Drying of Pharmaceutical Powders Using An Agitated Filter Dryer

Wei Li

Submitted in accordance with the requirements for the degree of
Doctor of Philosophy

The University of Leeds

Institute of Particle Science and Engineering

December 2014

Acknowledgements

I would first like to express my gratitude to Professor Kevin J. Roberts and Tariq Mahmud for their help and supervision throughout the course of this research work. I very appreciate that I spent such a fulfilled time to work in the field of Chemical Engineering especially in process engineering an area that I am so interested in. I am deeply grateful to them that they introduced me to the field of chemical engineering a discipline that I am much more proficient in.

I would also like to thank the technical staff in School of Chemical and Process Engineering, in particular Steve Caddick, Peter Dawson, John Cran and Simon Lloyd for their support in building up the experimental facilities needed for this research as well as for carrying out repairs and relocating to the filter dryer rig. I would also like to extend my appreciation to Stephen Terry from electronics workshop for his help for developing and implementing the LabVIEW system needed to control the experimental rigs used. I wish to thank all my colleagues in my group and Ulrike for providing such a pleasant working atmosphere.

I am grateful to my industrial supervisor, Dr. Mayling Yeow from Pfizer, Sandwich, UK and to Dr. David Am Ende, and Dr Mark Maloney from Pfizer, Groton, CT, USA who used to or still being worked in Pfizer company by giving me their valuable time and support during designing the drying rigs as well as though the most of research work.

I would like to thank the David Slate from Process Systems Enterprise (PSE) for helping me to implement and inspect the models developed in this work using gPROMS software.

I would also like to thanks Samal Mukayeva, who finished her master degree in University of Leeds in October, 2014, for her help in carrying out the experimental work on particle drying from mixed-solvents.

The financial support provided by EPSRC and Pfizer is gratefully acknowledged through the award of Dorothy Hodgkin Scholarship.

I am indebted to my mum for her continuous emotional and spiritual support, providing me with a sheltered harbour and for being as brilliant a guide as I could ever have wished for.

Abstract

The drying of pharmaceutical powders following their isolation via crystallization and filtration is examined using a laboratory-scale agitated filter dryer (AFD). Vacuum contact and through-circulation convective drying with and without agitation of aspirin powders with pure and mixed solvents are studied through an integrated experimental and modelling approach.

Experiments were carried out under different operating conditions by using aspirin particles and water/water-ethanol as typical solid-solvent systems. Two approaches were used to study the drying behaviour of aspirin: 100 µL small-scale drying using thermal gravimetric analysis (TGA) and 5 L medium-scale drying in a laboratory AFD. While the TGA tests provided a better understanding of drying kinetics as functions of temperature, vacuum level, solvent type and particle size, the AFD study revealed the effects of industry-relevant operating parameters (such as the heating rate, vacuum level, agitation speed and regime, gas flow rate, and initial solvent content) on the drying of aspirin particles.

In the TGA experiments, the constant and falling rate periods are observed for drying with pure water, while only the falling rate period is observed for pure ethanol and water-ethanol mixed solvents. In the laboratory-scale AFD experiments, drying cycle time is found to decrease with increasing agitation speed, vacuum level, heating power supplied and gas flow. The critical solvent content is determined by identifying the transition point on the temperature-time and the torque-time plots during the drying process. Particle size distribution and morphology analysis of aspirin particles before and after drying with agitation indicate that the particles tend to agglomeration at lower stirring speeds while they are prone to attrition at higher speeds. An increase of the circularity of the particles with the increase of the agitation speed is observed due to attrition effect.

Drying models based on a lumped-parameter (LPM) approach are developed for the static and agitated bed vacuum contact drying and combined LMP and distributed-parameter model (DPM) for the convective drying. Within this modelling approach, only one parameter that is the critical solvent content needs to be estimated from experimental results compared to other LPMs which greatly reduced the degree of parameter estimation. These computationally expedient models can be used for the prediction of drying time in a fast and reliable way. The model equations are implemented

in gPROMS software and the models are applied to simulate the experiments carried out in the 5 L AFD. The vacuum contact drying experiments were also simulated using a DPM embedded in the gPROMS software. The modelling results of LPM were compared with that obtained using the DPM. Overall, a good agreement between the calculated and measured drying curves is obtained and the measured drying times are well predicted at varied drying conditions.

This research presented the following improvements over the current studies on powder bed drying with limited research on organic crystalline materials and mixed solvent: holistic studies on drying behaviour with varied external drying conditions as well as internal material properties using different scale apparatus: TGA and AFD. Over the previous LPMs on powder bed drying, the modelling approach presented the following improvements: the models developed in this work need less parameter estimation. Three consistent approaches to measure the required parameter at the laboratory scale have been described in this work. The models provide a potential for industrial application on AFD drying.

Table of Contents

List of Tables

List of Figures

Nomenclature

Nomenclature

A_V	Interfacial area of solids per unit bed volume $(A_V = A_i/V)$	$m^2\ m^{-3}$
A	The heating wall area in contact with the wet-cake	m^2
A_b	Cross sectional area of the vessel	m^2
A_i	Interfacial area of solid particles	m^2
C, n	Adjusting constant	-
c_p	specific heat capacity	$J\ kg^{-1}\ K^{-1}$
$c(r)$	the solubility of particles at radius r	$kg\ m^{-3}$
d_p	Diameter of a single particle	m
D	Diameter	m
Fr	Froude number $(=\frac{(2\pi n)^2 D}{2g})$	-
$\dot{G}$	Gas flow rate	$kg\ m^{-2}\ s^{-1}$
ΔH_s	Latent heat at adiabatic saturated temperature	$J\ kg^{-1}$
ΔH_v	Latent heat of solvent vaporization	$J\ kg^{-1}$
k_{vap}	Rate constant	s^{-1}
k_{pro}	Propositional constant	-
l	Free path of the gas molecules	m
Le	Lewis number $(=Sc/Pr)$	-
m	Mass	kg
$\dot{m}_v$	Drying rate	$kg\ s^{-1}$
M	Molecular weight	$kg\ mol^{-1}$
n	Rotational frequency of the mixing device	s^{-1}
Nu	Nusselt number $(=\frac{\alpha_{gs} D}{\lambda})$	-
P	Pressure	Pa

P_{cap}	Gas-phase pressure through the capillary pressure	Pa
P_{sat}	Vapour pressure that would be in equilibrium with the local temperature	Pa
Pr	Prandtl number $(=\frac{c_{p,g}\mu}{\lambda_g})$	-
$\dot{Q}$	Rate of heat transfer	W
$\dot{Q}_{gs}$	Rate of heat transfer from forced convection	W
$\dot{Q}_{in}$	The heat actually entering the cake	W
$\dot{Q}_{gs}$	The rate of heat transfer from hot gas to the wet solid	W
$\dot{Q}_{js}$	The rate of heat transfer from jacket to the wet solid	W
q	Heat flux	$W\,m^{-2}$
r	Radius	m^{-1}
R	Gas constant (=8.314)	$J\,mol^{-1}\,K^{-1}$
Ra	Rayleigh number $(=\frac{g\beta\rho c_p(T_{wo}-T_\infty)D_{wo}^3}{\nu_{air}\lambda_{air}})$	-
Re	Reynolds number $(=\frac{D_p\dot{G}}{\mu})$	-
Sc	Schmidt number$(=\mu/\rho\kappa_{dif})$	-
T	Temperature	ºC
T_{aver}	Average temperature	ºC
T_S	Adiabatic saturated temperature	ºC
T_B	Boiling point of solvent	ºC
T_W	Wet bulb temperature	ºC
T_∞	Ambient temperature	ºC
t_R	Fictitious rest time during agitation	s
u	Fluid velocity	$m\,s^{-1}$
u_r	Rotational speed	rpm
ν	Local volume fraction	-

v^*	Residual saturation of ν	-
V	Volume	m^3
W	Power input	
X	Solvent content of wet solid $(= m_v / m_{ds})$	-
X_C	Critical solvent content	-
X_e	Equilibrium moisture content	-
Y	Gas humidity	-
z	Distance from the heating wall	m
Z	Depth of the cake	m

Greek symbols

α_{gs}	Convective heat transfer coefficient	$W m^{-2} K^{-1}$
α_m	Mass transfer coefficient	$kg m^{-2} s^{-1} pa^{-1}$
α_i	Overall heat transfer coefficient	$W m^{-2} K^{-1}$
α_{wp}	Heat transfer coefficient for a single particle	$W m^{-2} K^{-1}$
α_{rad}	Radiation heat	$W m^{-2} K^{-1}$
α_{ws}	Contact heat transfer coefficient	$W m^{-2} K^{-1}$
λ	Thermal conductivity	$W m^{-1} K^{-1}$
δ	Roughness of the particle	-
κ_D	Diffusivity	$m^2 s^{-1}$
κ_P	Permeability	m^2
υ	Kinetic viscosity	Pa s
μ	Dynamic viscosity	Pa s
ρ	Density	$kg m^{-3}$
σ	Stefan-Boltzmann Constant $\sigma = 5.67 \times 10^{-8}$	$W m^{-2} K^{-4}$
τ	Torque	N m

Subscript

0	Initial condition for t=0
1	Inlet position of the agitated vessel
2	Outlet position of the agitated vessel
a	Air
agi	Agitation
aver	Average
c	Cake
d	Dry
ds	Drying solid
dz	Dry-zone
eff	Effective
fc	Free convection
g	Gas phase
l	Liquid phase
p	Particle
s	Solid phase
sat	Saturated condition
ull	Ullage space
v	Vapour phase
V	Volumetric
vap	Vaporization
vf	Vaporization front
w	Wall
W	Wet bulb
wi	Inner wall of the vessel in contact with cake
wo	Outer wall of the vessel corresponding to wi
ws	Transfer from heating wall to solid phase
wz	Wet-zone

List of Abbreviations

AFD	Agitated filter dryer
API	Active pharmaceutical gradient
BET	Brunauer–Emmett–Teller theory
DPM	Distributed-parameter model
DSC	Differential Scanning Calorimetry
FDA	Food and drug association
LPM	Lumped-parameter model
LOD	Loss on drying
ODE	Ordinary differential equation
PDE	Partial differential equation
PSD	Particle size distribution
SOP	Standard Operating Procedure
TGA	Thermo-gravimetric Analysis
VCD	Vacuum contact drying

Chapter 1
Introduction

1.1 Research background

In the manufacture of active pharmaceutical ingredients (APIs), the final drug substance and key intermediates are often isolated through crystallization as solids. In order to recover these crystalline pharmaceutical powders from their crystal solution/mother liquor, a series of physical and chemical separation operations are usually employed. Drying through thermal vaporization and/or vacuum induced is usually the last separation step following crystallization, filtration and washing, the latter used to remove the undesirable solvent from adhering to the solid particulate product. The problem of maintaining relatively low solvent content and especially the control of water activity to prevent microbial proliferation exists in all stages of pharmaceutical production.

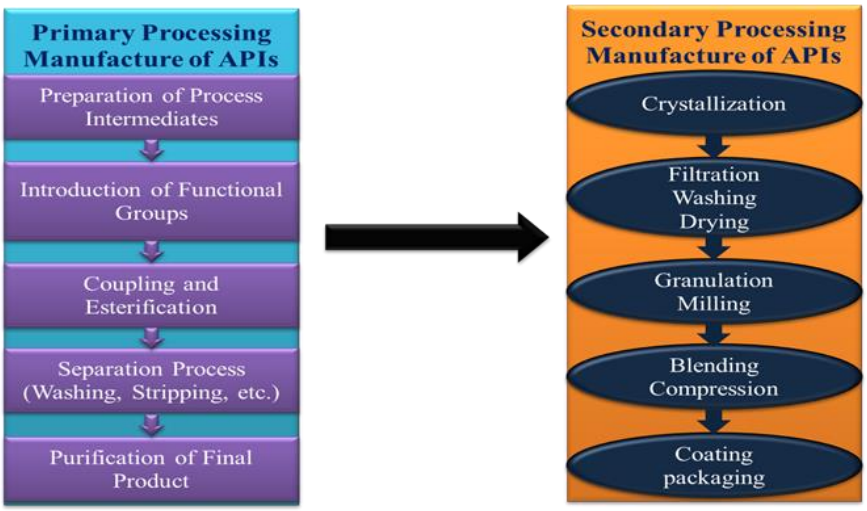

Figure 1.1 Schematic diagram highlighting the main unit operations used in the industrial processing of pharmaceutical ingredients

Considerable effort is made in terms of the design of crystallization processes in order to obtain the required chemical quality and physical properties including filterability, particle size distribution for further subsequent downstream processes. The particle properties attained after crystallization may be compromised during the downstream filtration and drying processes. Drying, as one of the final stages of the pharmaceutical production process, may cause deterioration of the pharmaceutical product by making it especially susceptible to microbial growth due to any unremoved organic solvent. Drying can be quite complicated process with

simultaneous heat and mass transfer accompanied with physical and chemical transformations. During drying, the heat transfer can be achieved by convection, when hot gas comes directly contact with the wet material, or by conduction, when heat is transferred to the wet material through a hot surface. Contact drying occurs as a result of the vaporization of liquid by supplying heat to wet material. Contact drying especially under vacuum conditions is often employed for thermal-sensitive and oxygen-sensitive pharmaceuticals to avoid thermal decomposition. Although the importance of drying and its effective control has been recognised for many years, it can still be quite unpredictable due to many of the uncertainties that are involved in the process. Many active pharmaceutical ingredients (APIs) and excipients are heat sensitive and require rigid temperature control to avoid degradation.

In the pharmaceutical industry, the agitated filter dryer (AFD) is frequently used for both filtration, washing and drying of crystalline intermediates and APIs. By combining these unit operations into one single equipment, AFD provide many advantages including excellent containment since the filtered, wet-cake does not need to be transferred to a separate dryer. AFD is very popular in the pharmaceutical industry because of their closed design and their ability to operate under vacuum. Working under lower pressures greatly reduces the solvent vaporization temperature hence allowing drying at lower temperatures optimal for handling temperature-sensitive materials. Such processing challenges for thermo- and oxygen-sensitive APIs containment to minimize the potential for worker exposure afforded through the use of AFD have given rise to the wide spread adoption of the AFD of the pharmaceutical industry.

To lessen the attrition and agglomeration effect on the drying product, different agitation modes are applied to AFD units. Intermittent agitation in static bed drying or starting agitating at a specific level of loss on drying (LOD) are the most commonly used approaches for vacuum contact drying. Therefore, to provide better design for this dryer and to optimize the drying processes, validated and reliable models are needed to predict the drying profile and drying time precisely. Thus the use of a model for predicting the drying curves can be used to optimise industrial drying process as well as to compare drying technology. The prediction of the end-point of drying process and suggestion of time for sampling as well as prediction of the start point of the agitation are very useful information in the pharmaceutical manufacturing in a manner which is both economic and effort-saving. Real-time model-predictive process control is useful for the comparison of different agitation regimes, and different operating conditions such as vacuum pressure, nitrogen flow, jacket temperature and cake volume, together with comparison of different solvents,

comparison of dryer geometric parameter designs. Through this process optimization as well as dryer design and selection can be facilitated [1].

In lumped-parameter models, which also called concentrated parameter models, Ordinary Differential Equations (ODEs) are developed [2] with the assumption of spatially-averaged variables (usually including temperature and moisture content). In distributed-parameter models, two dimensional variables as functions of both time and space are considered leading to the need for the use of Partial Differential Equations (PDEs) in the model as a result. Distributed-parameter models can further be classified as either continuum [3] or discrete. In continuum models, the porous wet-cake is taken as a continuum with constant or smoothly varying values of effective transport properties and the heat transfer equations are described by Fourier's law while mass transfer equations by Darcy's law. In particle scale models [4], the transport properties can be acquired through experimental measurement or obtained computationally from simulations on reconstructed porous media at the micro-scale.

Experimental studies are also used to better understand drying principles during the drying process. Study of agitated drying on crystalline particles have been carried out using an experimental studies [5] by Lekhal et al. who studied the effects of drying conditions on crystal morphology. The results showed that attrition and agglomeration competed with each other continuously and influenced the crystal morphology at certain moisture contents. Attrition was found to play a role when the drying rate was very low due to more particle/particle collisions occurring due to the long drying time. When drying rate increased, with higher temperature and lower pressure, agglomeration was found to play a role during the drying period. When needle-like crystals are dried [6], Lekhal et al. also found that the larger crystals were more sensitive to attrition whilst most of the attrition was found to occur during the falling rate drying period. Whereas the agglomeration process was found to dominate, the moment when the crystals size was found to enlarge was when the Critical Moisture Content (CMC) was exceeded.

The agglomerates initially grow from highly saturated aggregates containing a large portion of inter-particle pore space populated by saturated solution. During the drying process, the liquid within a group of particles vaporises in the first place and moves to the surface by diffusion [7]. When this process continues, the remained liquid content decreases with those left building liquid bridges which causes agglomerates formed at this point. If the liquid in the agglomerates contained dissolved substances, then re-crystallization can be expected to take place resulting in a layer of crust being formed on the surface of agglomerates. This phenomena is more

liable to take place for low temperature drying conditions especially in vacuum drying. In this situation, the crust can become very dense whereas under the crust surface the agglomerates can still be quite wet producing dry granules with a high moisture content inside. Without the application of external force or pressure, such a situation can be very dangerous for storage as trapped liquid inside may transport and lump. Such granules are likely to be destroyed in secondary processing, for example in the tabletting and compression process, the liquid would be liberated giving rise to potentially severe processing problems.

Since agglomeration typically occurs when the product is too wet the approach taken here is to identify methods of characterizing the CMC such that the risk of agglomeration can be minimized if agitation occurs below the CMC. The CMC is typically defined as the break point between the constant rate period and falling rate period. Figure 1.2 illustrates the scope of CMC as well as its critical importance in drying process. Given the relationship between CMC and energy input (torque), different means of defining CMC are used in this work including the transition point at the temperature profile, drying curve as well as the torque profile during agitation. While the former two can be used either static or agitated bed. One of objectives of this thesis is to optimize the drying process by reducing cycle time and construct a predictive model for the domination of the CMC.

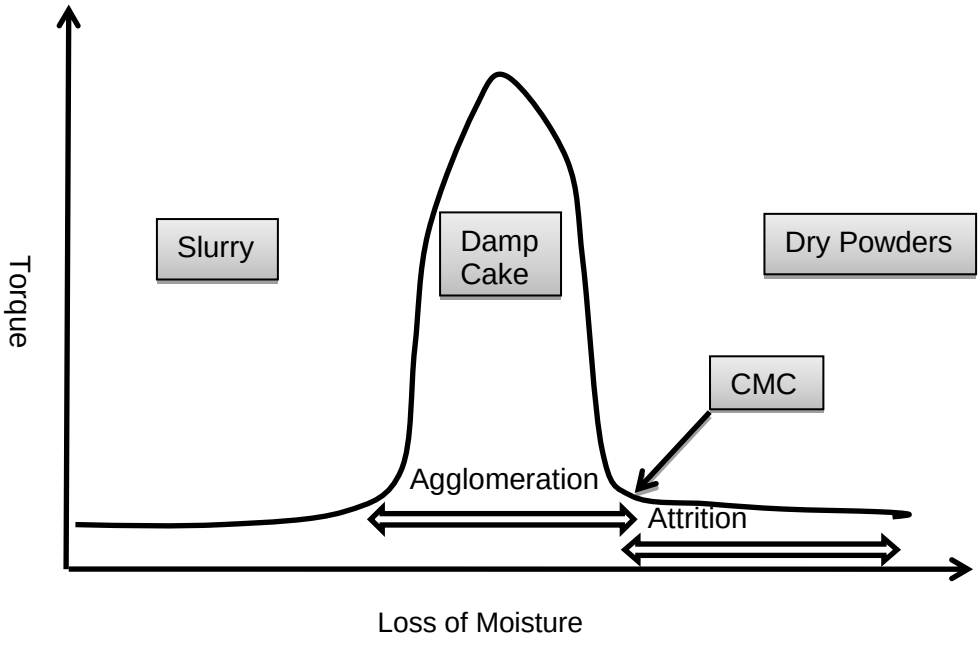

Figure 1.2 Torque against loss of moisture during drying process

1.2 **Motivation**

Amongst all separation process unit operations, drying is one of the most time-consuming stages with greater complexity when compared to other unit operations [4]. Therefore, to create more driving force for drying process, aggressive drying conditions by precipitating rate of heat transfer and mass transfer are used to minimize the drying cycle time in order to increase the productivity. For example, higher jacket temperatures and vacuum levels as well as incorporation of agitation can produce higher drying rates.

Despite the advancement in mechanical design for various types of dryers and widely used in industry, the mechanisms and principles for drying are still not clear enough. For example, the temperature profile and how moisture content distributed of volume wet-cake are not clear. The experimental technique is still not well developed for accurate measurement. On the other hand, models that have been developed can be used to predict the drying curves and through this to validate laboratory experimental work. Deviation between existing models and the actual situation still exists and validation only at the bench-scale results can be insufficient in terms of process scale-up. Precise prediction are thus needed for scale-up from laboratory to pilot plant AFD with stable and reliable models. Furthermore, most research has concentrated on the development of drying modes for direct dryers and indirect dryers separately though, and experiment or simulation work for predicting a combination of drying modes received less interest. Such a combination of more than one drying mode has the potential to create higher performance profiting ratio and enhance industrial production efficiency.

In the pharmaceutical industry, the major challenge during crystal materials drying is the preservation of the initial grain size and shape during the process by preventing the agglomeration and attrition phenomena. Regarding attrition, primarily caused by the mechanical impact of the stirrer blades on the individual particles or the mutual impact of adjacent particles, the simplest solution to this is either to reduce stirring intensity which related to stirring rate or the stirring duration. Intermittent stirring, which alternates the periods for stirring and no stirring, is frequently applied. The optimal stirring conditions can be investigated by calculating total drying times for different sequences of stirring and no stirring periods.

Furthermore, many pharmaceuticals are thermo-labile and oxygen-sensitive and any attrition and agglomeration phenomena occurring along with extreme drying conditions may have a unpredictable impact on the functionality and quality of the material being dried. It is important to note also that many APIs are shear sensitive,

so that agitation in the wet state can lead to agglomeration whilst in the dry state can lead to attrition. Agglomeration is undesired as it causes difficulties in discharging the dry-cake and hence prolongs the cycle time. Attrition can severely affect the downstream operations such as blending with excipients and tabletting. These can affect the particle shape and size distribution with a potentially negative impact on the drug product formulation. The best way to dry APIs is to minimise the effect of agitation in order to preserve particle integrity without producing lumps or fines. Therefore, the impact of drying process on the powder properties such as particle size distribution and particle morphology is clearly most worthy of more detailed study as currently there is a lack of effective tools which can be used to accurately predict AFD design and operation from both a micro (particulate behaviour) and macro (scale-up performance) perspectives.

1.3 **Aims and objectives**

To understand and predict scale-up performance in AFD, particularly the process analysing issues of powder morphology and size changes for further prediction the potential aggregation and agitation during agitated drying. As the operating conditions are complex, it is important to investigate current industrial concerns, the research questions are raised by Pfizer which the funding source.

- How to optimize operating conditions to reduce drying cycle time?
- Causes of agglomeration and relationships with critical solvent content?
- Is there a reliable and computationally expedient model to predict drying time?

To answer these questions, objectives have been set

- Previous studies on non-organic materials due to easily confined and reduced variability of the resultant drying sequences as the morphology of the particles and particle-solvent interactions. In order to build up the fundamental understanding of the filter drying process for organic materials in the light of the limited research on them, organic systems prone to form agglomerates are adopted for drying test..
- The particle size and morphology are investigated before and after agitated drying. The potential influence of solid-solvent interactions are investigated for resultant effects on agglomeration and attrition phenomena.
- To fully understand the way in which the material influences the drying process, knowledge of the complicated mechanisms of moisture movement that occur on the micro-scale is needed. Drying tests using TGA are carried out for further understanding drying kinetics.

- To predict drying time and drying behaviour in an AFD, computational expedient models are needed to be developed and to test the models reliability and consistency the models required to be validated through a series of representative pharmaceutical experimental studies.
- Therefore as part of this work a comprehensive investigation to determine the distribution of temperature within the cake using flexible thermocouples are performed as accurate and fast-response measurement provides a better understanding about the drying process.
- Investigation into optimization of drying conditions: types of drying (convective & contact drying); Lumped parameter model for vacuum contact drying with and without agitation will be developed. Lump-parameter drying model for through-circulation convective drying for static bed will be developed.
- The relationship between temperature and solvent content profile was closely associated as can be illustrated in Figure 1.3 The solvent content and temperature profile will be recorded online during the drying process for a better understanding of drying behaviour.

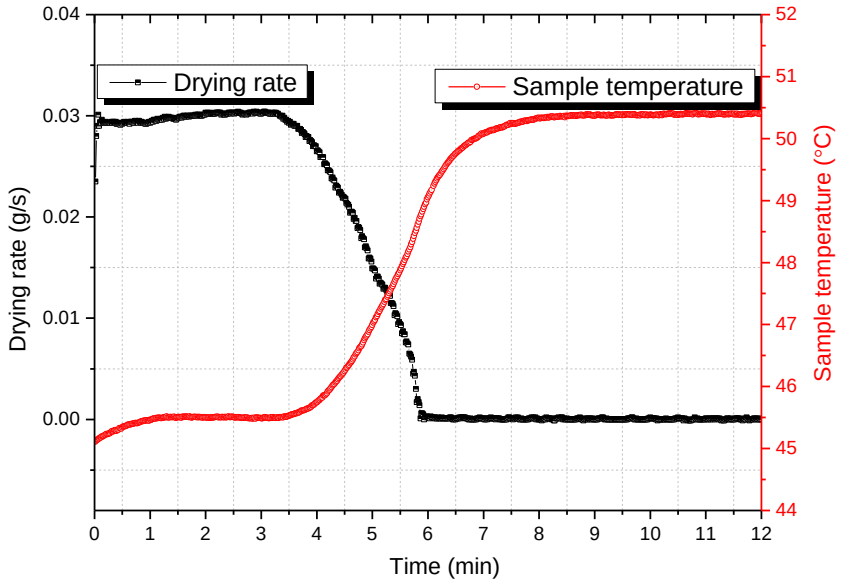

Figure 1.3 Example of drying curve (—) and relative sample temperature (—) for drying aspirin/water system using TGA at 50 ºC, constant-rate period from t = 0-3.5 min, falling-rate period from t = 3.5-15 min

- Different analytical techniques are used to characterise the critical solvent content includes online tracking the cake temperature, solvent content and power input of the wet-cake.
- Explore different approaches to develop reliable and convenient models based on experimental validation. To validate model, experimental studies will be

carried out through a bench-scale AFD instrument which can be operated under different drying conditions under both contact and convective drying.

- The model will be implemented into gPROMS software by solving ODEs and PDEs to investigate the practicability and performance of the drying models.
- An untested distributed-parameter model recent developed by PSE company for vacuum contact drying will be introduced and validated in this work and further compared with lumped-parameter model.

1.4 **Project management**

1. This project is support by Dorothy Hodgkin Postgraduate Awards from The Engineering and Physical Sciences Research Council (EPSRC) as well as Pfizer (from 2010 to 2011 in Sandwich, UK) and (from 2011 to 2013 in Groton, Connecticut, USA)
2. The collaboration with Pfizer includes a site visit to pilot plant in Sandwich, UK at 15th - 21st February, 2011. Also teleconference was held every one month aimed at research work discussion and issue communications. Work reports were done by every monthly meeting.
3. The modelling development and validation cooperated with Process Systems Enterprise (PSE) was accomplished by a site visit to London, UK at 10th -21st November, 2013.
4. The basis of bench-scale agitated filter dryer was originally built up by PhD student Amber Geddes with thesis ‘The Filtration and Drying Behaviour of Organic Crystals with Varied Morphologies following their Batch Crystallisation’ (2003).
5. The for water/ethanol mixed solvents drying experiments using bench-scale AFD were carried out by MSC student Samal Mukayeva in 2014 July-August.

Table 1.1 Timeline of project management

The improvement and modification of bench-scale AFD	12.2010 - 12.2011
Small-scale TGA drying experimental research	12.2010 - 12.2011
Experimental work carried out using bench-scale AFD	01.2012 - 08.2014
Model development for vacuum contact drying	06.2011 - 09.2011
Model development for convective drying	04.2012 - 08.2012
The implementation of drying models into gPROMS	08.2013 - 01.2014
Model validation using the existing experimental results	02.2014 - 09.2014

1.5 **Layout of the thesis**

A schematic diagram of the route-map for this thesis is given in Figure 1.4

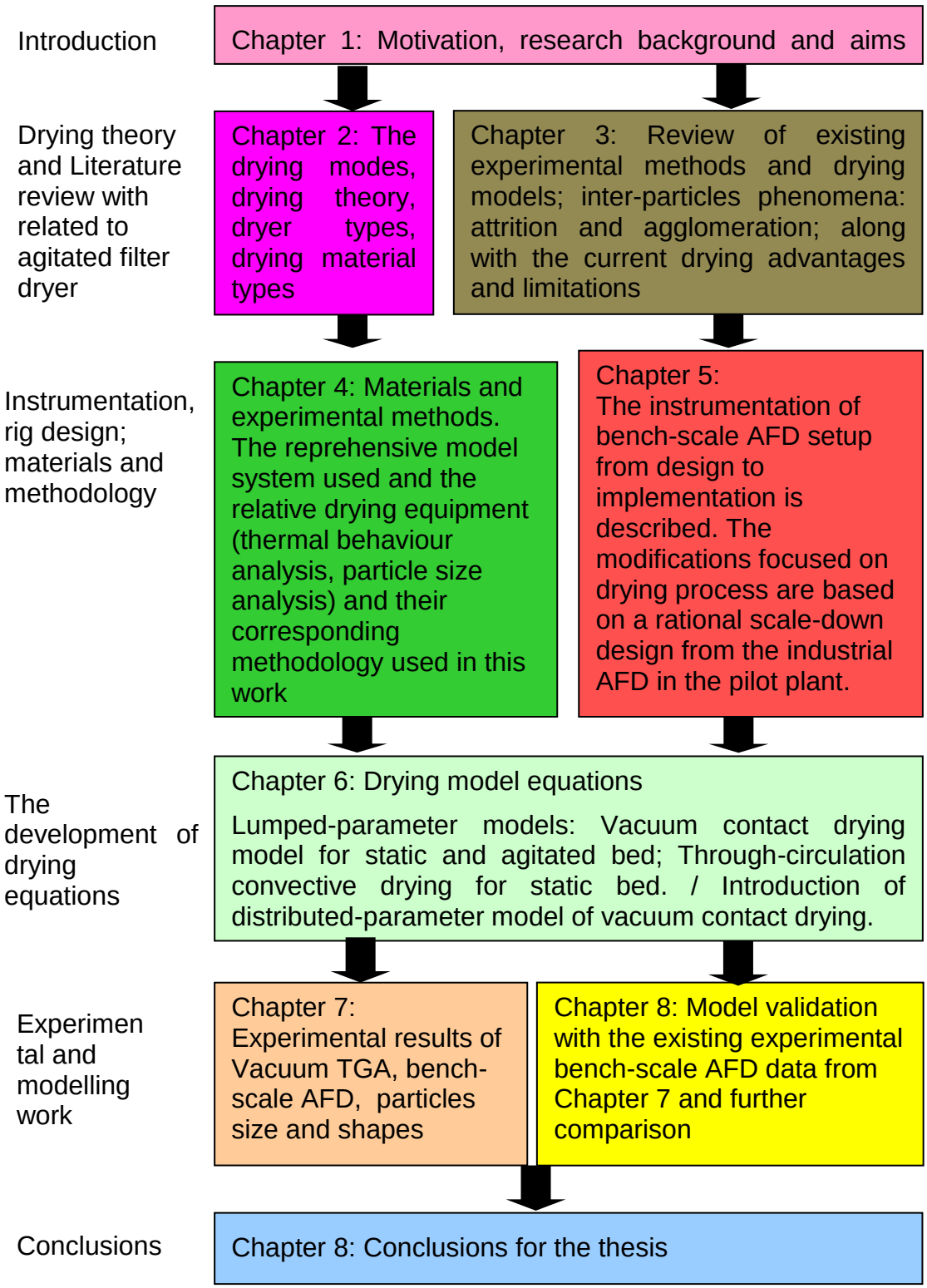

Figure 1.4 Illustrative route-map of the thesis chapters and a description of their content

Chapter 2
Drying theory

2.1 Introduction

In this chapter the basic theory concept concerning the thermodynamics and transport phenomena in the drying process are described. For drying is the removal of solvent either by vaporization or evaporation from different types of products including wet solids, solutions, slurries, and pastes. The most important thing in drying is to understand the mass and heat transfer mechanisms involved in drying for better predicting the future drying curves and variation of temperature profile symbolised. Drying is a complicated process with simultaneous heat and mass transfer accompanied with physical and chemical transformations. During drying, the heat transfer can be achieved by convection, when hot gas comes directly contact with the wet material, or by conduction, when the heat is transferred to the wet material through a hot surface. Solvent transport within the wet bulk material occur in different mechanisms.

2.2 Basic drying theory

Drying occurs in a heterogeneous system involving solid, liquid, and vapour so generally it is can be a distillation but taking place at a rather complex circumstance. The phase transformation occurs by vaporizing from liquid phase for distillation while drying takes place from wet solids after filtration process particular for pharmaceutical particles. For most pharmaceutical materials, specific requirements have to be satisfied when drying the sample due to water activity within pharmaceutical solids influences the process abilities including flow properties, compaction, hardness; as well as drug properties consisting of the chemical stability, microbial stability dissolution rate of dosage forms of pharmaceuticals, proteins, biopharmaceuticals, nutraceuticals and phytochemicals [8]. In the case of drying APIs, the acceptable levels of residual solvent should meet the basic requirements presenting including safety (solvent toxicity), regulatory and stability requirements regulated by FDA [8].

The moisture content is defined by mass of moisture per mass unit of bone-dry solid in percentage which means the moisture percentage on a dry solid basis ($X = m_v / m_{ds}$). There is also another definition for analysing the loss weight of drying process The moisture content of the bed is expressed as loss on drying of the

solvent (LOD). LOD is defined by Weight of solvent in sample per mass unit of the wet sample weight in percentage [9]. The moisture existing in the wet solid can be distinguished into different types according to the moisture levels (see Figure 2.1)

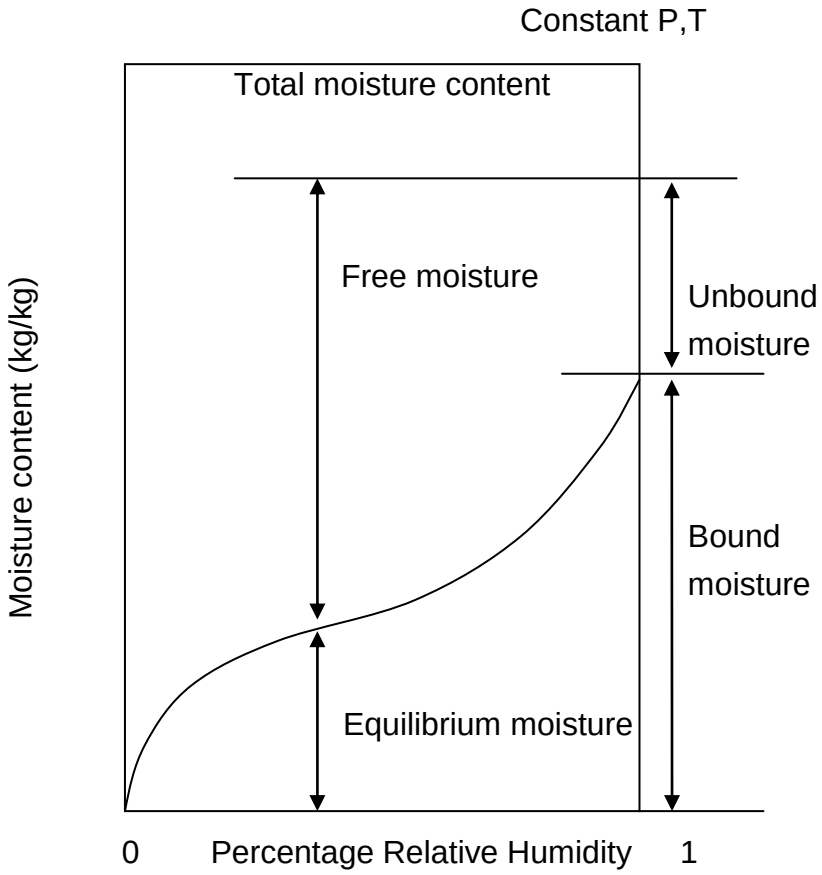

Figure 2.1 Types of moisture involved in the drying of solid [10, 11]

Figure 2.1 shows the relationship between varied terms of moisture existed in the wet materials. Free moisture is the part of moisture that the moisture content beyond equilibrium moisture content while below that is equilibrium moisture. The free moisture can be removed by drying process under given percentage of relative humidity. After exposure of the wet solid sufficiently long enough for dry air, an equilibrium to be reached, the solid will attain a definite point called equilibrium moisture content.

The sorption and desorption curves were obtained by wetting and drying the solid. For drying process, the capillary contains more moisture than sorption of wetting process. Materials with bound moisture are called hygroscopic. Bound moisture has a pressure less than normal vapour pressure. Bound moisture can also be defined as moisture kept in chemical form. Water of hydration in inorganic crystals is one example of bound moisture dissolved in the solid. The presence of crystal water strongly reinforces the adsorption capacity. The vapour pressure of such moisture is

much less than the true vapour pressure. The determination of how many hydrates inorganic salts can form is determined on not only the temperature and also the relative humidity of the gas in contact with the crystals.

When the relative humidity percentage reaches 100%, water in the solid is called bound moisture. Hygroscopic materials usually contains bound water and for system like this, the vapour pressure is less than the normal pressure at the same temperature. For this circumstance, the liquid water restrains to very small diameter capillaries which has a lowered vapour pressure due to the concave curvature of the surface. The sorption and desorption curves can be measured by wetting and drying the solid. While in drying process, because the capillary pores contains more liquid than wetting process so the desorption curve has a lagging effect [12] (see Figure 2.2). The equilibrium relative humidity is water activity (Figure 2.2 in x axe) presented as a percentage. The equilibrium moisture content of aspirin increased as increasing of the water activity at constant temperature for both adsorption and desorption curves together with the sigmoid shape sorption curves all indicated that aspirin as an hydroscopic material [13]. It can be seen that for the same level of relative pressure, the quantity of adsorbed water for sorption process is less than that in desorption process in 25ºC (Figure 2.2 a). This hysteresis effect became less obvious as temperature increased to 30 and 40ºC (Figure 2.2 b and c)

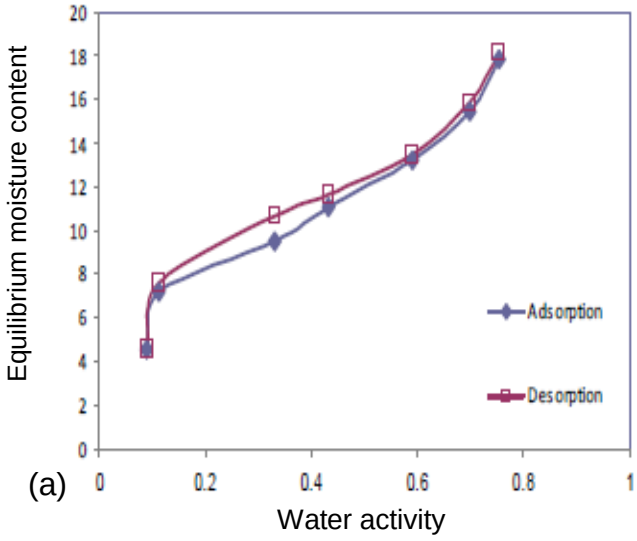

(a)

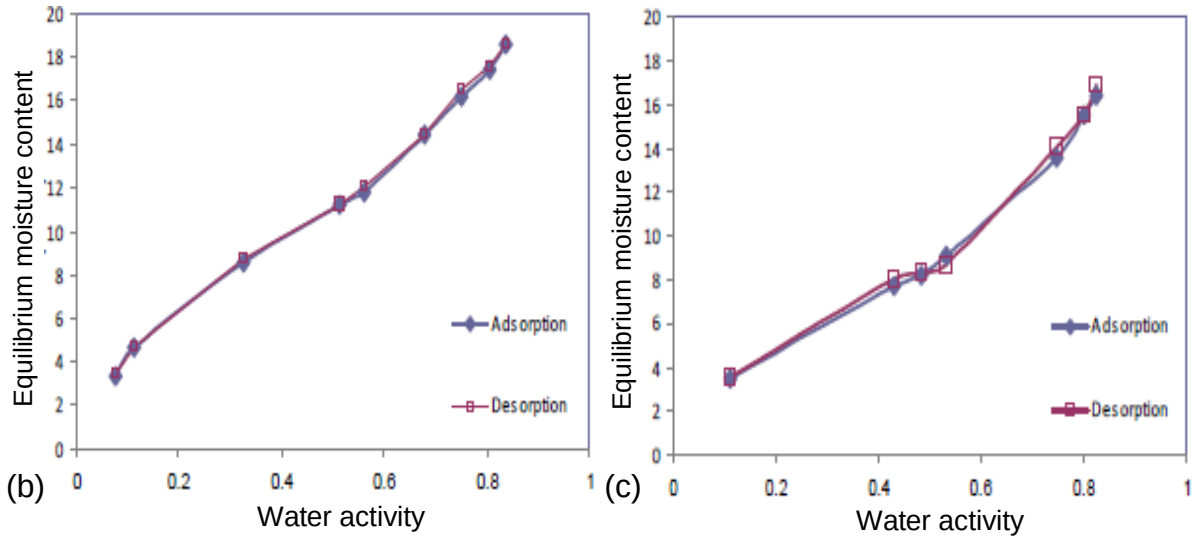

Figure 2.2 Example of curves of moisture desorption (—) and adsorption (—) isotherms of aspirin measured by BET method at (a) 25ºC; (b) 30ºC; (c) 40ºC offered [13]

As mentioned above, moisture in a solid may be either unbound or bound. Two methods are used to remove the unbound moisture: evaporation and vaporization [10]. Evaporation occurs at the normal boiling point where moisture vapour pressure is equal the atmospheric pressure. This is usually used to dry the material without risk of thermal damage and decomposition. Correspondingly, if the boiling point is lowered by lower the pressure to vacuum level and then this is vacuum evaporation. Continuing lower the pressure reach the tripe point of the liquid, there is no liquid phase exists and the solvent will be frozen also well known as freeze-drying and this evaporation caused by sublimation.

Another method to remove the unbound moisture is vaporization. Vaporization occurs when the air or more commonly nitrogen heated passes through the wet solid and supply the heat for the moisture directly. During vaporization, cooling effect can be observed in the process. In Figure 2.3, the air is cooled by the solvent vaporization, the mass transfer occurs when the moisture is carried away by the flowing dry air. The saturation vapour pressure of the moisture over the solid is less than the atmospheric pressure.

For convective drying experiment, during constant-rate period, the temperature of the drying surface, is the so-called wet bulb temperature. The heat transfer of the steady state in this period can be expressed as

$$\dot{Q} = \alpha_{gs}\left(T_g - T_W\right) \qquad 2\text{-}1$$

Also the heat supplied is all used for solvent evaporation, hence, the heat flux also can be given by

$$\dot{Q} = \dot{m}_v \Delta H_W \qquad 2\text{-}2$$

For mass transfer from the solid phase to the gas phase is given by:

$$\dot{m}_v = \kappa_D \left(Y_W - Y_g \right) \qquad 2\text{-}3$$

As can be seen from Figure 2.3, as corresponding to different drying regimes, similar temperature regimes can be observed. The temperature profile (Figure 2.3c), responding closely with the solvent movement within the wet-cake.

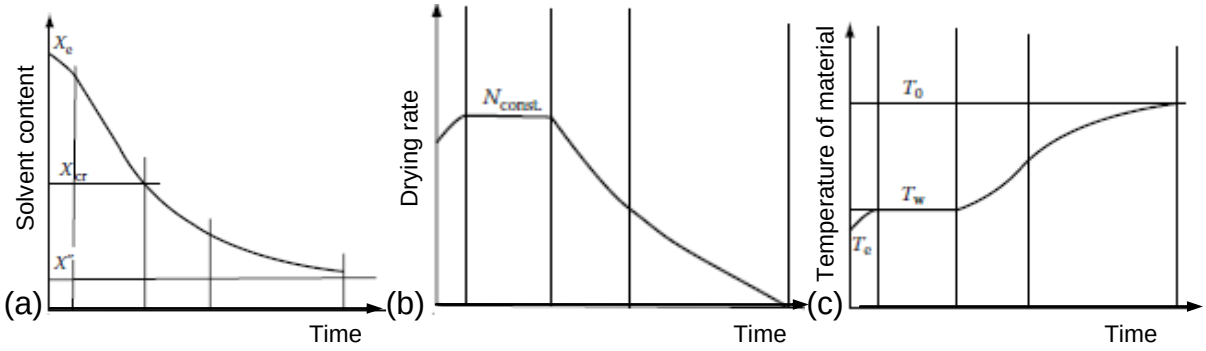

Figure 2.3 Example of (a) solvent content, (b) drying time and (c) temperature profile vs. time of convective drying process [14]

For nowadays, the two terms become more indistinct and for this work the term vaporization will be used for all the circumstances.

So far, techniques on online monitoring vacuum dryer include Near infrared spectroscopy (NIRS); mass spectrometry (MS); moisture meter, digital balance. However, some probes are only designed to detect the water content of the wet-cake rather than the organic solvents which are also important to pharmaceutical drying process. Furthermore, some probes are very sensitive to the external conditions and very difficult to install to the existing equipment make the online tracking are always being an issue. The methodology of collecting and weighing samples is still trustworthy and used by a lot drying process.

Vacuum drying is widely used in pilot plant for drying of pharmaceutical intermediates and drug substances. The monitoring of solvent content is not only a matter of the degree of the dryness of the products, also it can help track down the problems and targeting the time intense issue as well as productivity. [15]

Some work used NIRS technology to track the solvent content in pilot plant drying process [16, 17]. In such design, the probe was put in direct contact with the wet materials, the covalent molecular bonds can be excited by infrared radiation..

Because water shows a very strong absorption within the middle infrared range, it is a strong methodology to obtain the moisture content within a material. However, this method is very sunlight sensitive and most online tracking is water content determination. Mass spectrometry was also used for multiple solvents, which could be done by non-invasiveness as also can be referred as moisture meter. The MS has been used for online measurement of pharmaceutical drying process [18] in a vacuum tray dryer in pilot plant, the different drying regimes were also tracked down from MS monitoring.

2.3 **Drying types**

There are three modes of drying in terms of the way of heat transfer in porous media: convection, conduction and radiation. According to the mode how the heat is supplies to the moisture for vaporization can be divided into direct-heat (also called convection) dryers and indirect-heat dryers which provides heat to the material indirectly by conduction and/or radiation from a hot surface.

For this work, the former two modes will be focused. The direct drying, by heat transfer from a hot gas, and indirect, by heat transfer from a hot wall. The hot gas could be air, combustion gas, steam, nitrogen, or any other nonreactive gas. Conductive drying occurs as a result of vaporization of liquid by supplying heat to wet material. Contact drying especially under vacuum condition is employed for thermal-sensitive and oxygen-sensitive pharmaceuticals to avoid thermal decomposition. The extreme situation for vacuum drying is freeze drying where the moisture in the feed material is already frozen, the frozen ice will be sublimed to gas state by contact, convective or radiant heating. The advantage of freeze drying is that the structure and properties of the material to be dried stayed in the same morphology during the sublimation process while barely mass transfer occurred for the solvent is always frozen.

Contact drying is an indirect method of removal of a liquid phase from the solid by the application of heat, and is accomplished by the transfer of liquid from the surface of the solid into an unsaturated vapour phase. It is widely applied to industries that process chemical catalysts, food, pharmaceutical and other products. For the driving force for contact drying is the temperature difference hence higher contact surface temperatures can easily get approaching the boiling point of the solvent shows faster drying performance. The vaporising temperature for contact drying is the saturation temperature under the prevailing vapour pressure hence it can be calculated from Antoine’s equation [19].

For vaporising temperature within convective drying, dry-bulb and wet bulb temperatures are usually used. In general, the temperature in a direct-heat dryer is complex to determine and can vary from the inlet to outlet of the dryer. However, when the dryer operates isobarically and adiabatically with all of the energy needed for moisture vaporization, is supplied from hot gas by convective heat transfer, in addition, there is no energy required for heating the wet solid to the vaporization temperature. Then it is assumed that the moisture being vaporised is free liquid, exerting the full vapour pressure at the surface of the wet solid. This temperature of vaporization is referred to wet bulb temperature. The dry-bulb temperature is differentiated from wet bulb temperature that the former one measures the temperature of air shielded from radiation and moisture and it is true thermodynamic temperature. The way to measure wet bulb temperature can be achieved by covering the bulb of the thermometer with a wick saturated with the moisture. Also wet bulb temperature can be obtained by referring to psychrometric chart or using the equation below for calculation [20]:

$$T_W = T - \frac{\Delta H_v^W}{C_P}\left(\frac{1}{\mathrm{Le}}\right)^{2/3}\left(Y_W - Y\right) \qquad 2\text{-}4$$

While $\mathrm{Le} = \mathrm{Sc}/\mathrm{Pr}$ is the Lewis number, $\mathrm{Sc} = \mu/\rho\kappa_{dif}$ is Schmidt number representing momentum diffusivity/mass diffusivity; $\mathrm{Pr} = c_P\mu/\lambda$ is Prandtl number representing momentum diffusivity/thermal diffusivity. According to equation 2-1, for the constant pressure in convective drying, the parameters $\Delta H_v^W, C_P, \mathrm{Le}$ nearly remaining constant in a normal range of temperature; and then the possible changes for the value of the wet bulb temperature in a direct drying process lies in temperature (T) and moisture content of the gas (Y) will be the main factors influence the extent how much the moisture will be removed away to the flowing gas.

2.4 **Transport mechanisms**

For moisture to be vaporised from a wet-cake, it must be heated to the a temperature at which the vapour pressure of the moisture exceeds the partial pressure of the moisture in the gas in contact with the wet solid. In an indirect dryer where little or no gas is used to carry away the moisture as vapour. The partial pressure if the moisture approaches the total pressure and the temperature of evaporation approaches the boiling point of the moisture at the prevailing pressure as long as the moisture is free liquid at the surface of the solid. If the moisture interface recedes into the solid, a temperature higher than the boiling point is needed at the solid-gas interface to transfer the heat for evaporation from that interface to

the liquid-gas interface. In addition, if the moisture drops to a point where it is all sorted by the solid, the vapour pressure of this sorted pressure is less than the pure vapour pressure and an even higher temperature id required to evaporate the moisture. In a direct-heat dryer, similar situations can occur except that the temperature at which moisture evaporation occurs is dependent on the moisture content of the gas.

The rate at which drying is accomplished is governed by the rate at which these two processes proceed. Heat is a form of energy that can cross the boundary of a system. Heat can, therefore, be defined as “the form of energy that is transferred between a system and its surroundings as a result of a temperature difference.” There can only be a transfer of energy across the boundary in the form of heat if there is a temperature difference between the system and its surroundings. Conversely, if the system and surroundings are at the same temperature, no heat transfer across the boundary takes place.

Convection relies on the movement of a fluid in porous material. Conduction relies on transfer of energy between molecules within a porous solid or fluid. The driving force of both of heat flow is related to the temperature difference created for the transfer of energy to take place. The greater the temperature difference, the faster the heat transfer will be. Conversely, the lower the temperature difference, the slower will be the rate of heat transfer. Hence, when discussing the modes of heat transfer, the rate of heat transfer is much more considered for drying characteristics rather than that defines the rather than the quantity of heat.

Most vacuum drying is contact drying and the rate of heat transfer is controlled by contact resistance at the inner wall of the jacketed vessel and conduction into the material being dried. The difference between the batch operation and continuous operation can be distinguished by the mode of operation with respect to the material being dried. The batch operation usually has a led production rate wherever the continuous can handle big amount of production rate. Equipment for batch operation includes tray dryers and agitated dryers.

Diffusion of moisture through solids occurred when drying of porous particles. Diffusion is a molecular process, it is mainly of random movement of individual solvent molecules. If the water molecules within a material are of freely migration, they tend to diffuse from high moisture concentration zone to lower zone, to counteract the reducing moisture gradient and equalizing the concentration of moisture.

If liquid moisture occurs when there is a concentration difference between the depths of the solid and the surface. The moisture diffusivity usually decreases with decreased moisture content. So the diffusivities are usually average values over the range of concentration used. Since the rate of evaporation is quite fast, the resistance is very low, compared to the diffusion rate through the solid in the falling-rate period. As explained in the next sections, the rate limiting mechanism may be superficial evaporation or internal transport of water, depending on the conditions.

It is assume that the moisture being evaporated is free liquid and exerting with full vapour pressure. At the surface of the solid, there is evaporating temperature referred to wet bulb temperature. It can be measured by covering the bulb of the thermometer with a wick saturated with the moisture. In order to determine the possible change in the wet bulb temperature of the wet solid, in a direct-heat drying process, pressure, temperature and moisture content of the gas are all the main factors influence the extent how much the moisture will be removed from the wet-cake.

2.5 **Dryer types**

Dryers, according to the mode how the heat is supplies to the moisture for evaporation can be divided into direct-heat (also called convection) dryers, when hot gas is flowing through the solid and indirect-heat (also called contact) dryers when the energy is indirectly transferred to the wet material through a hot surface. In such a case, a wide variety of heating fluids can be selected including the hot water, steam, dowtherm, hot oil and molten salt etc.

Conductive drying is also called boiling drying which has a similar process as evaporation. The liquid evaporates at the prevailing pressure and the only difference between contact drying and evaporation is drying occurs at a much lower final moisture content. In an indirect dryer, such as vacuum contact dryer, where little or no gas is used to carry away the moisture as vapour, the partial pressure approaches the total pressure of the closed system. The temperature of evaporation approaches the boiling point of the moisture at the prevailing pressure as long as there is free moisture exists at the surface of the solid.

There is maximum temperature for the material for the product is temperature sensitive material. When material is easily combined with oxygen, becomes explosive and dusty during the drying or when the solvent is valuable, toxic and flammable, contact drying can be applied. In addition, vacuum and agitation can also be employed into contact drying for material tends to agglomerate without agitated.

Most vacuum drying is contact drying and the rate of heat transfer is controlled by contact resistance at the inner wall of the jacketed vessel and conduction into the material being dried.

Dryer can be divided into batch operation and continuous operation with respect to the material being dried. The batch operation usually has a less production rate while the continuous can handle large amount of feedstock. Tray dryers and agitated dryers are belonging to batch operation. Tray dryers are available for vacuum operation and with indirect heating. In one configuration, the trays are placed on hollow shelves that carry condensing steam and act as heat exchangers. Heat is transferred by conduction to a tray from the top of the shelf supporting it and by radiation from the bottom of the shelf directly above the tray. Typical performance flowchart for cross-circulation and through-circulation tray dryers are shown in Figure 2.4.

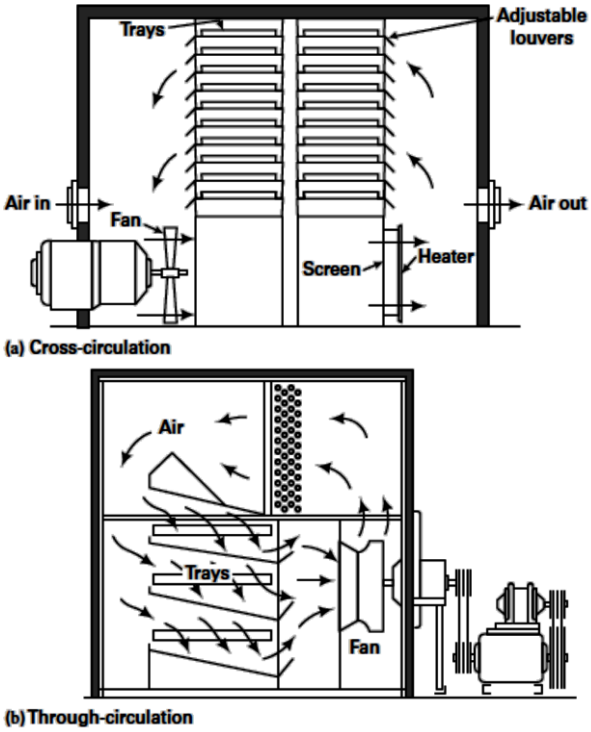

Figure 2.4 Tray dryers for batch convective drying offered [20]

Agitated dryers is designed to be enclosed for the following reasons: the material being dried easily combined with oxygen, becomes explosive and dusty during the drying; to keep the solvents dissipating if the solvents are valuable, toxic and flammable. Agitated dryer also designed for the materials tend to agglomerate without agitation. AFD is a particular design of agitated dryer to lessen the unwanted agglomeration effect on drying products. In the past, filtration and drying steps were carried out in separate unit operations. Typically a centrifuge filter and tray dryer

were combined together. Both the filtration and drying processes are time-consuming and labor as well as manufacture waste.

The most concerning is the containment issue for the exposure of irritating toxic and flammable organic solvents used during transferring process from a filter to a drying which will cause great damages to human body. AFD is an innovative filter and dryer equipment which can overcome this disadvantage by performing filtration and drying process consequently in one single unit (Figure 2.5). AFD are more commonly used in laboratory and pilot plant chemical engineering especially pharmaceutical industry currently. For AFD equipment is often operated under vacuum condition so that this unit is also used to dry granular thermal sensitive and oxygen sensitive products by utilising a vacuum, which has the benefit of lowering the boiling point of the liquid by reducing its vapour pressure, resulting in the reduction of both the solids temperature and the duration of the drying process. the details of bench-scale AFD design according the industrial AFD will be described in Chapter 4.

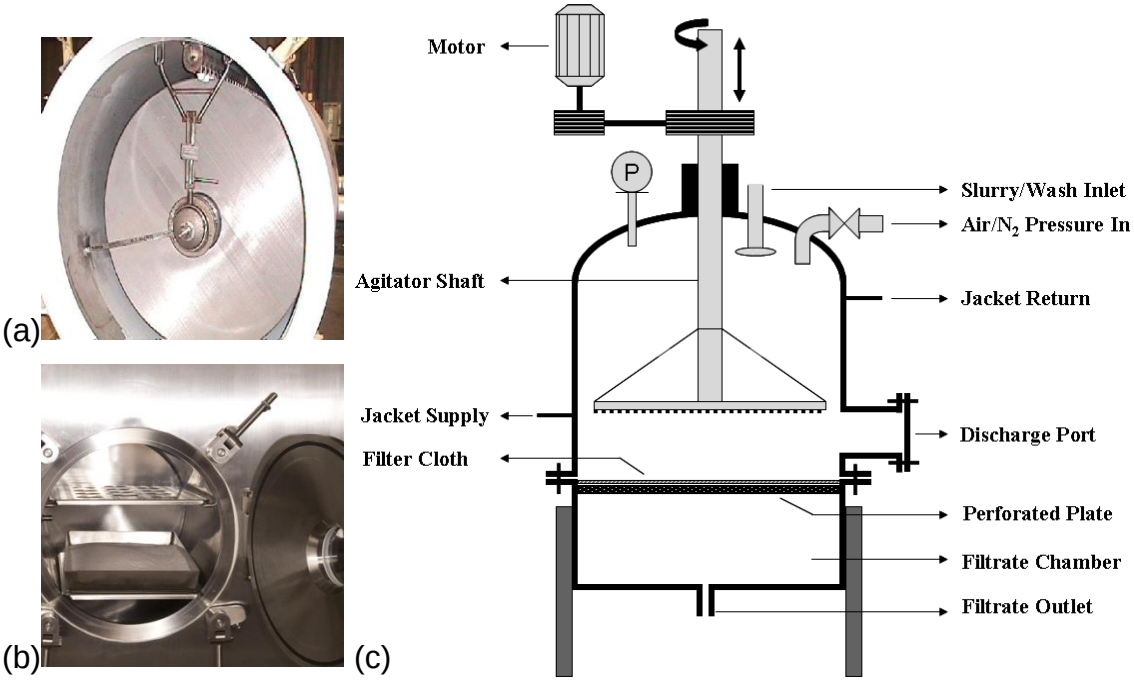

Figure 2.5 (a) photo of centrifuge filter; (b) photo of tray dryer; (c) cross-sectional representation of an AFD [21]

The development of agitated filter dryer (AFD) equipment and techniques evolved over last decade and are well appealed to the manufacturer once employed for industry. The widely use of commercial AFD in pharmaceutical engineering receives great concern. Vacuum contact drying theory related to AFD either experimentally or in simulation aspects is extensively researched. The transport and separation process takes place in a single unit involving heat transfer and mass transfer at the

same time. Most of vacuum contact drying processes use inert gas e.g. nitrogen as a drying gas purging through the system to help remove the residual vapours from the solid. The combination of vacuum contact drying and convective drying is considered as an efficient method to optimize drying process.

For contact drying, the liquid is often vaporised over the boiling temperature which causes overheating for thermal sensitive materials. Two methods is applied to reduce the possibility of thermal damage: reduce drying time by reducing the thickness of the wet-cake or reducing temperature by descending prevailing pressure. Hence vacuum contact drying is broadly used which has high thermal efficiency, since only a small fraction of the energy lost inside the dryer rather than convection or radiation. Therefore, operating costs for contact dryers are usually low, and the environmental impact is small.

Agglomeration and attrition is one of inevitable phenomena by using filter dryer equipment which may had bad alteration to the quality of final product. The effects of these two phenomena should be lessened to minimum. The agitation speed and stirring periodic intervals as well as the shape and size of the impeller and vessel both influence the agglomeration and attrition phenomena.

Most dryers are operated at near atmospheric pressures. A slight positive pressure avoids in-leakage from outside, which may not be permissible in some cases. If no leakage is permitted to the outside, then a slight negative pressure is used. Vacuum operation is expensive and is recommended only if the product must be dried at low temperatures or in the absence of oxygen or has flavours that are generated at medium- or high-temperature operation. High-temperature operation tends to be more efficient since lower gas flow rates and smaller equipment may be used for a given evaporation duty. Availability of low-temperature waste heat or energy from solar collectors may dictate the choice of a lower temperature operation. These dryers will then be large in size. Freeze drying is a special case of drying under vacuum at a temperature below the triple point of water; here water (ice) sublimes directly into water vapour. Although the heat required for sublimation is several fold lower than for evaporation, vacuum operation is expensive. Freeze drying of coffee, for example, costs two to three times more than spray drying. On the other hand, the product quality and flavour retention are better.

2.6 **Drying periods**

For the fixed dry air flowing in a direct heat dryer it was observed experimentally that generally the exposed surface is initially covered by a film of liquid. The most basic

and essential kinetic information on drying is presenting explicitly from a drying curve. Drying curve is obtained by differentiating moisture content with respect to time and multiplying by the ratio of the mass of dry solid to the interfacial area of contact (Figure 2.6). A drying curve describes the drying kinetics and explains the different stages during drying. Material properties, particle size or cake thickness of the drying material, and operation conditions etc. can both affect the drying curve [19].

Drying curves shows some common features for most materials to be dried. Both convective and contact drying can be divided into three drying periods: induction period, constant-rate period and falling-rate period. Here shows an example of general contact drying curve in red colour in Figure 2.6: The first induction period occurs when initially heating the material to the a certain temperature. Constant-rate period occurs when the surface of the wet-cake remains wet enough to maintain the vapour pressure of water on the surface. In this period, there will be moisture transfer to the surface by capillary flow. Once the surface dries sufficiently, the drying rate will decrease a lot and this is called falling-rate period. There is a transition between constant-rate and falling-rate periods of drying occurring at the critical point which known as CMC point. This gives rise to the second drying stage of the first falling rate period, the period of unsaturated surface drying. On further drying, the rate at which moisture move through the solid as result of concentration gradients between the deeper part and the surface is the controlling step.

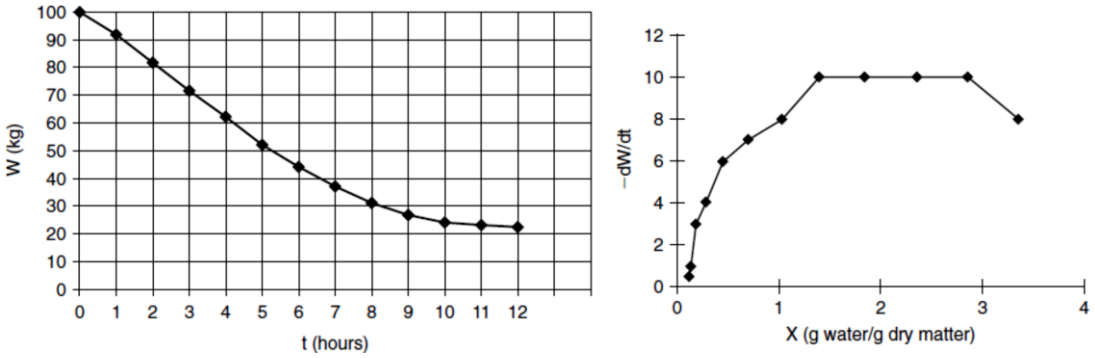

Figure 2.6 The plot for loss weight of moisture against time (left); the plot for rate of drying (right) [22]

The first induction stage occurs when initially heating the wet-cake to the boiling point. The rate of drying increases as water is removed. The rate of drying is increased may be ascribed to the warming-up or the pores opening effects etc. Only a negligible amount of solvent is evaporated during this stage. This stage is so short that usually it could not be observed in drying curves hence often omitted in the calculation of drying time. For this test, the induction period is so short and it can be

barely seen and the reason for that is this small-scale experimental makes the heating up process very easy to commence.

At the second stage of constant-rate period, the temperature of the material is maintained at the boiling point and it may rise slightly as the product becomes more concentrated resulting in rising of the material viscosity. Most of the liquid in the wet-cake is evaporated during this stage. The rate of drying is governed by the rate of heat transfer, occurs when the surface of the wet-cake remains wet enough to maintain the vapour pressure of water on the surface. In this period, there will be moisture transfer to the surface by capillary flow [23]. During this phase the product is still fairly wet, and the evaporation rate is constant, limited by the external rate of heat transfer. The drying curve appears as a straight line. The product temperature during this phase is equal to the boiling point of the liquid fraction at the operating pressure.

Once the surface dries sufficiently and there is not enough liquid diffusing through the pores to surface, the drying rate will decrease and this is called falling-rate period. At this stage, the drying rate decreases and asymptotically approaches zero if the equilibrium moisture fraction is reached. The liquid evaporated in this period is bound more tightly to the product on the surface and in the pores inside the particles, resulting in a lower vapour pressure and consequently a higher boiling point. The bed temperature will rise during this phase. Most of the residual water in the product is adsorbed in the capillaries and porous channels, therefore removal of water now takes place by desorption, until the desired final moisture content reached.

For specific wet-cake that high viscosity of the concentrated liquid and porosity may be created in the wet bed, causing further decrease in the rate of heat transfer, the overall heat transfer coefficient is reduced for the heat transfer resistance from the heating jacket to wet granular bed increases and drying rate slows down. However, the formation of porosity somewhat improves mass transfer rate though heat transfer dominates the transportation process. The temperature of the bed now rises gradually and tends approaching to the contact surface temperature.

Sometimes, two drying stages of falling-rate period can be observed due to various types of wet materials. The simultaneous drop in temperature gradient and overall heat transfer coefficient results in rapid declination of drying rate. This gives rise to the first drying stage of the falling-rate period, the period of unsaturated surface drying. In this stage, the surface is not covered by a continuous film of liquid. When the surface is completely dry, further drying causes the drying rate descending more rapidly. The controlling step is moisture move through the porosity as result of concentration gradients between the deeper part and the surface.

If the moisture content drops to a point where the liquid is all adsorbed by the solid, the vapour pressure of this point is less than the pure vapour pressure and an even higher temperature is need to vaporise the residual moisture. The major rate-controlling factor in contact drying is heat transfer rather than mass transfer which has a weaker influence on the process, which is similar to distillation. If the moisture interface recedes inwards to the solid, temperature greater than the boiling point needs to maintain to the vaporization occurred at liquid-gas interface as well as overcoming the solid-solvent interaction.

If all the solvent molecules in a material are free to migrate, they tend to diffuse from a region of high moisture concentration to a region of lower moisture concentration, as time going the moisture gradient tends to decline and equalize. Therefore, In the second stage of falling-rate drying period, the moisture diffusivity usually decreases with decreased moisture content. Although the diffusivities used are usually average values, since the rate of evaporation is quite fast, the resistance is very low, compared to the diffusion rate through the solid in the falling-rate period. To determine the rate limiting mechanism, the dominant rate control step could be either superficial vaporization or internal transport of liquid and it depends on the operating conditions, material properties, pore geometry & structure, and wall composition of the porous medium.

According to the classical theory, the porous medium is treated as continuous the moisture content and temperature are volume-averaged quantities. However, many different drying mechanisms occur at the pore level (Table 2.1).

Table 2.1 The possible mechanisms for drying at pore level [24, 25].

a) Liquid movement under capillary forces
b) Diffusion of liquid caused by concentration gradient
c) Surface diffusion adsorbed at solid interfaces in liquid layers
d) Water vapour diffusion in air-filled pores, caused by differences in partial pressures
e) Water flow under differences in total pressure
f) Flow caused by shrinkage and pressure gradients
g) Flow caused by gravity
h) Flow caused by a vaporization condensation sequence

2.7 **Conclusion**

Drying is the removal of solvent either from aqueous or organic solvent solution. The basic dryers that are used for pharmaceutical drying process are introduced. Different drying periods along with drying kinetics are sketched. The distinctive drying stages with regarding to different mass and heat transfer mechanisms are described. The comprehensive interpretations of drying stages are essential to understanding experimental drying behaviours as well as modelling applications. The basic drying theory included in this chapter: two common modes include contact and convective drying usually used industrial filter dryer equipment are described. The thermophysical and transport properties for packed beds that are essential to drying process are descried.

Chapter 3
Literature review

In this chapter the basic theory concept concerning the thermodynamics and transport phenomena in the drying process are described. The development of agitated filter dryer (AFD) equipment and techniques evolved over last decade and are well appealed to the manufacturer once employed for industry. The widely use of commercial AFD in pharmaceutical engineering receives great concern. Vacuum contact drying theory related to AFD either experimentally or in simulation aspects is extensively researched. The transport and separation process takes place in a single unit involving heat transfer and mass transfer at the same time. It is also considered as one of the most suitable process for drying thermal sensitive and oxygen sensitive pharmaceutical chemicals due to the specific desired characteristics of AFD. Most of vacuum contact drying processes use inert gas e.g. nitrogen as a drying gas purging through the system to help remove the residual vapours from the solid. The combination of vacuum contact drying and convective drying is considered as an efficient method to optimize drying process.

3.1 Experimental work

3.1.1 Solid-solvent binding and sticky issues

When doing modelling work, it all starts with mostly spherical, free-flowing particles in that this will eliminate the particle shape and surface energy influences and allow the researchers to focus on the drying conditions. However, the real system involved in drying is much more complicated and this gives a huge infinite possibilities of the drying consequences due to the existence of stickiness issue and increase the difficulty to understand the drying of the real system. Stickiness is a phenomenon frequently encountered when manufacturing and drying powders [26]. Stickiness can be referred as flow resistance or agglomeration caused by stickiness for particle-particle and particle-walls. Cohesion and adhesion are used to defined two phenomena caused by stickiness.

Cohesion is an internal particle property which is decided internal particle forces. Particles are coming into contact and stick to each other by forming an agglomerate until the shear forces are bigger than cohesive forces then the bonds inside will be broken. Caking, which is formation of lump in a powder bed with a certain temperature and moisture content. Cohesion is very disadvantageous for the drying

process while on the other hand, to effectively make use of the stickiness properties agglomeration, some processes like wet granulation aimed at create free-flowing structure products, are also widely used. Usually, granules in agglomeration are formed consisting of numbers of individual particles.

For the second definition, adhesion, is an interfacial property which measures forces holding the powders to the surface of other materials. Particles will stick to a surface unless the bond between particles and surface is broken in case that applying forces bigger than the adhesive force. So this phenomenon is usually used to describe the powders sticking to the hot surface as the depletion of the water from the wall area the particles tends to form a solid bridge at the inner wall surface especially for contact drying that had a hot surface.

The reasons result in stickiness have been addressed that particles are brought together by collision or stick to each other. Particle size enlargement may begin as soon as liquid is added to an agitated powder mass and continue on well after completion of liquid addition. However, if insufficient liquid is added then the particle size is decided by nucleation conditions. Whether a permanent bond generates or not depends on a wide range of factors including the mechanical properties of the particles and whether liquid binder is at or near the particles surfaces [27]. During agitation process, granules gradually consolidate resulting in increasing liquid pore saturation thus mechanical properties changes. That is to say, consolidation has a prominent effect on granule growth behaviour. The particle size enlargement induces by coalescence or aggregation known as balling based on varied forces according to different binding mechanisms. The binding mechanisms of size enlargement of agglomeration are defined and classified into five mayor groups:

Table 3.1 Binding mechanisms of agglomeration [28, 29]

I. Solid bridges

- Mineral bridges, sintering bridges
- Chemical reaction
- Partial melting
- Hardening binders
    a) crystallization of dissolved substances
    b) deposition of suspended colloidal particles

II. Adhesion and cohesion forces in not freely movable binders

- Highly viscous binders, adhesives
- Adsorption layers (below approximately 3-5nm thickness)

III. Interfacial forces and capillary pressure at freely movable liquid surface

- Liquid bridges
- Capillary forces at the surface of aggregates filled with liquid

IV. Attraction forces between solid particles

- Molecular forces
  a) Van der Waals's forces
  b) Chemical binding forces (valence forces)
- Electrostatic forces
- Magnetic forces

V. Interlocking bonds (form-closed bonds)

Furthermore, none of real particle surfaces are smooth, the degree of the adhesion is determined the particle size or particle size distribution within the same range of adhesive materials.

Adhesion for larger particles like hundreds of micrometres are not likely to form agglomerates unless binders exist for the toughness of surfaces reduced the effective contact distance. However, this phenomenon is distinguished from bulk cake containing large amount of fine powders. In such conditions, porosity known as the relative void volume as well as the coordination numbers known as the sum of all contact points and near points between the adhesive objects [7, 28].

Various complex binding and attraction forces aggregate together like interrelated system and lead to agglomeration even if too large particles exist. The agglomeration tendency will be extremely high in case that wide particle size distribution within the volume cake where fine powders filling in the large voids. Solid bridges can be developed by capillary condensation due to liquid bridges in wet-cake or recrystallization for solid in miscible solvent [28].

Solid particles can form hard agglomerates with solvents trapped inside [21]. This phenomenon exists commonly in AFD. Several methods can be applied to lessen agglomeration. One is to control the agitation mode or agitation speed and period. Another method is to change the proportion of mixture solvent during washing step. Research showed that the degree to agglomeration is concerning with the solubility

of the solvent that needs to be removed. If the solubility of the solvent is very high, the crystals will dissolve in the solvent then agglomeration is easily formed.

During a drying process, very large agglomerates can be produced which are usually unwanted for their low dissolution rate resulting in undermining drug's bioavailability as well as the subsequent processing. Multitude forces produced from different binding mechanisms keep particles in agglomerates from moving apart. For example, in the case of low viscosity solvents like water, capillary forces are dominant while electrostatic forces and van der Waals forces are not important when particle size larger than 10μm [29].

Schæfer et al. found that agglomeration is related to impeller speed and power input [30], apparatus variables[31] and particle size and shape [32]. He found that agglomeration is a function of impeller speed and power input [30] and that higher impeller speed led to larger and more rounded pellets. Furthermore, the agglomerate growth depended on the power input from the agitation. It is desirable to measure the power consumption during the process for the agglomerates growth is reflected by the power consumption. And the power input is primarily controlled by the impeller speed. Agglomeration is related to effects of apparatus variables [31]. Schæfer found that curved impeller blades in the 8-L mixer produced a high power input and a smooth spherical shape rather than plane impeller blades resulted in a lower power input and irregular agglomerates. Agglomerate growth is different in different scale mixers (8-L and 50-L). This difference mainly because differences in movement of the mass, power input and product temperature. Different particle size and shape also effects on agglomeration [32]. Schæfer used two chemicals mannitol and lactose for melt pelletization and found that the plate-like shape particles produced irregular shape agglomerates. When increasing content of regular shape particles in mixture gives rise to smoother and more spherical agglomerates. Either plate-like or needle-like shape of particles resulted in irregular agglomerates, wide size distribution and large amount of loose lumps in the product. An alternative method to reduce the disadvantages is to admixing proper spherical filler such as lactose to modify the final products and produce stronger agglomerates.

The degree of agglomeration is dependent on the liquid viscosity of the agglomerates, liquid saturation [33] and product temperature [34]. The granule size distribution and agglomerate growth mechanisms are affected by the viscosity and by the initial particle size of the binder. For example, if lower viscosity liquid and slightly lower liquid saturation were used, less sticky agglomerates would be produced.

The agglomerate growth was affected by the product temperature because a higher temperature caused a lower binder viscosity cause a higher deformability of the agglomerates and thus promote agglomerate growth by coalescence [34]. A critical viscosity exists for the solvent phase. If viscosity exceeds this value, conspicuous increase for agglomerates and formation of lump will come about. This critical value bear upon with factors influencing growth and/or affecting the strength of the agglomerates. But increasing the product temperature is prone to thermal decomposition. Water of crystallization started to vaporize from the lactose monohydrate when the product temperature exceeded about 80°C and this vaporization gave rise to increase the solid surface area and the intra granular porosity of the agglomerates and hence that the agglomerate growth became delayed. This indicated that adjustable temperature during process may help to control the agglomerate growth.

Another factor influences agglomeration is binder viscosity. A higher binder viscosity resulted in a lower initial agglomerate growth and in a higher subsequent growth rate. The effect of binder viscosity on agglomerate growth was reflected in the power consumption of the impeller motor [35]. A higher binder viscosity will increase the dynamic pendular liquid bridges force and thus the tendency for agglomerate growth by coalescence. At the other hand, a higher viscosity will also decrease the deformability of the agglomerates simultaneously hence that reduce the tendency for agglomerate growth. How the effect of viscosity on agglomerate growth will depend on the balance between these counteracting effects. This balance is affected by process variables such as impeller speed as well as product variables such as initial particle size thus these interact together to influence the agglomerate growth. In addition, higher viscosity give rise to lower surface plasticity of the agglomerates and as a result forming an irregular shape of agglomerates. On contrary, lower binder viscosity results in high deformability of the agglomerates and an elongated pellets due to the shearing forces. The agglomerate strength is concerning with binder viscosity and impeller speed.

3.1.2 Factors involved in drying

3.1.2.1 Crystallization effect

Lee et al. [36] found that when different crystallization routes for acetaminophen could affect the drying process: for moisture within the cake flowed through pores by capillarity and to some extent by surface diffusion. Small pores developed greater capillary forces than large ones, and small pores could consequently pull water out of the large pores and much more difficult to pull out water from small pores. After the constant-rate period, as the water at the surface was depleted, the large pores

within the wet-cake tended to empty first either transferred to the surface or transferred to small pores. Larger pores and narrower particle size distribution implies a faster drying rate for the wet-cake due to the relatively large crystal growth rate and high frequency of aggregation. While if smaller pores forms for the crystal bed, because of the strong adhesion during agglomeration originated from van der Waal attraction force and solute−solvent interactions. If the drying rate is low and the strength of capillary forces at a given point in a small pore is high. It also mentioned that recrystallization occurring across the wetted area during water evaporation will be more likely to promote the unwanted formation of solid bridges among particles. This irreversible lumping phenomenon will adversely affect the particle size distribution as well hindering the drying progress.

During a drying process, agglomeration is most mutual outcome generated from recrystallization. Large agglomerates are usually undesirable due to their low dissolution rate, which may affect a drug's bioavailability. Crystal size enlargement is mostly due to wet crystals coming into contact. Whether or not a collision between two or more crystals results in a permanent bond depends on a wide range of factors, including the mechanical properties and morphology (size and shape) of the crystals [27]. Crystals are held together by liquid bridges due to capillary and viscous forces. These forces keep them from moving apart. In the case of low viscosity solvents, such as water, capillary forces are dominant. Other types of interparticle forces, which can lead to crystal agglomeration, such as electrostatic forces or van der Waals forces, are insignificant in wet systems where particles are larger than 10μm [29]. Agglomeration is a strong function of the crystal properties and morphology.

3.1.2.2 Operating conditions

During a drying process agglomeration can produce very large particles. Large agglomerates are usually undesirable due to their low dissolution rate, which may affect a drug's bioavailability. Crystal size enlargement is mostly due to wet crystals coming into contact. Whether or not a collision between two or more crystals results in a permanent bond depends on a wide range of factors, including the mechanical properties and morphology (size and shape) of the crystals [27]. Crystals are held together by liquid bridges due to capillary and viscous forces. These forces keep them from moving apart. In the case of low viscosity solvents, such as water, capillary forces are dominant. Other types of interparticle forces, which can lead to crystal agglomeration, such as electrostatic forces or van der Waals forces, are insignificant in wet systems where particles are larger than 10μm [29]. Agglomeration is a strong function of the crystal properties and morphology. Schaefer [33, 37] showed that interlocking between plate-like or needle-like crystals produces

agglomerates with low strength. Schaefer [32] also showed that a mixture of needle-like or plate-like crystals and spherical ones generates stronger agglomerates. The strength of the agglomerates is further increased if crystals of irregular shape are used [37]. From the above discussion, it becomes clear that during drying, attrition and agglomeration depend on the drying conditions (temperature, shear rate, vacuum, moisture content) as well as on the mechanical properties and morphology of the solid material (size, shape, hardness). The development of a fundamental understanding of these two phenomena is therefore necessary for any rational design and scale-up of industrial dryers. In this work, an experimental procedure is used to characterize the morphology of l-threonine crystals during agitated drying.

Lekhal et al. [5, 6] studied the influences of different drying conditions including jacket temperature, agitation speed and vacuum level on drying kinetics and particle size distribution as well as morphology of final crystals. They found that attrition dominated the change of particle properties when the drying rate was low and/or the shear rate was high while agglomeration was on the contrary. In order to optimize drying conditions, processes involved alternating periods of stirring and no stirring, or, starting agitation at a certain solvent content. For the former process, the influence of contact drying under intermittent stirring on drying kinetics was investigated by Michaud et al. [38] They found that to reach a higher drying rate with a relatively low stirring period, the optimum duration of periods with stirring was determined to be at least larger than the rest step duration [1] and also there is a critical point by alternation the durations of periods with stirring and without stirring aims at reducing the attrition and agglomeration phenomena. The definition of rest step duration was first raised by Schlünder and his colleagues [39, 40] in 1980s which indicated the time needed to reach a perfect mixing. Schlünder et al. contributed significantly to the understanding of contact drying operations in mechanically agitated powder beds under vacuum as well as inert gas conditions. The heat transfer from walls in mechanically agitated beds is often described by a penetration model.

In the pharmaceutical industry, crystal morphologies can vary widely (e.g., needle-like, plate-like) and their behaviour during drying can differ from that of KCl. In particular, it is of interest to examine if a critical moisture content exists for other materials. In addition, if a critical moisture content is indeed a general feature, it can be expected that its value will be a function of the mechanical properties of the material and the crystal morphology. Moreover, it is not clear if there exists a single critical moisture content that applies to both attrition and agglomeration. In this

investigation, we use image analysis to characterize needle-like l-threonine crystals and to quantify their behaviour during agitated drying.

3.1.2.3 Characterization of powders involved in drying

Powder technology has been developed for characterization of powders for the design of storage and transport systems. Tests and equipment have been and are being developed for measuring the flow properties of powders [26]. However, apart from the problems concerning the location of shear planes and the distribution of stresses in the sample, these tests and equipment are not applicable to wet powders and at elevated temperatures. Considering the complexity and varied properties of wet powders, existing dryer models are dealing mostly with spherical free-flowing particles. One of the discrepancies that observed from the practical conditions of dryer performance is that many materials tend to form agglomerates inside the dryer and to adhere to the walls comparing to the predictions of the models. Drying behaviour and transport through the dryer of these agglomerates is much different from that of single spherical particles. How to incorporate these issues to models are pragmatic for dryer design and even for the transportation and storage for the final product.

After drying process, one of the most obvious consequences is the solvent removal from the solid. However, this is not the only changes involved in drying process. When studying the drying of potassium chloride in an agitated dryer, Lekhal et al. [5] used light microscopy to track the crystal size changes. They found that attrition mainly takes place at low drying rates and/or at high agitation speeds. In wet granulation studies, by colouring the tracer granules, some of the tracer granules broken formed small fragments. It was observed that larger granules larger than 1 mm were more likely to break than the small ones. Attrition is affected by the particle properties including size, shape and hardness as well as the status of drying such as drying time, shear rate, temperature, pressure, moisture content, etc. It has also been that attrition rate is affiliation to the particle shape especially that particles with spherical shape are less prone to attrition or breakage. And the influence of a given material hardness, a crystal with a cubic shape will show more resistance to attrition than particles with a needle-like shape.

It has been researched that if crystals of different physical properties (morphology and hardness) exhibit similar behaviour under the same drying conditions. It can be stated that the physical phenomena of attrition and agglomeration are independent of particle morphology. In an agitated drying process, attrition can lead to the generation of dusty fines. The fines can increase the bulk density of a light product, but they can also be a nuisance and a hazard in the collection of the product (e.g.,

dust explosion) [26]. Also, due to the poor flowability of fines, attrition can seriously impact the subsequent blending stage (when mixed with excipients) and the final tableting process. Crystal size reduction takes place as a result of particles colliding with one another or with the agitator. It can also take place due to stresses induced by temperature or pressure changes inside the drying chamber. Several experimental techniques have been used to identify crystal attrition during drying.

As using paste-like products like a china clay-water suspension as model system for drying study [41], the drying rate was measured by condensing the vapour in the brine-cooled condenser and measuring the condensate mass continuously over the time of the experiment.

The influence of temperature and pressure on drying kinetics of Z-(3-benzoylphenil propionic acid) - ketoprofen, in a vacuum dryer on laboratory scale [42]. Ketoprofen is a pharmaceutical product, produced from xylene. To produce ketoprofen of high purity, the content of xylene has to be removed completely. The melting point of ketoprofen is relatively around 95 °C while the bubbling point of xylene is relatively high 138 °C. so it is necessary to dry ketoprofen at lower temperatures and pressures. To determine the drying curve, a built-in balance was used to monitor the moisture content with time vacuum drying with radiation heat transfer mode.

3.1.2.4 Scale up problems

The first step in design and scale-up is to understand which mechanisms are controlling the process. All the mechanisms are discuss above and once the dominant mechanisms being established, operating practices and control strategies will also be developed.

Usually the lab-scale experiment was commenced to save materials and energy. A method used here is performing a scale-up from a 200 g bench-scale 500 ml reacted vessel drying process to production scale (approximately 1000 kg) [43]. Hoekstra et al. utilising a mathematical model, improved on the model developed by Schlünder et al. [39, 40] in 1980s, has been developed to simulate bench-scale drying processes. This simulation is used to determine the unknown mixing parameters by regression analysis. The authors postulated one additional heat transfer resistance to the existing common four heat resistances: from the external heating medium to the vessel wall, through the vessel wall, from the vessel wall to the first layer of particles and from the first layer of particles to the bulk materials. So the fifth heat transfer resistance, is product dependent but not related to the intensity of agitation. It is considered that this term is related the interaction between the solvent and the solid at higher solvent content during the constant-rate period. A good prediction of drying

time is fulfilled by considering this additional heat transfer coefficient term. However, the physical meaning of it is not fully understood. In their work, this model is used to predict the eight drying processes on production scale. For five out of eight cases the developed method accurately predicted drying behaviour. However, in three remaining cases the model did not apply due to extreme stickiness or aggregation during drying for Schlünder model is originally developed for free flowing particles. For three different types of contact dryer: a tumbler dryer, a filter dryer, and a Loediger dryer were used to validate the model and good results were obtained so the estimation method is presumed be used for most of contact dryers.

Murru et al. [1] investigated the scale-up issues of vacuum contact drying with intermittent agitation both in experimental and modelling approach. The mathematical model of vacuum contact drying is based on differential transient heat and energy balances while to model validation and parameter estimation a small-scale experimental apparatus is used. The authors validated the model using the small scale drying rig and then for the estimation of drying times of six different pharmaceutical compounds at the pilot-plant scale over a range of drying conditions: pressure 15-200 mbar, temperature 45-70 °C and solvents using acetone, water, methanol, n-propanol, and isopropyl acetate. The calculated drying times has a good agreement that the mean difference between predicted and actual drying times for the six compounds was less than 9 %. This is considered as an improvement over current semi-empirical approaches to vacuum contact drying scale-up.

However, the current drying models is still mostly relying on the parameter estimation and the drying mechanisms have difficulty in correlating to solid-solvent types. The parameter estimation still relies on experimental accumulations rather than using a systematic method relevant to solvent properties. Furthermore, the stickiness and agglomeration issue is still a huge challenge either for the real drying experiments or the model validation research.

3.1.3 Material and solvent types

The drying conditions for different types of material and solvent are listed in Table 3.1 showing the varied operating conditions using in the drying history to dry organic and nonorganic materials.

Table 3.2 Comparison of different agitated contact drying experiments and models

Solute/ solvent system	Particle shape	Agitation type	Pressure	Cake preparation	Temperature (°C)	Heating type	Heating surface	Vessel size (volume/ Diameter)	Particle characterize-ation	Type of study	Drying models	References
-	Granulate porous	CA	V/ A	N	50-90	EH	B	240mm	N	E/M	PM	Schlünder and Mollekopf 1984 [40]
Aluminium silicate/ water	Granulate porous	CA	V	N	50-90	EH	B	240mm	N	E/M	PM	Tsotsas and Schlünder 1986 [44]
Aluminium silicate/ isopropanol	Granulate porous	CA	V	N	50-180	EH	B	289mm	N	E/M	PM	Heimann and Schlünder 1988 [45]
Zeolites/ water	spherical	CA	V	N	70-90	EH	B	289mm	N	E/M	PM	Forbert and Heimann 1989 [46]
Alumina beads/ water	Spherical	CA	A	N	70-130	EH	B	240 mm	N	E/M	PM	Gevaudan and Andrieu 1991 [47]
Lactose/ Water	unknown	CA	V	N	10-70	EH	B	NA	N	E/M	LPM	Nastaj 1994

												[48]
Kieselguhr, S-PVC, pharmaceuticals/water, methanol	unknown	CA	V	N	75-80	EH	S	1, 60, 250, 1000L	N	E/M	PM	Thumer 1994 [49]
Ketoprofen/water	unknown	S	V	N	40-60	EH	S	NA	N	E/M	DPM	Skansi et al. 1997 [42]
Disodic tiludronate/Water /acetone	unknown	S	V	N	50-70	EH	B	NA	N	E	NA	Laurent et al. 1999 [50]
Potassium chloride/water	cubic	CA	V	Y	50-70	JV	S/B	100mm	Y	E	NA	Lekhal et al. 2003 [5]
Glass beads/water	Spherical	S	V	N	60	JV	S/B	50mm	N	E/M	DPM	Kohout et al. 2004 [4]
l-threonine/water	Needle-like	CA	V	Y	50-70	JV	S/B	100mm	Y	E	NA	Lekhal et al. 2004 [6]
Sewage sludge/ water	unknown	CA	V	Y	260	JV	S/B	200L	N	E	NA	Dewil et al. 2005 [51]
Glass beads/ water	Spherical	CA	V	N	54-70	JV	S/B	100-150mm	N	E	NA	Kohout et al. 2005 [52]
unknown	unknown	S	V	N	-	JV	S/B	NA	N	M	DPM	Kohout et al. 2006 [3]

Sodium carbonate/ isopropanol	Spherical	S	V	Y	40-52	JV	S/B	100mm	N	E/M	DPM	Kohout and Štěpánek 2007 [53]
Potassium chloride/ water	Cubic	IA	V	N	38-46	JV	S/B	100mm	N	E/M	LPM	Michaud et al. 2007 [54]
Potassium chloride, monohydrate lactose/ water	Cubic	S	V	N	56.3-57.2	JV	S/B	100mm	N	E/M	LPM	Michaud et al. 2008 [2]
Potassium chloride/ ethanol	Cubic	IA	V	N	38.6-46.4	JV	S/B	100mm	N	E/M	LPM	Michaud et al. 2008 [38]
Sewage sludge/ water	unknown	CA	V	N	200	JV	S/B	200L	N	E/M	PM	Deng et al. 2009 [55]
Sewage sludge/ water	unknown	CA	V	N	200	JV	S/B	200L	N	E/M	PM	Yan et al. 2009 [56]
Pharmaceutical compounds /acetone, water, methanol, n-propanol, isopropyl acetate	unknown	S/IA	V	N	50-70	JV	S/B	100mm	N	E/M	PM	Murru et al. 2011 [1]
Glass beads, lactose	Spherical	CA	V	N	45-80	JV	S/B	2L	N	E/M	DEM	Sahni et al.

monohydrate /ethanol												2011[9]
Bis-solvate/ethanol	unknown	CA	V	N	50-70	JV	S/B	600mm	N	E/M	PM	Nere et al. 2012 [57]
Cellobiose octaacetate /methanol	Needle-like	CA/IA	V	Y	60	JV	S/B	150mm	Y	E	NA	Hamilton et al. 2013 [58]
Glass beads, lactose monohydrate /ethanol	Spherical	CA	V	N	45-80	JV	S/B	2 L	Y	E	NA	Sahni et al. 2013 [59]
Glass beads, lactose monohydrate /ethanol	Spherical	CA	V	N	45-80	JV	S/B	2 L	N	E/M	CFM/LBFM	Sahni and Chaudhuri 2013 [60]
L-Threonine	needle-like	CA/IA	A	N	30-50	JV	S/B		Y	E	NA	Ende et al. [61]

Meaning for abbreviations in the table:

Agitation type: No agitation (NA); Continuous agitation (CA); Intermittent agitation (IA); Static (S)

Pressure: Vacuum pressure (V); atmosphere pressure (A)

Cake preparation: Yes (Y); No (N)

Heating type: Jacketed vessel (JV); Electronic heater (EH)

Heating surface: Side (S); Bottom (B)

Dry powder characterization: Yes (Y); No (N)

Model validation: Experimental work (E); Modelling Work (M)

Drying model: lumped-parameter model (LPM); distributed-parameter model (DPM); penetration model (PM); Discrete element model (DEM); Contact force model (CFM); Liquid bridge force model (LBFM)

Volume size: Not applicable (NA)

3.2 Modelling work

As discussed before, drying models can be classified into multi-scale models. This multi-scale is hierarchy model according to different research objects. Parameters obtained from distributed-parameter and particle-scale models can be used for lumped-parameter model. Effective transport properties (permeability, effective thermal conductivity) are depending on the moisture content and solid-phase microstructure which can be acquired by reconstructing length-scale of wet particle assembly based on capillary networks. The transport properties obtained from particle-scale model are then used in distributed-parameter models of heat and mass transfer with phase change in porous media at the continuum length-scale. Then different boundary conditions may be set up or individual drying configurations corresponding to system geometry or the means of heat supply varies among different dryer modes. Finally, at the length scale of the entire process unit, spatially averaged quantities obtained from the lumped-parameter models, such as the average moisture content and temperature or the overall drying rate, can be related to macroscopic design and operating variables (batch size, temperature, pressure, etc.) [3]. Modelling study of vacuum contact drying is sprouting out and keeps growing in the last three decades aims at developing a better understanding of the effects of operating parameters on drying kinetics by saving production and labour costs. Different modelling techniques for contact drying in both static and agitated beds have been employed [11,13-15]. This section is organised as follows: the modelling review of vacuum contact drying for a static and agitated bed; and then review on through-circulation convective drying; finally the transport properties involved in the drying process.

3.2.1 Vacuum contact drying for a static bed

As mentioned before in the experimental research, agitated drying may cause particle breakage and agglomeration and then impact the transport process as well as product property. Hence, agitation must be minimally and effectively utilised combined with the static bed drying. Furthermore, the static bed drying also has the advantage to figure out solvent diffusion and thermal conduction behaviour for vacuum contact

drying, the modelling research on for static bed drying is important and indispensable.

Drying models of different complexity can be divided into two categories: LPM and DPM [1]. Furthermore, DPM comprises continuum and discrete models. In this work, the LPM and continuum DPM are researched extensively. DPM defines that all variables are spatially dependent rather than time dependent only. Hence, the state variables (temperature and moisture distributions) are functions of both time and space, and the model therefore has the form of PDEs [17-19]. However, these models usually need lengthy and complicated calculating procedures. Conversely, in LPMs, the state variables (temperature and solvent content) are only functions of time and the whole system is assumed to have uniform bulk properties. Both DPM and LPM have advantages and disadvantages: DPM helps developing understanding of physical and chemical transformations based on the knowledge of heat transfer and mass transfer theory during the drying process. However, due to lack of effective techniques for real measurement in either temperature or solvent content distribution inside the wet bulk material. LPM can be one way of studying modelling by avoiding these uncertainties and also no lengthy and complicated calculating procedures needed for these models.

The current LPM basically developed from a classic vaporization front theory. This phase change front approach was first developed by Plank [62, 63] for one dimensional semi-infinite medium. Conduction with phase change was characterized by a moving interface, which separated the target body into two phases [63]. Since the physical chemical properties of material changed due to the phase transformation, a discontinuity found in temperature gradient at this moving interface. Hence, there were different temperature function assigned to each phase. A moving front involved in a phase change is governed by a non-linear boundary condition based on energy balance due to discontinuity [64]. Then this approach was applied to contact drying, this moving interface, also a vaporization front, moving from the heating wall towards the centre of the bed. This made the assumption within conductive drying that the drying rate was controlled by the heat transfer rate between the heating wall and the bulk material while the cake was completely dry between the wall and the vaporization front. Different temperature profiles formed at the sides of the vaporization front.

In LPM, uniform spatial variables including temperature and solvent content were presumed. The model equations were mostly in form of ODEs. The steady state DPM with classical vaporization front proposed by Kohout et al. [3] and further developed by Michaud et al. [2] based on mass and heat transfer mechanisms are both used to simulate both the constant and falling rate periods.

In the constant-rate period, the rate mass transfer from the wall to the cake surface was described by Darcy's law. Hence, the mass transfer rate was expressed as:

$$\dot{m}_v = \frac{\kappa_P \rho_v}{\eta_v}\left(\frac{P_{ull} - P_{sat}}{Z}\right) \tag{3-1}$$

Where κ_P is vapour permeability in the packed bed; $P_{ull} - P_{sat}$ is the pressure difference between the ullage space and the saturation temperature at the wall temperature; Z is the cake height.

While the heat flux against the heating wall is given by:

$$\dot{Q} = \alpha_{ws} A\left(T_w - T_{sat}\right) \tag{3-2}$$

In steady state, the heat supplied is all consumed by solvent vaporization, hence:

$$\dot{Q} = \dot{m}_v \Delta H_v \tag{3-3}$$

During this period, the average solvent content decreased from initial conditions to a critical solvent content, the average solvent content changed with time is expressed as:

$$\frac{\mathrm{d}X}{\mathrm{d}t} = -\frac{\dot{m}_v}{m_{\mathrm{ds}}} \tag{3-4}$$

During falling-rate period, a vaporization front developed and moved from the heating wall towards inside the wet-cake, dividing the entire cake into two zones: a drying zone between the heated wall and the vaporization front and a wet zone between the vaporization front and the free surface of the bed. In the wet zone, the solvent content was presumed to be uniform.

The vapour transfer rate then can be expressed by

$$\dot{m}_v = \frac{\kappa_P \rho_v}{\eta_v}\left(\frac{P_{ull} - P_{sat,vf}}{Z - z_{vf}}\right) \tag{3-5}$$

where z_{vf} was the distance from the heating wall to the vaporization front; κ_P represented the vapour bed permeability. $P_{ull} - P_{sat,vf}$ represented the pressure difference between the ullage space and the saturation temperature at the vaporization front. Meanwhile, one more heat resistance developed during this period, the thermal conductive resistance for the dry-zone. Hence, the rate of heat transfer at the vaporization front was given by:

$$\dot{Q} = \frac{T_w - T_{sat,vf}}{1/\alpha_{ws} - z_{vf}/\lambda_{ds}} \qquad 3\text{-}6$$

Michaud et al. further modified this model into a model with varying solvent supply vaporization front by introducing linear variation in the solvent content at the vaporization front which alternatively smoothed a transition point to a certain range rather than the classical constant critical solvent content. This modified version, when applied to the falling rate period, only one parameter required fitting while two extra parameters estimation needed to work out. For the classical vaporization front model, the solvent vapour permeability of the cake as well as the critical solvent content were obtained through parameter estimation using fitting drying curves from experimental results. Nastaj [10] used a similar vaporization front model to simulate the falling rate period during the vacuum contact drying in packed beds of selected biotechnology products. A good agreement between simulations and experiments was observed but only applied to the case with small the bed depth (2mm).

More complicated DPMs were developed by Kohout et al. [3, 4, 53] were frequently used and widely validated. In their research, two DPMs were applied to simulate the drying rates of non-porous glass beads packed bed in a cylindrical vessel: a general dynamic model and a specific steady state model. The second model were simplified by setting the boundary conditions for the moving vaporization front. A quasi-steady-state assumption was made rather than to calculate the heat and mass transfer in the entire domain dynamically. The second model was valid in the case where the liquid phase transfer from inside the wet-cake to the heating wall by capillary flow was faster than the vapour evanished from the wall area during the constant rate period. According to the second model, during the constant-rate period, the vaporization basically occurred in a thin zone near the heating wall, and the drying rates were governed both by heat transfer at the wall as well as by vapour mass transfer through the powder bed. This model

was based on dynamic differential heat and mass transient transfer mechanisms. This model based on a static layer of nonporous solid particles of depth Z within a cylindrical vessel of radius R with heating supplied by a circulating jacket . The vacuum was created from the top with the evacuation port as shown in Figure

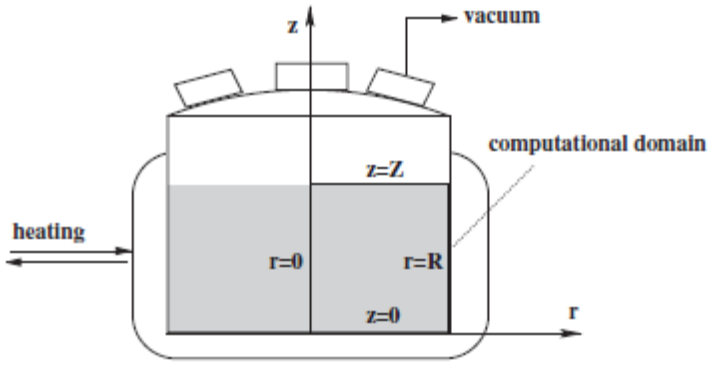

Figure 3.1 Schematic of the vacuum contact dryer and computational domain with boundary conditions in Kohout's work [Kohout 2006]

The mass transfer in the liquid phase including the capillary flow is given by:

$$\rho_l \frac{\partial v_l}{\partial t} = -\rho_l \nabla u_l - \dot{m}_v \qquad 3\text{-}7$$

Likewise, the mass transfer in the gas phase including vapour diffusion is given by:

$$\frac{\partial(\rho_g v_g)}{\partial t} = -\nabla(\rho_g u_g) + \dot{m}_v \qquad 3\text{-}8$$

The energy balance across the powder bed is given by:

$$\langle \rho c_p \rangle \frac{\partial(T)}{\partial t} = -\nabla\left[\left(\rho_l c_{p,l} u_l + \rho_g c_{p,g} u_g\right)T\right] - \Delta H_v \dot{m}_v + \nabla(\lambda_{eff} \nabla T) \qquad 3\text{-}9$$

The fluid velocities of liquid u_l and gas could be calculated from Darcy's Law. As the fluid laminate flow condition confined by this law, the use of it into vapour phase flow needed to be considered. According to Kohout et al, [3], for the relative bigger pore sizes and higher vacuum levels assumed.

With proper parameter investigation and boundary conditions set for the specific cases, the simulation started from a uniform temperature and moisture profile, and the gas phase was saturated at the prevailing temperature. The drying equations was solved by applying second order finite difference discretisation in space. The solvent volume fraction and temperature spatial profiles as function of time were obtained in this case.

The solutions to the resulting set of PDEs describing heat and mass transfer above were carried out. The vaporization front was found to originate from the heat source (heated walls) for large permeability, and from the mass sink (head-space) for low permeability. The calculated drying curves showed well agreement with the experimental results. For further extension of this DPM, Murru et al. [1] applied this model into vacuum contact drying of scale up performance of several real pharmaceutical compounds under different pressure and temperature, and for different solvents.

3.2.2 Vacuum contact drying under stirring condition

As discussed above, the consequences caused by mechanical agitation are much more complicate and difficult to predict, besides, fierce agitation can aggravate particle breakage and form big lumps. Studies on vacuum contact drying of free flowing, mechanically agitated granular beds were extensively described in the research papers of Schlünder et al.

An effective model named, penetration model, used to describe vacuum contact drying of free flowing mechanically agitated particulate material is comprehensively presented in the papers of Schlünder and Mollekopf and Tsotsas and Schlünder. This model was widely used for agitated drying of sewage sludge, crystalline materials, paste-like products, food materials have been reported in these papers. The penetration model postulated that the mixing process was constituted of a series of successive minor static packed bed stages. For the interval between each packed bed drying period, it was linked by the instantaneous and perfect mixing (Figure 3.2). The penetration model, considering that the drying rate of either packed beds or mechanically agitated beds under contact drying was controlled by the contact heat transfer resistance at the surface followed by the heat penetration resistance of the wet bulk [65]. The basic principle of the penetration model was to apply the convenient vaporization front and series resistances approach developed for stirring off periods to a stirred bed drying by substituting the real continuous stirring process by a fictitious sequence of rest steps during which the bed was static and then interrupted by instantaneous adiabatic and perfect mixing of the bed. The scheme of temperature and solvent content profiles through the bed during the fictitious rest steps of the stirring on periods is also presented in Figure 6.4. In this penetration model, if the particulate material is mechanically agitated, a random distribution of dry, partly wet and wet material is expected to form a

random distribution of transport resistances partly in series and partly in parallel.

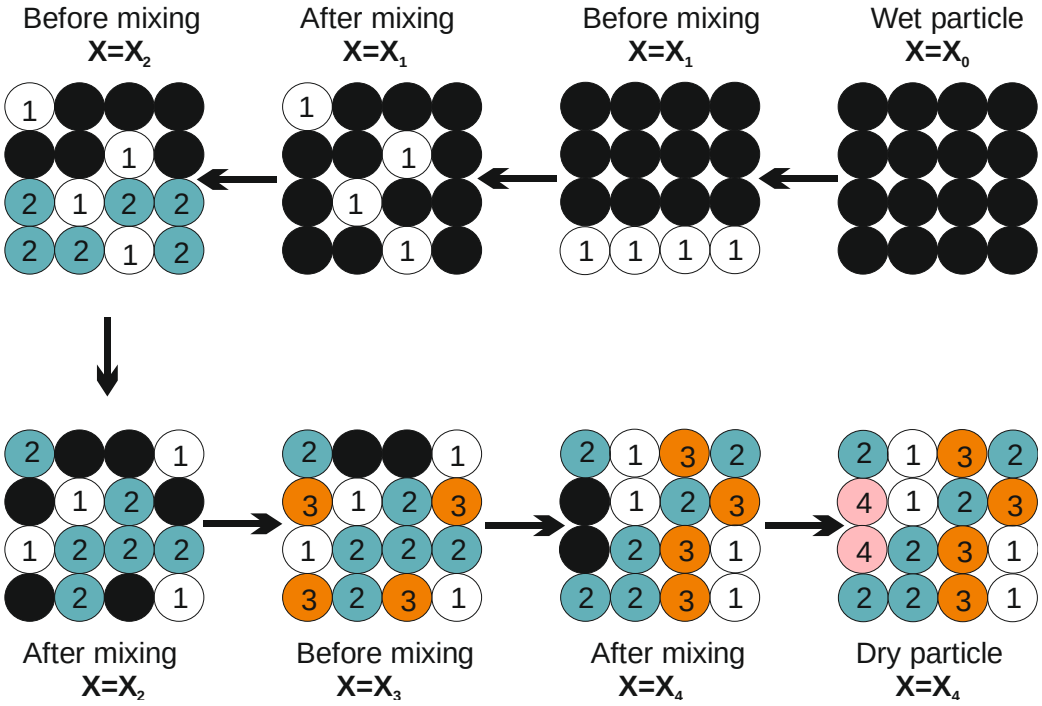

Figure 3.2 Stirred process for wet and dry particles in the penetration model adapted from [66]

In Both resistances can be predicted from model equations with sufficient accuracy. The equations for contact resistance and bulk penetration resistance for packed beds calculated from physical properties are used for many simulations recently. Whereas an empirical parameter, the so-called mixing number needs to be brought in to predict the bulk penetration resistance for mechanically agitated beds aimed at describe the random particle motion. A penetration model, needed to define the actual time for contact drying for a mechanically agitated bulk bed because in stirring bed the actual contact time is unknown. Thereafter, empirical correlations have been established, which connect the actual contact time with the time scale of the mixing device [65].

The penetration resistance is obtained by resolution of Fourier's equation for a moving front. Neumann's solution and Fourier's equation postulated for constant wall temperature supplied between the hot surface and the vaporization front for each static period as well as the position of the vaporization front allowing the penetration resistance to be calculated:

$$\dot{m}_v = \frac{\dot{Q} \cdot \exp\left(-z_{vf}{}^2\right)}{\Delta H_v} \qquad 3\text{-}10$$

For the dry bed, according to Neumann's solution, this reduced instantaneous position of the vaporization front z_{vf} is determined by the relationship:

$$z_{vf} = \frac{Z}{2\sqrt{\frac{\lambda_{ds}}{(\rho c_p)_{ds}} t}} \qquad 3\text{-}11$$

In this approach, the bed of particles is viewed as a continuum with effective bulk properties. The penetration model indicates that the mixing process is constituted of a series of successive minor static packed bed stages. For the interval between each packed bed drying period, it is linked by the instantaneous and perfect mixing. Each individual drying consequent stage is the so called fictitious static bed drying period. According to the definition of the vaporization front in static bed drying, the particles between the vaporization front and the heated surface are treated as completely dry, whereas beyond the front, all the particles are uniformly wet. The stirred bed still follow the vaporization front theory used in the packed bed however this vaporization front was destroyed and disappeared by every instantaneous mixing. The vaporization front of agitated bed mainly differentiated from that of static bed is that every fictitious stage this fictitious vaporization front always moves from the edge of wet-cake towards the centre of the cake. Between static periods, the perfect mixing assumption resets the vaporization front to the heat surface and this cycle is repeated using the new solvent level.

Deng et al. [55] used the penetration model to simulation the sewage sludge agitated contact drying process. It was found that the penetration model has a good agreement. It also showed that the power input (toque) change with three different phases: paste, lumpy and granulate phases. The drying behaviour of very sticky material has been predicted using this penetration model. it shows good agreement between the experimental data and simulation results. For pasty sewage sludge shows complete different properties comparing to free-flowing powder bed for it is more difficult to dry and it has great solid-solvent bonding. Contact drying experiments were carried out in a Nara-type paddle dryer to study the drying kinetics of sewage sludge in the presence of air. Dittler et al. [41] used this model to

simulate the contact drying of pasty material. The penetration model for the vacuum contact drying was used to simulate the sludge drying kinetics in their study. Their research indicates that the sludge drying kinetics of the particulate phase can be satisfactorily described by the model. The contact resistance between the hot surface of dryer and dry bed as well as the penetration resistance of the bulk were calculated and the good agreement obtained.

The heat transfer from walls in mechanically agitated beds is often described by a penetration model. In this approach, the bed of particles is viewed as a continuum with “effective” properties. The penetration model indicates that the mixing process is constituted of a series of successive minor static packed bed stages. For the interval between each packed bed drying period, it is linked by the instantaneous and perfect mixing. Each individual drying consequent stage is the so called fictions static bed drying period. As known, the definition of the vaporization front in static bed drying, the particles between the vaporization front and the heated surface are treated as completely dry, whereas beyond the front, all the particles are uniformly wet. The stirred bed still follow the vaporization front theory used in the packed bed however it is moves faster than packed bed in that the agitation accelerated the mass transfer rate and better use of heat source. For each static period, this fictitious vaporization front moves further to the centred of the cake. Between static periods, the perfect mixing assumption resets the vaporization front to the heat surface and this cycle is repeated using the new solvent level.

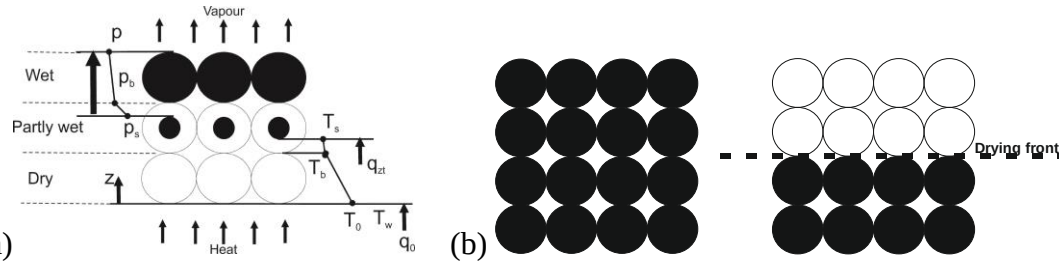

Figure 3.3 (a) the heat and mass transfer resistances in contact drying adapted from [66], (b) the packed static bed drying with a vaporization front

The heat supplied must overcome three heat transfer resistances: the contact resistance at the hot surface, the bulk penetration resistance and the penetration resistance of the particle (Figure 3.3). Vapour removal must overcome two mass transfer resistances: the permeation resistance within the particles and the permeation resistance through the bulk.

Since the first agitated filter dryer was used in 1970 used, it is a great progress for pharmaceutical industry for this instrument combines two unit operations into one single unit. It saves a lot time and manufacture cost. Since the appearance of first AFD instrument, it has been over 40 years. However, it still faces the challenges agitated filter drying process. Not only because the blur criteria between the filtration and drying process but also the scale-up problem from single particle to innumerable particles bed. First of all, the breaking point lies in filtration and drying is so difficult to define. The degree of filtration will affect drying process since these two processes are carried out sequentially. Also the bed properties changed and effective physical and chemical properties have to be used which is completely different from single particle characteristics. In addition, the agitation the flowing particles also cause change in particle morphology and size. To preserve the initial particle size and integrity is so important during manufacturing process.

The time constant may be correlated with the revolution frequency of the stirrer or drum, n, according to the relationship. The length of the fictitious static contact period, t_R, also the time needed for a perfect mixing is related to efficiency of during particle mixing. Contact duration is correlated with the rotational frequency, n, of mixing device:

$$t_R = \frac{\mathrm{N}_{\mathrm{mix}}}{n} \qquad 3\text{-}12$$

where, the mixing number $\mathrm{N}_{\mathrm{mix}}$, is the number of revolutions necessary to achieve a perfect mix and n is the rotational frequency of the mixing device. The mixing number depends on the mixing device and the mechanical properties of the powder bed, and is a function of the Froude number, Fr.

$$\mathrm{N}_{\mathrm{mix}} = C\,\mathrm{Fr}^{x} \qquad 3\text{-}13$$

The definition of function of the Froude number, Fr, is given by:

$$\mathrm{Fr} = \frac{(2\pi n)^2 D}{2g} \qquad 3\text{-}14$$

The fictitious static contact period, t_R, was expressed as follows:

$$t_R = \frac{C}{n}\left[\frac{(2\pi n)^2 D}{2g}\right]^x \qquad 3\text{-}15$$

where D is the diameter of the disc or drum, and g is the gravitational constant. The values of C and x are adjustment constants and evaluated from the experimental data.

The time-averaged heat penetration coefficient for partly wet bed can be defined in his work: the thermal resistance between the vessel wall and the first layer of solid particles is represented by the contact heat transfer coefficient. This parameter can be calculated representing the contact heat resistance from the wall the particles. The methods to calculate contact heat transfer coefficient and bulk penetration heat transfer coefficient were further developed by Schlünder [39]. Heat transfer properties between packed beds, moving beds, stirred beds and immersed surfaces can be predicted from the physical properties of the solids and gases, provided that the actual surface area, the equivalent surface roughness and the actual contact time are known. The actual contact time is identical with the residence time for packed beds and for moving beds as well, provided plug flow exists. For stirred beds the actual contact time may be correlated with the stirrer speed by an empirical function, the so-called mixing number. This mixing number was found to be a mechanical property of the system and depends on the stirrer design as well as on the particle frictional characteristics.

Then a model developed to predict the drying of mechanically agitated bulk material wetted with a binary mixture [45]. Since liquid diffusion effects could not be considered in the penetration model, the drying behaviour of a single particle became important. This modified model had common elements with the previous models in that substituting after each fictitious timeless mixing steps there followed an inoperative period rather than a continuous mechanical mixing process. A validation [46] for the statistic model [45] showed that this model could be also applied to mechanically agitated, coarse, hygroscopic bulk material. Furthermore, this modified approach from

Forbert and Heimann offered the possibility of introducing the drying behaviour of a single particle which is not consider in the model.

According to equations developed from Schlünder and Mollekopf, the dominant resistance for vacuum contact drying are contact resistance and bulk penetration resistance. Agitated contact drying experiments were carried out in a cylindrical lab-scale paddle dryer to study the drying kinetics of sewage sludge under partial vacuum conditions. Yan simulated the experimental results for Agitated Contact Drying of Sewage Sludge under Partial Vacuum Conditions using the penetration model developed by Schlünder to explore the drying mechanisms [56]. Different drying parameters including system pressure, temperature, agitation speed and dryer volume parameter on the drying kinetics were studied both experimentally and theoretically. The results the experimental and simulated drying rates were in acceptable agreement in case that the temperature difference between dryer and sludge was small. Nevertheless, if the temperature discrepancy was large, a crust is likely to form on the surface of the sample. It is this crust causing the drying rate departing markedly from the calculated ones. The fundamental parameter of this model was the fictitious rest step duration t_R, which accounts in a lumped way for particles trajectories induced by the stirrer motion and which had to be estimated for each particular dryer/powder system.

$$\dot{m}_{v,aver} = \frac{1}{t_R}\int_0^{t_R} \dot{m}_v \mathrm{d}t \qquad 3\text{-}16$$

In the frame of the penetration drying model, the transition from one fictitious rest step (i) to the next one (i+1) was assumed to take place by an instantaneous perfect mixing resulting in uniform solvent content over the entire bed. Consequently, the bulk solvent content at the beginning of the next (kþ1) rest step may be calculated by the following relation:

$$\frac{\mathrm{d}X}{\mathrm{d}t} = -\frac{\dot{m}_v}{m_{\mathrm{ds}}} \Rightarrow \frac{X_{i+1} - X_i}{t_R} = -\frac{\dot{m}_{v,i}}{m_{\mathrm{ds}}} \qquad 3\text{-}17$$

Moreover, the fictitious rest step duration was equal to the ratio of a fitting parameter called the mixing number, $\mathrm{N}_{\mathrm{mix}}$, and the stirrer rotation speed, u_{agi}, according to the following equation:

$$t_R = \frac{\mathrm{N}_{\mathrm{mix}}}{u_r} \qquad 3\text{-}18$$

Modified literature models were successfully applied to simulate the evolution of the average solvent content (ethanol) of potassium chloride bed during vacuum contact drying with intermittent stirring. Our new modelling approach incorporated the following modifications: the introduction of a jacketed vessel heat transfer coefficient and an accumulation term for the heating wall temperature; the application of alternate static bed and stirred bed conditions; and modelling of all the three drying phases, namely the constant rate phase, the transition phase, and the falling rate phase. Moreover, several validation experiments were carried out with different operating conditions to identify the values of the unknown model parameter. The optimal stirring conditions were investigated by calculating total drying times for different sequences of stirring and no stirring periods [54].

Modified literature models were successfully applied to simulate the evolution of the average solvent content (ethanol) of potassium chloride bed during vacuum contact drying with intermittent stirring [38]. Our new modelling approach introduced the following modifications: taking account of jacketed vessel wall heat transfer coefficient; taking account of an accumulation term in the heat balance for the heated wall; application of alternate static bed and stirred bed conditions; modelling of all the three drying phases, namely the constant rate phase, the transition phase and the falling rate phase. Several identification and validation experiments were carried out with a reliable laboratory vacuum contact dryer at different operating conditions. A good agreement between the simulated and experimental drying curves was observed and the experimental drying times were also very well predicted by the improved model with six fitting parameters in the most complicate case. The duration of periods with stirring and without stirring were optimized with the aim to obtain high mean drying rates with a low total stirring time in order to reduce the attrition and agglomeration phenomena.

Calculated drying curve based on penetration model was compared with the measured drying rate curves for contact drying of paste-like aqueous suspensions of china clay [41]. Neglecting mass transfer effects and assuming that the particle size distribution of the product remains constant, the penetration model is able to describe both the paste regime and the particulate regime of the drying process over the whole moisture range. Measured and calculated drying rate curves are in good agreement for a variety of drying parameters.

In Murru's work, the author introduced a simulation method which was periodically approximation for intermittent agitation by re-setting the initial conditions. The resetting is achieved by spatial averaging of the temperature profiles:

$$T_{aver} = \frac{\int_V \langle \rho c_P \rangle T \mathrm{d}V}{\int_V \langle \rho c_P \rangle \mathrm{d}V} \qquad 3\text{-}19$$

spatial averaging of the moisture content profiles

$$v_{aver} = \frac{1}{V} \int_V v_l \mathrm{d}V \qquad 3\text{-}20$$

However, this method was only valid for very short agitation time with properly mixed cake at the end of stirring on period as well as homogenous mixed within the entire cake.

3.2.3 Through-circulation convective drying

In order to avoid agglomeration due to agitated drying in a wet state, circulation of convective drying prior to vacuum drying is preferred or replacing water with other proper washing solvent [61]. Meantime, complete static vacuum drying takes very long cycle time. Both of the method can accelerate drying process, however, to find a proper washing liquid needs extensive research work on different organic solvents. Hence perform convective drying in an AFD is great interest in the pharmaceutical industry. In order to analyse convective drying in packed beds, different types of models were developed to predict drying time.

For convective drying of porous media, most of the previous research agreed that the characteristics of drying models included internal and external mechanisms of moisture and heat transfer as well as structural and thermodynamic assumptions [67]. The drying rate during constant rate period was influenced by external conditions including temperature, gas velocity, and gas water activity. The main resistance could related to the heat transfer from the fluid to solid or the mass transfer away from the solid. During the falling rate period, in porous solids the mechanisms to describe the phenomenon including liquid and vapour diffusion, surface diffusion. hydrodynamic or bulk flow, and capillary flow [68].

For deep bed drying, PDE models contains coupled balance equations were used to described water and energy balances of both product and drying air.

In these models, moisture and temperature gradients in product and air were considered [69-74].

Numerical simulation of grain drying in a vertical cylindrical bed was investigated by Mhimid et al [75, 76]. In their work, both convective and contact drying were studied with an imposed hot air flow and a conductive heat flux at the wall. Two mathematical models of heat and mass transfer through granular medium: two temperature model in which the local temperature was not in equilibrium and one temperature model which was in inverse.

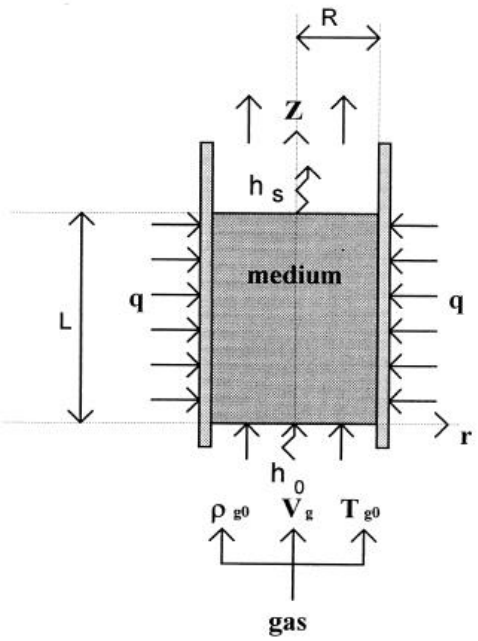

Figure 3.4 Sketch of the fixed bed with convection and conduction heat supply [76]

The governing equations of the heat and mass transfers relying on two dimensions: radial axe r, and axial axe z.

Vapour mass conservation equation comprised vapour diffusion in two dimensions due to heat convection from circulation hot air as well as conduction from the heated wall area. The mass transfer equation was expressed as follows:

$$\varepsilon \frac{\partial \rho_v}{\partial t} + \frac{\partial \left(\rho_v V_g\right)}{\partial z} = \dot{m}_v + \frac{1}{r}\frac{\partial}{\partial r}\left[r \rho_g \kappa \frac{\partial}{\partial r}\left(\frac{\rho_v}{\rho_g}\right)\right] \qquad 3\text{-}12$$

where ε and κ were the bed porosity and effective diffusivity respectively.

While the air flowing from the bottom to the top, taking vapour away from the system:

$$\varepsilon \frac{\partial \rho_a}{\partial t} + \frac{\partial \left(\rho_a V_g\right)}{\partial z} = 0 \qquad 3\text{-}21$$

The energy balance within the bed was given by:

$$\begin{aligned} &\varepsilon \rho_g c_{p,g} \frac{\partial \left(T_g\right)}{\partial t} + \rho_g c_{p,g} V_g \frac{\partial \left(T_g\right)}{\partial z} \\ &= \alpha_{gs} A_V \left(T_s - T_g\right) + \dot{m} c_{p,v} \left(T_s - T_g\right) + \frac{1}{r} \frac{\partial}{\partial r} \left[r \varepsilon \lambda_g \frac{\partial \left(T_g\right)}{\partial r} \right] \end{aligned} \qquad 3\text{-}22$$

The energy balance within the bed was given by:

$$\begin{aligned} &\left(1-\varepsilon\right) \rho_s \left(c_{p,s} + X c_{p,l}\right) \frac{\partial \left(T_s\right)}{\partial t} \\ &= \alpha_{gs} A_V \left(T_g - T_s\right) - \dot{m} \Delta H_v + \frac{\partial}{\partial z} \left[\left(1-\varepsilon\right) \lambda_g \frac{\partial \left(T_s\right)}{\partial z} \right] + \frac{1}{r} \frac{\partial}{\partial r} \left[\left(1-\varepsilon\right) r \lambda_g \frac{\partial \left(T_s\right)}{\partial r} \right] \end{aligned} \qquad 3\text{-}23$$

where α_{gs} and A_V are the convective heat transfer coefficient from gas to solid phase and the interfacial area of the solid particles respectively.

The convective heat transfer coefficient used here is given by

$$\alpha_{gs} = \frac{\lambda_g}{d_p} \left(2 + 1.8 \, \mathrm{Pr}^{0.33} \, \mathrm{Re}^{0.5}\right) \qquad 3\text{-}24$$

The drying rate equation was obtained from experiments. A finite volume method was used to solve the mathematical equations. The numerical simulation gives the time and space evolution of temperature when the lateral area of the cylinder is heated by a constant density flux and a constant temperature. Four governing equations for gas and solid phase were developed for heat and mass transfer separately.

A analytical method for simultaneous heat and mass transfer of convective drying process for carrot sliced in slab form was described [77]. The proposed model considers the evaporative heat transfer at the surface of product. The one dimensional non-steady mass transfer by moisture diffusion within a homogenous material was given by:

$$\frac{\partial X}{\partial t} = \kappa \frac{\partial^2 X}{\partial z^2} \qquad 3\text{-}25$$

where κ was the diffusivity.

The energy balance within the materials was expressed as:

$$\rho_s D_c c_p \frac{\partial T_s}{\partial t} = \alpha_{gs}\left(T_{ull} - T_c\right) + \alpha_m \Delta H_v \left(P_{ull} - P_c\right) \qquad 3\text{-}26$$

This equation indicated that convection heat transported from air to the material being dried were used for partly elevation the temperature of materials and partly for solvent evaporation.

The value of convective heat transfer coefficient depends on the interstitial air flow pattern as well as the conductivity of flow gas [78]. The calculation of convective heat transfer coefficient in packed beds was investigated since 1970s, the experimental data were with the empirical or semi-empirical expressions of convective heat transfer coefficient.

The data presented in Figure 6 were fitted favourably with the equation with Nusselt number:

$$\mathrm{Nu} = \left(0.5\,\mathrm{Re}^{\frac{1}{2}} + 0.2\,\mathrm{Re}^{\frac{2}{3}}\right)\mathrm{Pr}^{\frac{1}{3}} \qquad 3\text{-}27$$

In Equation 3.12, Nusselt numbers depended on the Reynolds number and Prandtl Number. The data in Figure 7 covered an enormous range of packed beds on the extensive study by Taecker and Hougen [79]. The materials used in their research comprising three sizes of Raschig Rings, one size Partition Ring, and two sizes of Berl Saddles. Their range of particle geometries is certainly extensive and yet the results can be correlated with a single equation provided one uses the appropriate Nusselt number and Reynolds number. This is shown more clearly in Figure 7 where all the data obtained by Taecker and Hougen are plotted along with all the data of Glaser and Thodos for spheres and cylinders indicated that equation 3.12 relative accurate calculation of convective heat transfer coefficient.

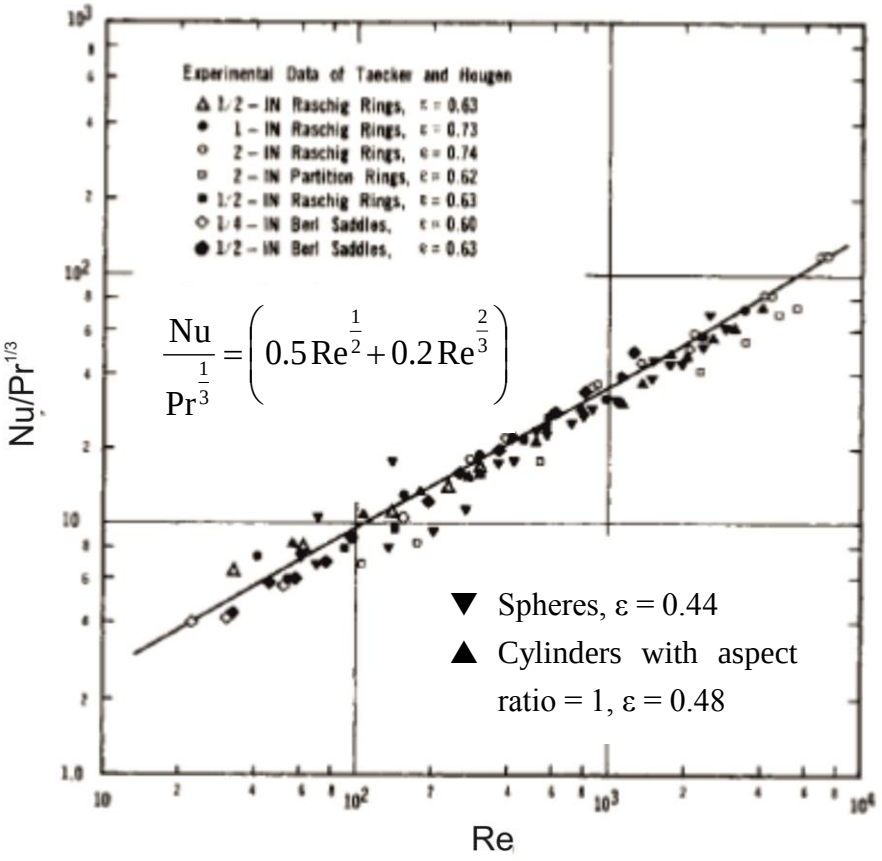

Figure 3.5 Heat transfer to gases flowing in packed beds

Another expression of heat transfer coefficient using semi-empirical correlation depending on Nusselt number relating to Reynolds and Prandtl numbers was given by [80, 81]:

$$Nu = 0.664\,Re^{\frac{1}{2}}\,Pr^{\frac{1}{3}} \qquad 3\text{-}28$$

The use of equation for further calculation of α_{gs} in packed beds can be found in the drying of food and sewage sludge materials [74, 82].

3.2.4 Transport phenomena and boundary conditions

The transport phenomena at the boundary of the material appears to take place in a thin film inside the porous medium at the interface between the product being dried and the vacuum chamber. This film, called Transition Layer, is defined as the location where the pressure drop from the saturated pressure to the pressure of the vacuum chamber occurs. This pressure drop induces a vapour flux at the interface between the porous medium and the vacuum chamber, and determines the heat and mass transfer at the boundary of the material [83].

During the drying process, the thickness of the transition Layer varies and regulates the intensity of the mass flux. Thus, at the beginning of the drying process, the Transition Layer is small and the mass flux is limited by the power of the vacuum pump. Thereafter, the Transition Layer thickness increases and the mass flux is regulated by the physical properties of the material.

The heat transfer resistance between the hot surface of the vessel wall and the first layer of the powder bed is characterized by a contact resistance. While the contact heat transfer coefficient, α_{ws}, including three aspects: heat transfer from the vessel wall to single particle, from the vessel wall to the free flowing gas as well as the heat transfer from radiation. All the three aspects can be calculated from the equation developed by Schlünder et al. [39]:

$$\alpha_{ws} = \phi_A \alpha_{wp} + (1-\phi_A)\frac{2\lambda_g / d_p}{\sqrt{2} + (2l + 2\delta)/d_p} + \alpha_{rad} \qquad 3\text{-}29$$

where d_p is solid particle diameter, ϕ_A is a plate surface coverage factor and is of the order of 0.80, δ is the roughness of the particle surface, l is the free path of the gas molecules, λ_g is the gas thermal conductivity, α_{wp} is the heat transfer coefficient for a single particle, α_{rad} is the radiation heat transfer coefficient. According to the foregoing assumption made, the radiation heat is ignored so in this case $\alpha_{rad} = 0$.

Hence, α_{wp}, the heat transfer coefficient for a single particle, is given by [39]

$$\alpha_{wp} = \frac{4\lambda_g}{d_p}\left[\left(1 + \frac{2l + 2\delta}{d_p}\right)\ln\left(1 + \frac{d_p}{2l + 2\delta}\right) - 1\right] \qquad 3\text{-}30$$

The modified mean free path of the gas molecules, l, is expressed by [39]

$$l = 2\frac{2-\gamma}{\gamma}\sqrt{\frac{2\pi R T_{aver}}{M}}\frac{\lambda_g}{p(2c_{p,g} - R/M)} \qquad 3\text{-}31$$

The solvent constant can be obtained by integrating the following equations:

$$\frac{\mathrm{d}X}{\mathrm{d}t} = -\frac{\alpha_{ws} A(T_{wi} - T_B)}{m_{ds}\Delta \mathrm{H_v}} \qquad 3\text{-}32$$

The transition layer is identified as the location where the pressure dropped from the saturated pressure to the vacuum pressure with regards to the

vacuum chamber. The vaporization front is delimited the area where the free liquid is not in a discontinuous state.

The transition layer as one of main variables of the drying process pertinent to the transition layer velocity. The driving force of intensity of gas flux at the interface between the porous media and vacuum chamber is the variations of drying layer thickness. Mathematical models are powerful tools to help engineers understand drying processes. Predictions are made from the appropriate sets of differential and algebraic equations, together with physical properties of the drying medium and drying material [10].

Waananen concludes that how to develop a fundamental drying model and tasks that must be accomplished before developing a model [68]. First is to identify the controlling resistances that is the dominate resistance coming from energy transfer or mass transfer and resistance from external or internal. Second is once the controlling resistance identified, correspondingly mechanisms should be defined. mechanisms if internal mass transfer resistance controls the drying process, then moisture movement mechanisms either diffusion, capillary or bulk flow should be identified. Once the mechanisms are identified, structural and thermodynamic assumptions have to well established where boundary conditions are closely connected to the mathematical description of the drying process.

Michaud et al. [2] studied the vacuum contact drying of crystalline powders with intermittent stirring and packed beds. a new model is developed based on the classical “vaporisation front” model. In the classical vaporization front model, In the study of Martin’s work, he found that for very small particles, the constant-rate may disappear. The transition layer is identified as the location where the pressure dropped from the saturated pressure to the vacuum pressure with regards to the vacuum chamber. The vaporization front is delimited the area where the free liquid is not in a discontinuous state. The transition layer as one of main variables of the drying process pertinent to the transition layer velocity. The driving force of intensity of gas flux at the interface between the porous media and vacuum chamber is the variations of drying layer thickness.

3.3 Conclusion

This section draws upon the above perspectives and presents an integrated experimental and modelling study for the recent drying pharmaceutical

materials in filter drying equipment. The mechanisms that are related to agglomerations and solid-solvent interactions are described extensively.

The unit operations of the drying stages associated with particle properties were also described. By reviewing the key features for the experimental and modelling part of drying process, this will facilitate the following work presented in this thesis.

That is the reason the combined drying will to some extent weaken the adhesion effect. That is why we suggest convective drying at the beginning as the water content reduced to a certain amount and then the contact drying will be used.

Chapter 4
Design modification and commissioning of a lab-scale AFD

4.1 Introduction

The filter dryer equipment is a versatile machine which can perform filtration/drying at the same time in a single unit. This combined unit alternatively gets rid of the step that transferring materials from separate filter to dryer instrument which is laboursaving as well as timesaving. In this chapter, targeting the fulfilment of the investigation the performance of drying performance of a filter and dryer, a lab-scale 5 L AFD was instrumented based on an existing vessel, which built up originally for investigation of filtration behaviour [amber Geddes]. This lab-scale AFD was In order to fully online monitor solvent content, temperature, power input, pressure during drying process, with an extensive research on process analytical techniques, the relevant and optimism instrument were selected and installed considering the scope of the geometric, operational, parameter factors. After extensive rig testing and calibration, the data collected from the finished rig were used for validation of drying models developed in chapter 6.

4.2 Design principle of a lab-scale AFD

4.2.1 Industrial prospective

The schematic of design for pilot plant scale AFD is shown in Figure 4.1. This unit is widely applied in industry, including the manufacturing process of various chemicals, pesticides, insecticides, dyes, food products and pharmaceuticals etc. This equipment can carry out its operation in an airless environment for sensitive materials, and can be adapted for producing sterile and poisonous products. The material of filter plate can be made of sintered plate or filter cloth (from 5μm to 50μm). The agitator shaft can be solid which is used in normal temperature status or hollow shaft with rotary joint which is used in heating status. The blade type includes two leafs or three leafs with the drawknife or without the drawknife. It can also heat the material if needed. The rotation, up and down of the agitator are driven by Hydraulic system. Clockwise and anticlockwise rotation of blender aims at performing

the smoothing and plough during the drying process. The up and down of the bottom of the impeller will be adjustable with washing and drying process. The operation of the filtration process is similar to a leaf filter. The driving force for filtration can either generated from pressure upstream using the air/N_2 pressure inlet or vacuum downstream beneath the filter plate. The slurry as well as wash inlet can either take the slurry ready to pour or from upstream crystallizer. The washing liquid also uses the same port for washing the organic solvent after filtration step. Finally, all the product can be removed from the discharge port as drying finished.

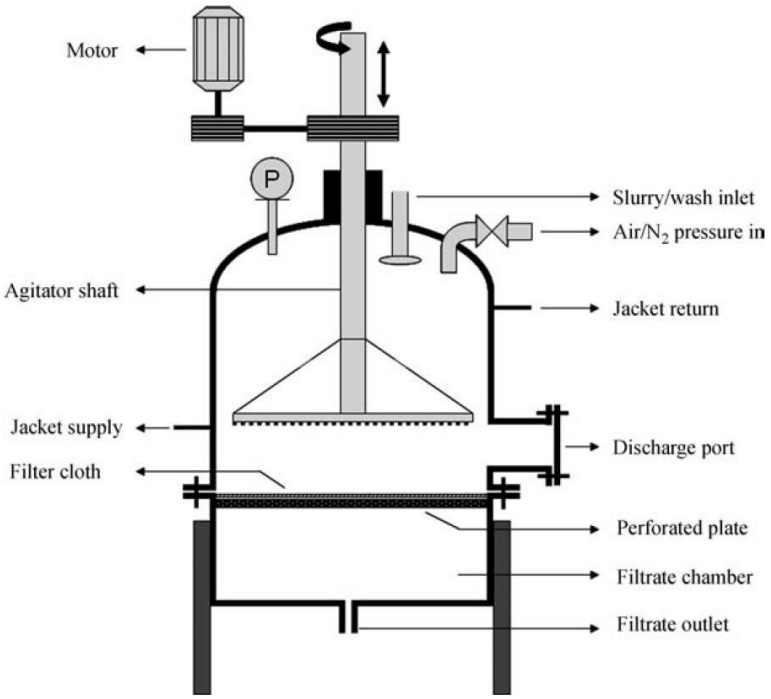

Figure 4.1 Cross-sectional representation of industrial filter dryer [21]

4.2.2 Description of the existing bench-scale AFD (Amber Geddes's work)

A 5 L bench-scale AFD rig was built in a previous project [84]. In that project, the perform experiments under different operating conditions. The design of the vacuum contact dryer instrumentation in the laboratory is shown in Figure 4.2. The main part of the laboratory dryer was constituted by a 5-L jacketed cylindrical vessel. The dryer basis is adopted non-contaminating construction material, stainless steel. The dryer is heated by electrical heating band insulated by silicone rubber (maximum power: 158 Watts). The jacket temperature is controlled by tuning the amount of power supplied to

evenly distributed electric resistance wires wrapped tightly onto the surface of the cylindrical vessel. The silicone rubber laminate allows a high temperature tolerance up to 200 ºC and good electrical insulating properties. To avoid thermal decomposition vacuum condition can be achieved by connecting the vacuum pump to the vacuum port. It should be noted that the vacuum ports are at the top in the ullage region of the vessel. The purpose of using this chemistry-resistant vacuum control box is to stabilize vacuum level as well as to ventilate the system. The vessel was 169mm wide and 300mm high. The bottom plate of this vessel was made of stainless steel and supported a temperature probe in contact with the first layer of the powder bed at the vessel wall. The vessel side wall contains a customised glass window enabling the process to be observed. Two absolute pressure transducers were fixed to the vessel walls which take the measurement above and under the cake online. Four flexible thermocouples can bend anywhere in contact with the bulk of the powder bed and take the measurement of temperature distribution during the drying process. All these variables are recorded online through LabVIEW system. The different types of analogue input and output parameters are show in Figure 4.2.

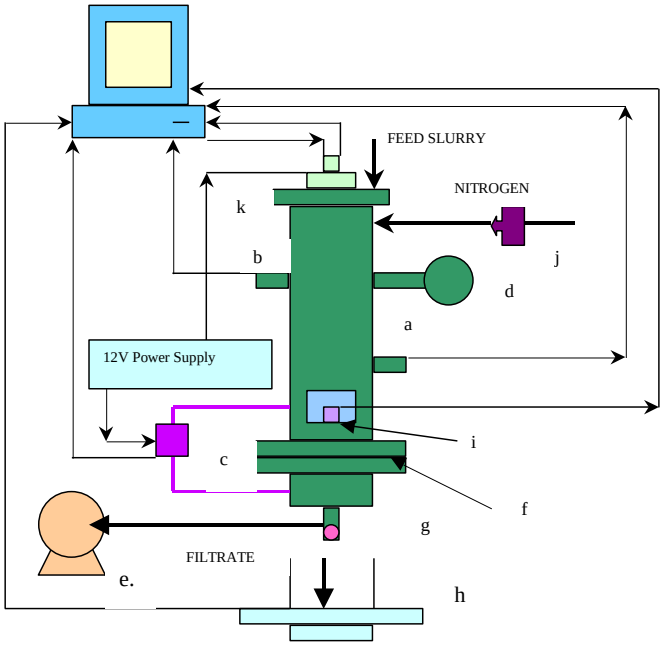

Figure 4.2 Schematic diagram of automated pressure filter-dryer rig set-up to determine the characteristics of cakes produced from the filtration of mother liquor slurries a.) temperature, b.) pressure transducer, c.) differential pressure transducer d.) pressure relief valve, e.) vacuum pump with catch-pot f.) stainless steel wire mesh g.) 3-way valve h.) electronic balance i.) moisture content (arbitrary value) j.) flow controller and k.) motor and stirrer developed by Geddes [84]

As it may apply pressure or vacuum inside this unit, it has to be a closed system. To keep this in mind, a few joint parts have to make sure to be airtight. A feedport with glass window produced by West Technology System Ltd. (Bristol, UK) allows the top view of the vessel. This viewport replaces a blank off cap and uses a standard NW centring assembly and clamp for sealing. The diameter of the viewport is 40mm. A side window is made of curved transparent Perspex to observe the phenomena inside the vessel. It is sealed by binding agent between the perplex window and steel vessel with length at 11cm and height at 11cm.

(a)  (b) 

Figure 4.3 Photograph of (a) the vacuum pump and two flask catchpots (b) the 5 L bench-scale filter-dryer developed by Geddes [84]

4.2.3 Modification base on the existing bench-scale AFD

The lab-scale AFD presented here is a miniature of pilot plant AFD with the similar design of geometric parameters.

As the vessel is inherited from previous study introduced in session 4.2.2, the drying study starts from the instrumentation of this existing lab-scale AFD by applying a number of key modifications. The basic dimensions are shown in Figure 4.8.

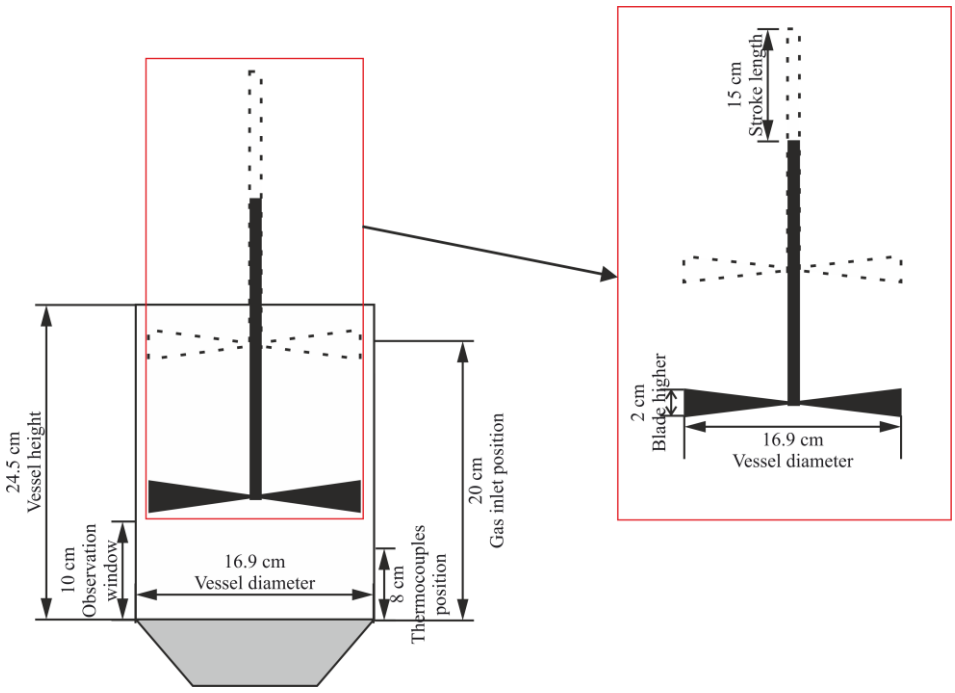

Figure 4.4 Dimensions of lab-scale AFD

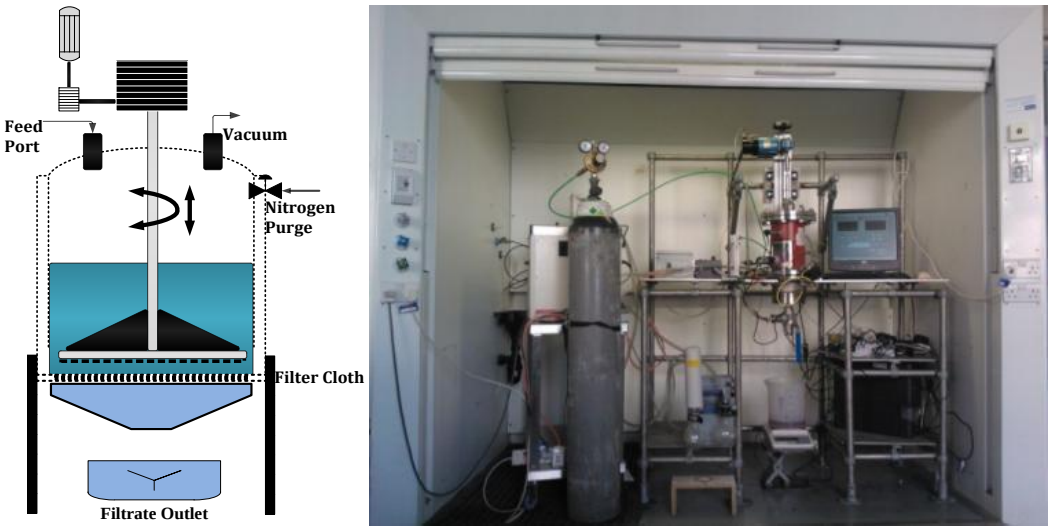

Figure 4.5 The lab-scale AFD in a fume cupboard

4.2.3.1 Humidity sensor

To monitor the solvent content during the through-circulation convective drying process, the humidity sensor is built into the jacketed vessel from setup for the Lab-scale AFD is shown in Figure 4.8.

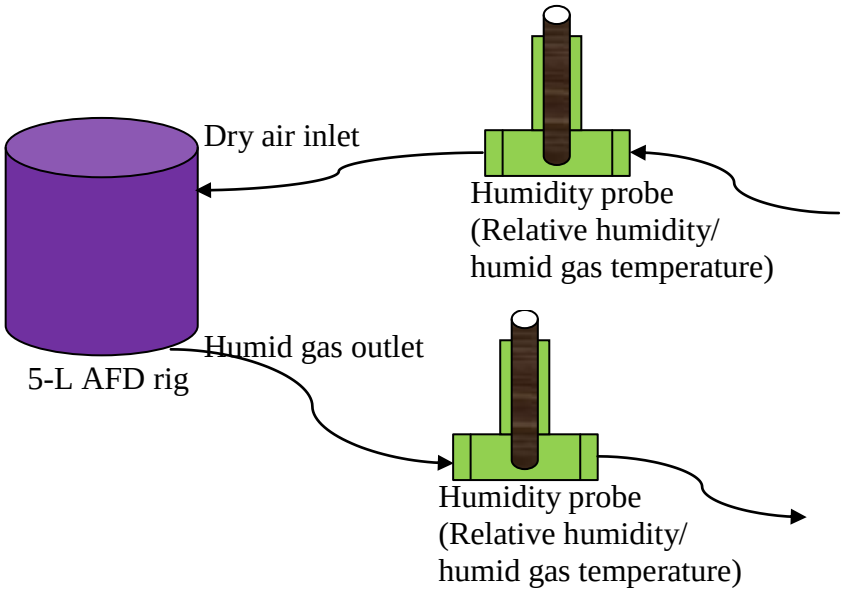

Figure 4.6 Simple schematic setup for the Lab-scale AFD

The combined PCMini52 digital relative humidity and temperature probe is manufactured by Michell Instruments Ltd. (Cambridgeshire, UK). The mini probe provides two linear analogue outputs for temperature and relative humidity; furthermore, this mini probe allows to monitor temperature and humidity changes in the drying line. After extensive field tests the probe was selected not only due to its resistance to contamination as well as its small size. With the miniature size, the simplicity and robustness the PC Mini52 humidity and temperature sensors can be easily installed in the target field by connecting to the agitated vessel used a T-type tube design. The T-type tube is shown in Figure 4.8, the humidity probes installed on both the inlet and outlet positions of the agitated filter dryer to allow the humidity of the gas directly passing through the AFD to be measured. The tips of the probes were both placed at the centre of the tube allowing the humid gas completely cover the sensing element of the probe. .

Due to the specification of the sensor a specific T-type tube with an adequate seal at the top adjacent to the lead has to be made. A combination of PTFE sealing washers and silicone sealant as well as “O” rings were utilised to make the position the sensing part accurately sit in the centre of the tube. With regard to 2 parallel threads fitted into the body make it more easily utilised by using standard enots fittings to the commonly used air supply tubes. The diagram of basic design of T-type tube parts were shown in Figure 4.9. As shown in the Figure, the long cylindrical shape of humidity probe is difficult to obtain the accurate experimental data unless an enclosed

work environment was created for the sensing tips. Hence, T-type tube parts were designed to allow the gas that passing through AFD to be measured. The photo of final T-type tube parts was shown in Figure 4.10 which shown a satisfactory data recording system.

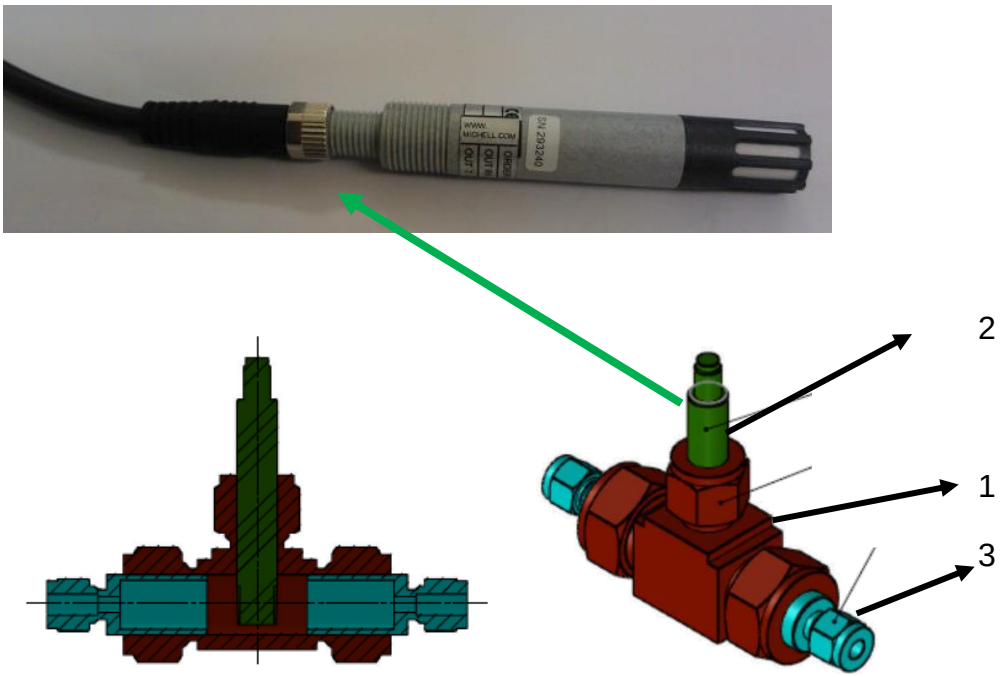

Figure 4.7 Schematic diagram of T-type tube parts

The basic dimensions used to manufacture the T-type tube parts were shown in Table 4.1.

Table 4.1 T-type tube parts for humidity sensor

Item No.	Part
1	12mm x 18mm T-type tube
2	PCMini52 Humidity/temperature sensor
3	1/4 X 3/4 enots Adaptor

Figure 4.8 The photo of T-type tube fitted with the humidity sensor

4.2.3.2 Temperature control

A silica band adjacent to the outer wall of the vessel controlled by electricity can be heated through varying the heating power inputs. The heater on/off can be easily controlled by the control panel. The resistance of the band is measured so the heat flux of the heating band is also known. Thermocouples: 4-wire thermocouples can measure temperature distribution along radial and axial direction by easily put the thermocouples to certain positions. However, temperature data measured from thermocouples can only be collected under circumstances that without agitation. Once applied agitation, the thermocouples should have been interfered by stirring impeller. The thermocouples will be tuned to above the agitator in order to get temperature profile during agitation.

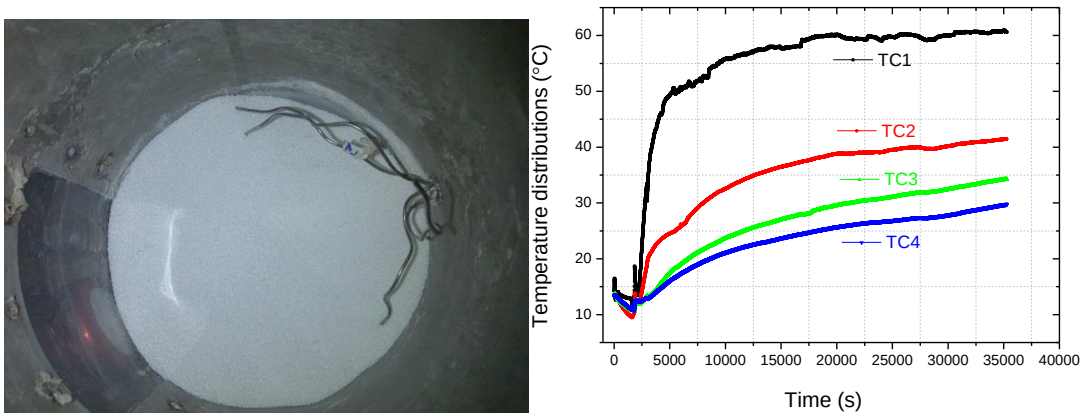

Figure 4.9 Photo of flexible thermocouples and example of temperature profile at different locations within the wet-cake

In order to test the reproducibility of thermocouples used in this experiment, the temperature profile of heating up a dry-cake was plotted in Figure 4.10. It can be seen that the red, green and blue lines representing different locations within the dry-cake are almost similar to each other (within ± 0.5°C)

when the system temperature become stabilized. The temperature of thermocouples are very similar during the long time range, however, there is 12 ºC difference between the wall and the entire cake. This could be result from the heat loss by free convection and radiation (see section 6.2.1.4).

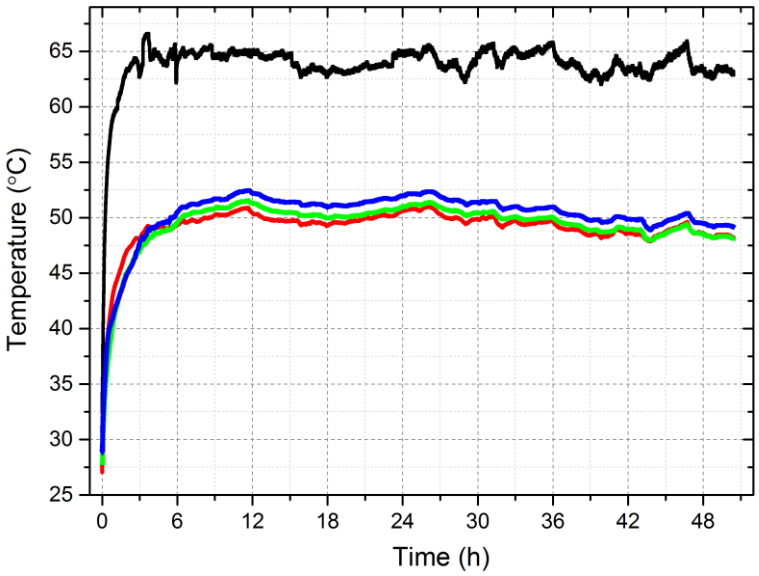

Figure 4.10 The temperature distribution at different locations: wall area (——), first layer of particles (——), middle of radius (——), centre of the wet-cake (——) for the dry-cake at heat power 128 Watts

4.2.3.3 Vacuum condenser

A Vacuubrand MZ 2C + AK + EK 180W vacuum pump, with two round bottom flask catchpots, figure 3.3, was chosen as it allowed a maximum pumping speed of 1.7/2.0 m^3hr^{-1} with an absolute vacuum of 10 mbar (25bar with gas ballast attached).

The first catchpot prevents drainage of contaminated condensate back into the pump. The maximum absolute outlet pressure was 2 bar with the maximum differential pressure between the inlet and outlet being 1.1 bar. The motor had protection in the form of a cut-out device and an exhaust waste vapour condenser with relief valve. The motor was covered with thermal insulation to avoid condensation from the humid gas. The second round bottom flask was used at the inlet port, to act as a separator.

In order to avoid throttling losses, the length of the connecting pipe was kept as short as possible and the diameter as large as the 3-way valve on the base of the rig, connecting the filter to the pump. Using a flexible rather than rigid pipeline reduced the effects of vibration. The 3-way valve also allowed isolation of the pump from the vacuum system as the pump needed to warm

up before pumping liquid in significant amounts so as to avoid damage to the diaphragm and valves.

4.2.3.4 Nitrogen/air flow & pressure transducer

The inlet nitrogen or dry air flow into the vessel is controlled by a regular flowmeter. The maximum flow of the flowmeter is 12 L/min is falling in the scope as can be seen in Table 4.2

Table 4.2 The gas flows from scale-down calculation

Parameter	Gas inlet flow
Industry	500 - 1000 L/min/m^2
Laboratory	11.2 - 22.4 L/min

Two absolute pressure transducers from Gems Sensors (Basingstoke, UK) were installed to at the top and bottom of the vessel separately to detect any pressure vibration above and beneath the wet-cake (Figure 4.12). This pressure transducer can be used at wet environment such as measurements of liquid and gas. This capacitance sensor has fast-response characteristics and signal conditioned electronic circuitry provided a highly accurate, linear analogue output proportional to pressure.

Figure 4.11 One of the pressure transducers installed onto the top of the vessel wall

The actual pressure inside the vessel is measured by the pressure transducers that any change of the pressure can be detected which helps explain and further understand the drying behaviour. Figure 4.6 shows an example during the filtration and drying process. the high pressure at the beginning indicates that the sample starts with filtration and step into vacuum contact drying as the pressure level goes down. However, the

pressure level during drying is not maintaining constant and there is sudden changes in the period. Combining with the temperature data they can fairly explain the drying behaviour.

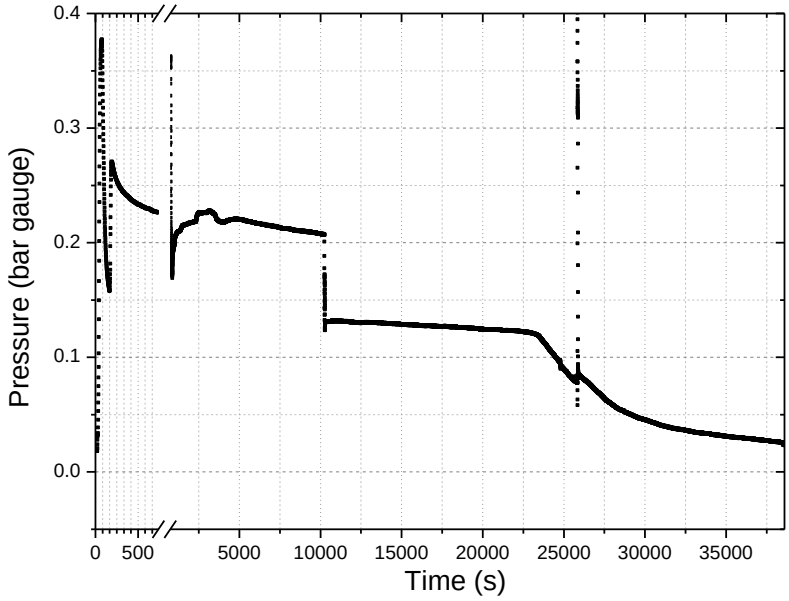

Figure 4.12 Example headspace pressure variation with time measured by pressure transducer

4.2.3.5 Movable agitator with reversing motor

The powder was mechanically agitated by a four-blade stirrer driven by an electric motor. A shunt wound dc sd11c gear box from Parvalux Electric Motors Ltd. (Bournemouth, UK) is used in order to performing smoothing the surface of the wet-cake and ploughing during drying the wet-cake. The stirrer rotational speed could be set in the range of 0 to 100 rpm. The solvent vapour flowing out the vessel was condensed by means of a vacuum condenser cooled with Haake chiller running by a certain ratio of mixed solvent-ethylene glycol and water. The temperature of circulating coolant can be set down to -10 ºC which is cold enough to condense the vapour. The total mass of the solvent condensate, the inside wall temperature, and radial distribution of temperatures inside the bulk material, the pressure above and under the wet-cake were continuously recorded throughout the duration of the contact drying experiments by every second. A 4 cm glass window feedport was fixed to the top of the lid allowing feeding the slurry and viewing from the top. A side window made of curved transparent Perspex allows observe visualised particle aggregation phenomena occurred during agitated drying process. Due to the stirrer acting as different roles in the serration processes, the motor is mounted to a linear sliding

system to smooth the surface and stir deep inside the cake. The photo of lab-scale AFD is shown in Figure 4.15.

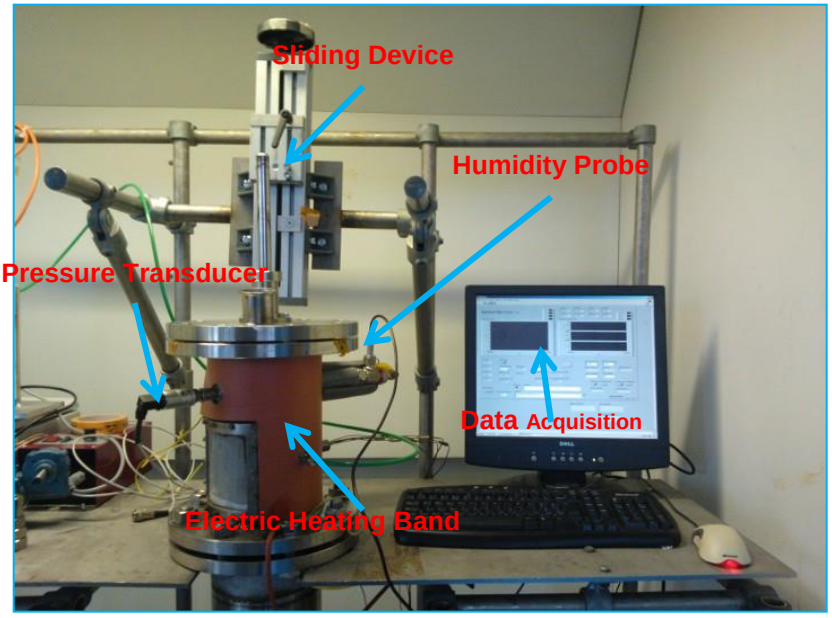

Figure 4.13 Photograph of 5 L lab-scale agitated filter dryer

Here shows examples of temperature distributions and torque recorded against time during drying period. Figure 4.17 shows the temperature distribution during agitated drying process at stirring speed 20 rpm. The wet-cake forms agglomerated lumps from the beginning the drying process. The temperature difference at three locations is big at the initial drying stage due to agitation at the higher solvent content. As the moisture removed from evaporation, the big lumps gradually break into small aggregates which can be seen from Figure 4.17 that the temperature has a critical change at around t=3.5h. This evidence also can be seen from Figure 4.17 that the torque increases first as more and more agglomerates formed at the beginning and reach to the a peak at around t-3.5h (which is similar to phenomenon observed from the temperature distribution) then followed by a critical change. The torque then reduced gradually as the wet-cake become drier. The solvent content is not enough to bind the all the particles together. The particles at this stage are rather like free flowing particles.

A current meter also installed to measure torque of impeller. Actually the torque was transformed by power input to the unit via writing a program relating the relation between the power and torque.

$$\text{Power (kw)} = \text{Torque (N} \cdot \text{m)} \cdot 2\pi \cdot \text{Rotational Speed (rpm)}/60000$$

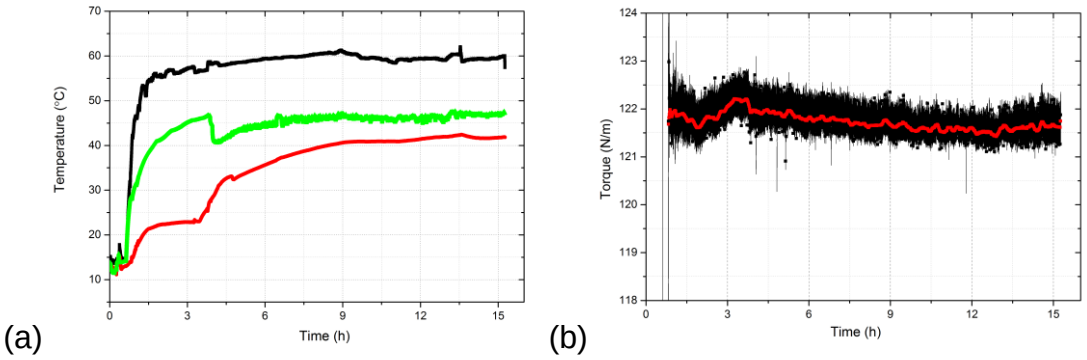

Figure 4.14 (a) temperature distribution at different locations : first layer of particles (——), middle of radius (——), centre of the wet-cake (——); (b) experimental torque data (——) and smoothed data (——) varied with time during agitated drying process

Figure 4.15 The gearbox with an impeller fixed to a linear positioning slides adapter

Impeller has to command plough and smoothing function when perform different actions. A self-made four-bladed impeller with 45° inclining angles (Figure 4.16) is made of stainless steel with shaft bearing inserted in the middle of vessel. The shaft bearing is sealed in the lid and connected to a linear system on the top. The gaps between impeller and vessel wall/bottom are 1cm and 2mm separately. Linear position slide from MiniTec UK Ltd (Basingstoke, UK) is fixed on the top of the vessel to adjust the level of the agitator. Raising and lowering the impeller can be controlled by turning the handle of the adjusting unit. The Adjusting Unit VEN 45 X 90 S has a length

of stroke at 100mm to perform different function of plough and smoothing. A reversing controller was connecter to the motor system allows the agitator rotate at both clockwise and anticlockwise directions by simply press the switch button.

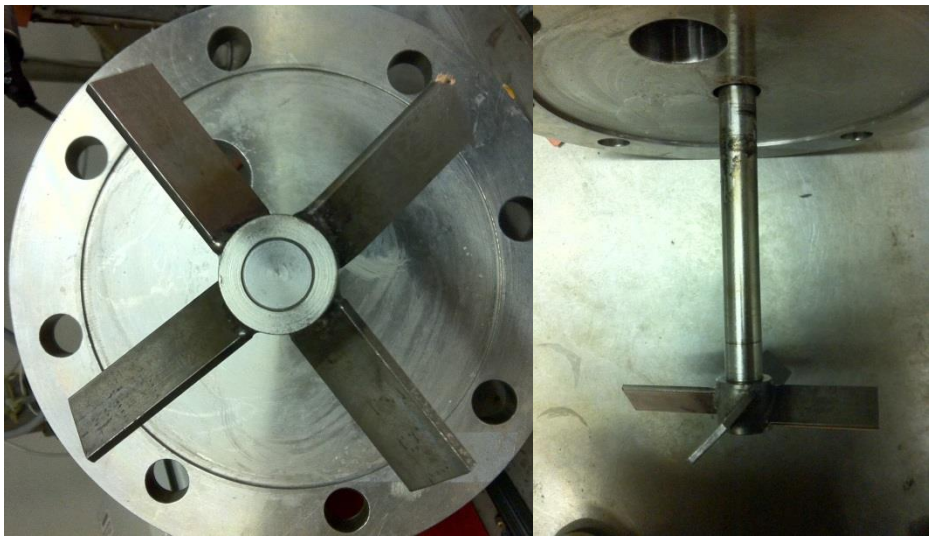

Figure 4.16 The bottom view and side view of the stainless steel stirrer of the lab-scale AFD

Four through-circulation convective nitrogen drying experiments were carried out in the lab-scale AFD rig. Three experiments were carried out without agitation and one with agitation. The nitrogen flow for the four experiments was set to 12L/min for each experiment. The stirring speed was set to 12 rpm according to the equation by scale down from industry to the lab:

$$\frac{\text{Stirring speed}_{\text{Industry}}}{\text{Stirring speed}_{\text{Laboratory}}} = \frac{\text{Inside Diameter}_{\text{Laboratory}}}{\text{Inside Diameter}_{\text{Industry}}}$$

Table 4.3 The stirring parameters from scale-down calculation

Parameter	Industry	Laboratory
Inside wall diameter	62 cm	16.9 cm
Stirring speed	3-8 rpm	11-29 rpm

4.2.3.6 Updated LabVIEW system

In order to record and control each of the individual filter variables automatically, it was necessary to create a programme employing LabVIEW (Laboratory Virtual Instrument Engineering Workbench). LabVIEW CompactDAQ General-Purpose I/O Modules from National Instruments

Corporation Ltd. (Newbury, UK) was used for acquiring data, performing online analysis together with a measurement system using LabVIEW system design software was used in this work to collect online data. LabVIEW is a graphical programming language that is used to create programs in block diagram form rather than using a text-based language. The LabVIEW software can do one command at a time, graphical (G) programming executes when its inputs are defined, thus parallel-branched executions can occur at the same time and so control multiple pieces of equipment. Graphical (G) programming also allows linear execution of certain parts of the program. This is particularly useful when data is first sent to an instrument where there is a lag before the data is returned, as in the case of the mass balance. This makes G programming specialised to data acquisition and instrument control as the program is visually displayed utilising instrument driver software called "Measurement and Automation" to control “actual instruments”. The previous study from Amber Geddes shows a LabVIEW design about the experiment, however, some new instrument are adding to the vessel, hence, an updated design of LabVIEW is made which is shown in Figure 4.12.

On-line computer data collection and control program includes: Two pressure transducer to measure the pressure inside the vessel and differential pressure can be measured through the actual pressure drop across the cake and medium. Installation of a gas flow meter mounted upstream of the vessel in order to control pressure within the vessel. A design of a PC controlled heater band to fit round the vessel and port holes. Addition of a bidirectional stirrer with a seal that allowed for stirring across the whole diameter of the vessel at low stirring rates and motor for the stirrer that controlled speed and allowed the torque of the stirrer to be measured.. Inclusion of several thermocouples to measure the temperature throughout the height, width and depth of the vessel. A vacuum pump was also fitted downstream of the filter unit, with a catchpot fitted to either side of the pump to collect the filtrate during the drying operation. PC compatible balance with a two-way RS-232 connection.

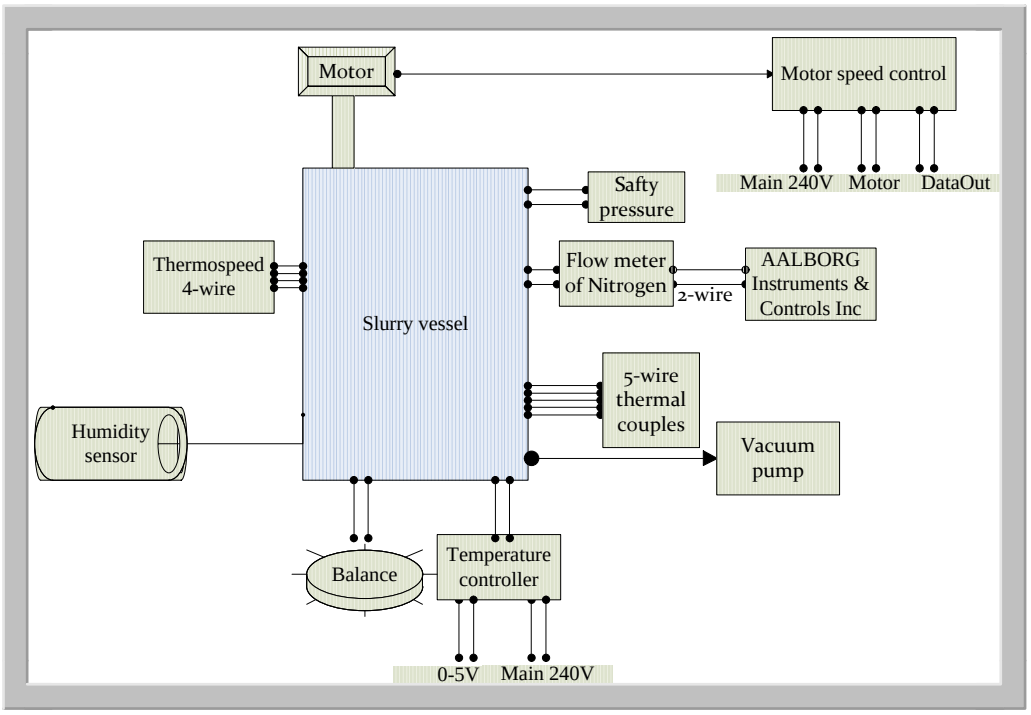

Figure 4.17 Schematic of data logging parts for Bench-scale AFD

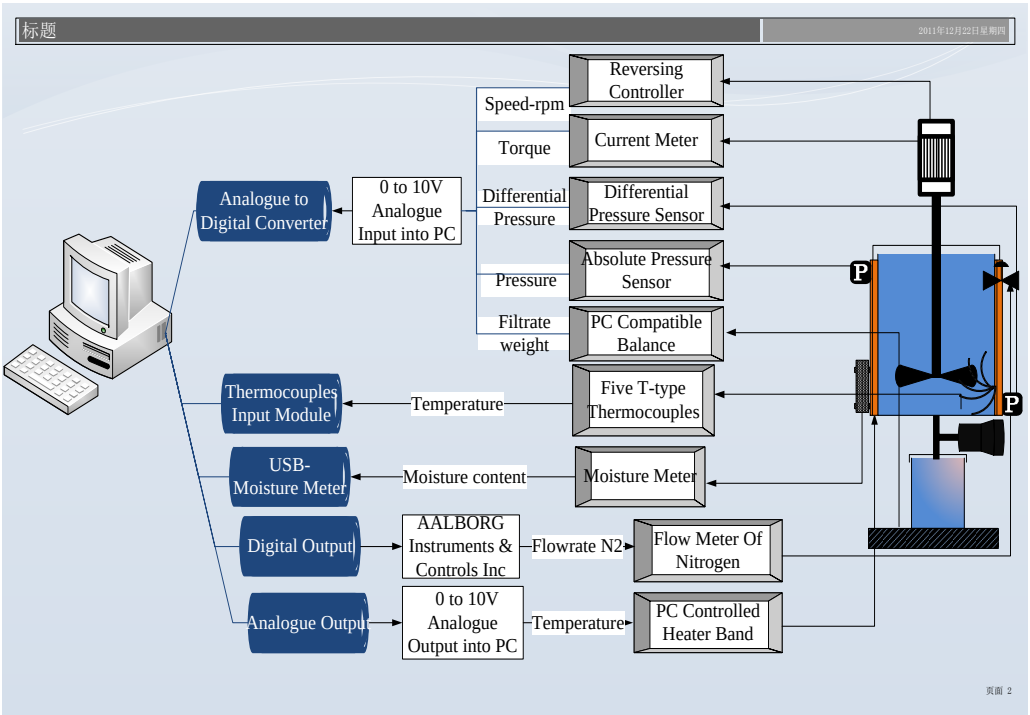

Figure 4.18 Schematic of data input and output parts between the LabVIEW software and the bench-scale AFD

4.2.3.7 Vacuum condenser

The moisture content tracked by the moisture meter is proved not too accurate for the drying process that contain much less water than the

filtration process. Hence, the vacuum condenser at the outlet is designed to connect to a digital balance which measures the condensate weight variation with time during the process. The condensate weight is directly reflected the vapour content. the vapour condensate trapped inside the second catchpot is shown in the digital balance which is recorded through data acquiring system.

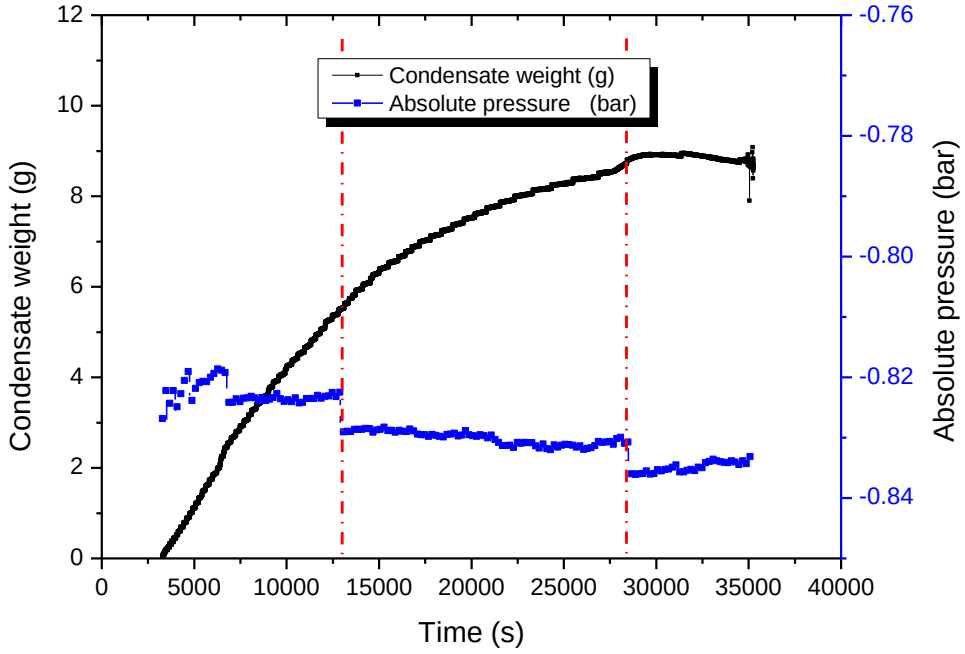

Figure 4.19 Pressure and condensate weight variation as time inside the vessel during drying process

4.2.3.8 Digital balance

A&D GX-2000 Digital balance from A&D Company, Limited (Abingdon, UK) was used in this work to record the weight and filtrate and condensate separately. The 3-way valve beneath at the downstream of the vessel can be functionalized as outlet seal and filtration separately. A vacuum pump with a condenser is connected to the inlet of the vessel in order to perform sucking the vapours above the wet-cake during vacuum contact drying rather than at the bottom considering the particles may clog and further wash away while pumping vacuum from bottom. The bottle used to collect filtrate was placed on the digital balance during filtration process while exchange for the bottle of concentrate during contact drying process (Figure 4.18).

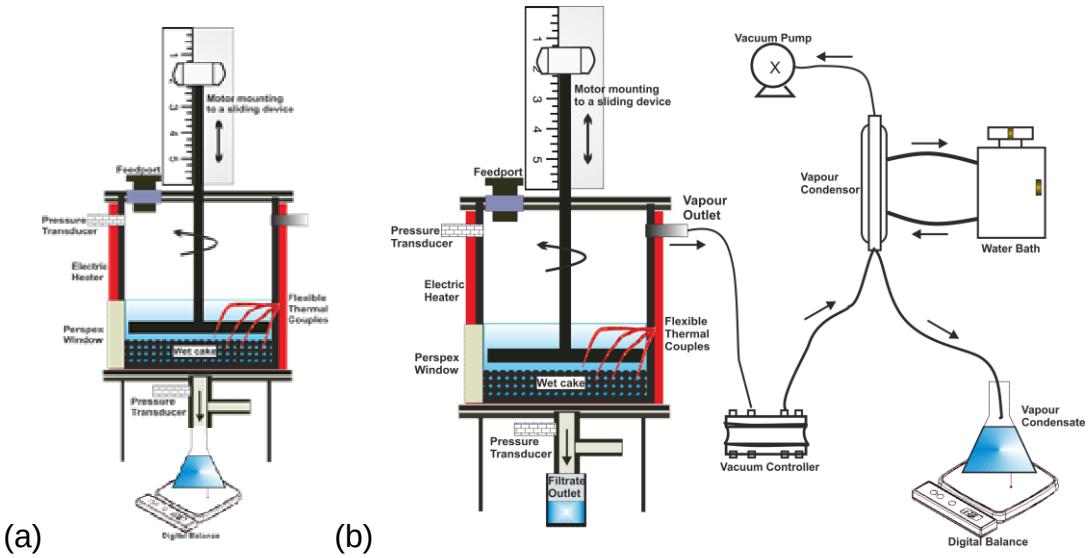

Figure 4.20 The sketch of lab-scale AFD – examples of (a) filtration setup (b) vacuum contact drying setup

4.3 **Conclusion**

To monitor solvent content variation with time, tracking the condensate weight for vacuum contact drying and humidity probe for through-circulation convective drying were chosen to investigate drying curves. The modification design of the existing bench-scale filter-dryer was detailed and performance and reproducibility utilising aspirin and water/ethanol commencement of series of drying of pharmaceutical materials investigated in chapters 5 and 7.

Chapter 5
Materials and methods

5.1 Introduction

This chapter describes the materials being studied and the methods used for this characterizations. The technical range from small-scale Thermal analysis instruments to medium-scale drying equipment using the AFD which has been described in Chapter 4. This work utilised aspirin powders, water and ethanol as representative model systems. The drying kinetics and particle properties were investigated through different data acquiring systems and then evolved into data analysis.

5.2 Materials

Aspirin as one of the widely used pharmaceutical materials with needle-like morphology and hydrophobic properties was selected to perform thermal analysis to investigate the effects of temperature and heating rates on drying time and drying rate. Aspirin crystalline particles used in TGA test were obtained by crystallizer. The particle size and surface area information is listed in Table 5.1. Distilled water and Ethanol were used as solvents. The physical properties about the solvents used in this work are shown in Table 5.2.

Table 5.1 Physical properties of solid and solvent

Cooling rate $\left(°\mathrm{C min}^{-1}\right)$	**Concentration**	**Specific surface area** $\left(\mathrm{m}^2\mathrm{g}^{-1}\right)$	**D10** $\left(\mu\mathrm{m}\right)$	**D50** $\left(\mu\mathrm{m}\right)$	**D90** $\left(\mu\mathrm{m}\right)$
1.0	7.75g/50ml 38% Ethanol/ water	0.14	60.7	168.1	427.1
0.7		0.12	68.8	225.1	522.7
0.5		0.09	70.2	239.4	548.7
0.2		0.08	103.2	346.6	642.2
0.1		0.07	70.3	275.7	564.8

Table 5.2 Physical properties of liquid and gas used in the experiment at 20 °C [19]

Materials	Ethanol (liquid)	Ethanol (vapour)	Water (liquid)	Water (vapour)	Dry air
Thermal conductivity $\left(Wm^{-1}K^{-1}\right)$	0.179	0.0139	0.602	0.019	0.026
Density $\left(kgm^{-3}\right)$	0.800	0.085	998.23	0.017	1.205
Specific heat capacity $\left(Jkg^{-1}K^{-1}\right)$	2400	1400	4181.8	1874	1.005
Latent heat $\left(Jkg^{-1}\right)$	1030000	-	2453000	-	-

For medium-scale drying experiment using lab-scale agitated filter dryer, the demanding for the test materials is comparatively large, hence the commercial aspirin material was used for the drying experiments. The aspirin used in the AFD were crystalline powders (Assay≥99.0%) obtained from Sigma-Aldrich Company Ltd. (The Old Brickyard, Dorset, UK). The aspirin powders obtained here were not mono-dispersed particulates. In fact, contact drying of polydispersed powders is much more difficult than that of mono-dispersed particulates due to the increased viscosity. For polydispersed powders, especially for those containing polymodal size distributions, void fraction may be considerably smaller than that of monosized powders. Size distribution resulted in closest packing within the filter cake where small particles can fill in the voids between the large particles. Hence, powder flow and cohesivity are strongly depending on the particle size and shape. The powders show cohesive properties as well as poor flowability when possessing large amount of smaller particles and large aspect ratio. In this work, the basic features of solid particulate products are examined, which are relevant for adequate process design and best performance of post-processing. The basic physical properties of aspirin obtained from literature and experimental tests are shown in Table 5.3. The specific heat capacity and thermal conductivity value are sited from literature while the rest of the value in the table are obtained from experimental tests.

Table 5.3 Physical and thermal properties of aspirin crystals [85]

Properties	Aspirin
Specific heat capacity $\left(Jkg^{-1}K^{-1}\right)$	2200
Thermal conductivity $\left(Wm^{-1}K^{-1}\right)$	0.1
Density $\left(kgm^{-3}\right)$	1400
Porosity	0.4
CE Diameter Mean $\left(\mu m\right)$	26.03
Melting point (ºC)	143.7
Decomposition temperature (ºC)	110-120

The data of aspirin particle size and morphology are shown in Figure 5.1 b and c. These data were obtained using Morphology G3 (see section 5.1.2.3). Figure 5.1 b shows needle-like particles with bimodal size distribution as revealed in Figure 5.1 c. The processing challenges of filtering and drying such particles with wide particle distributions have been addressed [61]. It has been reported in their work that wide particle size distribution with excess of fines generated from crystallization process led to cake hardening. This could happen even without agitation in tray dryer.

(a) 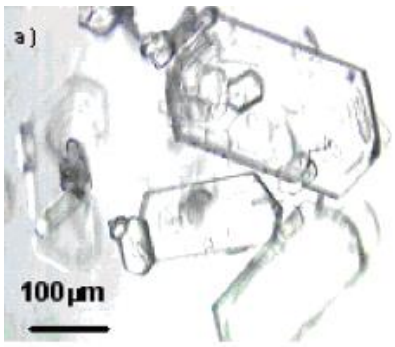

(b) 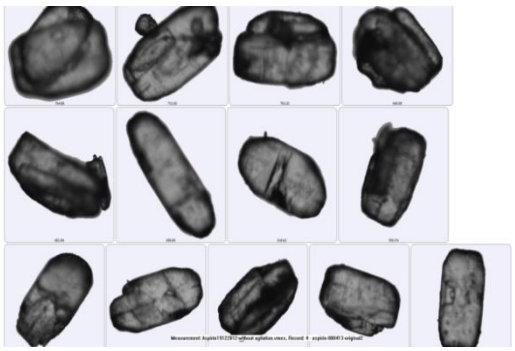

(c) 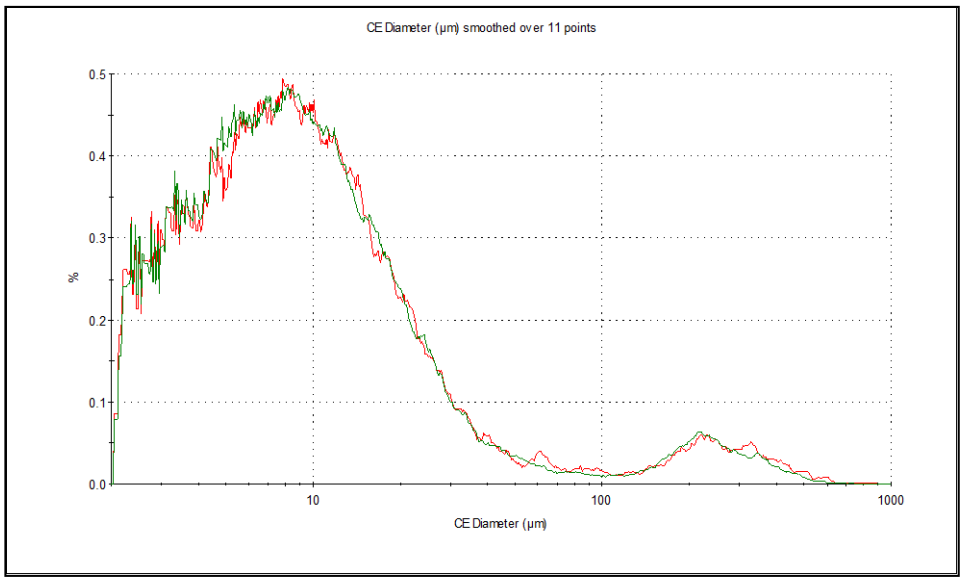

Figure 5.1 Particle property of aspirin: (a) crystal morphology obtained from literature offer [86]; (b) particle morphology and (c) particle size distribution of observed the aspirin crystals

In order to compare the effects different particle size and shape of the same material on the drying behaviour, the drying behaviour of aspirin agglomerates are also being investigated here. The morphology of the agglomerates observed from microscope optics is shown as follows.

(a) 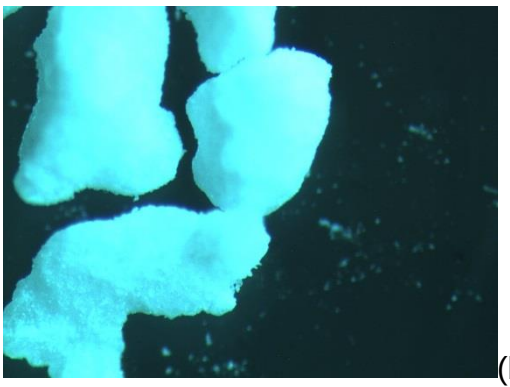 (b) 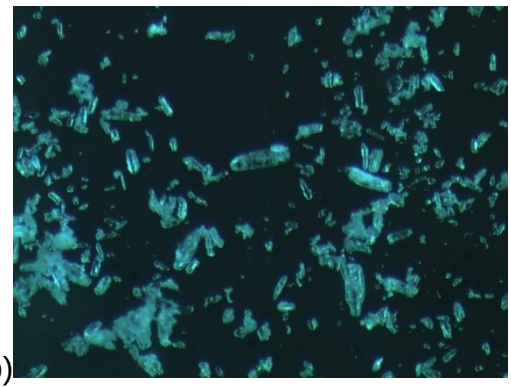

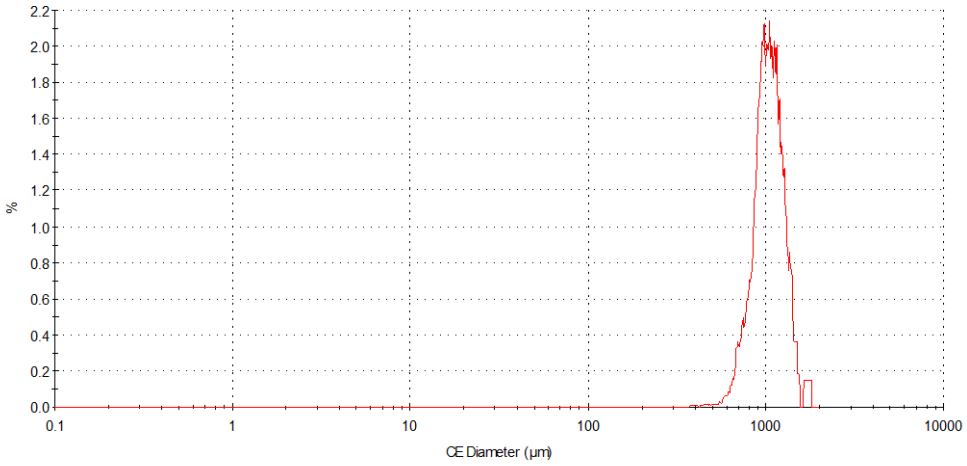

(c)

Figure 5.2 (a) The morphology of aspirin agglomerates; (b) the crystals composed the agglomerates by grinding a single agglomerate; (c) particle size distribution of observed the aspirin agglomerates

5.2.1 Apparatus

Thermal analysis instruments includes DSC (differential scanning calorimetry) and TGA as the basic technology to characterize sample materials over a very wide temperature range. The thermal analysis instrument used in this work is Mettler Toledo.

5.2.1.1 DSC

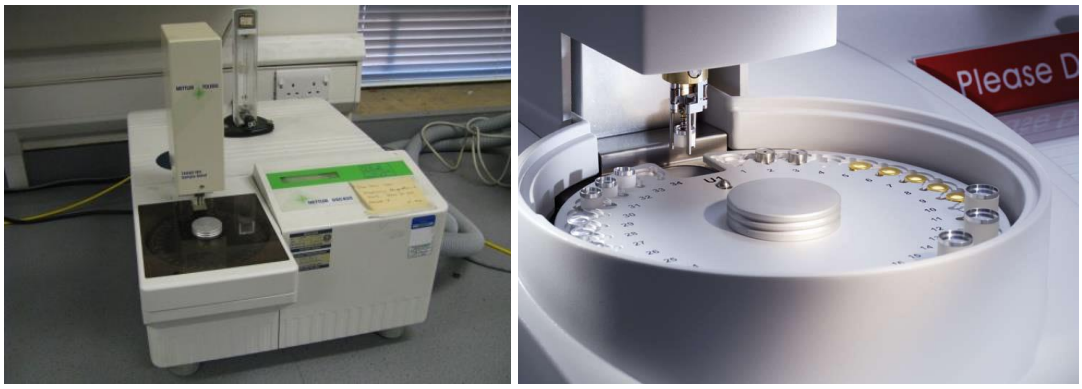

Figure 5.3 DSC instrument (left); the automation of sample robot (right)

DSC is a thermal analytical technique in which the difference in the amount of heat required to increase the temperature of a sample and reference is measured as a function of temperature. DSC measures enthalpy changes in samples due to changes in their physical and chemical properties as a function of temperature or time. Results from DSC will help to comprehend about the decomposition temperature of pharmaceutical materials. This is very important when processing thermal sensitive pharmaceutical crystals.

5.2.1.2 TGA

TGA is a type of testing performed on samples that determines changes in weight in relation to change in temperature. Such analysis relies on a high degree of precision in three measurements: weight, temperature, and temperature change. TGA/SDTA851e (Figure 5.4 a) and TGA/DSC 1 STARe from Mettler-Toledo Ltd. (Leicester, UK) are used for pure water and mix solvent drying tests separately. The mass of a sample is measured when it is heated cooled or held isothermally in a defined atmosphere. A typical TGA curve shows the mass loss steps relating to the loss of volatile components (moisture, solvents, monomers), polymer decomposition, combustion of carbon black, and final residues (ash, filler, glass fibres). As many weight loss curves look similar, the weight loss curve may require transformation before results may be interpreted. The weight loss curve against temperature will have qualitatively predict in drying process. It is mainly used for the quantitative analysis of products.

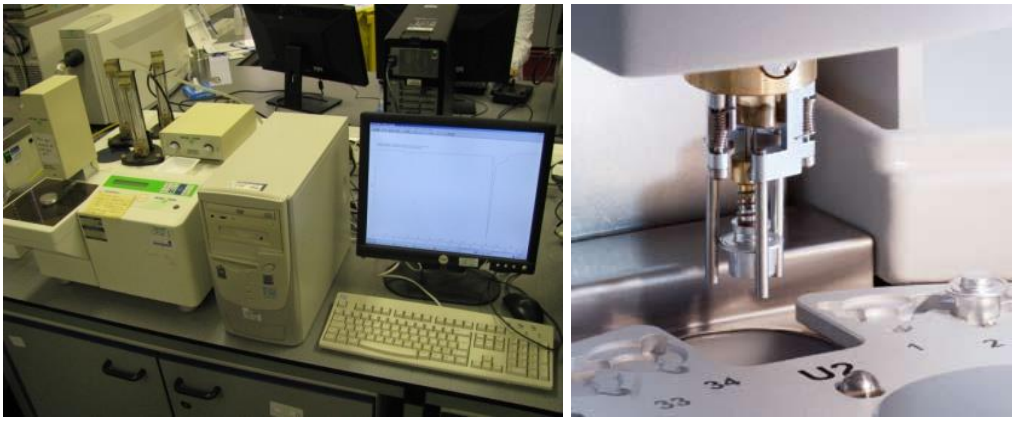

Figure 5.4 TGA instrument (left); aluminium crucible in the automation robot (right)

For most of the contact drying experiment, it is very popular to perform at vacuum conditions for contact drying and the liquid is often vaporised over the boiling temperature which causes overheating for thermal sensitive materials and longer cycle time. Two methods are applied to overcoming thermal damage as well as decreasing drying time are to reducing the thickness of the wet-cake or reducing temperature by lessen prevailing pressure. Hence, a vacuum system is built up and linked to TGA instrument.

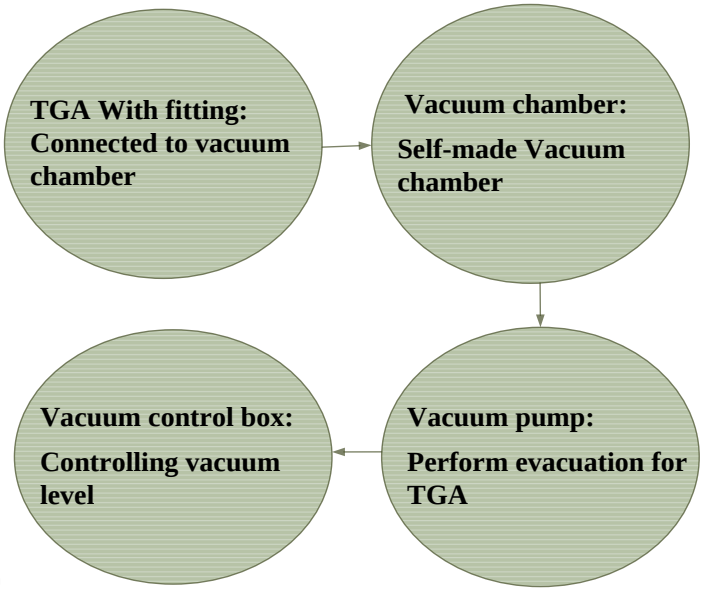

(a)

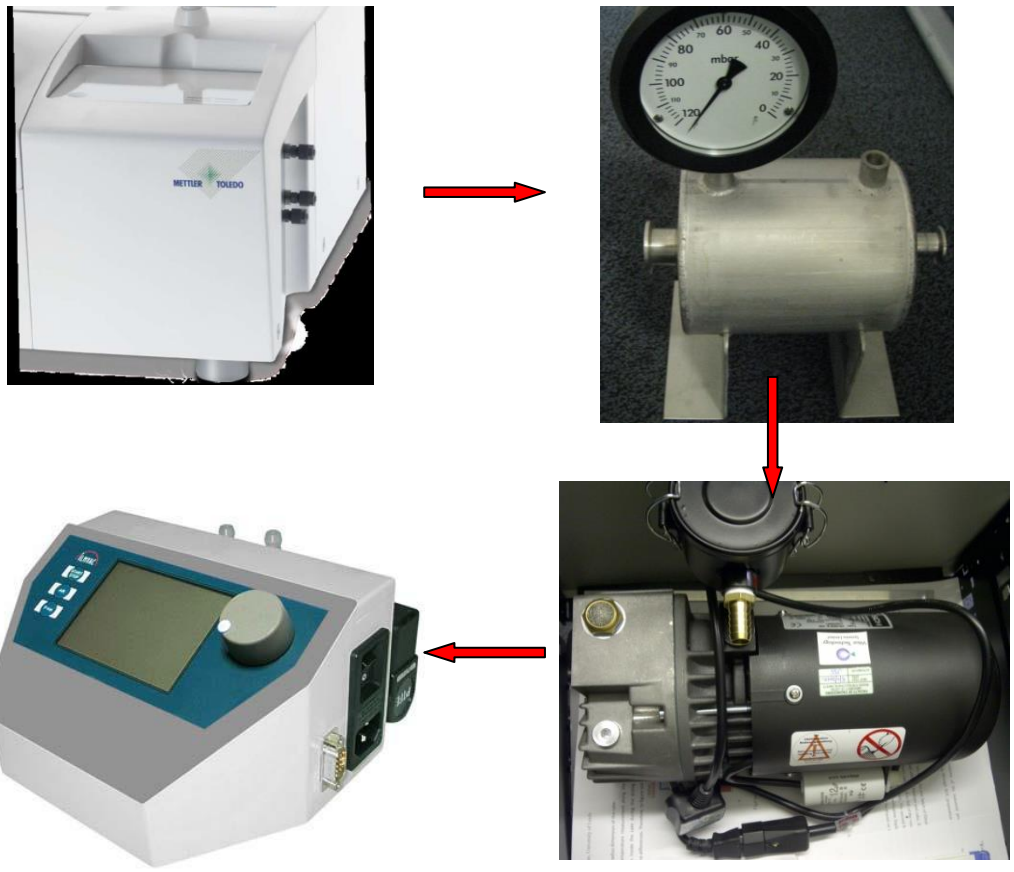

(b)

Figure 5.5 (a) the design of vacuum system connecting to TGA; (b) the actual equipment used to connect to TGA (follow the direction of the arrow): TGA instrument with the correspondingly fittings; self-design vacuum chamber to bridge the vacuum pump and TGA; small-scale vacuum pump; vacuum control box for controlling vacuum level

There is a fittings at the side of TGA instrument (Figure 5.5 a) which can be connected to the self-made vacuum chamber. The self-made vacuum chamber is designed with a pressure gauge which can tell the absolute pressure inside the chamber. Vacuum pump is connected to chamber next to perform evacuation within the chamber. A vacuum control box is set up at last to control the vacuum level at any pressure with minimum value at 10 mbar.

5.2.1.3 Particle size and morphology

(a) 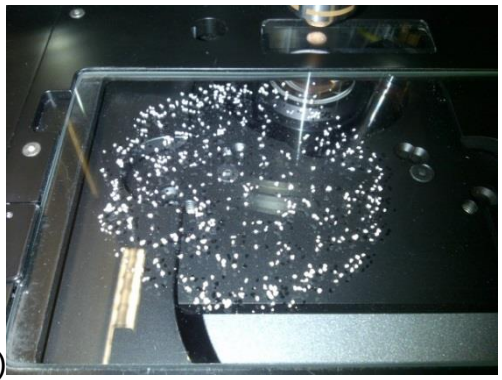 (b) 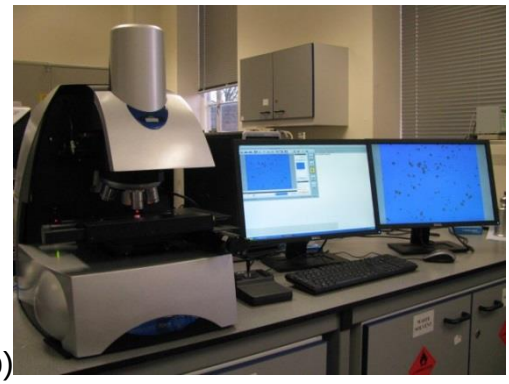

Figure 5.6 Photos of Morphologi G3 (a) sample dispersion plate (b) equipment and software analysis interface

To further knowledge of the particles behaviour during drying process, it is better to understand how a single particle behaves and whether there is the same trend for the rest of the particulate materials. A better way to do so is to observe the particle behaviour before and after the drying process. Morphologi G3 can meet these demands by scanning over ten thousands of particles at a given time and provide the size and shape information. This equipment developed by Malvern Instruments Ltd. (Malvern, UK) using static automated imaging which can analyse particle size range generally from 0.5µm to 1000µm. For dry powder measurement it usually uses fully automated dispersion unit (Figure 5.6 a). The dispersing nozzle helps to produce a homogeneous distribution of powders on the observation glass plate.

The SOP commonly is controlled by the dispersion pressure, injection time and sample settling time which related to the status of initial particles. In this work, the SOP was set to 0.8bar for the dispersion pressure, 60s for injection time and for 60s sample settling time for the similar type of materials to minimise the sensitivity of instrument intervention and

repeatable results can be maintained. Magnification (5x) lens was chosen as the measurement lens which commonly covering the particle size 6.5-420µm. The analysing tool utilising Morphologi G3 software provides the information of individual particle images as well as the scattergram plot of the size and shape variables. Figure 5.7 shows the two results of circular equivalent diameter distribution of same aspirin crystals. In which you can see that the repeatable results can be obtained by using same SOP for each experimental test.

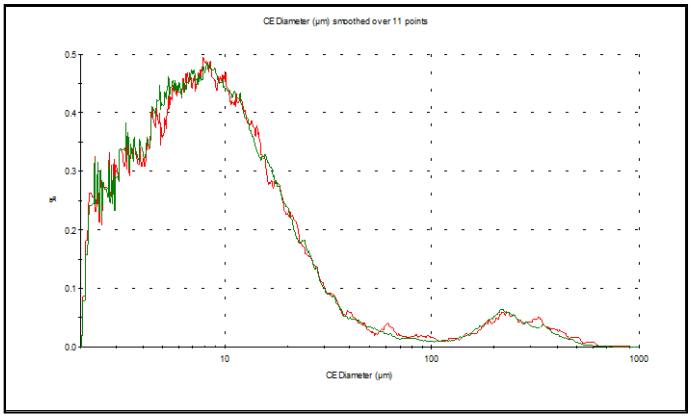

Figure 5.7 Twice observation of aspirin crystals from Morphologi G3

5.2.1.4 Lab-scale AFD

The bench-scale AFD is the miniature of pilot plant AFD with the similar geometric parameter design. The Bench-scale AFD is grounded on the previous work of Amber Geddes whose concentration on filtration process. There is a clear lack of fundamental understanding of the filter drying process for organic materials due to the limited research that has been carried out. This bench-scale AFD is already introduced in Chapter 4. The operating procedure is described as follows.

5.2.2 Experimental methods

The equipment using for thermal analysis of aspirin/water pure solvent system which was separate TGA (model ?) and DSC (model ?) unit, while the analysis of aspirin/water & ethanol mixed solvents system using Simultaneous Thermal Analysis TGA/DSC 1 STARe unit offered by Mettler Toledo UK Ltd (Leicester, UK).

5.2.2.1 DSC test

(a)  (b) 

Figure 5.8 (a) The standard aluminum crucible (40µl) and its cover for TGA; (b) crucible sealing press (right)

The experiment conducted in DSC equipment is by setting up heating programs in a crucible pan. At first, weigh a certain amount of Aspirin powders and put them into aluminium crucible and seal the aluminium with a cover with a crucible sealing press (Figure 5.7).

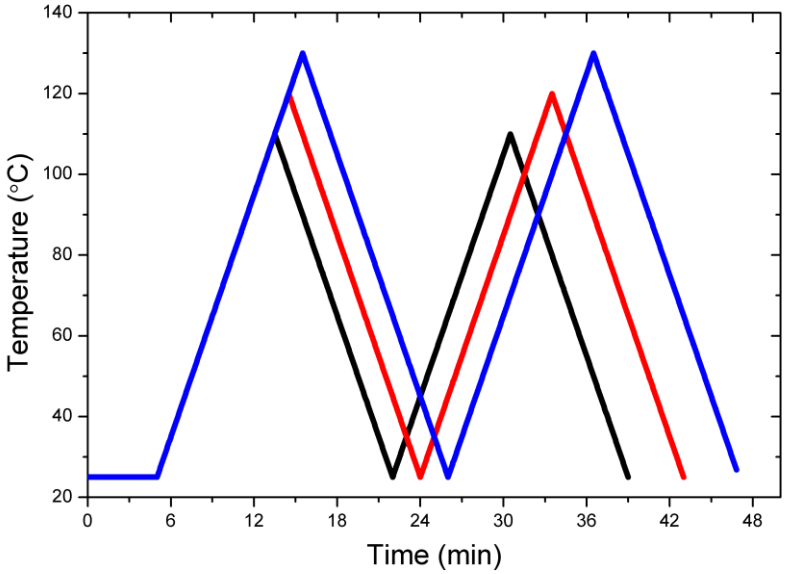

Figure 5.9 Temperature profile cycling at 110ºC (——), 120ºC (——), 130ºC (——) for DSC test

Use the temperature profiles shown in Figure 5.7 to perform cycle DSC tests with Nitrogen purging flow at 20 cm^3/min to obtain the isothermal drying behaviours at 50ºC, 60ºC and 70ºC respectively.

5.2.2.2 TGA test

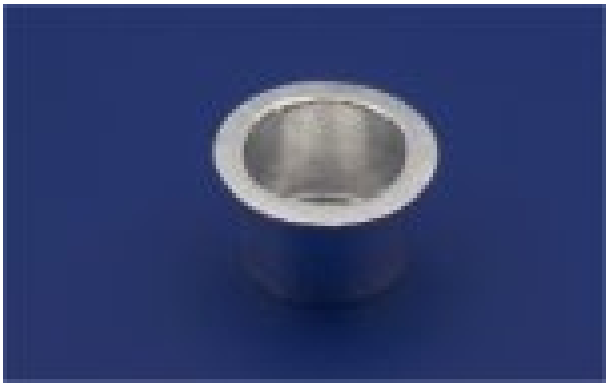

Figure 5.10 The aluminum crucible medium (100µl) for TGA

The wet-cake were prepared by stirring the mixture of solid/solvent to produce a homogenous slurry. The 100µl empty aluminium crucible pan (Figure 5.10) with dry as well as wet particles loading were weighed separately. The amount of solvent and solid loaded to the crucible pan were controlled to the similar level to keep the consistent initial solvent content. 5 consecutive reference temperature was set for TGA measurement from 30ºC to 70ºC with increment of every 10ºC. The maximum heating temperature 70 ºC fell well below the decomposition temperature of aspirin crystals. All the samples were dried to bone-dry materials as can be seen that the end weight of the sample pan would not been changed.

The Aspirin solid and solvent is mixed with a sharp knife to get a uniform state then smooth the surface at last. Similarly, the nitrogen purging flow is at 20 cm^3/min. The mixing solid and solvent is observed using an optical microscope to observe the surface moisture distribution. Figure 5.11 shows that the wet-cake was initially covered by a film of water on the surface of the particles evenly. After drying, the water adhere to the surface vaporized and the wet-cake became completely dry.

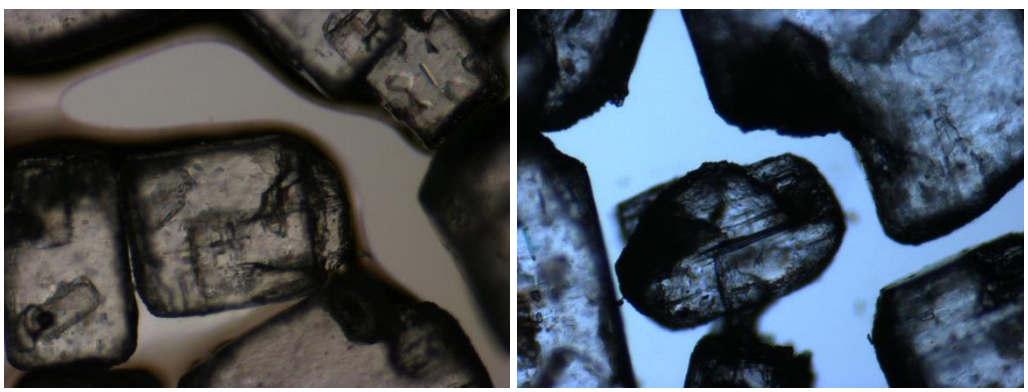

Figure 5.11 Microscopic images of aspirin crystals before (left) and after (right) drying

The vacuum drying of aspirin can be performed using the setup in Figure 5.5, the vacuum level ranging from 10 mbar to 1000 mbar. The vacuum is created instantaneously after the robot settling down the sample pan. As the drying rate increase as the vacuum level increases, the drying cycle time for each run is reduce which greatly reduced experiment span.

The drying of aspirin using TGA could be carried out under varied conditions including temperature, vacuum level, particle size distribution and ratios of mixed solvents.

5.2.2.3 Experimental method using lab-scale AFD

To reduce the variability of the results, the AFD experiments were performed following a consistent SOP as follows:

- Considering the aspirin dissolving in the solvent, saturated solution with aspirin in 1 kg distilled water was prepared. Approximately 3-5 g aspirin dissolved in 1 kg water at the prevailing temperature 20 ºC.
- Pre-weighed 1 kg aspirin powder and the solution were put into a beaker and stirring for a few minutes to keep aspirin solid suspended.
- The slurry was charged into the vessel via the feedport of the top. The feedport and the outlet were closed. The experiment is taken at room temperature.
- Nitrogen or dry air was bled into the vessel to pressure up to 1bar gauge. The outlet valve was opened to perform filtration process under the driving force of gravity and nitrogen pressure. In this process, the weight of filtrate was recorded.
- After the filtration process, a long thin tube was inserted into the vessel through the feedport to collect a small amount of wet-cake. The wet-cake was taken out to run a drying test separately and the initial solvent content is measured.
- The 3-way valve was switched from filtration (bottom open position) to drying (bottom close position). A condenser with a flask was placed downstream to collect the vapour. A coolant running through the condenser was set to - 5 ºC.

- The flask used to collect the vapour coming out of outlet was placed on a balance and the vapour weight recorded online during drying process.
- Thermocouples were put into the wet-cake along either the radial and axial direction of the wet-cakes depending on the experimental setup.

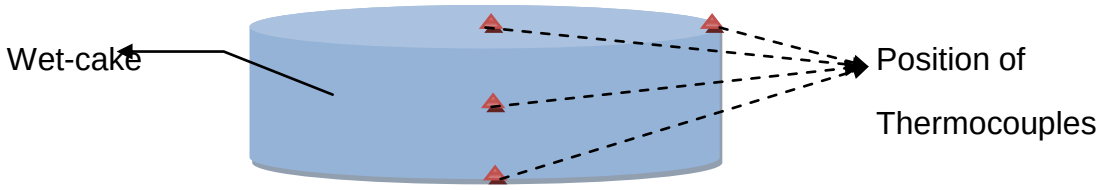

- The dry product was collected by opening the lid and the vessel was cleaned using water after this.
- During the drying process, moisture content, absolute pressure, temperature distribution in a static bed, nitrogen flow were recorded.

The diagram and schematic operating procedure of AFD was shown in Figure 5.12 and 5.13.

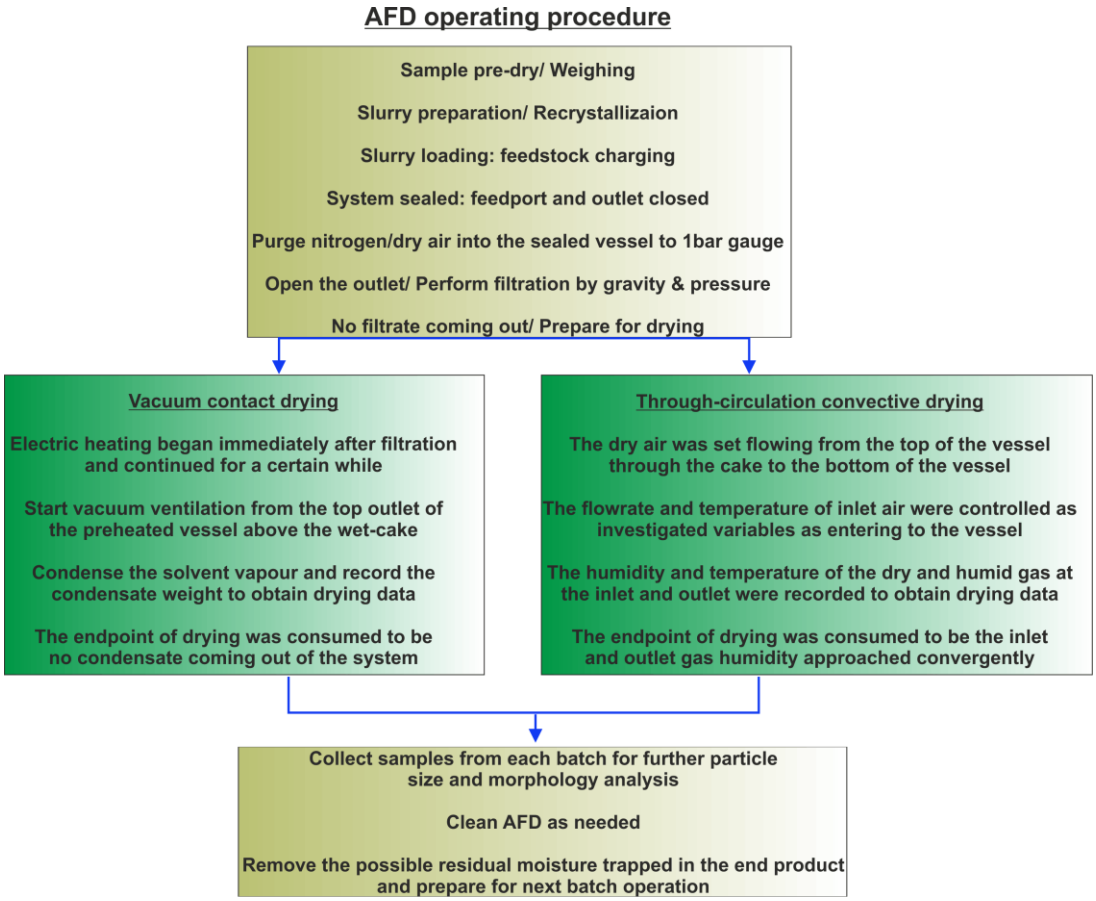

Figure 5.12 The diagram of operating procedure for lab-scale AFD in the laboratory

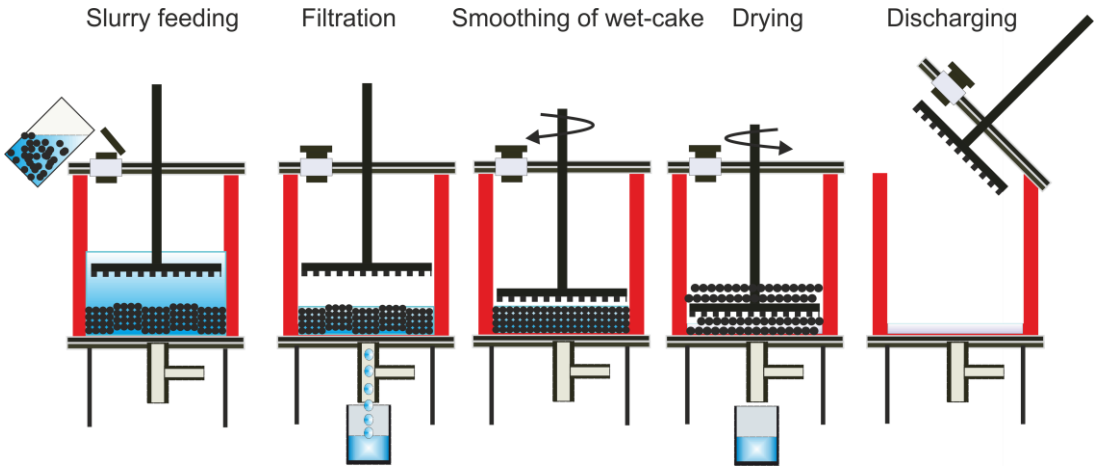

Figure 5.13 The schematic of operating procedure for lab-scale AFD in the laboratory

For this work, two types of drying including vacuum contact drying and through-circulation convective drying were examined. For each of these types of drying, the rig designs were slightly different.

For vacuum contact drying:

The powder was dried either static or mechanically agitated by a four-blade stirrer driven by an electric motor. A reversing motor controller is used in order to performing smoothing the surface of the wet-cake and ploughing during drying the wet-cake. The stirrer rotational speed could be set in the range of 0 to 100 rpm. The solvent vapour flowing out the vessel was condensed by means of a vacuum condenser cooled with Haake chiller running by a certain ratio of mixed solvent-ethylene glycol and water. The temperature of circulating coolant was set down to - 5 ºC which is cold enough to condense the vapour. The total mass of the solvent condensate, the inside wall temperature, and radial distribution of temperatures inside the bulk material, the pressure above and under the wet-cake were continuously recorded throughout the duration of the contact drying experiments by every second. The detailed setup for vacuum contact drying and instrumentation is shown in Figure 4.20. The locations of thermocouples within the wet-cake for measuring temperature profile radially are shown in the Figure 5.14.

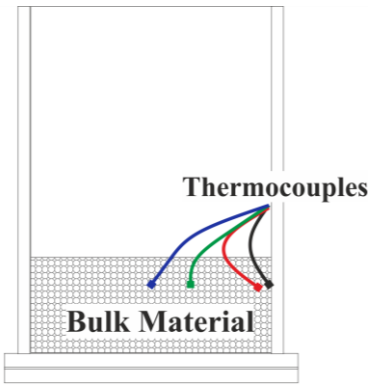

Figure 5.14 Thermocouple positions for vacuum contact drying of lab-scale AFD

For through-circulation convective drying:

For through circulation convective drying, there is slightly changes of the parts of rig (Figure 5.15):

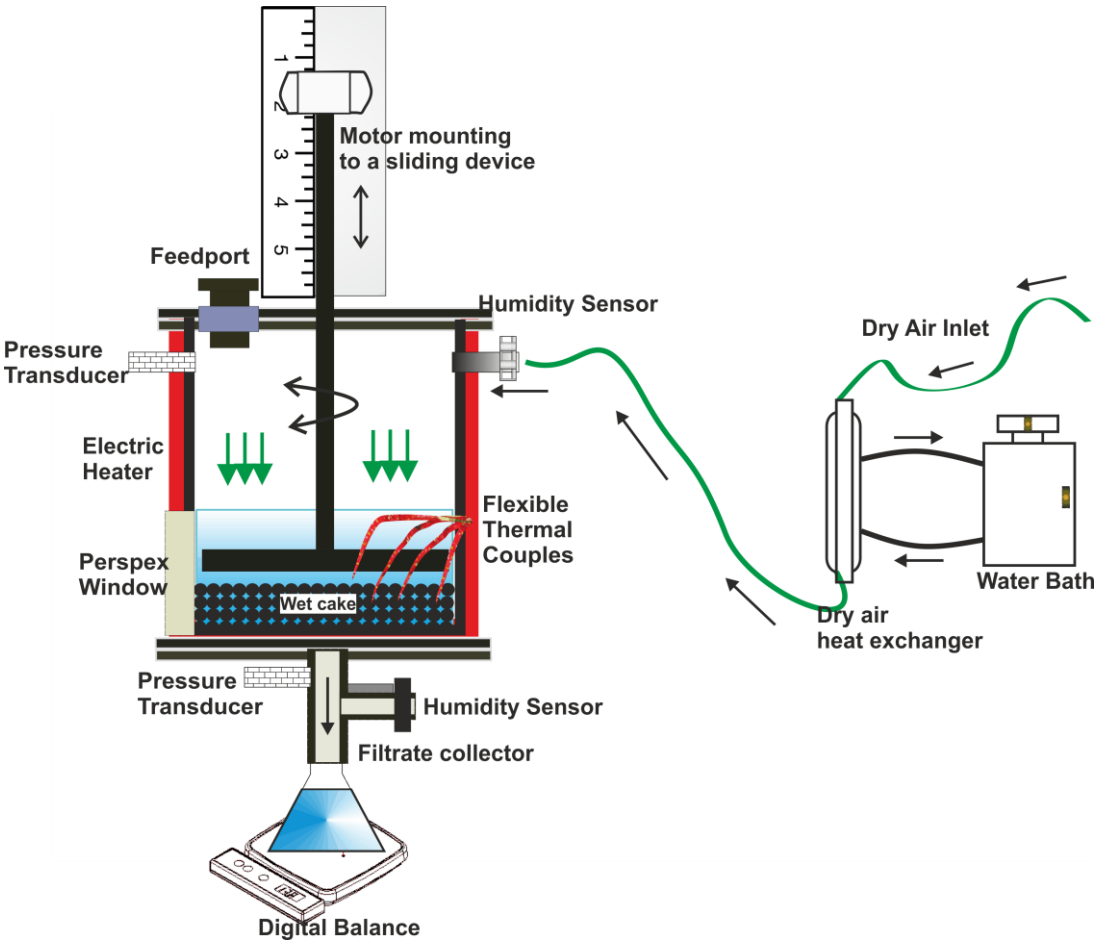

Figure 5.15 The design of through-circulation convective drying for lab-scale AFD in the laboratory

- The addition of heat exchanger at the inlet of the vessel to maintain the dry air temperature.
- Two humidity sensor were wired up to monitor the solvent content variation with time.
- Furthermore, the position of thermocouples are placed into the locations shown in the Figure 5.16.

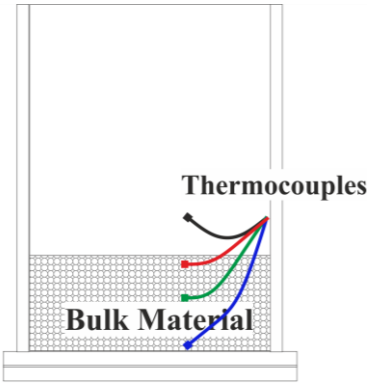

Figure 5.16 Thermocouple positions for through-circulation convective drying of lab-scale AFD

The range of experimental conditions using the bench-scale 5 L AFD rig are shown in the Table below. Experimental conditions for vacuum contact drying and through-circulation convective drying are shown in Table 5.4 and 5.5 separately.

5.3 Conclusions

This chapter provides a detailed description of the materials and apparatus utilised in this research work, describing the principles of the various techniques used to characterise the systems. The experimental procedure and apparatus used to carry out filtration and drying has been described in detail, with the results presented in Chapters 7.

Table 5.4 operating conditions for vacuum contact drying

Operating conditions	Trial 1	Trial 2	Trial 3	Trial 4	Trial 5	Trial 6	Trial 8
Jacket temperature (ºC)	66	70	75	70	70	70	70
Electric heating power (Watts)	128	146	157	157	157	157	157
Vacuum level (mbar)	150	150	150	150	150	150	150
Initial solvent content	31%	9.1%	8.9%	9.2%	12%	12%	10%
Agitation speed (rpm)	0 (static bed)	0 (static bed)	0 (static bed)	10	20	30	30 (20min off / 20mins on)

Table 5.5 operating conditions for through-circulation convective drying

Operating conditions	Trial 1	Trial 2	Trial 3	Trial 4	Trial 5	Trial 6
Inlet air temperature (ºC)	26-28	26-28	26-28	26-28	26-28	26-28
Inlet air flow (L/min)	8	10	12	12	12	12
Inlet air humidity (%)	0	0	0	0	0	0
Initial solvent content	15%	16%	18%	17%	14%	16%
Agitation speed (rpm)	0 (static bed)	0 (static bed)	0 (static bed)	10	20	30

Chapter 6
Drying equation

6.1 Introduction

A Drying model based on a lumped-parameter approach is developed for the static bed and a more rigorous model is developed incorporating agitation for the agitated bed drying. The models include both the constant- and falling-rate drying periods. In the former drying period, the heat transfer contact resistance between the inner wall and the first layer of particles are considered. For the later period, a vaporization front in both static and agitated beds is developed which moves towards the centre of the wet bed. An additional heat transfer resistance through the layer of dry particles between the inner wall and the vaporization front is considered.

6.2 Vacuum contact drying models: LPM and DPM

Three lumped-parameter models are developed for vacuum contact drying of static and agitated bed model while distributed-parameter model was introduced here from the work of Kohout et al. [3] and Murru et al. [1] for further comparison between the two types of model.

6.2.1 LPM for a static bed

In this case, the wall temperature is considered as varied value changing with the electric power supplied to the vessel wall. The ambient environment temperature is assumed to be constant during the experiment period. Since the power supplied is used for heat up the wall as well as heat loss to the air.

6.2.1.1 The constant-rate period

In this period, the solvent vaporises at a much lower temperature due to the very low pressure maintained in the head-space of the vessel. With the heating jacket supplying heat to the wet-cake, the temperature rises from the room temperature to the boiling point of the solvent and the solvent starts to vaporize. The rate of heat transfer to the wet-cake determines the rate of solvent vaporization. The drying model for the constant-rate period is based on the following assumptions:

- There are no gradients of temperature and solvent content inside the wet-cake.
- The heat supplied from the heating jacket is used for heating up the cake, also heating up the surrounding air as well as for the vaporisation of the solvent.
- Cylinder vessel surface area is small compared to surroundings.
- The room air is quiescent.

Figure 6.1 shows the diagram of heat transfer process when taking the heat supplied from the electric heating band as a constant known value. The calculation of convection heat to the ambient environment is calculated by the following equations [87].

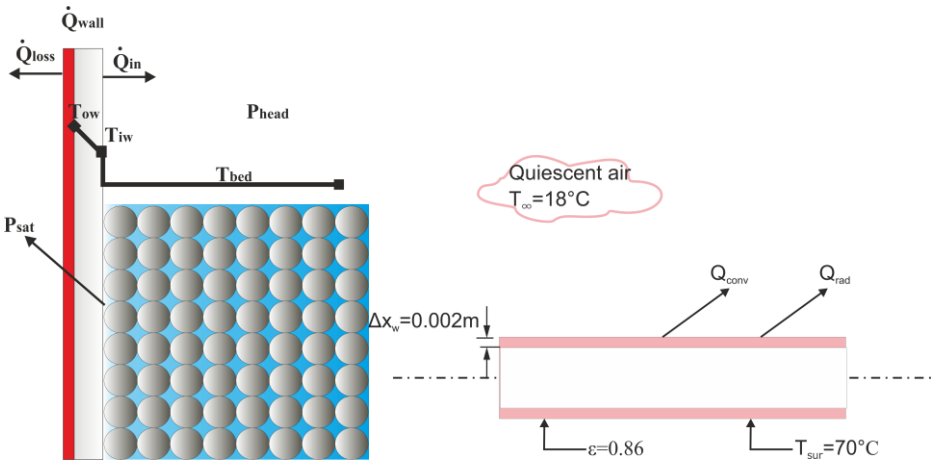

Figure 6.1 The schematic of a vacuum contact dryer during the constant-rate period

The heat supplied from the electric heating band is divided into two parts: one part goes into the wet-cake while the other part is dissipated into the ambient atmosphere. Hence, the total heat flow equation can be expressed as follows:

$$\dot{Q}_{total} = \dot{Q}_{in} + \dot{Q}_{loss} \qquad 6\text{-}1$$

In order to obtain the value of $\dot{Q}_{in}$, the heat loss is first calculated. The total heat loss per unit length of pipe is

$$\dot{Q}_{loss} = \dot{Q}_{gs} + \dot{Q}_{rad} \qquad 6\text{-}2$$

The heat loss to surroundings through heat convection is given by:

$$\dot{Q}_{fc} = \alpha_{gs} \pi D_{wo} \left(T_{wo} - T_{\infty} \right) \qquad 6\text{-}3$$

The convective heat transfer coefficient is calculated by:

$$\alpha_{gs} = \frac{\lambda_a}{D_{wo}} \mathrm{Nu} \tag{6-4}$$

where the diameter of outer wall, D_{wo}, is 0.179. The Nusselt number, Nu, for a cylinder under a wide Rayleigh number (Ra) range is given by

$$\mathrm{Nu} = \left\{ 0.6 + \frac{0.387\,\mathrm{Ra}_D^{1/6}}{\left[1 + \left(0.559/\mathrm{Pr}\right)^{9/16}\right]^{8/27}} \right\}^2 \tag{6-5}$$

where the Rayleigh number is given by:

$$\mathrm{Ra} = \frac{g\beta\rho c_p \left(T_{wo} - T_\infty\right) D_{wo}^3}{\nu_a \lambda_a} \tag{6-6}$$

where the thermal expansion coefficient, β, of air at atmosphere pressure, is calculated from the equation below:

$$\beta = -\frac{1}{\rho}\left(\frac{\partial \rho}{\partial T}\right)_P = \frac{1}{\rho}\frac{P}{RT^2} \tag{6-7}$$

Here a simplification is made in order to calculated the thermal expansion coefficient. Assume that for an ideal gas, the density of air is expressed as $\rho = PM/RT$.

In this case, the value of Nu is calculated to be 39 (Morgan's method) and 41 (Churchill and Chu's method) [87, 88], here an average value 40 of Nu is used.

The heat loss to surroundings through heat radiation is given by:

$$\dot{Q}_{rad} = \varepsilon \pi D_{wo} \sigma \left(T_{wo}^4 - T_\infty^4\right) \tag{6-8}$$

In this case, the emissivity for soft rubber band, $\varepsilon = 0.86$; the Stefan-Boltzmann Constant, $\sigma = 5.67 \times 10^{-8}$.

The agitated dryer vessel is considered as the hollow cylinder wall, where inner and outer wall are exposed at different temperatures. Hence, the wall temperature is function of time and position. The heat transfer through the hollow cylinder wall is given by:

$$\dot{Q}_{in} = \frac{\partial}{\partial t}\left(-\lambda_w A_w \frac{\partial T_w}{\partial x}\right) \tag{6-9}$$

The temperature distribution within the cylindrical wall in this case is neglected for the thickness of wall is very thin.

$$\frac{\partial}{\partial t}\left(-\lambda_w A_w \frac{\partial T_w}{\partial x}\right)=\frac{\lambda_w A_w}{\Delta x_w}\frac{\partial T_w}{\partial t} \qquad 6\text{-}10$$

Hence, the heat supplied from the heating wall to the wet-cake is given by:

$$\dot{Q}_{in}=\dot{Q}_{total}-\dot{Q}_{loss}=\dot{Q}_{total}-\alpha_{air}\pi D_{wo}\left(T_{wo}-T_{\infty}\right)-\varepsilon\pi D_{wo}\sigma\left(T_{wo}^4-T_{\infty}^4\right) \qquad 6\text{-}11$$

Now that the heat transfer to the wet-cake has been obtained, using above equation to solve the drying rate equations, the heat transfer across the vessel wall is used for solvent vaporization directly during the constant-rate period:

$$\dot{Q}_{in}=\dot{m}_v\,\Delta H_v \qquad 6\text{-}12$$

Through Figure 4.10, the temperature difference between the inner wall and dry-cake is 12 ºC, then, the contact heat transfer coefficient, α_{ws}, can be calculated from the equations above. The calculated parameters in this simulation case is shown in Table 6.1.

Table 6.1 Values of calculated parameters used in the model at 313 K

Parameters	Value	Unit
D_{io}	17.3	cm
D_{wo}	17.9	cm
L_{wo}	24.5	cm
T_{wo}	65	ºC
T_{∞}	15	ºC
Nu	40	-
Ra	1.5E7	-
α_{gs}	6.4	$W\,m^{-2}\,K^{-1}$
α_{ws}	31.33	$W\,m^{-2}\,K^{-1}$
λ_{air}	2.5E-5	m^2s^{-1}
β	3.95E-3	K^{-1}
λ_{air}	0.028	m^2s^{-1}
υ_{air}	1.8E-5	m^2s^{-1}
ε	0.86	-

$\dot{Q}_{total}$	127	W
$\dot{Q}_{rad}$	157	$W\,m^{-1}$
$\dot{Q}_{gs}$	170	$W\,m^{-1}$
$\dot{Q}_{in}$	48.5	W

Hence, the heat transfer coefficient from wall to solid, α_{ws} , is 31.33 $W\,m^{-2}\,K^{-1}$.

6.2.1.1 The falling-rate period

Figure 6.2 shows that during the falling rate period, the heat supplied from the electric heating band not only emits to the atmosphere and vaporise solvent, but also heat up the dry-cake. the temperature profile showing in Figure 6.2 indicated that process of transportation of heat within the vessel as well the outside heat movement.

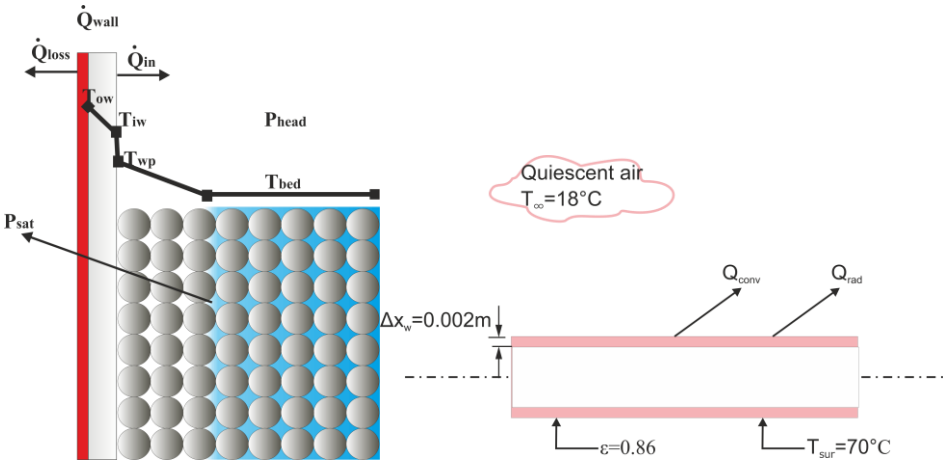

Figure 6.2 The schematic of a vacuum contact dryer during the falling-rate period

Being distinct from the constant-rate period, a vaporization front is developed which moves towards the centre of the wet-cake. The bed comprised of a coaxial internal cylindrical wet-zone and an external cylindrical dry-zone composed by completely dry powders during the falling-rate period. The wet-zone diameter shrinks from diameter of powder bed, D_c , to diameter of wet-zone, D_{wz} , shown in Figure 6.3 in that the vaporization interface decreases and the dry-zone is expanded.

During the falling-rate period, one more heat resistance is taken into account: the thermal contact resistance, α_{ds} , through the layer of dry particles between the inner wall and the vaporization front in addition to the

contact resistance at the vessel wall. The overall heat transfer coefficient, α_i, is calculated as the reciprocal sum of individual heat resistances [89].

$$\alpha_i = \frac{1}{\frac{1}{\alpha_{ws}} + \frac{1}{\alpha_{ds}}} \qquad 6\text{-}13$$

It should be noted that the width of the wet-zone, $D_{wz}(t)$, decreases as drying processes. In order to solve the relationship between the solvent content X and diameter of wet-zone $D_{wz}(t)$, the following assumptions are made in this condition [10]. The cake consists of two parts including a dry-zone with local solvent content equals to zero and a wet-zone with local solvent content equals to start point of solvent content of the falling-rate period, critical solvent content X_C. The schematic diagram of the cake is shown as follows.

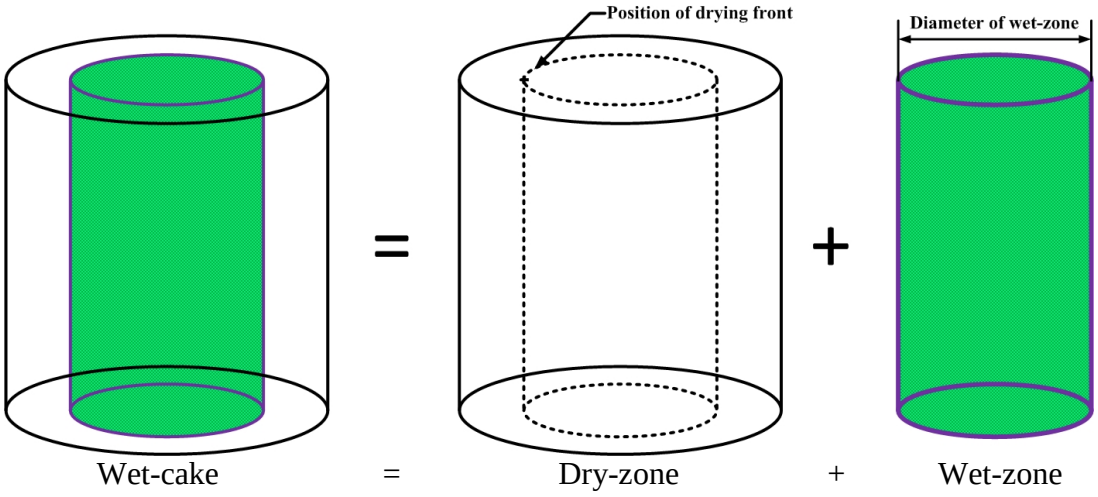

Figure 6.3 The diagram of local status of wet-cake during the falling-rate period

Table 6.2 The parameters and variables for different locations of the wet-cake

Cake position	Powder bed	Wet-zone	Dry-zone
Local solvent content	$X = X(t)$	$X = X_C$	$X = 0$
Volume of zones	$V_{wc} = \frac{\pi}{4} D_c^{\,2} L$	$V_{wz} = \frac{\pi}{4} D_{wz}(t)^2 L$	$V_{dz} = V_c - V_{wz}$

The solvent content inside the powder bed must be equalized no matter the distribution of the solvent content, then substituting V_c, $V_{wz}(t)$ and $V_{dz}(t)$ from the Table A.1, hence the mass of the solvent m_v can be expressed by

$$m_v = X(t)\rho_{ds}V_c = 0 \cdot \rho_{ds}V_{dz}(t) + X_C\rho_{ds}V_{wz}(t)$$
$$\rightarrow X(t)\rho_{ds}\frac{\pi}{4}D_c{}^2 L = X_C\rho_{ds}\frac{\pi}{4}D_{wz}(t)^2 L \qquad 6\text{-}14$$

The wet-zone diameter $D_{wz}(t)$ is expressed as

$$D_{wz}(t) = \sqrt{\frac{X(t)}{X_C}}D_c \qquad 6\text{-}15$$

According to the classical vaporization front theory[2], during the entire falling-rate period the local solvent content at the vaporisation front is considered as critical solvent content. In equation (6-93), the local solvent content of the wet-zone is equal to the critical solvent content (X_C).

The contact heat transfer coefficient is calculated according to the equation for the Conduction through a thick-walled tube [90]. The thermal contact heat transfer coefficient for the dry zone is given by:

$$\alpha_{ds} = \frac{\lambda_{ds}}{\left(\frac{D_c}{2}\ln\frac{D_c}{D_{wz}(t)}\right)} \qquad 6\text{-}16$$

where D_c is the diameter of the wet-cake, $D_{wz}(t)$ is the diameter of the wet-zone, λ_{ds} is the thermal conductivity of dry solid. In order to solve the drying equations the relationship between the diameter of wet-zone and solvent content has to be deducted.

Substituting $D_{wz}(t)$ in equation 6-10, the contact heat transfer coefficient is given by

$$\alpha_{ds} = \frac{4\lambda_{ds}}{D_c \ln\frac{X_C}{X(t)}} \qquad 6\text{-}17$$

Replacing $D_{wz}(t)$ in equation 6-9, then, the overall heat transfer coefficient, α_i, is given by

$$\frac{1}{\alpha_i} = \frac{1}{\alpha_{ws}} + \frac{1}{4\lambda_{ds}}D_{wc}\ln\frac{X_C}{X(t)} \qquad 6\text{-}18$$

Hence, the solvent content against time for the wet-cake during the falling-rate period is written as follows:

$$\frac{dX}{dt} = -\frac{A(T_{wi}\text{-}T_B)}{m_{ds}\Delta H_v}\left[\frac{1}{\frac{1}{\alpha_{ws}} + \frac{D_c}{4\lambda_{ds}}\ln\frac{X_C}{X(t)}}\right] \qquad 6\text{-}19$$

6.2.2 Agitated Bed Drying

6.2.2.1 Constant-rate period

During constant-rate period, the powder bed was stirred and the wet materials were continuously exposed to the heating surface. In this case, all the wet particles had even chances to direct contact with the hot surface. Hence, the heat transfer area of agitated bed was far more than that of static bed. An effective heat transfer coefficient is used here to represent the realistic contact area. The drying rate $\dot{m}_{v,agg}$ increased as agitation applied, hence, the drying rate equation was rewritten as follows:

$$\alpha_i A(T_{wi} - T_B) = \dot{m}_{v,agi}\Delta H_v \qquad 6\text{-}20$$

To solve the rate of mass transfer for vapour phase, the penetration model was applied, the details of this model was described in section 3.3.2.

6.2.2.2 Falling-rate period

For the falling-rate period, the solvent content changed from one fictitious rest step (i) to the next one (i+1) was assumed to take place by instantaneous perfect mixing. Consequently, the local solvent content at the beginning of the next (i+1) rest step may be calculated by the following relation:

$$X_{vf}(i+1) = X(i+1) \qquad 6\text{-}21$$

The duration of the fictitious static period, t_R, the mixing number N_{mix} can be found in the following equations:

$$N_{mix} = CFr^n \qquad 6\text{-}22$$

$$Fr = \frac{(2\pi n)^2 D_w}{2g} \qquad 6\text{-}23$$

$$t_R = \frac{N_{mix}}{u_R} \qquad 6\text{-}24$$

Here the mixing number related constants are shown as follows, the paddle type of drying is used in this case [91].

$C = 9$, $n = 0.05$.

Hence for different stirring speed u_R, the mixing number is given by

u_R	N_{mix}	t_R
10	9.12	1.01

20	9.50	0.47
30	10.18	0.30

each interval of drying t_R from static bed solvent content X_{i-1} to agitated bed solvent content X_i , using the same deduction developed for the relationship between the solvent content and diameter of wet-zone deducted previously, the diameter of wet-zone D_{wz} for agitated bed is expressed as follows:

$$D_{wz}(t) = D_c\sqrt{\frac{X_i}{X_{i-1}}} \qquad 6\text{-}25$$

Hence, the thermal contact heat transfer coefficient of dry solid can be written as

$$\alpha_{ds} = \frac{4\lambda_{ds}}{D_c \ln\left(\frac{X_i}{X_{i-1}}\right)} \qquad 6\text{-}26$$

Hence, the energy balance at the vaporization front for agitated bed is expressed by the following equation:

$$\frac{\left(T_{wi}\text{-}T_B\right)}{\frac{1}{\alpha_{ws}} + \frac{D_c}{4\lambda_{ds}}\ln\left(\frac{X_i}{X_{i-1}}\right)} = \dot{m}_v \Delta H_v \qquad 6\text{-}27$$

To solve this equation, the iterative method is used to solve the nonlinear differential equation of agitated bed drying process.

6.2.2.3 Boundary conditions

The heat power used in this case is 128, 144, 157 Watts respectively. The quiescent air temperature is 15 °C. The pressure at the headspace is set at 170 mbar. The thermal conductivity of the dry aspirin is 0.01 W/(m·K) [85]. The equation for constant-rate period and falling-rate period is different for the varied heat transfer coefficient. The solvent content as the variable is the function of time in the process and is solved by the following equations.

6.2.3 DPM for a static bed

6.2.3.1 Introduction

The distributed-parameter model originally developed by Kohout et al. [53] and then further examined for the scale-up of vacuum contact drying by Murru et al. [1]. Now it is implemented in gPROMS software by PSE

company. The model combines a mathematical model of vacuum contact drying, based on differential transient heat and energy balances. This model needs to fit three parameters include Evaporation rate constant k_{vap} , Proportionality constant k_{pro} and residual saturation v_r . The parameter estimation needs to be obtained by small-scale experimental tests.

6.2.3.2 Assumptions

The model is based on differential mass and energy balances in the wet-cake of specified geometry, whereby the wet-cake is regarded as a stationary porous solid with constant porosity but spatially and temporally variable moisture content (pore saturation) and temperature (Figure 6.4)

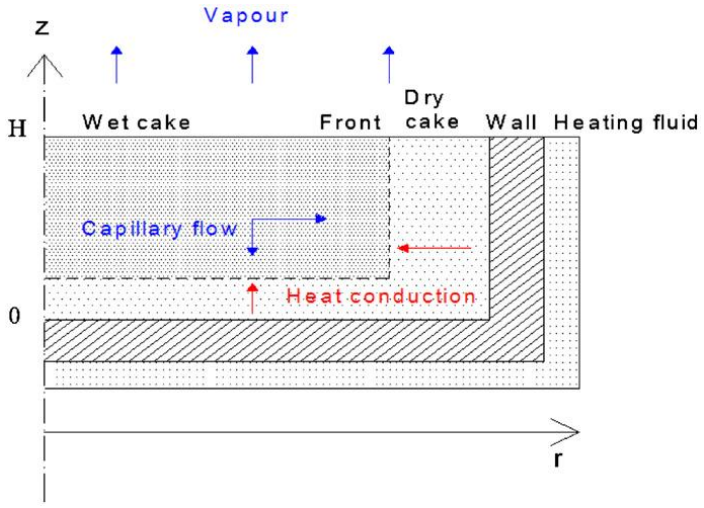

Figure 6.4 The scheme of heat and mass transfer during static vacuum contact drying in Nutsche filter dryer with axial symmetry offer by [1]

The principal model assumptions are:

- Mass vapour is free to flow within the pores wet-cake so that the mass transfer for the vapour phase is not the rate-limiting step.
- The mass transfer for the liquid-phase through the cake is described by the Richards equation with a linear approximation for the dependence of the apparent moisture diffusion coefficient on the moisture content.
- There is only conduction heat transfer and the heat dissipation is by evaporation with no other heat losses.
- The cake parameters include bed porosity and transport properties are spatially homogeneous and scale-independent.
- There is no solvent–solid interactions are considered.

- The liquid evaporation is described by a kinetic model assuming that the driving force is proportionally to a difference between the equilibrium and actual local vapour pressure.
- The physical properties of all materials are constant during drying and spatially homogeneous.

6.2.3.3 Model equations

The partial differential equations of a mass balance in the liquid phase and an energy balance on the cake (liquid and solid), which are coupled by a kinetic expression for the evaporation rate.

The mass balance for the liquid Phase is given by:

$$\frac{\partial v_l}{\partial t} = \nabla\left(\kappa_D \nabla v_l\right) - \frac{\dot{m}_v}{\rho_l} \qquad 6\text{-}28$$

The energy balance for the liquid Phase is expressed as:

$$\left\langle \rho C_p \right\rangle \frac{\partial T}{\partial t} = \nabla\left(\lambda_{eff} \nabla T\right) - \dot{m}_v \Delta H_v \qquad 6\text{-}29$$

ϑ_l (dimensionless) is the liquid phase volume fraction, T is temperature, t is time, $\kappa_D\left(\mathrm{m^2\ s^{-1}}\right)$ is the apparent liquid phase diffusion coefficient (more on this coefficient below), $\lambda_{eff}\left(\mathrm{W\ m^{-1}\ K^{-1}}\right)$ is the effective thermal conductivity, ρ is the liquid phase density, $\rho C_p\left(\mathrm{J\ m^{-3}\ K^{-1}}\right)$ is the mean volumetric heat capacity, ΔH_v is the latent heat of vaporisation, and $\dot{m}_v\left(\mathrm{kg\ m^{-3}\ s^{-1}}\right)$ is the local evaporation rate.

The evaporation rate is postulated to be proportional to the difference between the prevailing and equilibrium vapour pressure:

$$\dot{m}_v = \begin{cases} k_{vap}\rho_l\left(P_{sat} - P_g\right)/P_g & \text{if } \vartheta_l > 0 \\ 0 & \text{if } \vartheta_l \le 0 \\ 0 & \text{if } P_{sat} \le P_g \end{cases} \qquad 6\text{-}30$$

where $k_{vap}\left(\mathrm{s^{-1}}\right)$ is a rate constant, $P_g\left(\mathrm{Pa}\right)$ is the actual local vapour pressure, and $P_{sat}\left(\mathrm{Pa}\right)$ is the vapour pressure that would be in equilibrium with the local temperature. $P_{sat}\left(\mathrm{Pa}\right)$ can be evaluated from the Antoine equation. In this model, it is assumed that zero resistance to vapour phase mass transfer, hence the vapour phase pressure $P_g\left(\mathrm{Pa}\right)$ is constant and equal to the head-space pressure in all points of the gas phase.

To complete the set of governing equations, the mean volumetric heat capacity is calculated from the pure components and the phase volume fractions according to

The mean volumetric heat capacity is calculated from the pure components and the phase volume fractions according to

$$\left\langle \rho C_p \right\rangle = v_l \rho_l C_{p,l} + v_s \rho_s C_{p,s} + v_g \rho_g C_{p,g} \qquad 6\text{-}31$$

The phase volume fractions satisfy the following equations:

$$v_l + v_s + v_g = 1 \qquad 6\text{-}32$$

The local dependence of the effective thermal conductivity on the solvent content is calculated from the thermal conductivity of the dry and fully liquid-saturated porous medium (filter cake) using an expression proposed by [92]

$$\lambda_{eff} = \lambda_{ds} + \frac{v_l}{1 - v_s}\left(\lambda_{ws} - \lambda_{ds}\right) \qquad 6\text{-}33$$

Assuming capillary flow dominate mechanism of liquid phase migration in the filter cake, the mass flux of the liquid phase is given by Darcy's law

$$j_l = -\frac{\rho_l}{\mu_l} k(v_l) \nabla P_l \qquad 6\text{-}34$$

where $\kappa_P(\vartheta_l)[\mathrm{m}^2]$ is the relative permeability, μ_l $[\mathrm{Pa\,s}]$ is the liquid viscosity, and $P_l[\mathrm{Pa}]$ is the liquid phase vapour pressure, related to the gas-phase pressure through the capillary pressure P_C ,

$$P_C(v_l) = P_g - P_l \qquad 6\text{-}35$$

The apparent moisture diffusivity in the unsaturated porous media is expressed by:

$$D_l(v_l) = \frac{\kappa_P(v_l)}{\mu_l}\left(-\frac{\partial P_C(v_l)}{\partial v_l}\right) \qquad 6\text{-}36$$

A simple two-parameter linear relationship for apparent moisture diffusivity is given by

$$\kappa_D = \begin{cases} k_{pro}\left(v_l - v_l^*\right) & \text{if } v_l \geq v_l^* \\ 0 & \text{if } v_l < v_l^* \end{cases} \qquad 6\text{-}37$$

where v_l^* is the residual saturation for which the capillary pressure diverges and k_{pro} is a proportionality constant. Both adjustable parameters have to be

determined by fitting lab-scale experimental data but should be preserved upon scale-up.

6.2.3.4 The Boundary Condition for distributed-parameter model

At the centre of the cake $(\mathrm{r}=0)$,

$$\frac{\partial v_l}{\partial r}=\frac{\partial T}{\partial r}=0 \qquad 6\text{-}38$$

At the side and bottom walls area $(\mathrm{r}=\mathrm{R}\ \text{and}\ \mathrm{z}=0)$,

$$\frac{\partial v_l}{\partial r}=0 \text{ or } \frac{\partial v_l}{\partial \mathrm{z}}=0 \qquad 6\text{-}39$$

$$-\lambda_{eff}\frac{\partial T}{\partial r}=-\alpha_i\left(T_w-T\right) \text{ or } -\lambda_{eff}\frac{\partial T}{\partial \mathrm{z}}=\alpha_i\left(T_w-T\right) \qquad 6\text{-}40$$

At the top the filter cake $(\mathrm{z}=\mathrm{H})$,

$$\frac{\partial v_l}{\partial \mathrm{z}}=\frac{\partial T}{\partial \mathrm{z}}=0 \qquad 6\text{-}41$$

6.2.4 The link between LPM and DPM

There is so much similarities between the lumped- and distributed-parameter model, they are compared as follows: the temperature and solvent content used in the distributed-parameter model is spatially distributed and by set these two variables dimensionless, the heat transfer equations have the similar form. The fitting parameter of saturation rate constant is much similar to the critical solvent content in lumped-parameter model but the mechanisms behind them are different. However, it is different way to solve these two models, in addition, the lumped-parameter model needs much shorter time to get the simulation results compare to the distributed-parameter model .

6.3 Through-circulation convective drying

6.3.1 Introduction

In through-circulation drying in an agitated filter dryer, preheated hot nitrogen or hot air is passed downwards through a fixed bed of wet granular solids. Convective heat is continuously supplied from the hot gas and contact heat is supplied from the heating jacket, in the two heat transfer processes, the drying process may be divided into two stages the constant- and falling-rate period. The granular solids sedimentated on a filter plate so that the inlet dry

gas passes through the open spaces or voids between the solid particles and the moisture is carried away via the flowing gas passing though. At the same time, the heat could also be provided from external heating wall in order to . The temperature of the wet-cake starts to increase. At the same time, the nitrogen starts to flow through the bed from top to bottom. The schematic of drying process is showed in Figure 6.5 that while a hot nitrogen flows through a packed bed plug flow of the wet-cake as well as uniform radial temperature distribution in the wet-cake. The solvent vapour is removed by the hot nitrogen with a higher humidity than inlet gas humidity. Assumptions are made as follows.

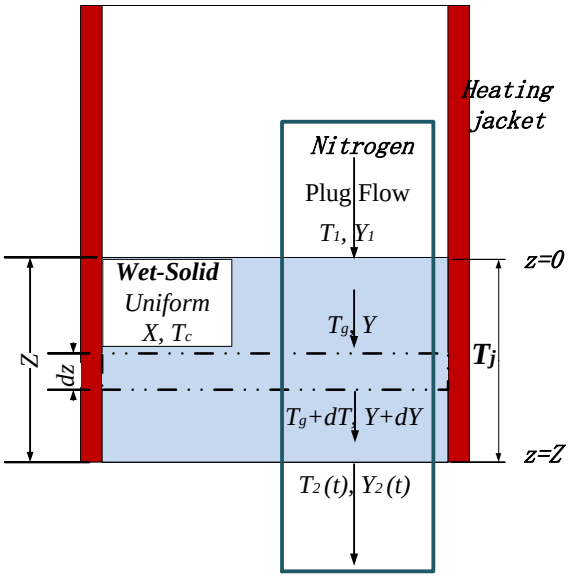

Figure 6.5 Mass and energy balances in an agitated filter dryer with through circulation if nitrogen through a wet-cake of solids

6.3.2 Assumption

- Gas flow from the inlet to outlet in the dryer is of plug type. In the gas phase, temperature and humidity gradient exist along the axial direction but uniformly distribute along the radial direction.
- In the solid phase, the temperature and solvent content are uniform throughout the bed and are only functions of time.
- Mass transfer of solvent in the gas phase by diffusion in the axial direction is neglected.
- There is no radiation heat transfer.
- No heat loss is considered in this system from the jacketed vessel to the atmosphere.

6.3.3 Derivation of model equations for combined convective and contact heating

In order to solve the problems regarding the mass balance and energy balance for convective drying process, take the whole system as two combined phases: gas phase and solid phase.

6.3.3.1 Gas phase equations:

As shown in Figure 6.6, nitrogen or dry air enters the wet-cake at a temperature T_{g1} and humidity Y_1, leaves at T_{g2} and Y_2.

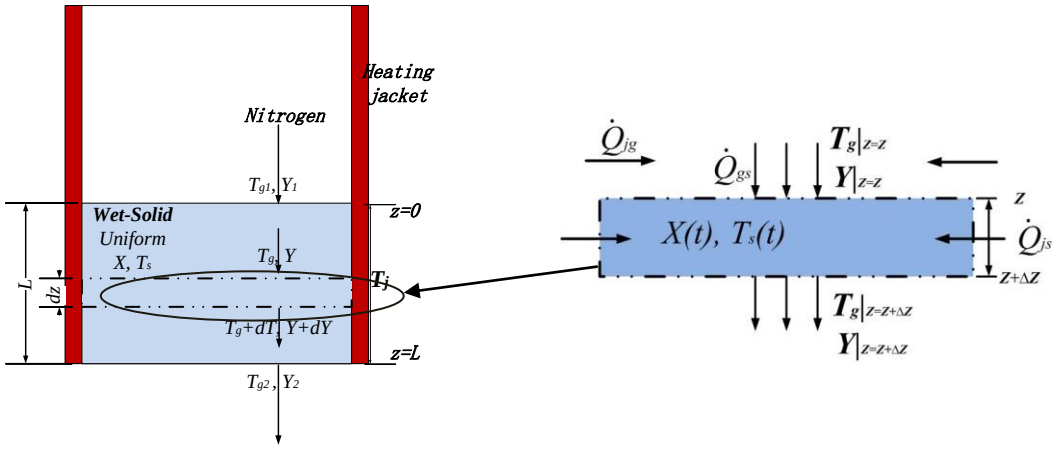

Figure 6.6 Mass and energy balances over a differential height dz at any location z within the gas phase

Mass balance equations

Due to the vapour pressure difference caused by the flowing gas within the open pores of the wet-cake, the vapour moved through the stagnant air film surrounded by the single wet particles. The driving force for convective drying is the water vapour pressure gradient between the drying surface and the main stream of the drying air.

Hence at any given location z, the amount of solvent removed from the wet-cake over a height differential height dz of the bed is equal to the difference of mass flux at the exit and entrance of the objected box shown in Figure 6.6. The rate of mass transfer can be expressed as follows [20]:

$$\begin{bmatrix}\text{Accumulation Rate}\\ \text{of solvent vapour}\end{bmatrix}=\begin{bmatrix}\text{Rate of input}\\ \text{of vapour}\end{bmatrix}-\begin{bmatrix}\text{Rate of output}\\ \text{of vapour}\end{bmatrix}+\begin{bmatrix}\text{Rate of generation}\\ \text{of vapour}\end{bmatrix}$$

$$0 = -\dot{G}A_{cs}dY + \dot{m}_v \frac{dz}{L} \qquad 6\text{-}42$$

where $\dot{G}\left[\mathrm{kg\,m^{-2}\,s^{-1}}\right]$, is the dry air flow; A_b, is the cross sectional area of the wet-cake; $\dot{m}_v = -m_{ds}\,dX/dt\left[\mathrm{kg\,s^{-1}}\right]$ is the drying rate of the cake.

The solvent vapour content changing against height differential dz in terms of solvent drying rate is given by:

$$\frac{\mathrm{d}Y}{\mathrm{d}z} = \frac{\dot{m}_v}{\dot{G}A_b L} = \frac{m_{ds}}{\dot{G}A_b L}\frac{\mathrm{d}X}{\mathrm{d}t} \qquad 6\text{-}43$$

Energy balance

For the process occurs at constant volume, at any given location z, an energy balance over a differential height between z and $z+dz$ yields:

$$\begin{bmatrix}\text{Accumulation rate}\\ \text{of total enthalpy}\end{bmatrix} = \begin{bmatrix}\text{Rate of input}\\ \text{of energy}\end{bmatrix} - \begin{bmatrix}\text{Rate of output}\\ \text{of energy}\end{bmatrix} + \begin{bmatrix}\text{Rate of generation}\\ \text{of vapour enthalpy}\end{bmatrix}$$

$$\dot{G}A_b\left(H_g\big|_{z+dz} - H_g\big|_z\right) = \left(d\dot{Q}_{gs} + d\dot{Q}_{jg} + d\dot{Q}_{js}\right) + \dot{m}_v\left(c_{p,v}T_g + \Delta H_v\right) \qquad 6\text{-}44$$

where $\dot{Q}_{gs}$ is the rate of heat transfer from hot gas to the wet solid; $\dot{Q}_{jg}$ and $\dot{Q}_{js}$ are the rate of heat transfer from the jacket to the gas and to the wet solid respectively.

In equation 6-50, the rate heat input and rate of enthalpy accumulated can be expressed as follows:

$$\dot{G}A_b\left(H_g\big|_{z+dz} - H_g\big|_z\right) = \dot{G}A_b dH_g$$

$$d\dot{Q}_{gs} + d\dot{Q}_{jg} + d\dot{Q}_{js} = \left[\alpha_{\mathrm{cov}}\left(T_g - T_s\right)A_S + \alpha_{jg}\left(T_j - T_g\right)A_w + \alpha_{jg}\left(T_j - T_s\right)A\right]\frac{dz}{L} \qquad 6\text{-}45$$

The enthalpy of humid gas per unit mass, H_g, is given by [10]:

$$H_g = \left(c_{p,dg} + Yc_{p,v}\right)T_g + Y\Delta H_v \qquad 6\text{-}46$$

where $c_{p,dg}$ is specific heat of drying gas and $c_{p,v}$ is specific heat of solvent vapour. Hence $c_{p,dg} + Yc_{p,v}$ represents the combined specific enthalpy of humid gas including dry gas and solvent vapour. Then enthalpy changes as differential height is expressed as:

$$\frac{dH_g}{dz} = \frac{d\left[\left(c_{p,dg} + Yc_{p,v}\right)T_g + Y\Delta H_v\right]}{dz} = \left(c_{p,dg} + Yc_{p,v}\right)\frac{dT_g}{dz} + \left(c_{p,v}T_g + \Delta H_v\right)\frac{dY}{dz} \qquad 6\text{-}47$$

By substituting the relative parameters using equations (6-48) and (6-52), (6-49) can be rewritten as:

$$\dot{G}A_b L\left(c_{p,dg}+Yc_{p,v}\right)\frac{dT_g}{dz}=\alpha_{gs}\left(T_g-T_s\right)A_S+\alpha_{jg}\left(T_j-T_g\right)A_w+\alpha_{jg}\left(T_j-T_s\right)A \qquad 6\text{-}48$$

6.3.3.2 Wet solid phase equations

Mass balance

The mass balance on the moisture in the wet solid phase at any location, z, is given by:

$$\frac{dX}{dt}=-\frac{\dot{m}_v}{m_{ds}} \qquad 6\text{-}49$$

where $A_S\left[\mathrm{m}^2\right]$ is the surface area of the solid particle; $\alpha_{gs}\left[\mathrm{Wm^{-2}K^{-1}}\right]$ is the convective heat transfer coefficient; $T_W\left[\mathrm{K}\right]$ is the wet bulb temperature.

Heat transfer equations

The energy balance for wet solid phase is given by:

$$\begin{bmatrix}\text{Rate of accumulation}\\ \text{of enthalpy}\end{bmatrix}=\begin{bmatrix}\text{Rate of input}\\ \text{of energy}\end{bmatrix}-\begin{bmatrix}\text{Rate of output}\\ \text{of energy}\end{bmatrix}-\begin{bmatrix}\text{Enthalpy of vapour}\\ \text{leaving the wet solid}\end{bmatrix}$$

$$m_{ds}\frac{\left(H_{ws}\big|_{in}-H_{ws}\big|_{out}\right)}{\Delta t}=\dot{Q}_{gs}+\dot{Q}_{jg}+\dot{Q}_{js}-\dot{m}_v\left[c_{p,l}\left(T_v-T_s\right)+\Delta H_v+c_{p,g}\left(T_g-T_v\right)\right] \qquad 6\text{-}50$$

where $\dot{Q}_{gs}$ is the rate of heat transfer from hot gas to the wet solid, $\dot{Q}_{js}$ is the rate of heat transfer from jacket to the wet solid.

The specific enthalpy of wet solid H_s per unit mass of dry solid is defined as:

$$\dot{Q}_{gs}+\dot{Q}_{jg}+\dot{Q}_{js}=\alpha_{\mathrm{cov}}\left(T_g-T_s\right)A_S+\alpha_{jg}\left(T_j-T_g\right)A_{sw}+\alpha_{jg}\left(T_j-T_s\right)A_{eff} \qquad 6\text{-}51$$

The enthalpy of the solid is described as follows:

$$H_s=\left(c_{p,ds}+Xc_{p,l}\right)T_s \qquad 6\text{-}52$$

Then the enthalpy changed with time in the wet solid can be expressed as

$$\frac{\left(H_{ws}\big|_{in}-H_{ws}\big|_{out}\right)}{\Delta t}=\frac{dH_s}{dt}=\left(c_{p,ds}+Xc_{p,l}\right)\frac{dT_s}{dt}+c_{p,l}T_s\frac{dX}{dt} \qquad 6\text{-}53$$

where $c_{p,ds}$ is the specific heat of dry solid, while $c_{p,l}$ is specific heat of the solvent liquid. Combining the equations (5.56), (5.57) and (5.59):

$$m_{ds}\left(c_{p,ds}+Xc_{p,l}\right)\frac{dT_s}{dt}+m_{ds}c_{p,l}T_s\frac{dX}{dt}+\dot{m}_v\left[c_{p,l}\left(T_v-T_s\right)+\Delta H_v+c_{p,g}\left(T_g-T_v\right)\right]$$
$$=\alpha_{\mathrm{cov}}\left(T_g-T_s\right)A_S+\alpha_{jg}\left(T_j-T_g\right)A_{sw}+\alpha_{jg}\left(T_j-T_s\right)A_{eff} \qquad 6\text{-}54$$

The temperature of wet solid changes with time is obtained and the equations above can be solved by solving the following equations:

$$m_{ds}\left(c_{p,ds}+Xc_{p,l}\right)\frac{dT_s}{dt}=\alpha_{\mathrm{cov}}\left(T_g-T_s\right)A_S+\alpha_{jg}\left(T_j-T_g\right)A_{sw}+\alpha_{jg}\left(T_j-T_s\right)A_{eff}$$
$$-\dot{m}_v\left[c_{p,l}T_v+\Delta H_v+c_{p,g}\left(T_g-T_v\right)\right] \qquad 6\text{-}55$$

6.3.3.3 Boundary conditions

Initial conditions at $t=0$:

- The temperature of wet-cake at the beginning equals to the room temperature of the wet solid: $T_s=T_{so}$
- The solvent content of wet-cake at the beginning equals to initial solvent content: $X=X_o$

At the inlet, $z=0$ (at the top surface of the wet-cake), following boundary conditions are applicable:

- The temperature of gas at the top surface of the wet-cake equals to inlet gas temperature: $T_g=T_{g1}$
- The solvent vapour content of gas at the top surface of the wet-cake equals to vapour content of dry gas which is zero: $Y=Y_1=0$

6.3.3.4 Solution techniques

There is a totally of four variables:

$$Time\,dependent\begin{cases}T_s=f_n(Time)\\X=f_n(Time)\end{cases}\qquad Height\,dependent\begin{cases}T_g=f_n(Height)\\Y=f_n(Height)\end{cases}$$

Four equations derived for these variables.

$$\frac{dY}{dz}=\frac{\dot{m}_v}{\dot{G}A_bL} \qquad 6\text{-}56$$

$$\dot{G}A_bL\left(c_{p,dg}+Yc_{p,v}\right)\frac{dT_g}{dz}=\alpha_{gs}\left(T_g-T_s\right)A_S+\alpha_{jg}\left(T_j-T_g\right)A_{sw}+\alpha_{jg}\left(T_j-T_s\right)A_{eff} \qquad 6\text{-}57$$

$$\frac{dX}{dt} = -\frac{\dot{m}_v}{m_{ds}} \qquad 6\text{-}58$$

$$m_{ds}\left(c_{p,ds} + Xc_{p,l}\right)\frac{dT_s}{dt} = \alpha_{gs}\left(T_g - T_s\right)A_S + \alpha_{jg}\left(T_j - T_g\right)A_w + \alpha_{jg}\left(T_j - T_s\right)A_{eff} - \dot{m}_v\left[c_{p,l}T_v + \Delta H_v + c_{p,g}\left(T_g - T_v\right)\right] \qquad 6\text{-}59$$

6.3.3.5 The fully convective drying model

Since a lumped-parameter model of combining of convective N_2/air drying with conduction heat has been developed, the model validation without conduction heat is less complicated. To develop convective drying equations, the terms related to contact heating in the equations in previous section can be dismissed. Then the equations for the convective drying model are given by:

$$\frac{dY}{dz} = \frac{\dot{m}_v}{\dot{G}A_b L} \qquad 6\text{-}60$$

$$\dot{G}A_b L\left(c_{p,dg} + Yc_{p,v}\right)\frac{dT_g}{dz} = \alpha_{gs}\left(T_g - T_s\right)A_S \qquad 6\text{-}61$$

$$\frac{dX}{dt} = -\frac{\dot{m}_v}{m_{ds}} \qquad 6\text{-}62$$

$$m_{ds}\left(c_{p,ds} + Xc_{p,l}\right)\frac{dT_s}{dt} = \alpha_{gs}\left(T_g - T_s\right)A_S - \dot{m}_v\left[c_{p,l}T_v + \Delta H_v + c_{p,g}\left(T_g - T_v\right)\right] \qquad 6\text{-}63$$

These four coupled differential equations will be solved together with the above boundary conditions using an appropriate numerical method in gPROMS programme.

6.3.3.6 The simplified convective drying model

A further simplification in the equations developed for the full convective drying model can be made to improve computing efficiency.

For the constant-rate period, it is assumed that the wet solid temperature is constant $\left(dT_s/dt = 0\right)$ at wet bulb temperature, T_W. In addition, the solvent vaporised at wet bulb temperature that is the vapour temperature here $T_v = T_W$. Hence the drying rate is expressed as:

$$\dot{m}_{vc} = \frac{\alpha_{gs}\left(T_g - T_W\right)A_S}{c_{p,l}T_W + \Delta H_v + c_{p,g}\left(T_g - T_W\right)} \qquad 6\text{-}64$$

where $\dot{m}_{vc}$ is the drying rate in the constant-rate period, the convective heat transfer coefficient between solid and gas , α_{cov} , can be obtained by [75, 76, 93]:

The solvent content, X , changes with time t during the constant-rate period is given by (6-66):

$$\frac{dX}{dt} = -\frac{\alpha_{gs}\left(T_g - T_W\right)A_S}{m_{ds}\left[c_{p,l}T_W + \Delta H_v + c_{p,g}\left(T_g - T_W\right)\right]} \qquad 6\text{-}65$$

For the falling-rate period, based on an empirical approach, it is assumed that the drying rate $\dot{m}_{vf}$ is a linear function of solvent content X through the equilibrium solvent content at X_e:

$$\frac{\dot{m}_{vc} - \dot{m}_{vf}}{\dot{m}_{vc}} = \frac{X_C - X}{X_C - X_e} \Rightarrow \dot{m}_{vf} = \dot{m}_{vc}\frac{X - X_e}{X_C - X_e} \qquad 6\text{-}66$$

$\dot{m}_{vc}$ can be replaced using equation (6-66):

$$\dot{m}_{vf} = \frac{\alpha_{gs}\left(T_g - T_W\right)A_S}{c_{p,l}T_W + \Delta H_v + c_{p,g}\left(T_g - T_W\right)}\frac{X - X_e}{X_C - X_e} \qquad 6\text{-}67$$

6.3.4 Boundary conditions

Following boundary conditions are applicable at $t = 0$ (at the beginning of drying process), $z = 0$ (at the surface of the wet-cake) and $z = H$ (at the bottom of the wet-cake).

$t = 0$, $z = 0$:

The gas temperature is equal to the temperature of inlet dry gas

$$T_g\left(t = 0, z = 0\right) = T_{in} \qquad 6\text{-}68$$

The initial gas humidity is equal to the humidity of inlet dry gas

$$Y\left(t = 0, z = 0\right) = Y_{in} \qquad 6\text{-}69$$

The initial solid temperature is equal to the room temperature of wet solid

$$T_{ws}(t=0) = T_{room-temperature} \qquad 6\text{-}70$$

The initial solvent content is equal to the solvent content of wet solid

$$X(t=0) = X_o \qquad 6\text{-}71$$

At the top of the filter cake

$$T_g(z=H) = T_{ws} \qquad 6\text{-}72$$

6.4 **The Solution technique**

The equation type for the lumped-parameter drying model is first-order nonlinear ordinary differential equations which can be solved based on variable time step/variable order Backward Differentiation Formulae (BDF). This has been proved to be efficient for a wide range of problems. The solution software used in this work is gPROMS from PSE.

6.5 **Conclusions**

The work presented in this chapter is focused on development of a one dimensional numerical model for demonstrating the effects of contact drying in an agitated filter dryer as well as a two dimensional model for convective drying by incorporating the vaporization front assumptions for falling-rate period and penetration model for agitated bed drying.

The LPM for vacuum contact drying is developed. In this model, only one parameter critical solvent content needed to be fitted from experimental curves, if the drying starts below the critical solvent content, then no parameter estimation needed, the drying time can be calculated from this LPM directly. The advantages of this model not only lie on its computational expedient characteristic with a relative reliable prediction, but also can be applied to any preliminary drying, no specific software needed for calculation.

Conduction heat supplied from the side wall and convection heat transfer from the hot air to wet-cake are modelled for AFD. The convective heat transfer through radial and axial direction of the bed were considered.

The critical solvent content is obtained from the parametric study to those of experiments performed under similar conditions.

The model was validated by comparing the calculated curves obtained from gPROMS implementation with the experimental data of the bench-scale AFD. The validation results was described in Chapter 8 and 9.

Chapter 7
Experimental results on TGA

7.1 Introduction

This chapter describes the small scale TGA drying experimental results. To investigate the heat and mass transfer mechanisms, small-scale experiments were carried out using TGA while medium-scale drying performances were investigated using a 5-L lab-scale AFD in section 8 and 9.

For small-scale thermal analysis instrument, the effects of temperature, pressure as well as particle size distribution on drying behaviour were investigated. Meantime, the pure water and ethanol as well the mixed solvents were also examined. The reproducibility and drying curves together with sample temperature changing with solvent content were all plotted to help understand the drying mechanisms. To further comparing the scale-up drying systems, the instrumentation of vacuum pump with TGA providing a fast and reliable data collection for vacuum contact drying. The data collected from TGA were used for basic parameter estimation of drying behaviour and understanding of heat and mass transfer mechanisms. The scale-up experiments were used for model validation and further parameter estimation. Thermal analysis of aspirin powders

In order to fully understand the thermal behaviour of aspirin, small-scale thermal analysis instrument has its advantages for very small amount of material is used in the experiment. In this section, the thermal properties and drying behaviour of aspirin were examined by DSC and TGA instrument respectively. The effects of temperature, solvent types as well as particle sizes were investigated in this work.

7.2.1 DSC: Thermal decomposition

The decomposition temperature of aspirin was obtained by setting a series of heating programs in DSC and then by observing the reproducibility of cycling curve for the first round and second round. The DSC curve in Figure 7.1 shows that the thermal behaviour corresponding to three different cycling heating programs. The heating method was set to heat up from the room temperature with a heating rate at 10ºC/min to 110 ºC, 120 ºC and 130 ºC

and repeat the temperature program again. Figure 7.1 (c) shows that the second heat flow curve was not coincidence with the first. The gap between the two cycles means that the aspirin crystals were damaged somehow due to the first heating history up to a comparatively high temperature at 130 ºC. While for lower temperatures at 110 ºC and 120 ºC, the heating curve for the second cycle was totally superimposed on the first one in Figure 7.1 (a) and (b) which indicates that the aspirin molecule has not been deteriorated yet. From the discussion above, the decomposition temperature of aspirin could be speculated to a value between 120 ºC and 130 ºC. Hence, for the following TGA and lab-scale AFD tests, all the experimental results would be reliable by performed set the operating condition well below 70º during the drying process.

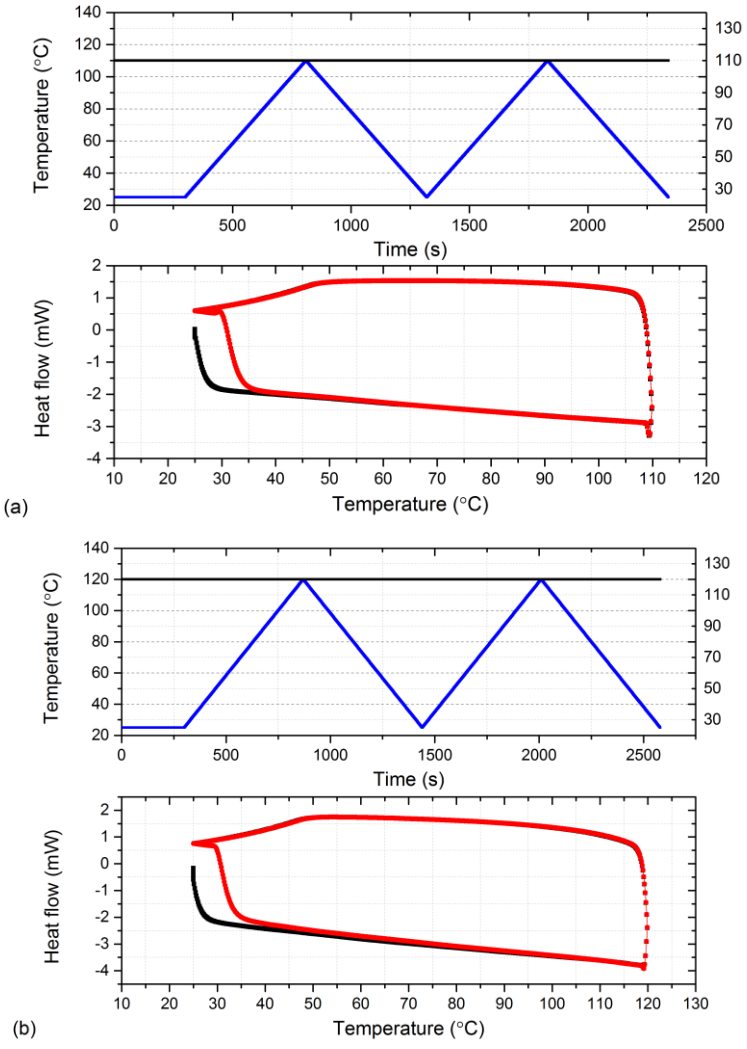

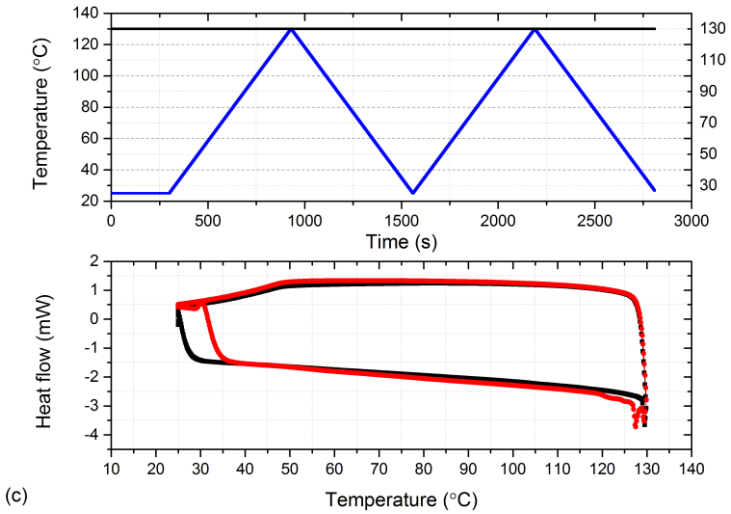

Figure 7.1 DSC temperature programs (——): two cycles at (a) 110ºC, (c) 120ºC (c) 130ºC with corresponding DSC curves for the first loop (——) and second loop (——) using aspirin dry powders as test material

7.1.1 Error of TGA: Reproducibility of data

The aim of this section was to evaluate the reproducibility the drying experiment conducted by TGA, lab-scale AFD as well as particle analysis. For mixed solvents drying using TGA, six solvent ratios covered 0%, 20%, 40%, 60%, 80% and 100% ethanol in water were chosen. For each solvent ratio, five experiments were carried out under the exact same operating conditions and the temperature was all set to 40 °C. The TGA drying tests of mixed solvent systems were done by a MEng project student, and included in Samal Mukayeva's dissertation [94]. The results were shown in Figure 7.2.

It can be seen that the drying curve for the pure solvent drying is quite replicable in Figure 7.2 (a) and (f). There are five colourised lines for each plot representing the five repeatable experiments carried out under the same operating conditions. While for the mixed solvents drying ranging from 20% to 80% ethanol aqueous solution the reproducibility is not good and the reason for that is due to the high volatility and lower boiling point of ethanol rather than water. Furthermore, due to the high volatility of ethanol, although the initial solvent content were intended to maintain at 150%, the solvent content at the beginning of drying may vary from batch to batch. It was found to be quite unstable for the moisture wet-cake that was rich in ethanol. The ethanol volatilized easily and fast considering the sampling and transferring period the ratio might be varied from the designed initial solvent mixtures. Volatility is the tendency of a substance to vaporize. Volatility is directly

related to a substance's vapour pressure. At a given temperature, a substance with higher vapour pressure vaporizes more readily than a substance with a lower vapour pressure. The vapour pressure for water and ethanol at 40 °C is 7.38 kPa and 13.45 kPa respectively [95]. According the vapour pressure for the solvent it can be well understood that the non-repeatable characteristics due to the inevitable lost during the sample preparation and transferring process. All these manual operations can lead to the inconsistency of the experiment.

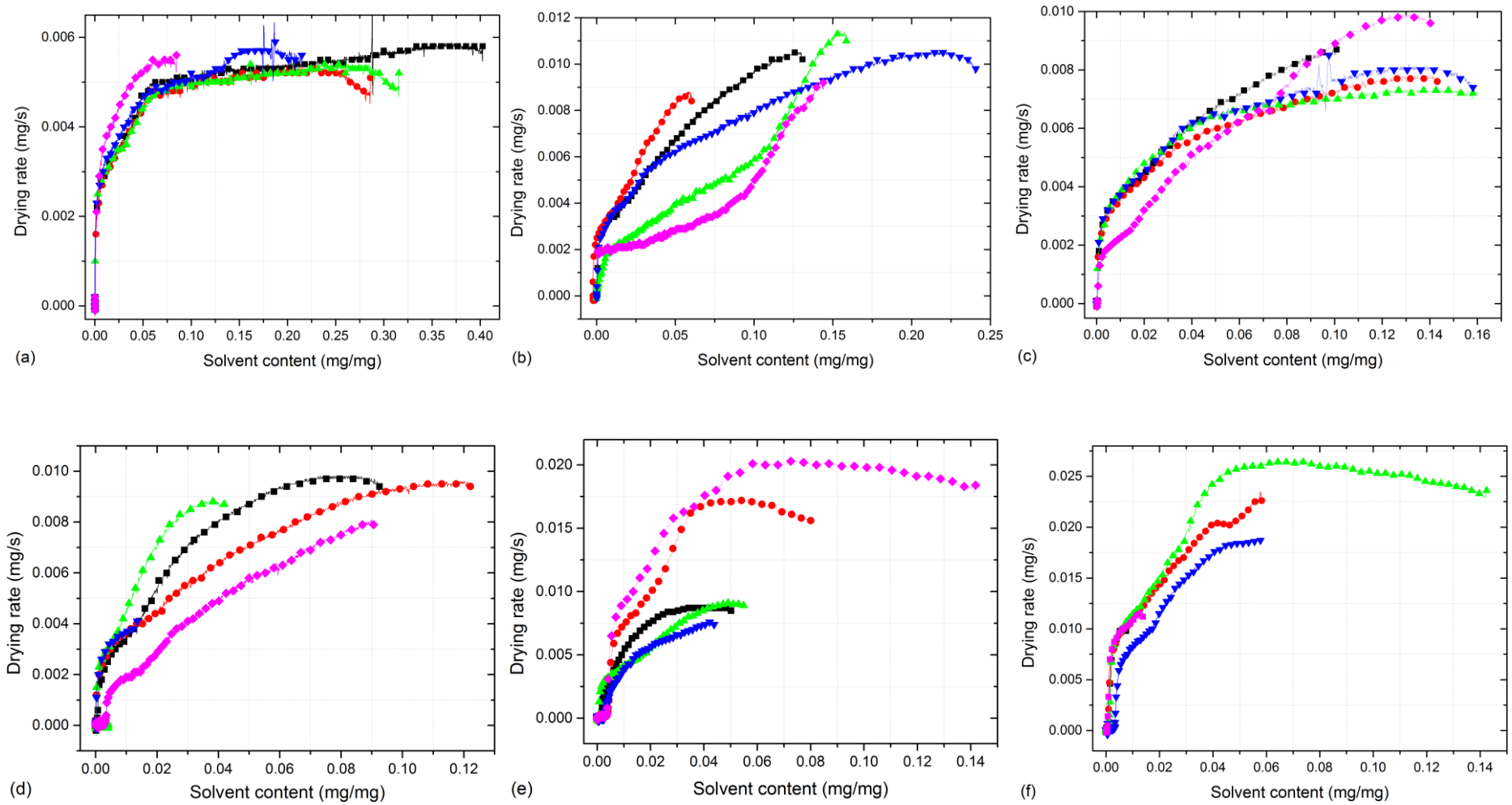

Figure 7.2 Investigation of reproducibility of drying rate versus solvent content at 40 °C at different solvent ratios: (a) 0% ethanol; (b) 20% ethanol; (c) 40% ethanol; (d) 60% ethanol; (e) 80% ethanol; (f) 100% ethanol

7.1.2 TGA: Effects of solvent type

In spite of the non-repeatable of mix solvent drying experiment, it is reasonable to pick the medium curve as the representative drying curve for each solvent ratio in that it neutralised the unsteady drying characteristic of ethanol and eliminated the extreme drying behaviour caused by the unstable liquid state of mixed solvents. The six drying curve were plotted together in Figure 7.3 for further comparison. Comparing the drying curves at different ratios it can be seen that the drying rate increases corresponding to the amount of ethanol in the mixture. The drying rate increased from 0.005 mg/s for pure water to 0.026 mg/s for pure ethanol. All the drying rates for mix solvents landed in between them. While the critical solvent content shifts to a smaller value by increasing the amount of ethanol in the mixture. The critical solvent content decreased from 0.065 for pure water to 0.02 for pure ethanol. It also can be observed that there is a ramping up period at the beginning of drying process for mixed solvents that are rich of ethanol (80% ethanol and pure ethanol). The reason for that is postulated that the higher solubility in ethanol than water leads to a recrystallization phenomenon which in turn restrain the drying the process. Hence the recrystallization process inclined the constant-rate drying rate to a slope.

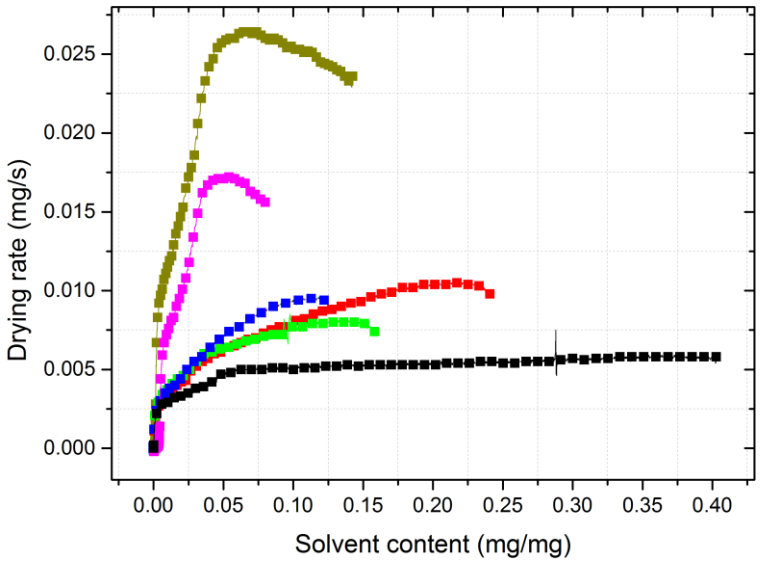

Figure 7.3 Drying rate versus solvent content at different solvent ratios: (a) 0% ethanol (——); (b) 20% ethanol (——); (c) 40% ethanol (——); (d) 60% ethanol (——); (e) 80% ethanol (——); (f) 100% ethanol (——)

Comparing the sample temperature against solvent content in Figure 7.3 the similar trends can be observed at different solvent ratios. As the vaporization of solvent progressed, the wet-cake becomes much drier during the drying

process. Apart from the appreciable loss of solvent weight, the vaporization has similar effect that that the baseline shifts in the exothermic direction due to the decreasing heat capacity of the sample corresponding to the increasing the ethanol content within the mix solvent.

The temperature of the wet-cake gradually increased to 44.5 °C when the wet-cake became bone-dry material. During the constant-rate period the surface of the solid covered by a film of mixed solvent, the vaporization of water and ethanol are occurred at the same time. The saturation temperatures for water and ethanol are different and it is lower for ethanol and higher for water. The samples with rich ethanol solvent mixture present a changing cake temperature in Figure 7.4c and d rather than a constant saturated temperature for rich water solvent system in Figure 7.4a and b during the constant-rate period. Hence, the sample temperature with rich ethanol solvent mixture in Figure 7.4c and d changes much faster than that in in Figure 7.4c and d.

Apart from the appreciable loss of weight, these reactions have another feature in common, namely that the baseline shifts in the exothermic direction due to the decreasing heat capacity of the sample.

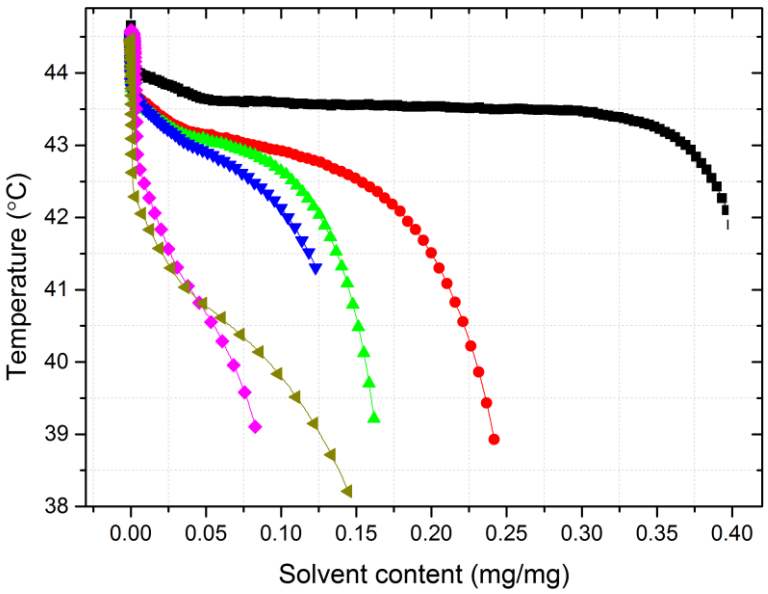

Figure 7.4 Temperature versus solvent content at different solvent ratios: (a) 0% ethanol (——); (b) 20% ethanol (——); (c) 40% ethanol (——); (d) 60% ethanol (——); (e) 80% ethanol (——); (f) 100% ethanol (——)

In order to better understand the mass and energy balance during the drying process, the heat flow for the wet-cake when drying progressed against solvent content were plotted in Figure 7.5. it can be seen that the heat flow become much faster from the constant-rate period to the falling-rate period for all the four solvent mixtures. For example, in Figure 7.5a, the heat flow before the transition point maintains at an average of 4 mW while beyond the transition point, the rate of heat transfer greatly reduced because of the decrease of the solvent content.

The critical solvent content is not only of material intrinsic property depending on the loads of material being dried, the rate of drying and the heat and mass transfer resistances of the wet solid [96, 97]. The critical solvent content only exists in the pure water drying but not observed in the mix solvent drying tests. The critical solvent content for 100% water is 0.065 (Figure 7.5a) and is 0.04 for 60% water mixture (Figure 7.5b) while it goes down to 0.025 for 60% ethanol mixture (Figure 7.5d) and 0.02 for 80% ethanol mixture (Figure 7.5d). Before the transition point, the heat is used for solvent vaporization. The vaporization of heat is 2408 kJ/kg for water while for ethanol is 846 kJ/kg at 40 °C. It can explain that the rate of heat transfer for water from the crucible wall to the wet-cake is much smaller (Figure 7.5a) than that of ethanol/water solvent mixture (Figure 7.5b, c and d).

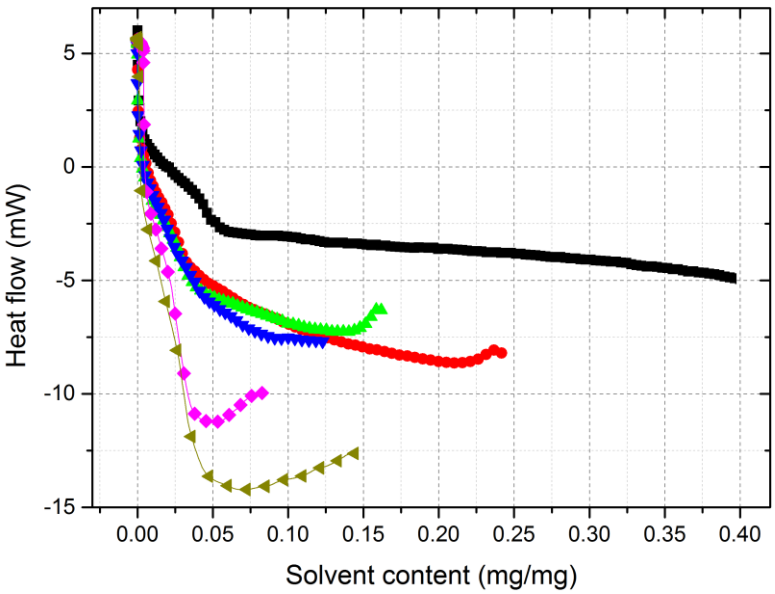

Figure 7.5 Heat flow versus solvent content at different solvent ratios: (a) 0% ethanol (——); (b) 20% ethanol (——); (c) 40% ethanol (——); (d) 60% ethanol (——); (e) 80% ethanol (——); (f) 100% ethanol (——)

7.1.3 TGA: Effects of furnace temperature

As discussed before, when use water as the drying solvent, the drying curve is comparatively reliable and repeatable. In addition, the decomposition point for aspirin is between 120 ºC and 130 ºC. Hence, five heating temperatures were chosen for testing the effects of temperature on drying ranging from 30 ºC to 70ºC and every interval for 10 ºC. To reduce the sensitivity to particle size, aspirin powders with particle size D_{50} at 275.7μm were used in this series of experiments. Figure 7.6 showed that the time needed to dry for each sample are 200 mins, 120 mins, 70 mins, 45 mins and 30 mins at 30, 40, 50, 60 and 70ºC respectively. Each drying test started from similar initial solvent content and dried to bone-dry products. It can be seen that less time was needed to dry at higher temperature.

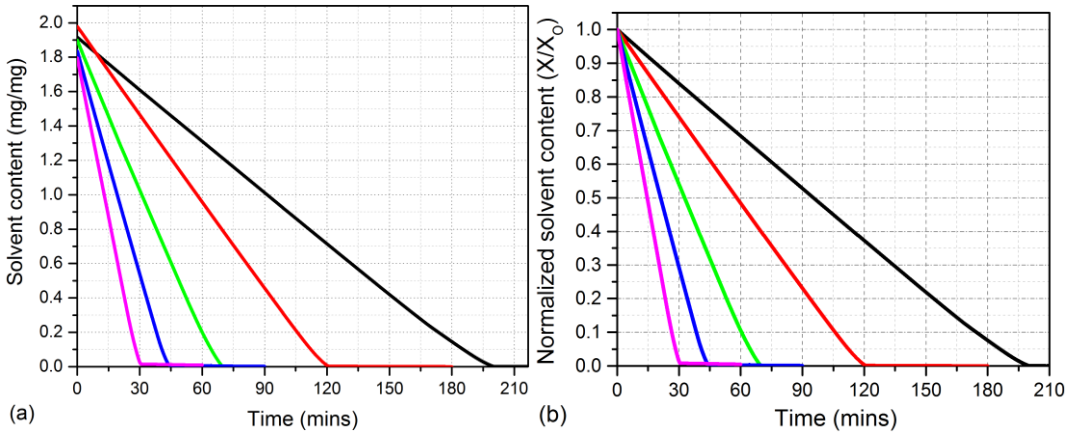

Figure 7.6 Plot of solvent content versus time (left) and normalized solvent content (Solvent content/Initial solvent content) versus time (right) with aspirin particle for D_{50}=275.7μm at 30 ºC (——), 40 ºC (——), 50 ºC (——), 60 ºC (——) and 70 ºC (——)

However, from Figure 7.7, as the temperature approaching to saturated temperature of the solvent, the degree of reduced amount of time for drying due to increasing temperature is not proportional to the degree of the growth of temperature.

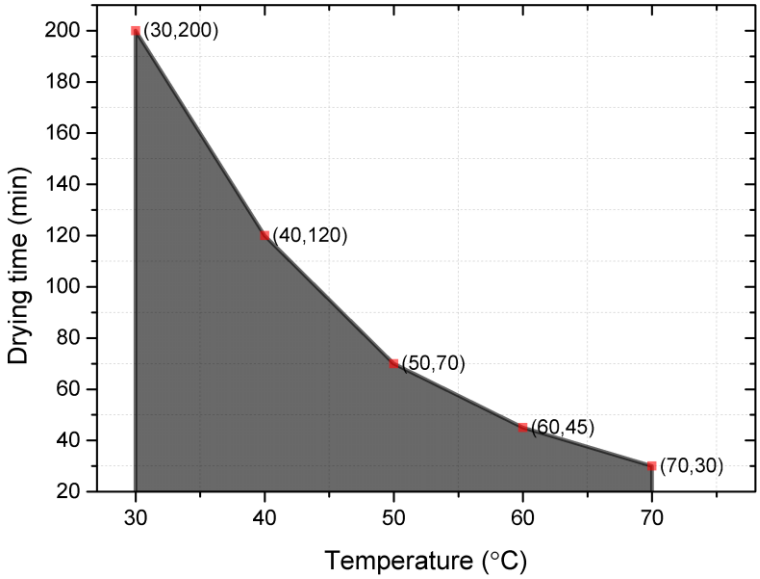

Figure 7.7 The tendency of time needed for drying aspirin particles (D_{50}=275.7μm) at different heating temperatures

Higher drying rate obtained from tests performed at higher temperature during the entire drying period shown in Figure 7.8. It can also been seen that the length of constant-rate period is apparently shorter at comparatively high temperature than that at lower temperature. The critical solvent content tends to shift to lower value as temperature decreased. The value of critical solvent content ranges from 0.3 at 70 ºC to 0.05 at 30 ºC. It can be deferred that aspirin crystals dissolved into solvent and recrystallized during vapour dissipated. At a higher temperature more and more small crystals tends to dissolve and when vaporization occurred, recrystallization from supersaturated solution made precipitated bigger particles as well as additive energy consumed leads to a shift of critical solvent content. The shift of size-dependent critical solvent content phenomenon can be proved in the following section.

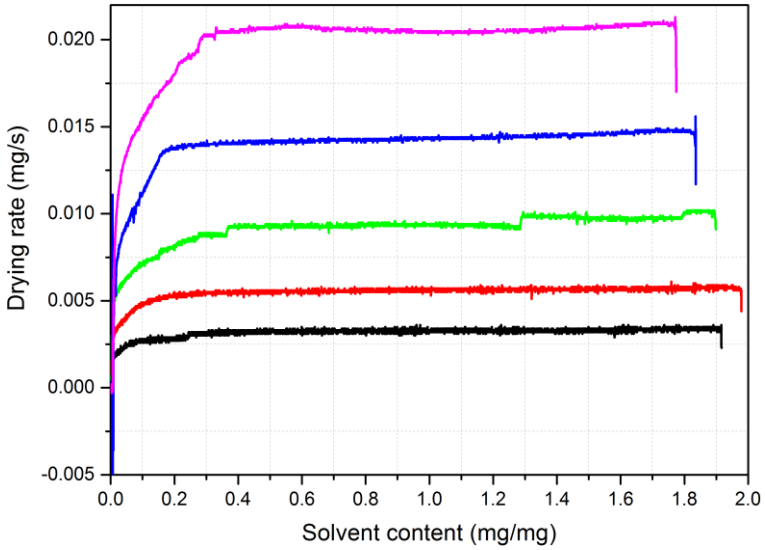

Figure 7.8 Plot of solvent content versus time (left) and normalized solvent content at 30 ºC (——), 40 ºC (——), 50 ºC (——), 60 ºC (——) and 70 ºC (——)

7.1.4 TGA: Effects of particle size distribution

Four batches of the aspirin samples obtained from crystallization at different cooling rate ranging from 0.1 °C/min to 1 °C/min were used for this investigation. The size properties of aspirin are given in Table 7.1.

Table 7.1 The size properties of aspirin crystalline powders

Cooling rate (ºC/min)	Concentration	Specific surface area (m^2/g)	D10 (µm)	D50 (µm)	D90 (µm)
1.0	7.75 g / 50ml Ethanol / water (38% in mole)	0.14	60.7	168.1	427.1
0.5		0.09	70.2	239.4	548.7
0.2		0.08	103.2	346.6	642.2
0.1		0.07	70.3	275.7	564.8

In order to investigate whether the critical solvent content is a particle size-dependent parameter, a series of particle sizes were tested with water and ethanol solvents. As can be seen in Figure 7.10 the drying rate for D_{50}=239.4 µm was found to be faster than particle with a D_{50}=275.7 µm at the beginning. However, the drying rate was found to slow down hindered by the recrystallization of aspirin by solvent evaporation. High solubility resulted more crystals dissolved in the solvent. The solubility of a particle increases as its size decreases according to the Gibbs-Thomson effect and it is described by [98]:

$$\ln\left[\frac{c(r)}{c^*}\right] = \frac{2M\gamma}{\nu RT\rho r} \qquad 6\text{-}66$$

where $c(r)$ is the solubility of particles at radius r, c^* is the normal equilibrium solubility, M is the molecular weight of the particle, R is the gas constant, T is the temperature, is the solid density, γ is the surface energy of the solid in contact with the solution.

The surface energy of the particle also plays an important role in the intermolecular force between the solid and solvent. As the particles precipitate, the ratio of surface area to cake volume becomes larger; the particle surface needs to adsorb more solvent molecules to cover the extra surface to maintain a certain surface energy (Figure 7.9). The solution becomes more saturated due to vaporization and more particles precipitated in the solid form from. This kinetic recrystallization process converted the unbound moisture inside the wet-cake to bound moisture so it made the solvent removal more difficult. More vaporization surface area dried faster; however, it is counteracted with recrystallization effects. For the particle size at 225.1 μm 168.1 μm the recrystallization effect was found to be overtaken by the effect that the surface area effect that makes drying the particles at smaller size slower.

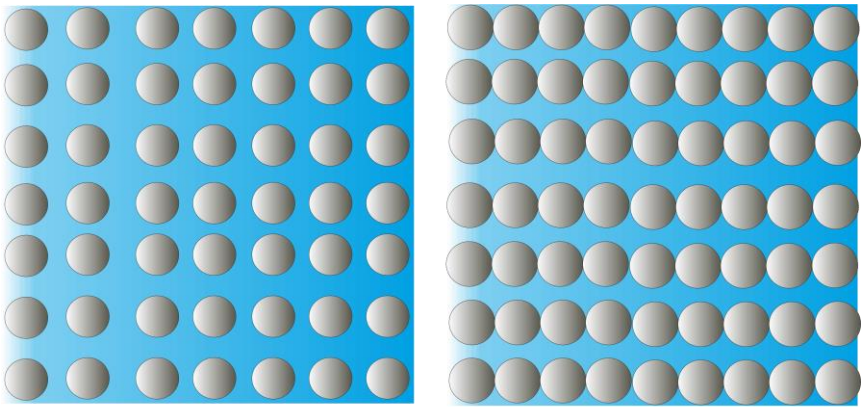

Figure 7.9 The diagram of particle density of the wet-cake: (a) at the beginning of drying, (b) after recrystallization

The drying curve in Figure 7.10 shows that samples with particle size D_{50} < 239.4 μm represents a slightly inclined constant-rate drying which is caused by the appearance of new surface area within the wet-cake makes drying more difficult. The critical solvent content is around 0.2 for smaller particles

(D_{50}=239.4 μm, 225.1 μm and 168.1 μm) while this value shifted to a higher value around 0.3 (D_{50}=275.7 μm) for large particles.

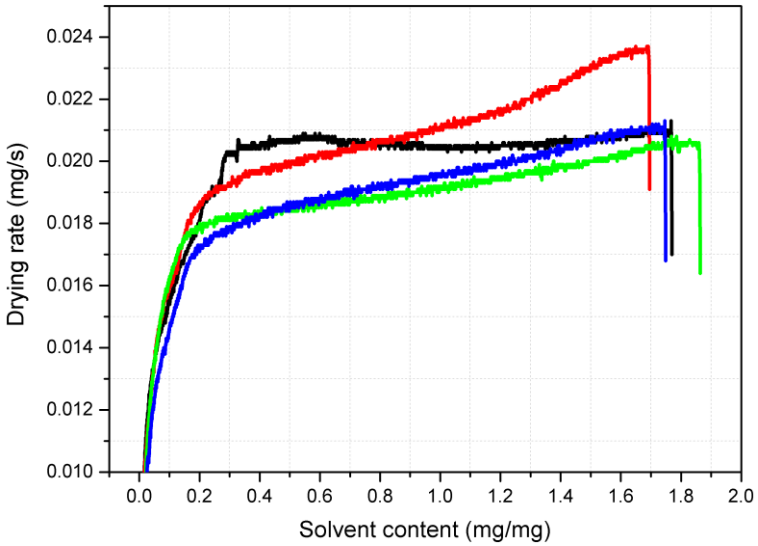

Figure 7.10 The drying rate against solvent content for aspirin powders in water at 70 ^{o}C with particle sizes as follows: D_{50}=275.7 μm (——), D_{50}=239.4 μm (——), D_{50}=225.1 μm (——) and D_{50}=168.1 μm (——)

Similar results are obtained from aspirin/ethanol wet-cake. From Figure 7.11 it can be observed that the higher drying rate is coming from sample with smaller particle size. The recrystallization effect is not as obvious as aqueous aspirin drying. This may be related to the physical properties of ethanol for the solvent is so volatile and less vaporization heat needed to vaporise that the solution has not got enough time to crystallize before the vaporization of ethanol. Hence, ethanol drying is much reflected the pure drying process without the disturbance of other transformation. Furthermore, the variation of particle size distribution has more influence on the drying rates during the constant-rate period rather than in the falling-rate period for during the falling-rate the drying curves nearly superimposed together. The reason for that is surface energy is more influential in strengthening the solid-solvent bonding (constant-rate period) rather solid-vapour bonding (falling-rate period). The critical solvent content is around 0.15 for larger particles between 239-275 μm while 0.1 for smaller particles between 165-225 μm which represents a slight shift of transition point to a lower value.

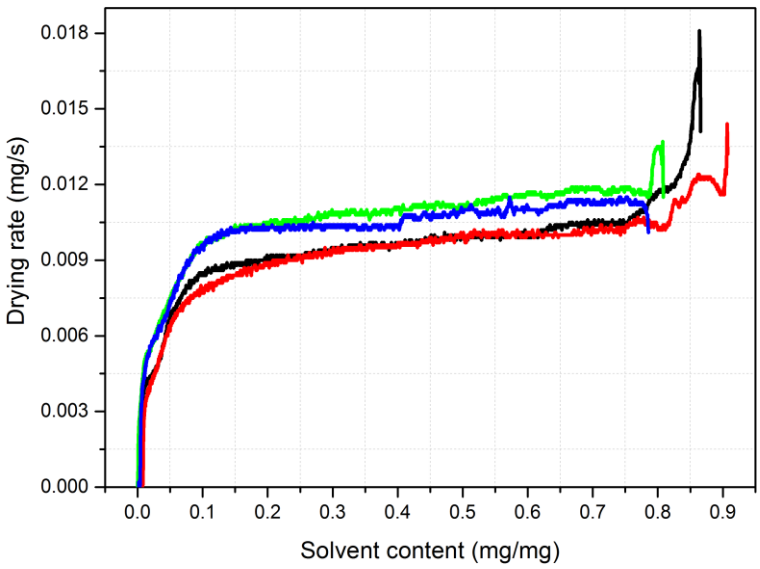

Figure 7.11 The drying rate against solvent content for aspirin powders in ethanol at 30 ^{o}C with particle sizes as follows: D_{50}=275.7 μm (——), D_{50}=239.4 μm (——), D_{50}=225.1 μm (——) and D_{50}=168.1 μm (——)

7.1.5 TGA: Effects of pressure

In order to investigate the influence of pressure on the drying behaviour, three vacuum conditions (10 mbar, 50 mbar and 100 mbar) as well as ambient atmosphere (1 bar) were tested. It can be seen in Figure 7.12 that the drying time is 12 min, 18 min, 22 min and 68 min for pressure at 10 mbar, 50 mbar, 100 mbar and 1 bar respectively. It is not surprising that the wet aspirin powders drying have a decreased cycle time to the vacuum level. The boiling point of the solvent is greatly reduced due to the vacuum condition: The boiling point of water is 7°C, 33°C, 46°C and 100°C at 10 mbar, 50 mbar, 100 mbar and 1 bar respectively [95]. Hence, when all the samples drying at same temperature of 50 °C the reduced pressure has much advantage in terms of facilitating the drying process.

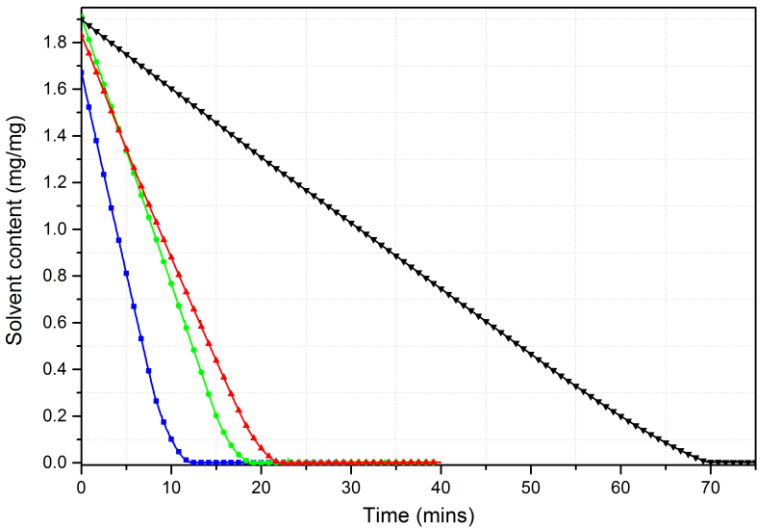

Figure 7.12 Solvent content against time at varied pressure: 1 bar (——), 100 mbar (——), 50 mbar (——) and 10 mbar (——) at 50 °C

It can also be shown from Figure 7.13 that decreasing the pressure from 1 bar to 10 mbar increases the heat transfer rate between crucible temperature and prevailing boiling point under corresponding pressure hence increases the drying rate. It can also be observed that the higher drying rate during constant-rate results in longer constant-rate drying period with the critical solvent content shifting to a reduced solvent content. The temperature profile against solvent content in Figure 7.14 shows that there is a clearly critical solvent content for each drying curve. The temperature remains constant as long as it is within the constant-rate period because only the unbound moisture is removed in this period. When constant-rate period ends, the temperature gradually approaches the set crucible temperature.

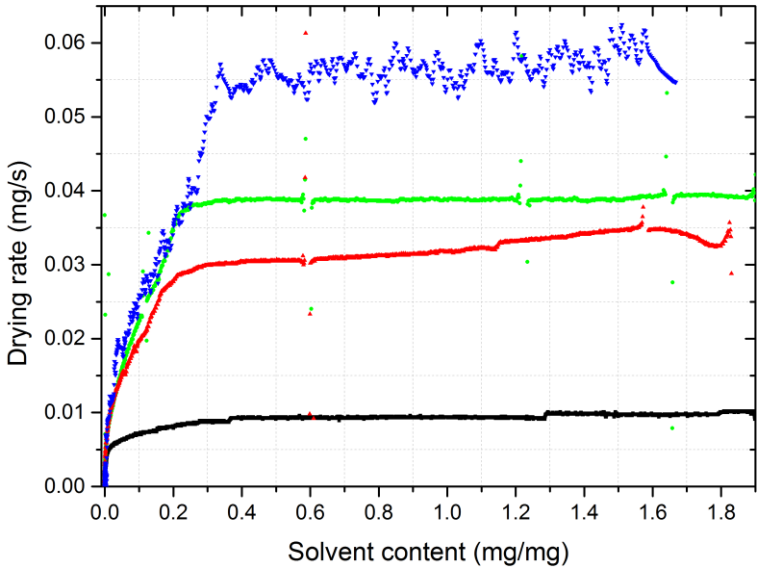

Figure 7.13 Drying rate against solvent content at varied pressures: 1 bar (——), 100 mbar (——), 50 mbar (——) and 10 mbar (——) at 50 °C

The critical solvent content drops from 0.3 for pressure at 10 mbar to 0.05 for pressure at 10 mbar. It has been found that for those drying conditions intend to increase the drying rate they all have a shifted critical solvent content compared to the mild drying conditions. The temperaure profile against time in Figure 7.15 shows that after a constant-rate drying period it enters the falling-rate period immediately for the vacuum level drying. However, for ambient pressure drying, there is a transition period between the constant- and falling-rate period and that is because under ambient pressure the moisture vapour gathered above the wet-cake and no extra forces to remove it which make the mass transfer rate slower from the wet-cake to the dense vapour.

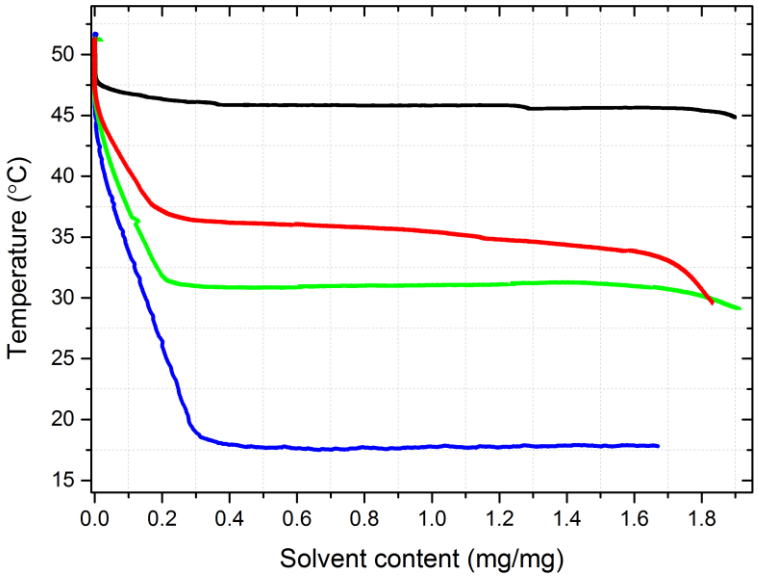

Figure 7.14 Sample temperature against moisture content at varied pressures: 1 bar (——), 100 mbar (——), 50 mbar (——) and 10 mbar (——)

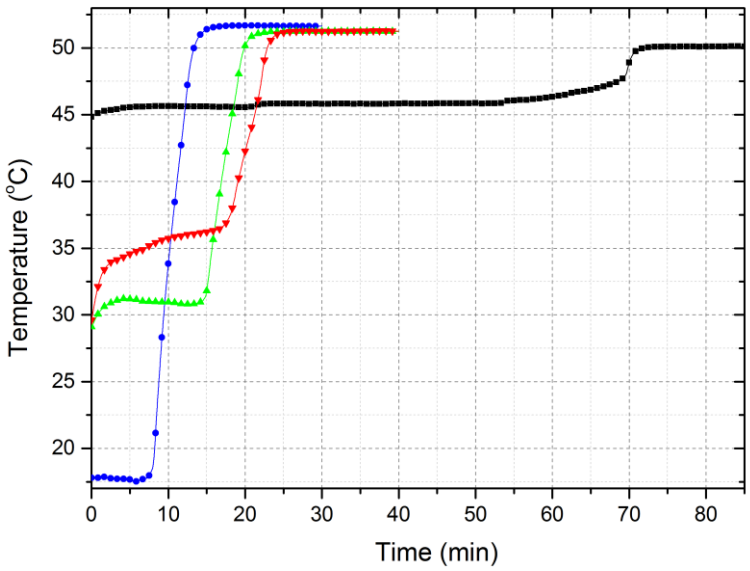

Figure 7.15 Wet-cake temperature against time at varied pressures: 1 bar (——), 100 mbar (——), 50 mbar (——) and 10 mbar (——) at 50 °C

Figure 7.16 illustrates that the variation of the solvent content with time for three different reference temperatures of 30 °C, 40 °C and 50 °C at 10 mbar. It can be seen from this figure that the drying time is reduced when the temperature is increased under the same the vacuum level but much shorter than that of the ambient pressure. Figure 7.17 illustrates that the calculated drying rate also increases as temperature increases. Furthermore, it can be seen that there is two stages during the falling-rate period at 30 °C while only one stage for experiment at 40 °C and 50 °C.

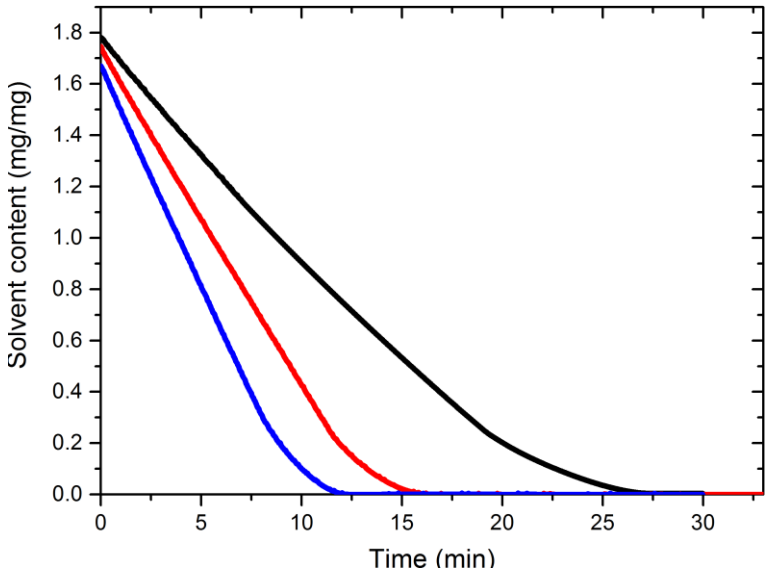

Figure 7.16 Solvent content against time at varied reference temperatures: 30 °C (——), 40 °C (——) and 50 °C (——) under vacuum condition of 10 mbar

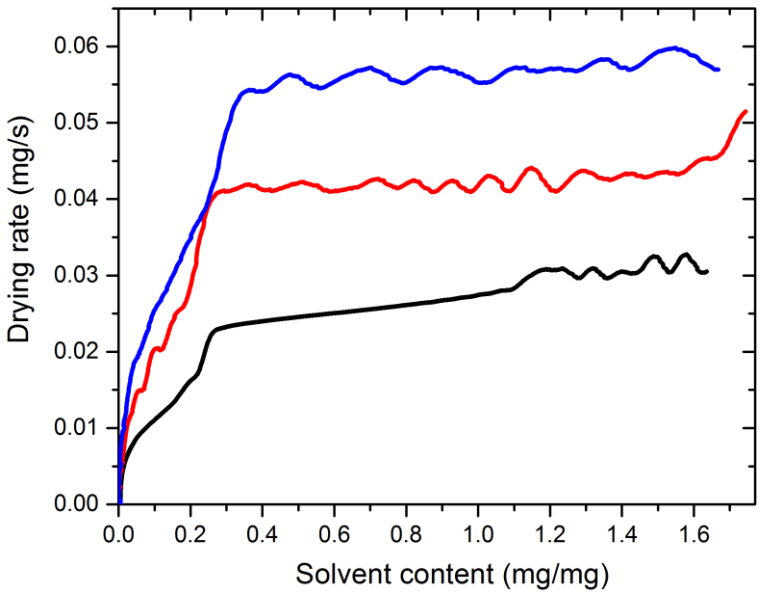

Figure 7.17 Plot of drying rate against moisture content at varied reference temperature: 30 °C (——), 40 °C (——) and 50 °C (——) under vacuum condition of 10 mbar

The two-stage for the falling-rate period also can be observed in the temperature profile changing with time shown in Figure 7.18. The reason for this is because at relative lower temperature 30 °C the liquid tends to coagulated which allows the moisture inside the wet-cake to rearrange hence the liquid in the pores of wet solids has more time to redistribute and begins to recede from the exposed surface. However, this new arrangement for the liquid phase is not applicable for 40°C and 50°C. The temperature profile in Figure 7.19 shows that the three samples all start at a constant temperature, after retain such value at a comparatively long stage for 40°C and 50°C, the sample temperature starts to rise up. However, the sample temperature at 30 °C was found to stay at the constant value for a short period with the relevant solvent content from 1.8 to 1.2 before entering into the first heating up period corresponding solvent content from 1.2 to 0.3.

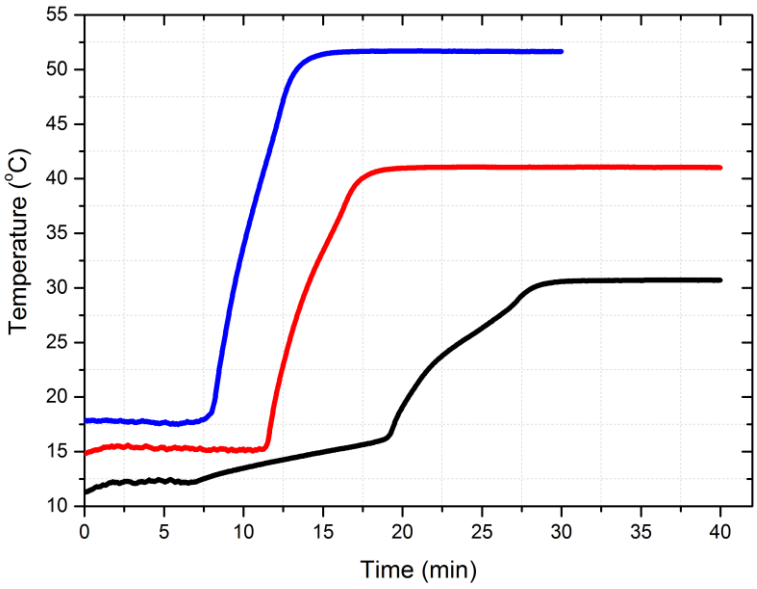

Figure 7.18 Plot of sample temperatures against time and moisture content at varied reference temperature: 30 °C (——), 40 °C (——) and 50 °C (——) under vacuum condition of 10 mbar

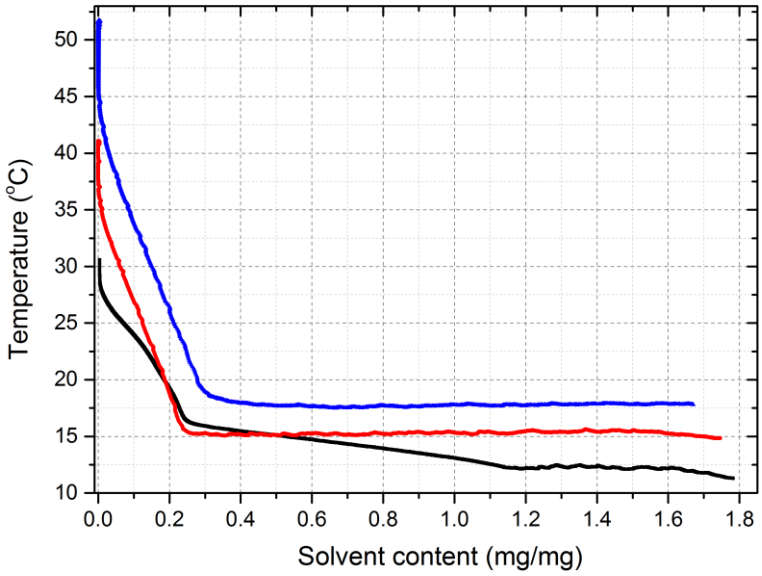

Figure 7.19 Plot of sample temperatures against moisture content at varied reference temperature: 30°C (——), 40°C (——) and 50°C (——) under vacuum condition of 10 mbar

7.2 **Conclusions**

The temperature for drying is quite a critical parameter: a higher temperature may cause recrystallization especially for sample particle size; while a lower temperature may result in two consecutive falling-rate periods, which is detrimental for an optimum drying time.

For water drying experiments, all drying curves can be observed a constant and falling rate period. However, the high ratio of ethanol in water drying tests shows that the missing the falling-rate period. The different operating conditions were examined by TGA tests. It is found that as the drying rate relies on the vacuum level, temperature, particle size, and solvent volatility.

TGA results shows that recrystallization effects may hinder the drying process especially for combinations of solid and solvent with low solubility profile when drying with a higher temperature and smaller particle size.

The critical solvent constant is also found to be related to the external operating conditions as well as particle size of the material being dried.

Chapter 8
Experimental and modelling results on vacuum contact drying

8.1 Introduction

The critical solvent is related closely to the agglomeration and attrition issues of drying process which can referred to Figure 1.2.As the small scale drying was investigated in section 7 which gave a profound understanding about the drying process. The parameters involved in critical solvent content were also investigated. In this chapter, the continuous study of critical solvent content were carried out in a lab-scale AFD, the way to determinate the critical solvent content in this work is described elaborately. To check the consistency of the experimental results, two consecutive experiments were carried out under the same conditions. The critical solvent content can be determined by the temperature profile, torque measurement as well solvent content during the drying process.

The process parameters including different heating power supplied, initial solvent content, agitation speed, types of solvents and materials were investigated for vacuum contact drying in a lab-scale AFD cake. The purpose of this chapter is to report on the experimental programme notably in terms of gaining an understanding of the effects of the setup of the experimental AFD apparatus processing conditions and filter cake parameters had on the drying process for aspirin-ethanol and aspirin-aqueous slurry.

The particle size distribution and morphology with related to agglomeration and attrition phenomena were also investigated using Morphologi G3 equipment which is a very powerful tool to analysing the particle properties before and after drying process. Analysis of the crystal size and shape distribution showed that attrition and agglomeration took place simultaneously during the process. The size distribution curve revealed that attrition dominated the drying process when the stirring speed was high while for low stirring speed, agglomeration became dominant.

8.2 Experimental results and discussion

8.2.1 Error of reproducibility

The reproducibility of experiment carried on using the AFD was examined and are shown in Figure 8.1 from which can be seen that two identical experiments produced closely similar results when the experiment were conducted using the same operating conditions.

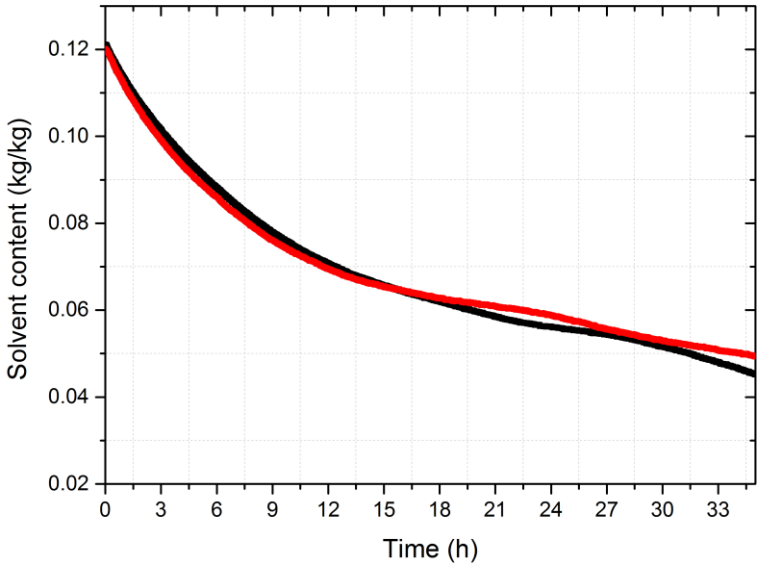

Figure 8.1 Two consecutive drying experiments performed in lab-scale AFD under same operating condition first drying (——) and second drying (——) at heat power 128 Watts

8.2.2 Test with water

The pure water drying test was performed to test the drying behaviour of water. From Figure 8.2 it can be seen that the condensate weight increases with time linearly for free water evaporation occurred in this case. Higher drying rate was obtained for higher vacuum level (0.2 bar). The drying rate for contact drying of pure water at varied vacuum conditions were shown in Table 8.1.

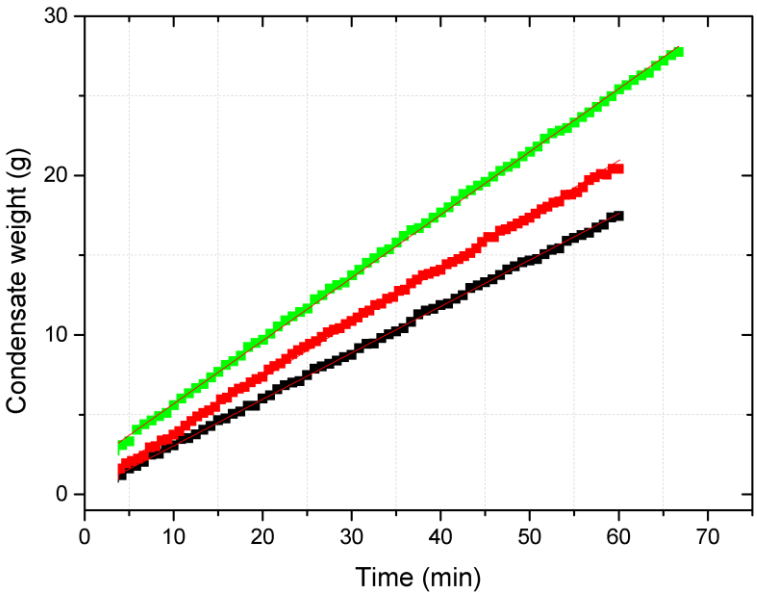

Figure 8.2 The condensate weight changing with time at headspace pressure 0.4 bar (——), 0.35 bar (——), 0.2 bar (——)

Table 8.1 The drying rates at different pressures for pure water at heating power 128 Watts

Pressure (bar gauge)	Drying rate (g/min)	R-square
0.2	0.00659	0.99941
0.35	0.00568	0.99598
0.4	0.00486	0.98177

Also it can be observed from Figure 8.3 that lower temperature difference were created for higher vacuum level. The temperature differences between the inner wall and bulk water were 13, 12 and 10°C at 0.4, 0.35 and 0.2 bar gauge separately (Figure 8.3). This indicates that at constant heating power, the solvent could be evaporated at higher temperature as the vacuum level increases. According to Antoine equation, the vaporizing temperature increases as the pressure decreases. Hence, at constant heating power condition, the rate of heat transfer decrease but the rate of mass transfer increases as the vacuum level increases.

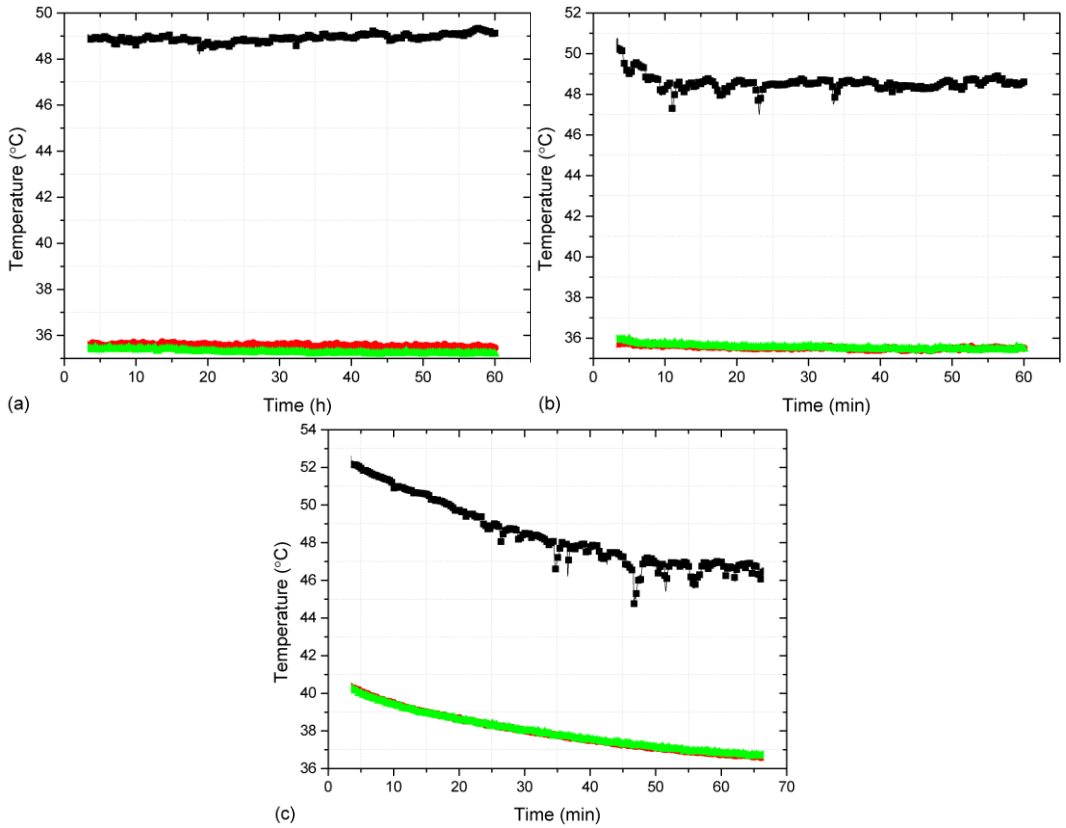

Figure 8.3 The temperature profile changing with time at wall area (——), middle of radius (——) and centre of the wet-cake (——) at pressure of (a) 0.4 bar, (b) 0.35 bar and (c) 0.2 bar

8.2.3 Effects of heating power

Figure 8.4 shows the temperature variation along radial direction inside the wet-cake with heating power at 146W (similar temperature distribution for 128W and 157W). It is believed that the wet-cake temperature changes correspondingly to the solvent content. Understanding how temperature was distributed inside the wet-cake was used to help understand the drying behaviour. The temperature at different locations is related to the local solvent content. The temperature gap reflects that wet bed close to the heating surface has the highest temperature and wet-cake for the static bed is dried layer by layer. When the temperature at centre of cake reach a certain limit at t=12h, the wet-cake dries much slower beyond this point. From the evidence of measured temperature and solvent content, the critical solvent content can be estimated to be 5-6%.

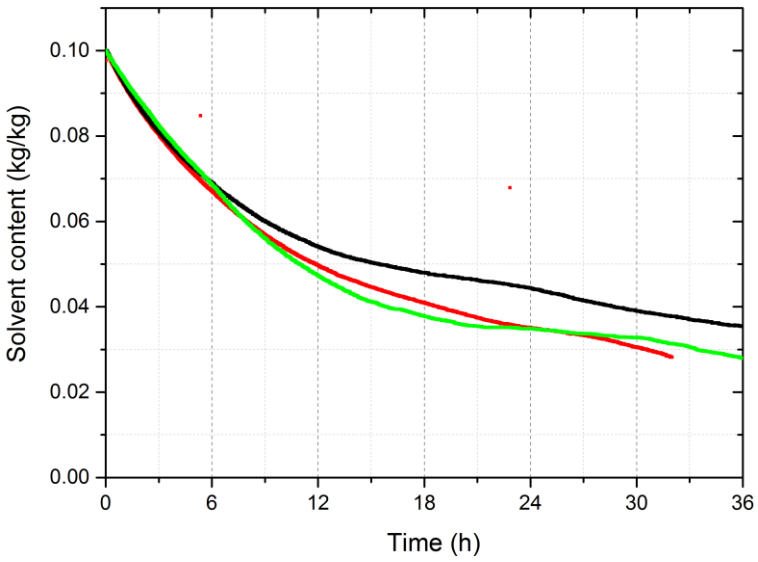

Figure 8.4 The solvent content against time for different heating power at 128W (——), 146W (——) and 157W (——)

The drying curve for heating power at 128 Watts in Figure 8.5 shows that the transition point in the drying curve is synchronised with that in the temperature profile. The temperature curves shows that the critical solvent content locates between 0.05 and 0.06.

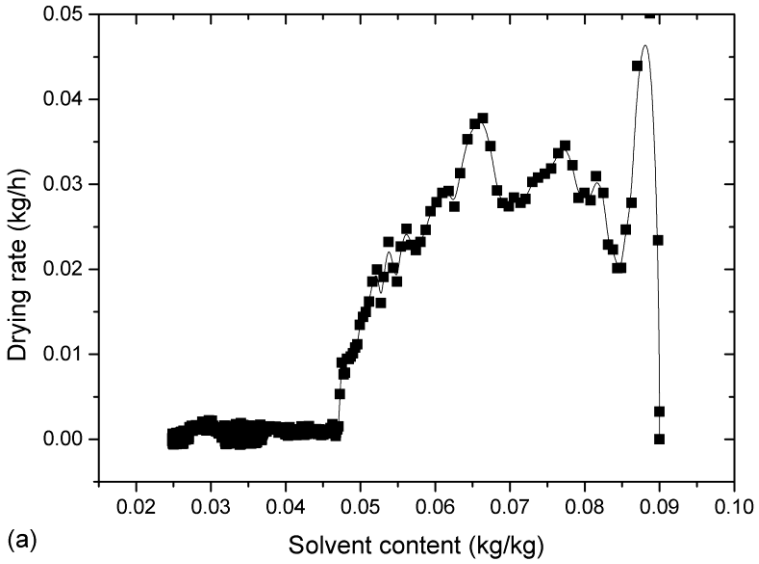

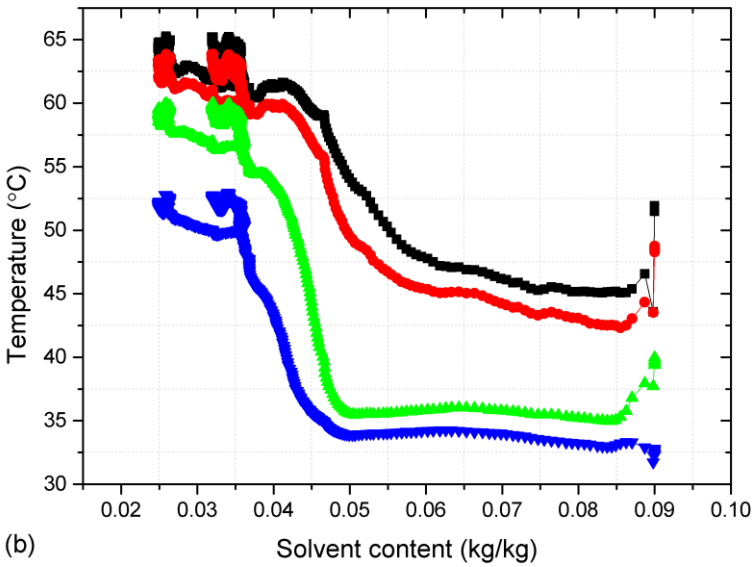

Figure 8.5 (a) drying curve and (b) temperature distribution at wall area (——), first layer of particles (——), middle of radius (——), centre of the wet-cake (——) changing with solvent content heating at 128 Watts

8.2.4 Effects of initial solvent content

The different initial solvent content was investigated. A crusting phenomenon is observed due to a high initial solvent content from the temperature distribution curves shows below (Figure 8.6) There has a temperature delay between the cake and the jacketed wall from t=0 to 24h, then follows by a suddenly increase of the cake temperature. It can be seen from the drying rate curve that there is increase at t=24h. Both the drying curve and temperature distribution indicated that the aggregation effect formed at a high solvent content and then as the solvent remained in the cake decreased, the bonding effect that caused by the water holding the aspirin particles was weakened. The temperature of the cake recovered rising up corresponding to the jacketed wall temperature. However, no such phenomenon observed from the lower solvent content experiments.

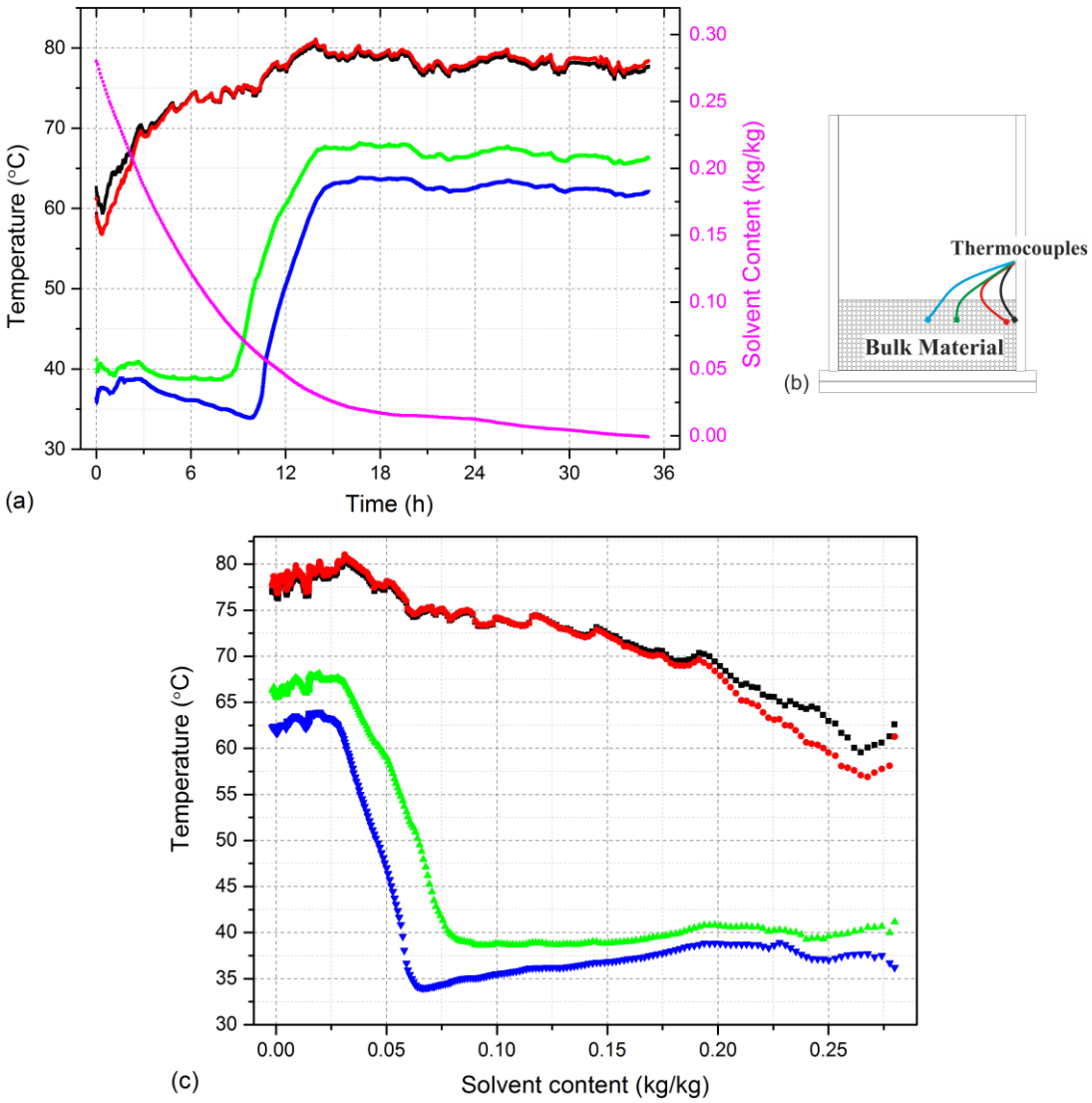

Figure 8.6 (a) The temperature distribution at different locations : wall area(——), first layer of particles(——), middle of radius (——), centre of the wet-cake (——) and solvent content against time (b) thermocouple positions inside the wet-cake (c) the temperature against solvent content with heating power at 157 Watts

8.2.5 Effects of agitation

However, in the agitated drying process, the surface of the cake formed a crusted shell resulting poor flowability. It can be seen in Figure 8.7 that the crust formed even in static drying. Basically, the formation of crust is resulted from liquid bridge among the solid particles. As the liquid evaporates, the solute precipitates from the slurry forms solid bridge.

(a) (b)

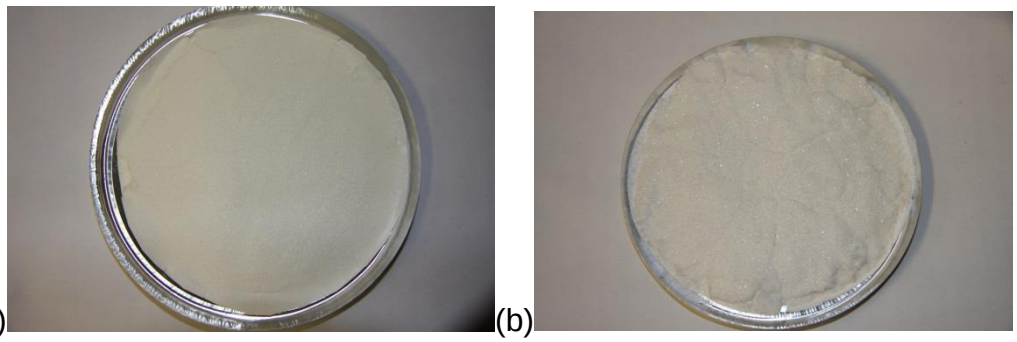

Figure 8.7 (a) The crust formation of dry aspirin after tray drying (b) the dry aspirin crust breaks lumps after applying an external force drying

After breaking the crust, the temperate of the cake tend to become uniform due to agitation effect. Comparing to the static bed, the drying time needed for agitation bed greatly reduced (Figure 8.8). With agitation effect, the cake formed a crust at the beginning. As more solvent removed from the wet solid, the solvent content for the crust decreased and the crust can be broken by the stirrer. The temperature profile shows that the crust formed from the beginning the drying process. As the drying progresses, the solvent content is not enough to hold the wet solid as a whole crust. The critical temperature changes at t= 4h shows that the big lumps started to break at this time.

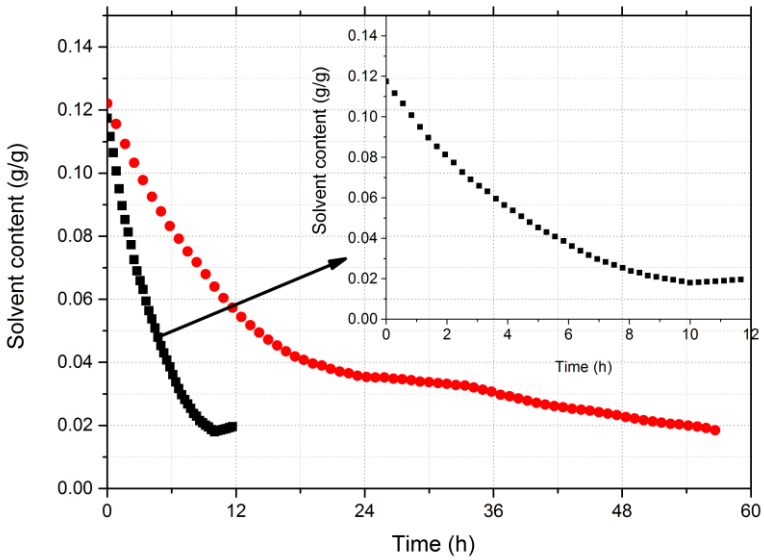

Figure 8.8 The solvent content for static bed (——) and agitated bed (——) against time with heat power at 157W and agitated speed at 30 rpm

Here shows temperature distributions and torque recorded against time during drying period. Figure 8.9 (a) shows the temperature distribution during agitated drying process at stirring speed 20 rpm. The wet-cake forms

agglomerated lumps from the beginning the drying process. The temperature difference at three locations is big at the initial drying stage due to agitation at the higher solvent content. As the moisture removed from evaporation, the big lumps gradually break into small aggregates which can be seen from Figure 8.9 (a) that the temperature has a critical change at around t=3.5h. This evidence also can be seen from Figure 8.9 (b) that the torque increases first as more and more agglomerates formed at the beginning and reach to the a peak at around t-3.5h (which is similar to phenomenon observed from the temperature distribution) then followed by a critical change. The torque then reduced gradually as the wet-cake become drier. The solvent content is not enough to bind the all the particles together. The particles at this stage are rather like free flowing particles.

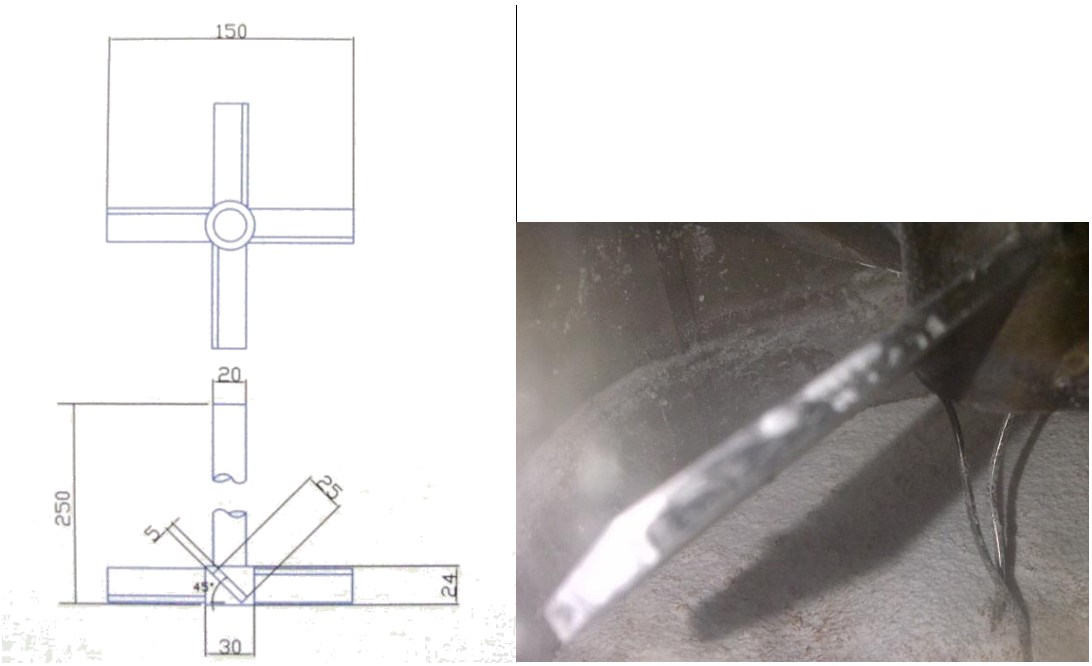

Figure 8.9 (a) The design of the stirrer used for agitation; (b) the local photo of the stirrer

In Figure 8.10 and 8.11, the all shows a relationship between the breaks of temperature curves and the sudden decreasing of the torque value.

The torque is calculated from the equations below:

$$\tau = \frac{W}{2\pi u_r} \qquad 8\text{-}1$$

where τ is the torque as applied agitation to the wet-cake, W is the power need to agitate the wet-cake and u_r is the rotational speed of the agitator.

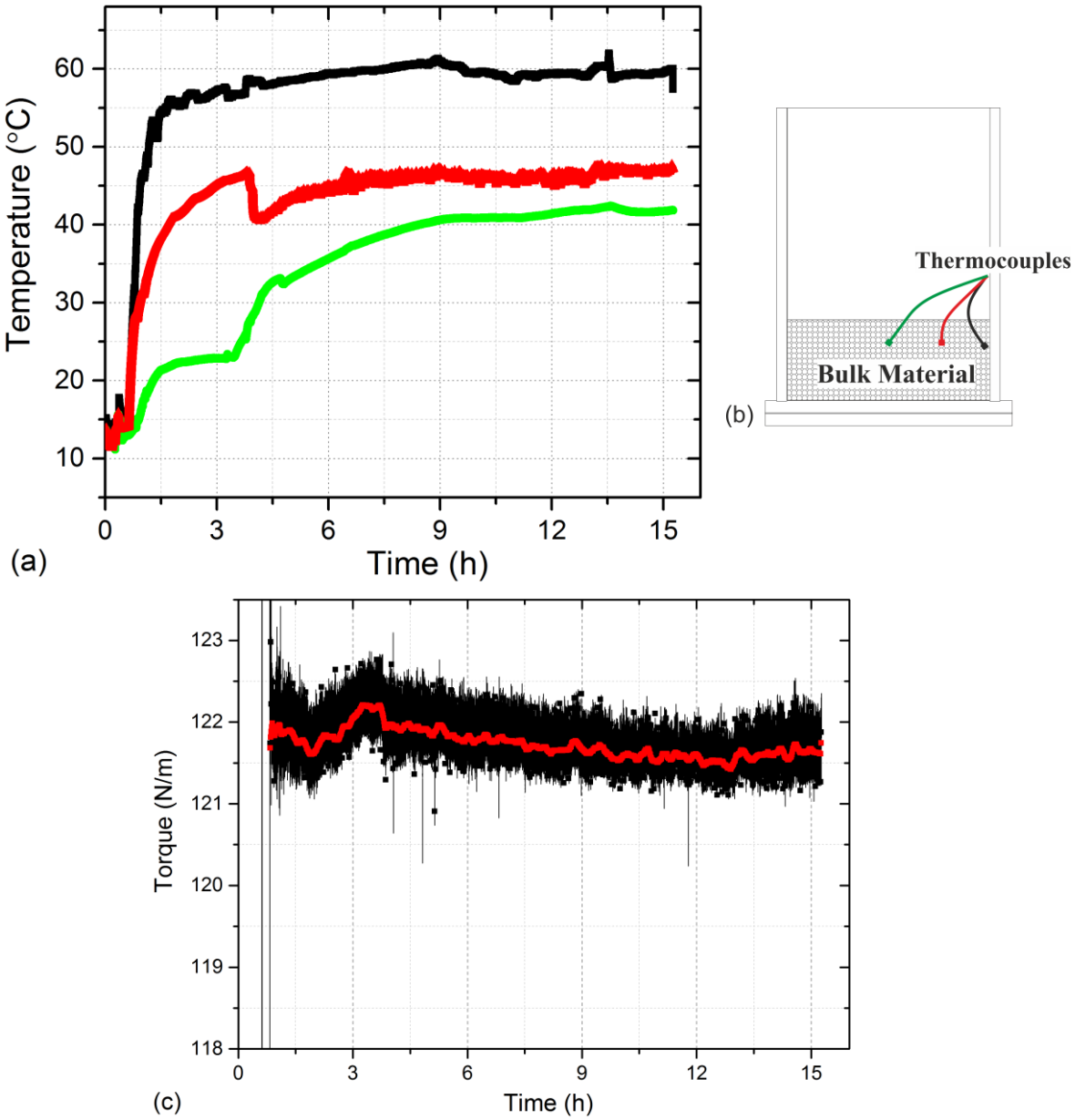

Figure 8.10 (a) temperature distribution at different locations: first layer of particles (——), middle of radius (——), centre of the wet-cake (——); (b) experimental torque data (——) and smoothed data (——) varied with time heat power at 128W and agitated speed at 20 rpm

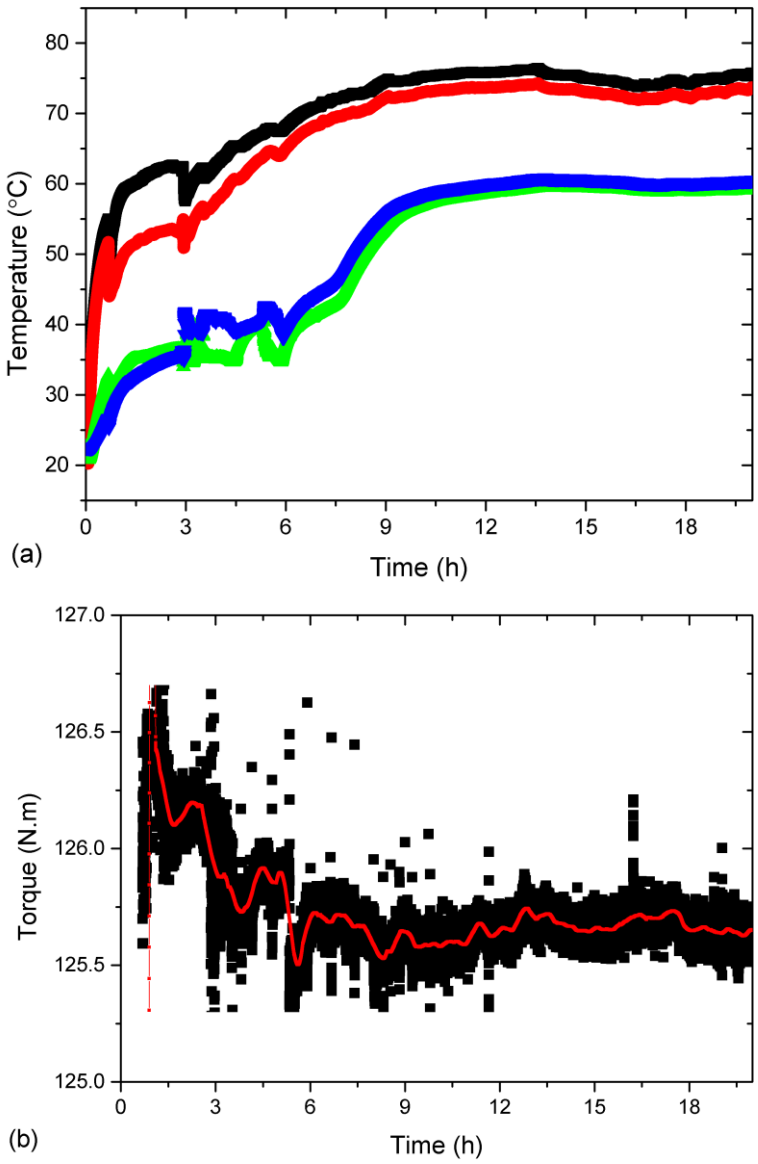

Figure 8.11 (a) The temperature distribution at wall area (——), first layer of particles (——), middle of radius (——), centre of the wet-cake (——) and (b) torque against time at heating power 157 Watts and continuous 30 rpm

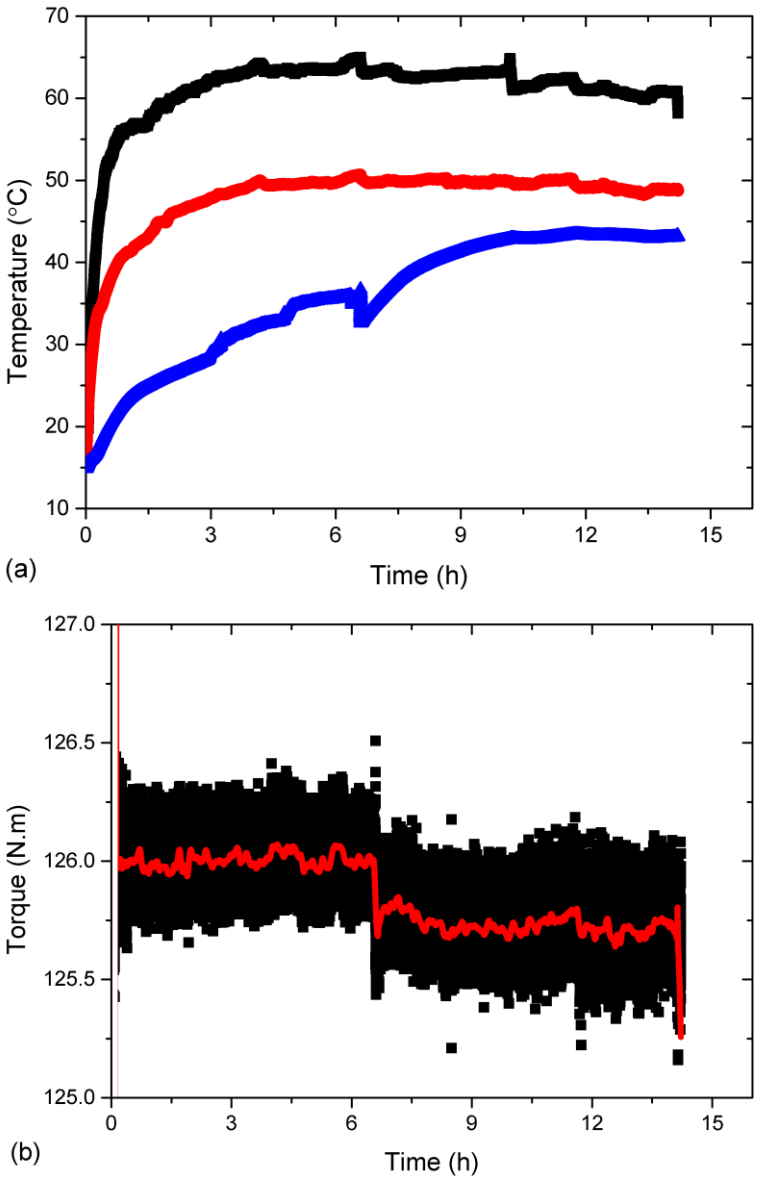

Figure 8.12 (a) The temperature distribution at wall area (——), middle of radius (——), centre of the wet-cake (——) and (b) torque against time at heating power 128 Watts and continuous 30 rpm

To restrain aggressive drying condition, intermittent agitation was used in this work. The drying under intermittent agitation is observed to be faster at the first half of drying process than that of continuous agitation (Figure 8.13). The reason for that may be caused by the big lumps being liable to form under continuous agitation hence restrained the rate of heat transfer while this suppression effect from agitation is alleviated to a certain extent. When the solvent content is less than critical solvent content, the drying under continuous agitation became faster than that of intermittent agitation as the agglomeration effect lessened and more free flowing particles released from agglomerates.

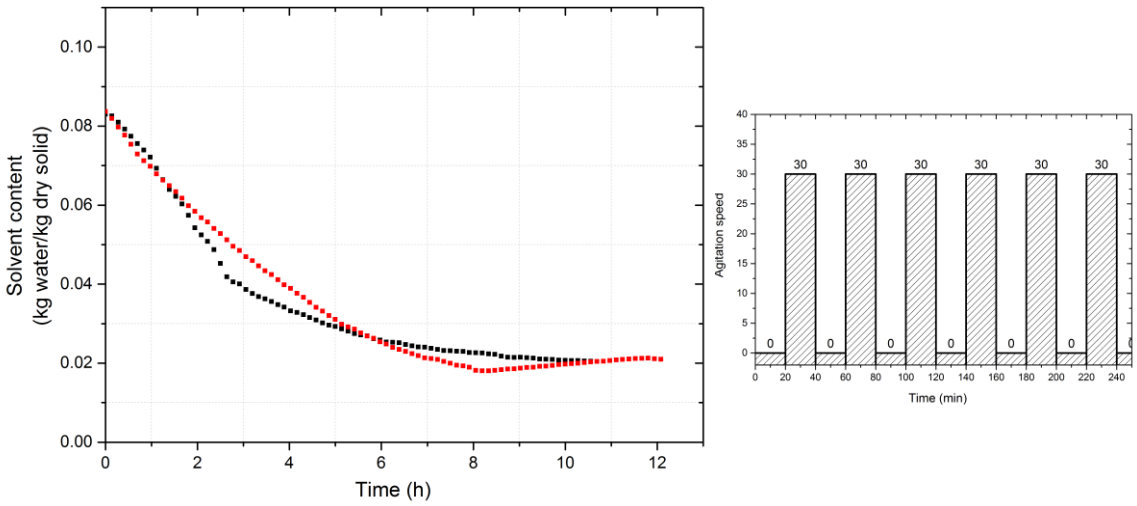

Figure 8.13 The solvent content for continuous agitated bed with agitated speed at 30 rpm (——) and intermittent agitated bed (20mins ON/ 20mins OFF) (the agitation regime shows at the right) (——) against time with heat power at 157 Watts

The temperature profile under intermittent agitation shows the wave change of temperature during agitation ON and OFF (Figure 8.14). For each static period, the temperature of the wet-cake goes up similar to static bed drying. For each agitated period, the dry and wet material was mixed together the temperature starts to decrease whenever agitation initiates. The absent of wave-shape for the temperature at the cake centre from 1.5h to 3h is caused by lumps formed by the first 20 mins agitation. As drying progresses, the big lumps breaks by the 6th agitation at t=220mins. The cake temperate reduced gradually as the agitation starts before t=6h and then temperature reaches homogenous state faster beyond t=6h. The reason for that may be caused by the worse flowbility at the beginning of drying process. After that, uniform temperature reached instantly within the wet-cake due to better powders mixing.

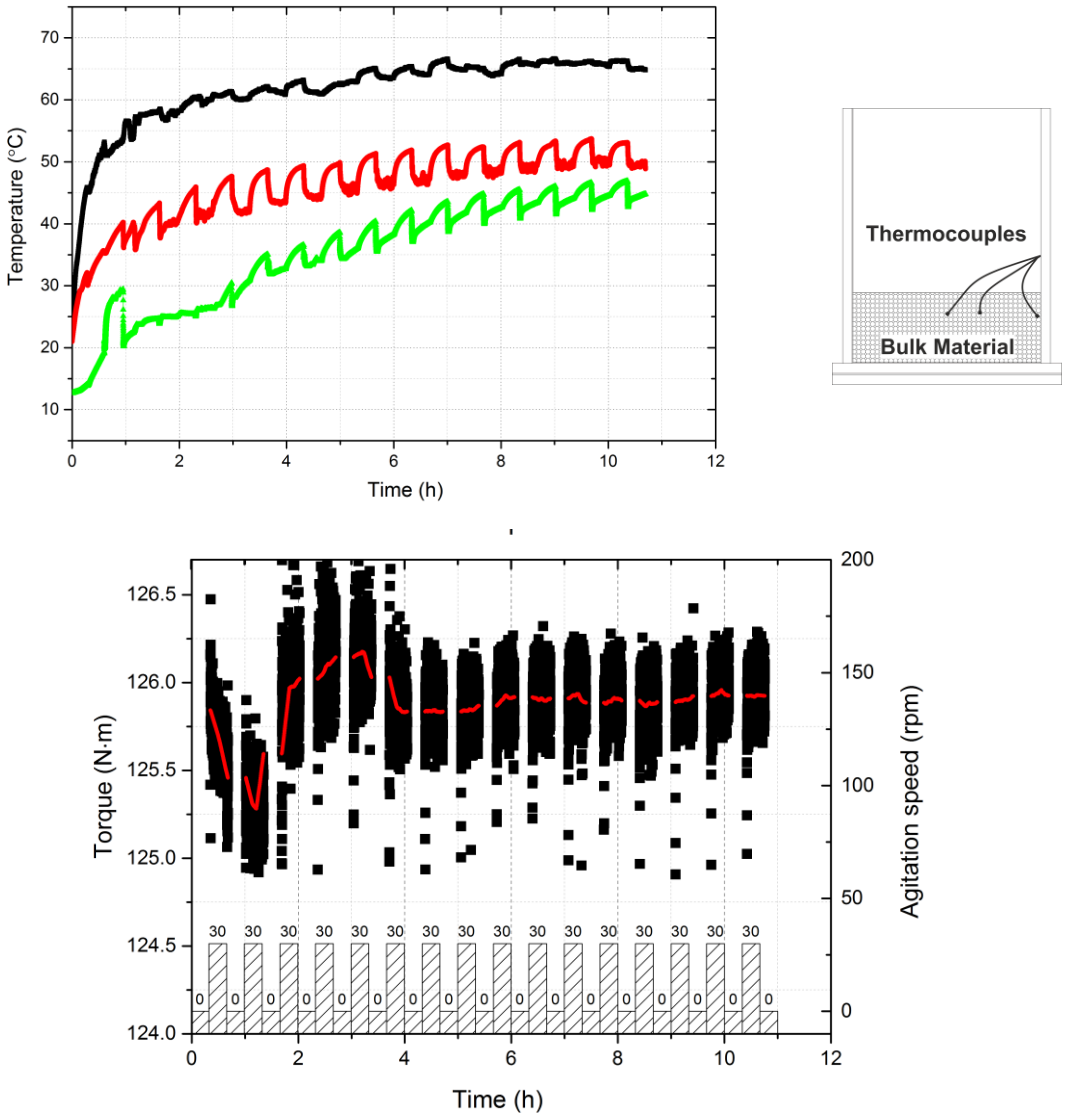

Figure 8.14 Temperature distribution at different locations: first layer of particles (——), middle of radius (——), centre of the wet-cake (——) against time (b) experimental torque data (——) and smoothed data (——) varied with time heat power at 157W and agitated speed at 30 rpm (20mins ON/ 20mins OFF)

8.2.6 Effects of solvent types

According to the previous screening results from TGA work, as long as the component of the mixed solvent is volatile, the results are difficult to reproduce; however, this reproducibility can be enhanced by choosing the edging ratios of the mixed solvent. In this case, 10% and 20% ethanol in water were investigated and the results were compared with the result drying with the pure water. Figure 8.15 shows that at the beginning of the drying process, the drying with ethanol mixed solvent is faster than pure water

drying. As the drying progresses, the volatile ethanol is running away from condensate collecting bottle, hence, the condensate weight is decreasing. The sample prepared in 20% ethanol in water is losing weight for the much ethanol slip away. While the weight for sample prepared in 10% ethanol in water is remaining constant is because the rate of weight losing is basically flat to condensate collecting rate.

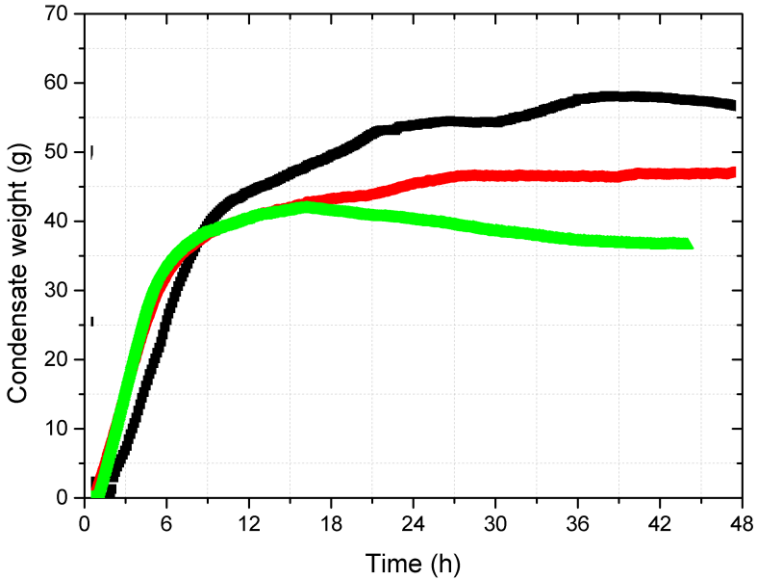

Figure 8.15 Concentrate weight against time for different solvent: pure water (——), 10 % ethanol in water (——) and 20 % ethanol in water (——)

The temperature profiles in Figure 8.16 shows that the drying of mixed solvent samples is greatly reduce the time needed for the centre of the cake rising up temperatures for the volatile ethanol molecules helps carry away the water vapour and greatly reduce the resistance of water removing from the wet-cake.

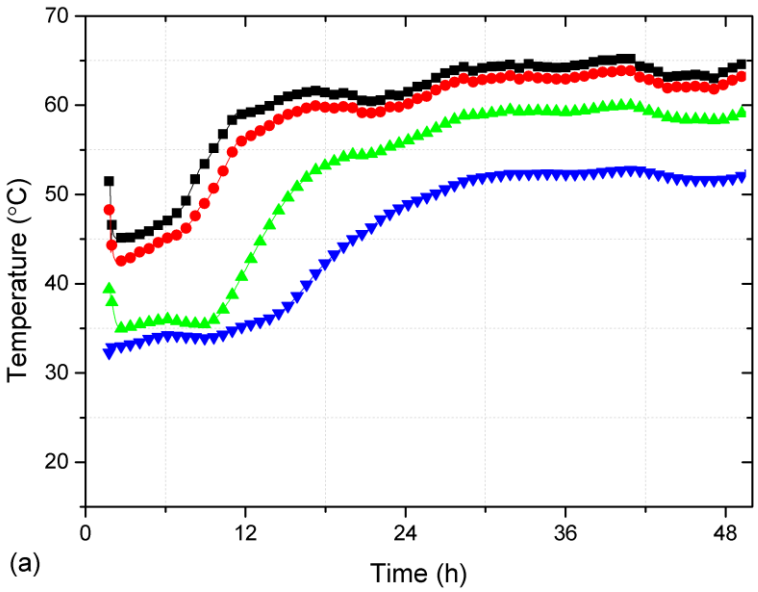
Temperature (°C)
Time (h)
70
60
50
40
30
20
0
12
24
36
48

(a)

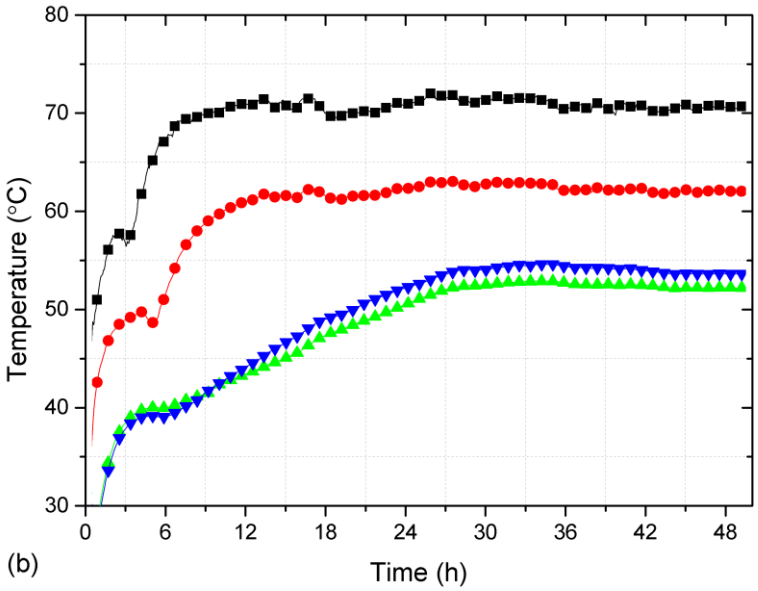
Temperature (°C)
Time (h)
80
70
60
50
40
30
0
6
12
18
24
30
36
42
48

(b)

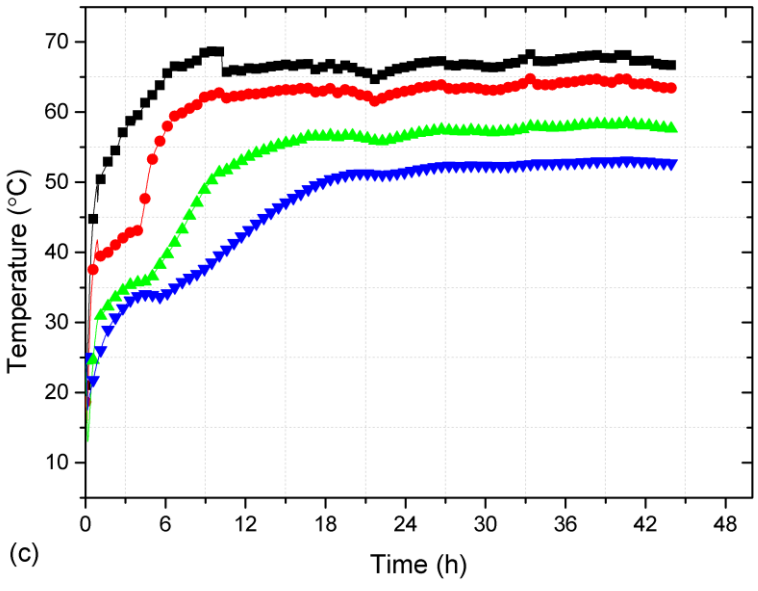
Temperature (°C)
Time (h)
70
60
50
40
30
20
10
0
6
12
18
24
30
36
42
48

(c)

Figure 8.16 Temperature distribution at wall area (——), first layer of particles (——), middle of radius (——), centre of the wet-cake (——) against time for different solvent: (a) pure water, (b) 10 % ethanol in water and (c) 20 % ethanol in water

8.2.7 Effects of material types

Two types of aspirin materials with different particle shape and size distribution was investigated: Aspirin crystals and aspirin agglomerates. Materials to be processed in the drying process can be either crystals and granulates. Hence it is necessary to investigate the drying behaviour between crystals and granulates. The drying time needed for aspirin granulates is far more than aspirin crystals (Figure 8.17). The morphology of aspirin crystal and granulates are displayed in Figure 8.17. It can be observed that aspirin granulates which form from aggregation of lot aspirin crystals must ha1ve a larger surface area than aspirin single crystals. The interfacial area of particles comes into play effects on drying kinetics. Hence the surface area and pore volume of granulates and crystals are investigated by Brunauer-Emmett-Teller (BET) Surface Area Analysis and Barrett-Joyner-Halenda (BJH) Pore Size and Volume Analysis.

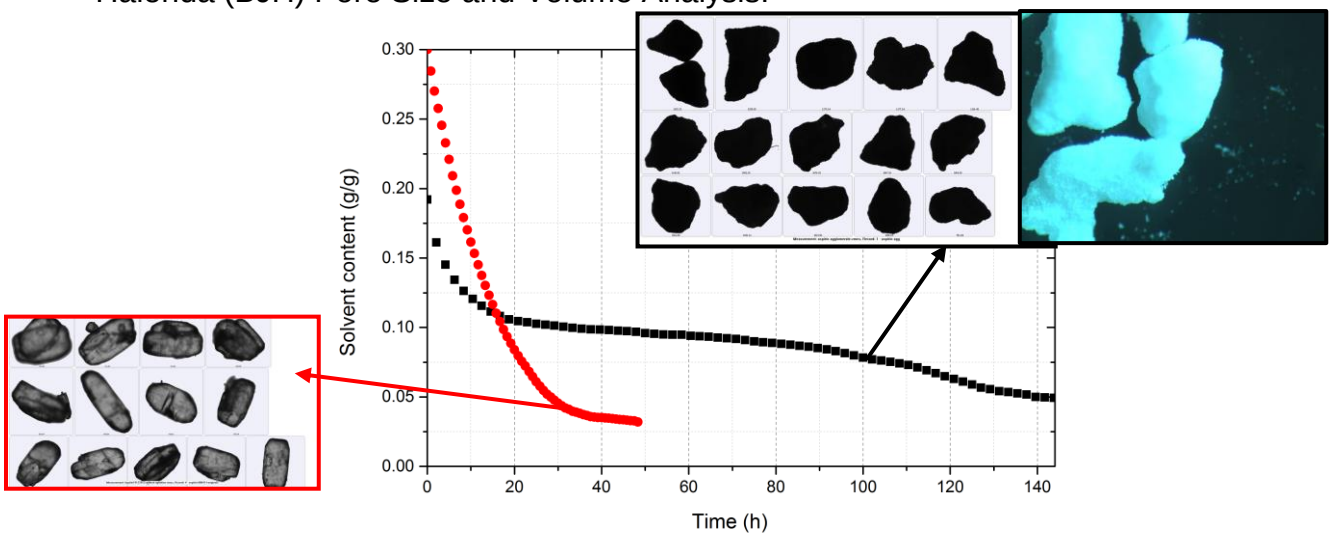

Figure 8.17 The solvent content of aspirin granulates (——) and aspirin crystals (——) against time with heat power at 157W

By evaluating the external area and pore area, the results show that granulate material has bigger surface area (0.2357 m^2/g) and pore volume (0.001169 cm^2/g) than crystalline material (0.502 m^2/g) and pore volume (0.000067 cm^2/g). The bigger surface area and pore size make aspirin granulates more capable of holding moisture inside the pore. It is more difficult to remove the moisture caused by bigger capillary force resistance

exist when existing of pores. Hence longer time is needed for the granular powders to dry than crystalline aspirin.

8.2.8 Particle size and morphology

The particle size distribution and morphology is investigated for stirring speed at 10 rpm and 30 rpm. The two inset figures of Figure 8.18 are the particle morphology of aspirin powders of before and after drying at second peak of 390μm separately. Broken crystals are observed for sample with agitation with stirring at 30rpm due to a high mechanical force is applied and sufficient to break the hydrogen bond and van der Waals for aspirin crystals.

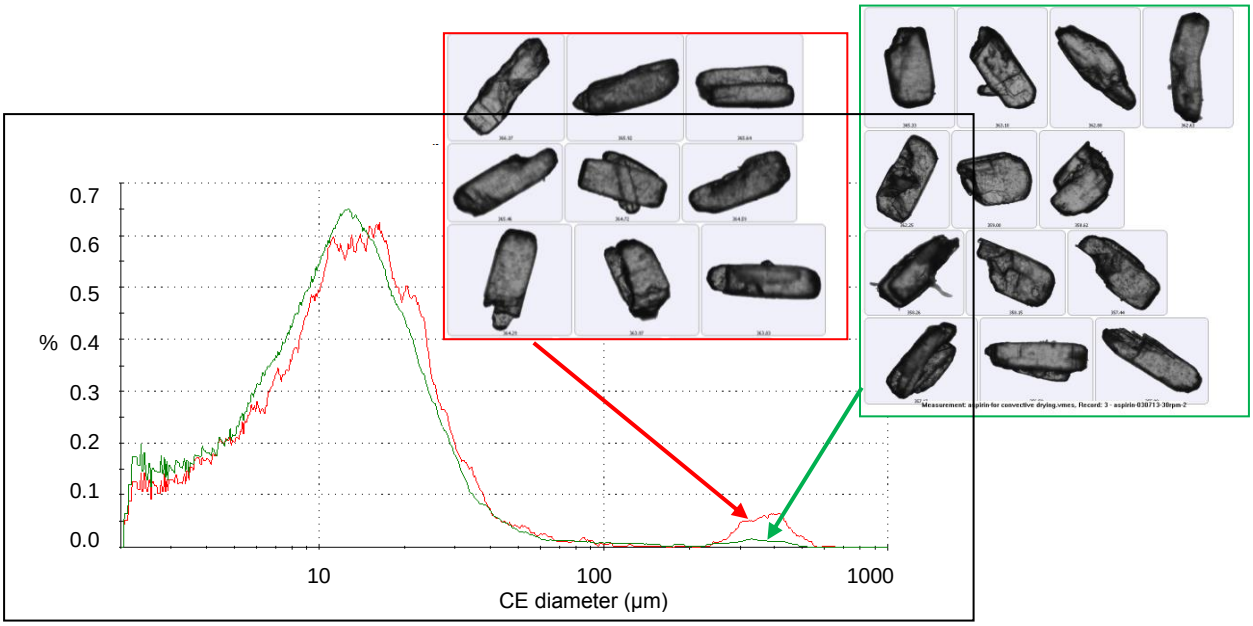

Figure 8.18 Particle size distribution before (——) and after continuous stirring (——) at 30rpm; particle shapes before (inside left) and after agitation at 30 rpm (inside right)

This attrition effect can be quantified by comparing the convexity distributions. The Convexity is a measure of the edge roughness of a particle and very sensitive to changes in edge roughness. So if attrition existed accompany the agitation process, convexity should decrease. For aspirin particles with agitation shows a lower convexity (Figure 8.19), indicating rougher edges formed due to attrition effects.

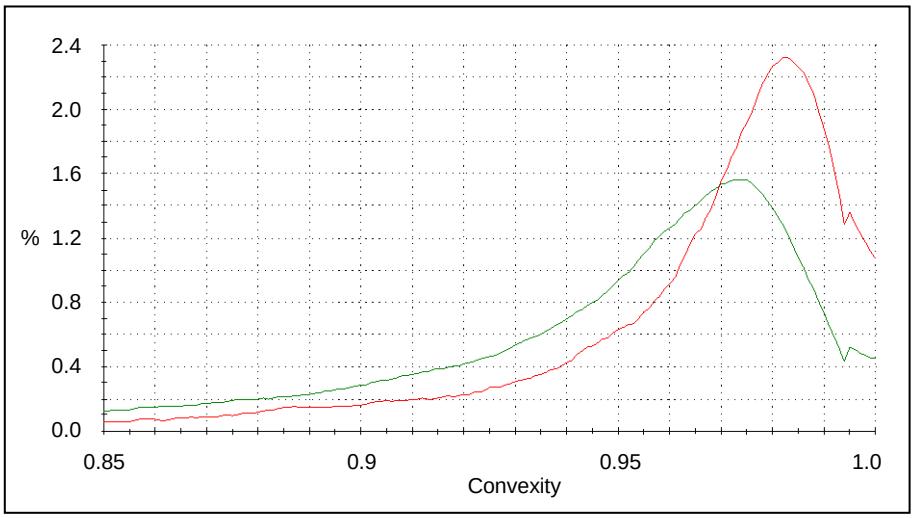

Figure 8.19 Convexity before (——) and after (——) continuous stirring at 30rpm

When reduce agitation speed to 10 rpm, evidence of agglomeration found from particle images after agitation (see inside Figure 8.20). At mean time, the particle size distribution slightly increased. It can be seen from Figure 8.20, the particle size of sample with agitation shift to bigger size compare to original particles as a result of agglomeration. It is found that the agglomeration caused by agitation at a very early stage in drying and attrition caused by agitated too much during drying process especially for dry powders.

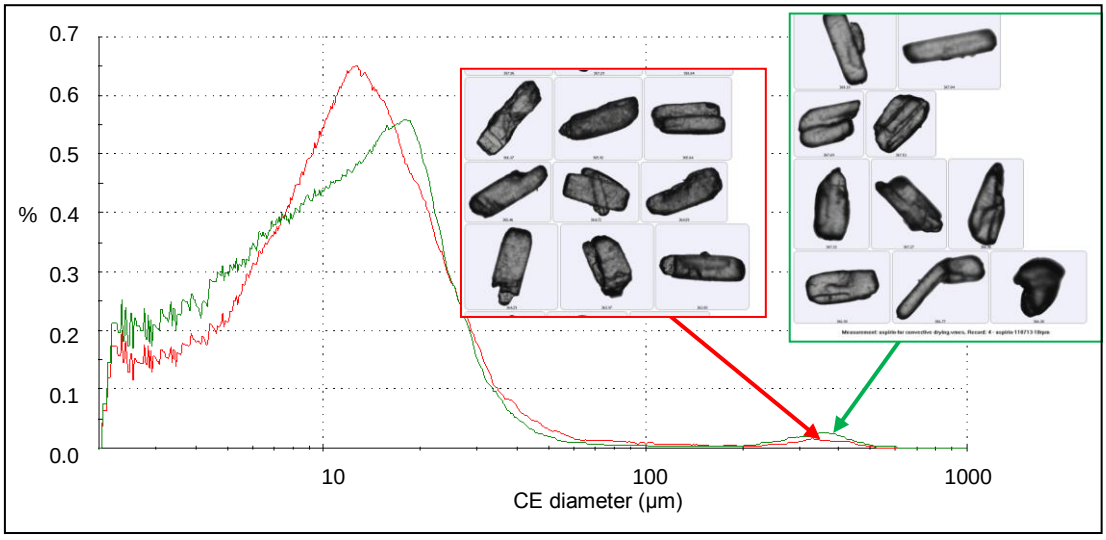

Figure 8.20 Particle size distribution before (——) and after (——) continuous stirring at 10rpm; particle shapes before (inside left) and after agitation at 10 rpm (inside right)

To quantitatively describe this phenomenon, circularity is investigated over a range of 10000 particles for each sample measurement using Morphologi

G3 which is referred to Chapter 3. Circularity is developed as a standard to measure how the particles are the closeness to a perfect circle. The circularity is sensitive to both overall form and edge roughness. For much rounder aggregates can be produced from agglomeration effect, hence by comparing the circularity distribution it can be considered as indicator of agglomeration effect. The sample with agitation at 10rpm presents a higher circularity (see in Figure 8.21) indicating that aggregation effects and polishing effects at mild agitation speed.

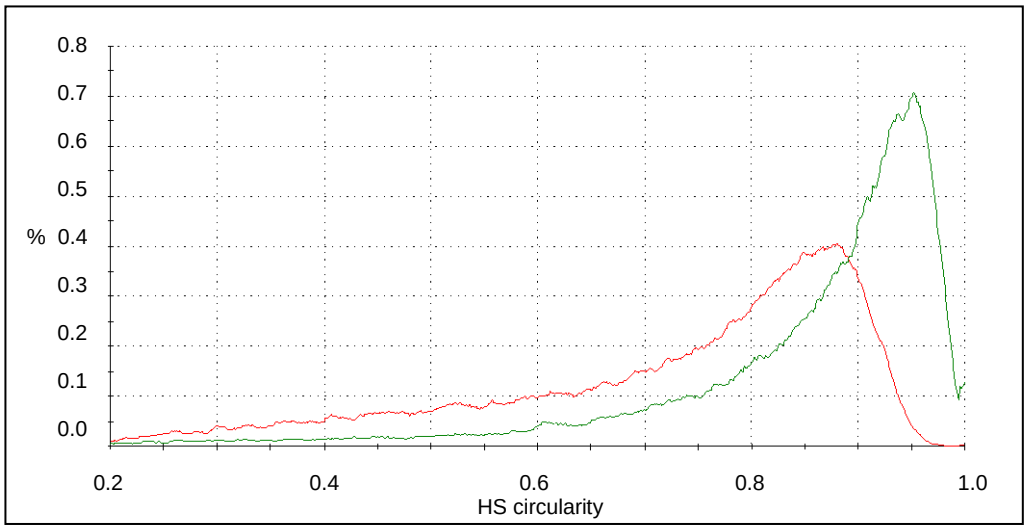

Figure 8.21 Circularity before (——) and after continuous stirring (——) at 10rpm

Due to the solid-solvent bounding between aspirin and water, it is found that the agglomeration formed at a higher initial solvent content even in static bed. And when agitated in higher solvent content beyond critical solvent content (4% for aspirin and water system), it has a high risk of forming big lumps. Stirring at the lower agitation speed can result in agglomeration while stirring at higher agitation speed may cause attrition (Figure 8.21). To adopt intermittent agitation can avoid such effects to some degree for intermittent agitation reduced the lumped-period from 4h for continuous agitation to 3h.

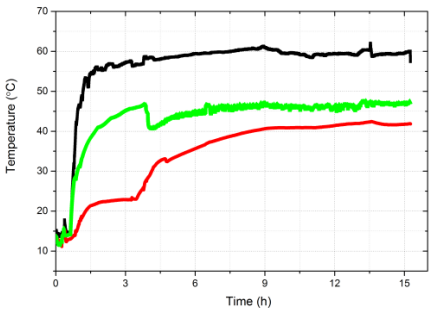

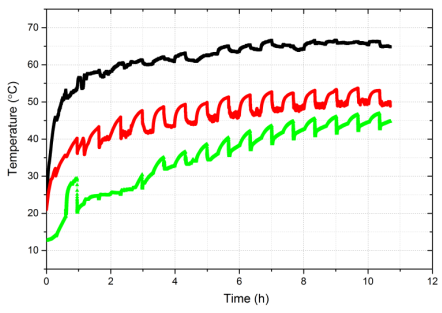

Figure 8.22 Temperature distribution at first layer of particles (——), middle of radius (——), centre of the wet-cake (——) against time (a) continuous agitation 30rpm, (b) intermittent agitation at 30 rpm

For the same material, the effects of surface porosity and particle size on drying process could play important role in drying kinetics. The bigger the surface area is, the slower the dry rate is. The huge pore volume inside the particles also impact on the drying rate in that the pores are capable of holding more moisture inside.

The simulation results have a good agreement with experimental results. Critical solvent content is believed to be related to solid and solvent properties. According to the simulation results, this critical solvent content does not change with agitation, initial solvent content, as well as temperature. But it actually changed between aspirin crystalline and granulated materials. A critical solvent content is fitted for both static and agitated bed at 4%.

The particle size was also compared before and after intermittent agitation. It can be seen that after intermittent agitation, the big crystals become smaller while the small crystals grow bigger in Figure 8.23. This phenomenon can be explained that the parallel effects with regards to agglomeration and attrition. For the combination of static and stirring bed within intermittent agitation mode, the crystal size is controlled by the dual effect of attrition and agglomeration.

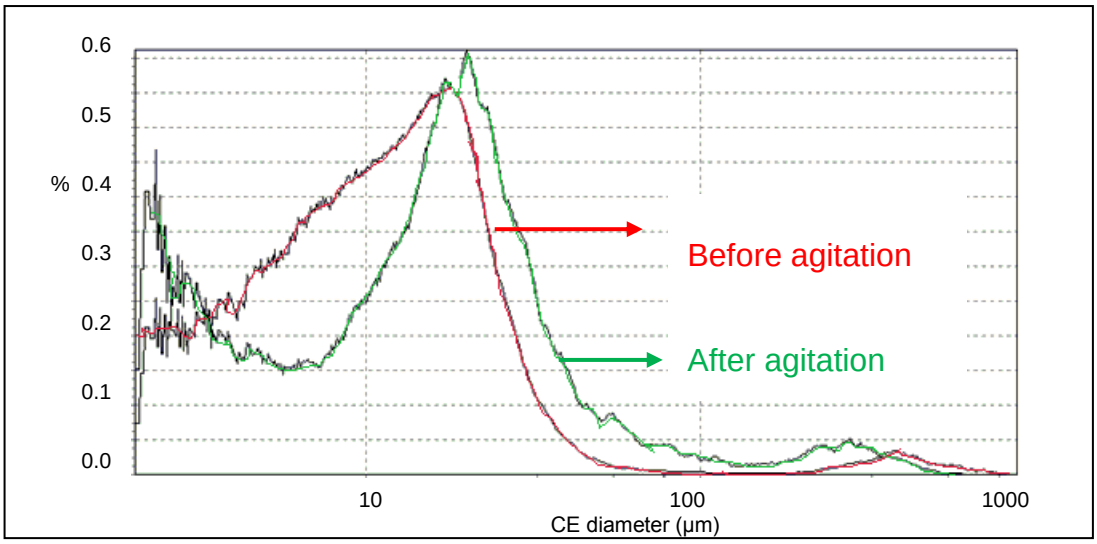

Figure 8.23 CE diameter before and after intermittent stirring at 30rpm

8.3 Simulation results and validation

8.3.1 Modelling validation of LPM

To validate the model, two experimental sets including static bed drying and agitated bed drying were applied in this work. The experimental conditions were described in Chapter 5 and referred to Table 5.4 and 5.5.

The results of the numerical simulation are presented as a curve giving the solvent content (Figure 8.24) at different times and compared with the experimental results. It can be seen that good agreement has achieved between the experimental and simulation results. The parameter needs to be optimised here is critical solvent content. Before scale-up, the parameter were verified using small-scale TGA with the same compound and solvent, dried at 40 °C. Although the agreement is good, the small difference still exists in the constant rate-period and may be attributed to the gap between particles and vessel wall as well as the fouling layer of particles stick to the wall. This makes the actual contact resistance much bigger than the calculated value. Furthermore, the materials used in these experiments are the same but reused and reslurry again. Due to the sample used each time is the same as the previous batches and this may cause the changes of physical properties. Therefore, small changes in the transport properties could be observed despite the fact that the same operating conditions used. This also can lead to the deviation between experimental and simulation results.

8.3.1.1 Static beds

While experimental trials 1-3 in Table 5.4 were simulated by solving LPM ODEs in gPROMS. Figure 8.24 shows the predicted results comparing the experimental drying curves. It was found from the experimental results in section 8.2 that the range of the critical solvent content was 5-7% in different operation conditions applied. In this simulation process, the values, every 0.1% increment from 5% to 7%, was fitted through comparing the square deviation and it was found that 6.2% was the optimal critical solvent content for all the drying sets.

The simulation results have a good agreement to the experimental results. However, there is a discrepancy at the transition period that the predicted values are smaller to the experimental data. That may be resulted from the cake properties may change during the drying process. When the cake

drying it tends to be shrink into the core as the vapour removed from the internal space of the particles. This change may cause more resistance for the mass transfer process which hinder the drying process to some degree. Hence, the actual drying rate is a bit smaller than the predicted value especially during the transition period. A transition period means a short period around the transition point. For certain circumstances, most drying transferring from constant-rate period to falling-rate period presents a transition period rather than a single transition point. For the liquid phase during this period has the effect to support the particles structures. Once the liquid phase within the pores was removed this may result in rearranging the existing location of particle blocks.

The values used for the simulation results are listed as follows.

The effective cake thermal conductivity, λ_c, is calculated as follows [14, 99]:

$$\lambda_c = \lambda_s^{\nu_s} \lambda_l^{\bar{\nu}_l} \lambda_v^{\bar{\nu}_v} \qquad 8\text{-}2$$

where, λ_s, λ_l, λ_v are the thermal conductivities of solid, liquid and vapour phases; $\nu_s, \bar{\nu}_l, \bar{\nu}_v$ are the volume fractions of solid phase, average volume fraction of liquid and vapour phase individually.

The volume fractions and porosity of the cake can be expressed as follows:

$$\nu_s + \bar{\nu}_l + \bar{\nu}_v = 1 \text{ and } \nu_s = 1 - \varepsilon \qquad 8\text{-}3$$

Table 8.2 Parameters used for the simulation process of vacuum contact drying

Parameter	Value	Unit
A_V	30	m^2
A	0.0075	m^2
m_{ds}	0.99	kg
P_{ull}	0.18	mbar
ΔH_v	2380	kJ/kg
Z	0.04	m
T_w	350	K
T_b	330	K
D_c	0.163	m

α_{ws}	33	$W\,m^{-2}\,K^{-1}$
ε	0.3	-
v_s	0.7	-
$\bar{v}_l$	0.0001	-
$\bar{v}_v$	0.3	-
λ_c	0.08	$W\,m^{-1}\,K^{-1}$

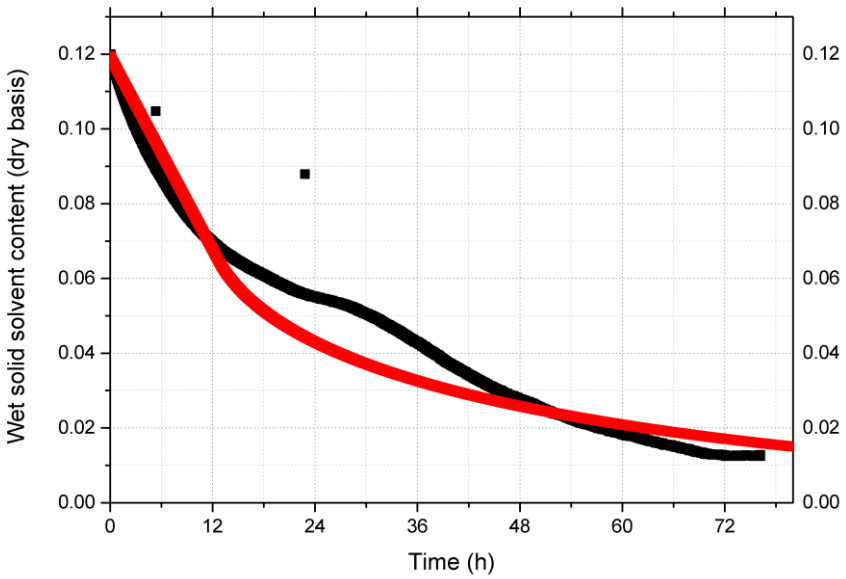

(a)

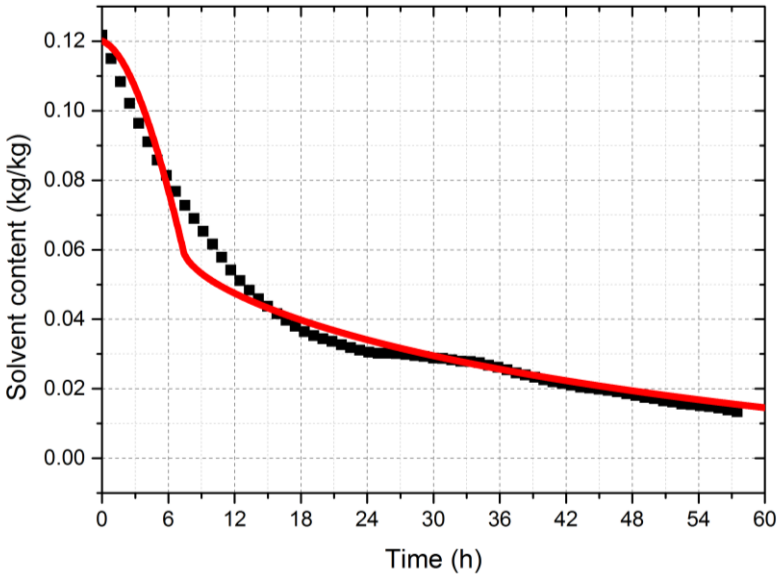

(b)

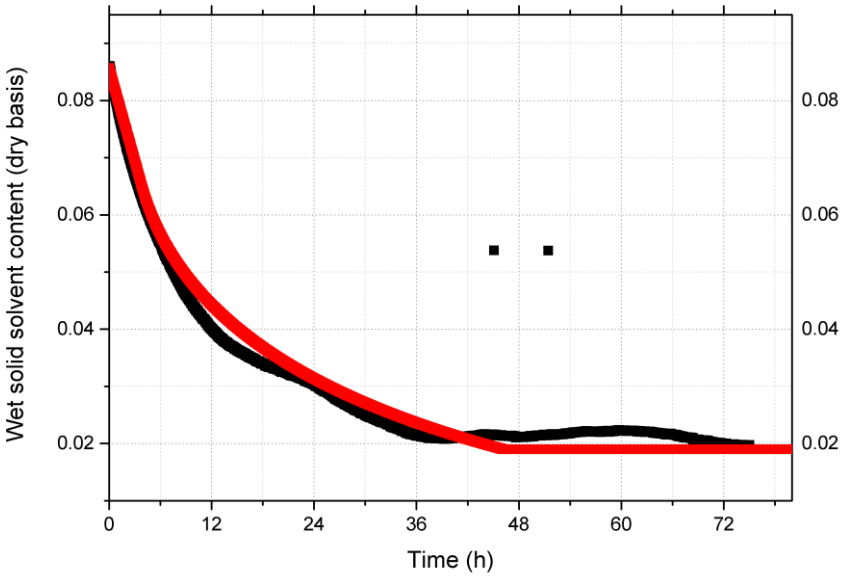

(c)

Figure 8.24 The simulation (——) and experimental result (——) for static bed contact drying with heat power at (a) 128 W; (b) 144 W; (c) 157 W

Compare to the model validation previous

8.3.1.2 Agitated beds

While experimental trials 4-6 in Table 5.4 were simulated by solving LPM ODEs with iteration process of agitation element in gPROMS. Figure 8.25 shows the predicted results comparing the experimental drying curves. In this simulation continued to employ the critical solvent content as 6%. Also the mixing number was estimated from the experimental trial 6 with agitation speed at 30 rpm. The equations used to calculate the mixing number were depicted in Chapter 6 and the mixed number was estimated to be 3. With this estimated mixing number to predict the drying behaviour of experimental trials 4 and 5 with agitation speed of 10 and 20 rpm. It is found that there is a little discrepancy for trial 5 while slight bigger discrepancy for trial 4. The reason for this may need to take consider the actual drying conditions that at higher agitation speed agglomeration effect aggravated that makes the estimation of mixing number distortion.

For the model did not consider any inter-particle interactions, hence when using this estimated mixing number (trial 6 in Table 5.4) to predict a range of agitation drying experiments, it can be found that the lower the agitation speed, the more discrepancy it is.

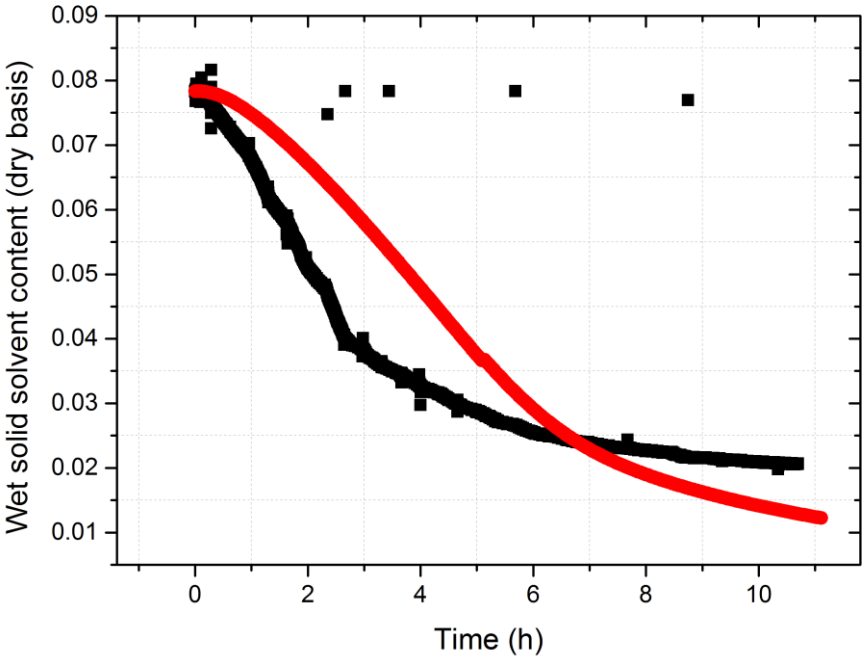
Wet solid solvent content (dry basis)
0.09
0.08
0.07
0.06
0.05
0.04
0.03
0.02
0.01
0
2
4
6
8
10
Time (h)

(a)

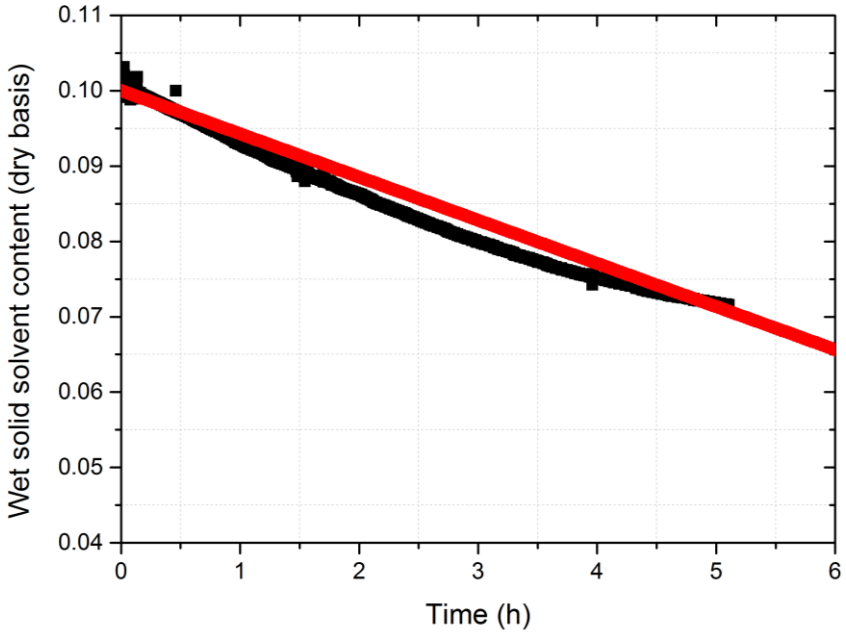
Wet solid solvent content (dry basis)
0.11
0.10
0.09
0.08
0.07
0.06
0.05
0.04
0
1
2
3
4
5
6
Time (h)

(b)

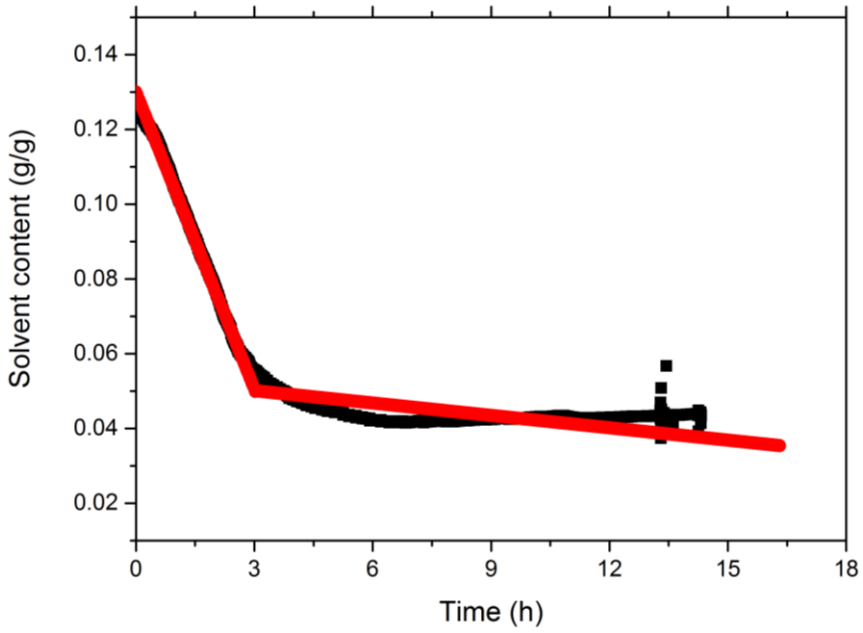

(c)

Figure 8.25 The simulation (——) and experimental result (——) for agitated contact drying under continuous agitation at (a)10rpm; (b) 20rpm and (c) 30rpm with heat power 157 Watts

Compare to the LPMs in previous work [2, 38], this model only one parameter critical solvent content needed to be fitted from experimental curves, if the drying starts below the critical solvent content, then no parameter estimation needed, the drying time can be calculated from this LPM directly. The advantages of this model not only lie on its computational expedient characteristic with a relative reliable prediction, but also can be applied to any preliminary drying, no specific software needed for calculation.

8.3.2 Modelling validation of DPM for static beds

Three fitting parameters were chosen from fitting the experimental operating conditions heat power at 128 W, 144 W and 157 W separately. And then the averaged values of fitting parameters were shown in Table 8.1. Using the average value of evaporation rate constant, residual saturation and proportionality constant to predict the experimental trials 1-3 in Table 5.4. It can be seen that good predicting trends for the distributed parameter model. However, there is discrepancy between the calculated curve and experimental data for the samples drying at heating power of 144 and 157 W in Figure 8.26. This may also be explained by particle interactions due to high heating input into the powder bed that the residual solvent was more sticky to the particles leading to aggregation even within the static bed.

Table 8.3 The three parameter using to fit in this model

Test	Evaporation rate constant	Residual saturation	Proportionality constant
Trial 1	3.00E-06	0.25	5.00E-09
Trial 2	5.00E-06	0.14	1.00E-07
Trial 3	3.00E-05	0.1	1.00E-05
Average value	1.00E-06	0.15	3.00E-06

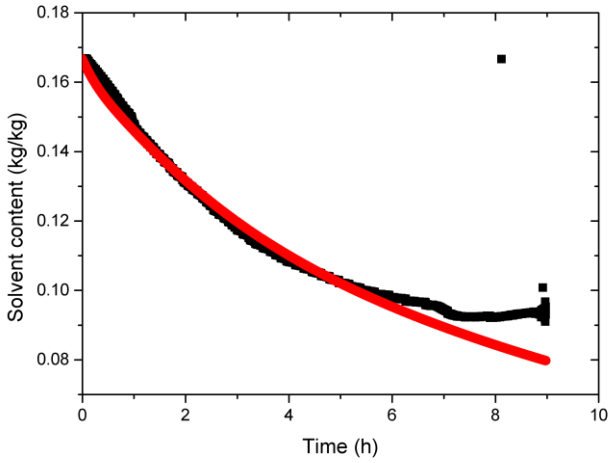

(a)

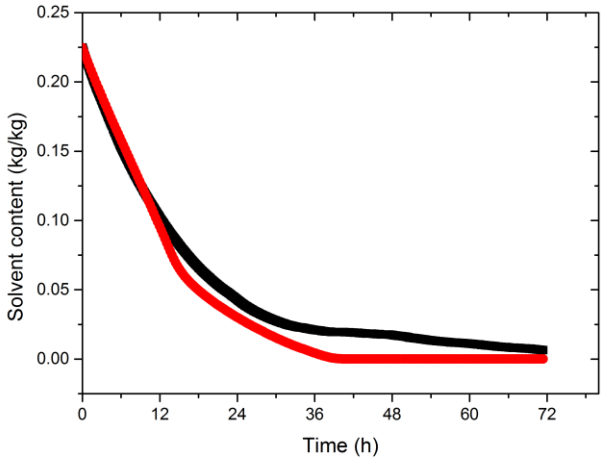

(b)

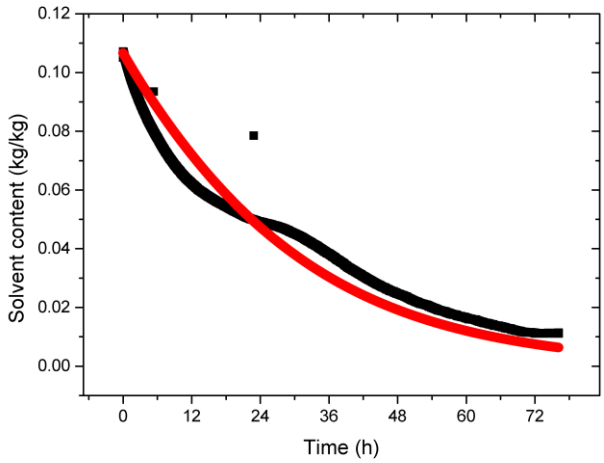

(c)

Figure 8.26 The simulation (———) and experimental result (———) for static bed contact drying with heat power at (a) 128 Watts; (b) 144 Watts; (c) 157 Watts

It can be seen there is good agreement between most of the calculated curves and experimental data especially for constant-rate period. The reason for the discrepancy mainly lies on the residual saturation is very sensitive parameter and it is most rely on particle and bed properties. Hence, any slight changes about the filter cake will lead to a different residual saturation. However the evaporation rate constant is relatively constant compare to the residual saturation for this parameter is related to the solvent vaporization.

The temperature profile of trial 3 (157 W) shown in Figure 8.27 is the experimental and calculated temperature curves. It can be seen that the simulation temperature curves have the similar trend to the experimental curves. The good prediction to the data at the wall area while some discrepancy to the temperatures of inside the wet-cake. The actual bed temperature variation with time seems to have very sharp changes at the transition point however the calculated curves are smoothly changing with time. The reason for that may be caused by the agglomeration effects and the changing of kinetic porosity of the bed during the drying process.

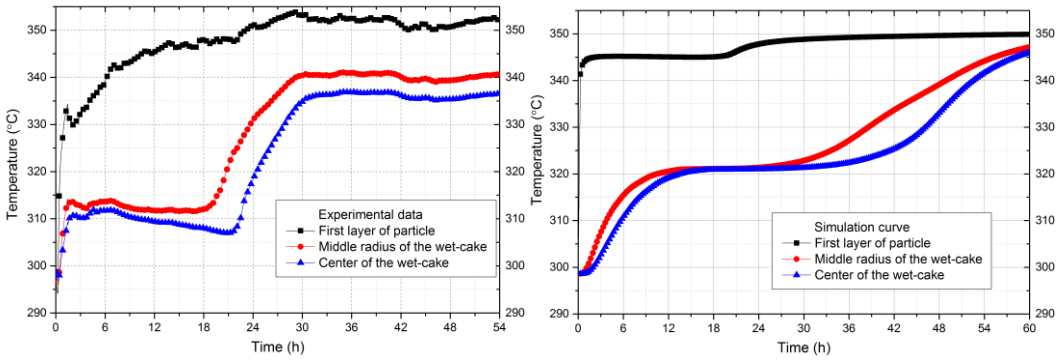

Figure 8.27 Experimental data (left) and simulation curve (right) for wet solid temperature distribution of vacuum contact drying

The DPM model [1] is only developed for intermittent agitation with very short stirring period, however, for the experimental cases in this work, with continuous agitation and intermittent agitation (ON/OFF=1:1) applied, the DPM model are not applicable. Hence, the DPM are not validated in vacuum contact drying of agitated beds in this work.

8.4 **Conclusions**

Temperature profile and torque has been proved be a consistent way to identify the critical solvent content. The outcome of struggling between the two effects also can be observed by particle size analysis. Every agitated drying process the torque value has consistent transition point to the temperature profile indicating that existence critical solvent content and the struggling between attrition and agglomeration effect.

Among different operation conditions investigated in this section, it is found that the drying rate relies on the heating power supply, the stirring speed, the solvent type as well as the PSD and the morphology of the materials being dried. The drying rate is found to be increased with the heating power supply, agitation speed, the proportion of volatile solvent in the mixed solvents.

Particle size decreases as the agitation speed increases due to attrition effect, while, particle size is observed to be increase at low agitation speed due the agglomeration issue.

The predicted drying curves for the vacuum contact drying process, are in reasonably a good agreement with experimental data for both the LPM and

DPM. This agreement is especially well matched in the constant-rate period while some discrepancy exited during the falling-rate period.

The following future work can be done: for experimental work, data collection of reliable solvent content distribution within the wet-cake provide more sources for model validation ; further optimising the agitation regime to reduce agglomeration effect; the multi types of solvents drying can be investigated.

Chapter 9
Experimental results on through-circulation convective drying

9.1 Introduction

In this chapter, the experiments for through-circulation convective drying were carried out in the lab-scale AFD. The effects of different dry air flow, agitation speed, initial solvent content on drying behaviours were investigated. A heat exchanger were installed at the dry air inlet to maintain the temperature of dry air to a certain level.

The models developed for through-circulation convective drying in section 6 were validation in this chapter. The models including differential partial equations were solved using the gPROMS software. The plot of LPM and DPM of the convective drying were compared with the experimental data. The temperature profile along the axial direction were also compared between the experimental and simulation results.

9.2 Experimental results and discussion

In this section, the effects of drying air flow, initial solvent content, agitation speed was investigated using medium-scale AFD rig. In order to get the drying curve, the relative humidity data directly get from the instrument is converted as follows:

Relative humidity is given by:

$$H_R = 100\% \times \frac{P_v}{P_{sat}} \qquad 9\text{-}1$$

Absolute humidity can be expressed as:

$$H = \frac{m_v}{m_a} = \frac{M_v P_v}{M_a (P - P_v)} \qquad 9\text{-}2$$

Replace P_v in equation (7-1):

$$H = \frac{\dot{m}_v}{\dot{m}_a} = \frac{M_v H_R P_{sat}}{M_a (P - H_R P_{sat})} \qquad 9\text{-}3$$

The mass flow of vapour within the gas phase is given by

$$\frac{\Delta m_v}{\Delta t} = \frac{M_v H_R P_{sat}}{M_a \left(P - H_R P_{sat}\right)} \dot{m}_a \qquad 9\text{-}4$$

By integrating equation (7-4), the mass of vapour weight is given by

$$\int_0^{m_v} dm_v = \int_0^t \frac{M_v H_R P_{sat}}{M_a \left(P - H_R P_{sat}\right)} \dot{m}_a dt \qquad 9\text{-}5$$

The increased vapour weight is equal to loss on solvent weight:

$$m_v = m_{so} - m_s \qquad 9\text{-}6$$

where m_{so} is the initial solvent weight remaining inside the wet-cake before drying starts.

where $A = 10.196213, \quad B = 1730.63, \quad C = 233.426 \qquad for \quad 0°C < T < 100°C$

H_R	Relative humidity	H	Absolute humidity
P_{sat}	Saturation vapour pressure	P_v	Vapour pressure
m_v	Mass of vapour	m_a	Mass of dry air
m_s	Mass of solvent	m_{so}	Initial mass of solvent

9.2.1 Effects of flow

To obtain the moisture content changing with time, the relative humidity against time were recorded at different flow ranging from 8 L/min to 12 L/min. It can be seen that the inlet dry air humidity is quite constant and low maintaining at 0.05% of relative humidity. For the outlet relative humidity in Figure 9.1, with the increase of gas flow, distinguish between the constant- and falling-rate periods become more obscure. As the drying progressing, the gradually loss of the constant-rate period in Figure 9.1 (b) and (c) indicates that the higher gas flows result in a faster cooling rate giving smaller crystals in the system while for lower flows there is more time for re-dissolving and re-crystallization. It is necessary to convert the relative humidity to the absolute humidity of the gas and then further get the moisture content changes.

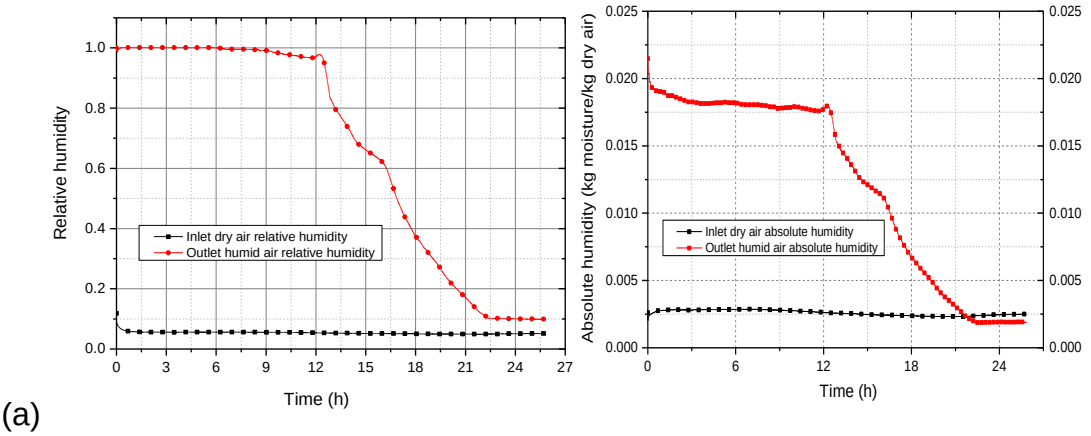

(a)

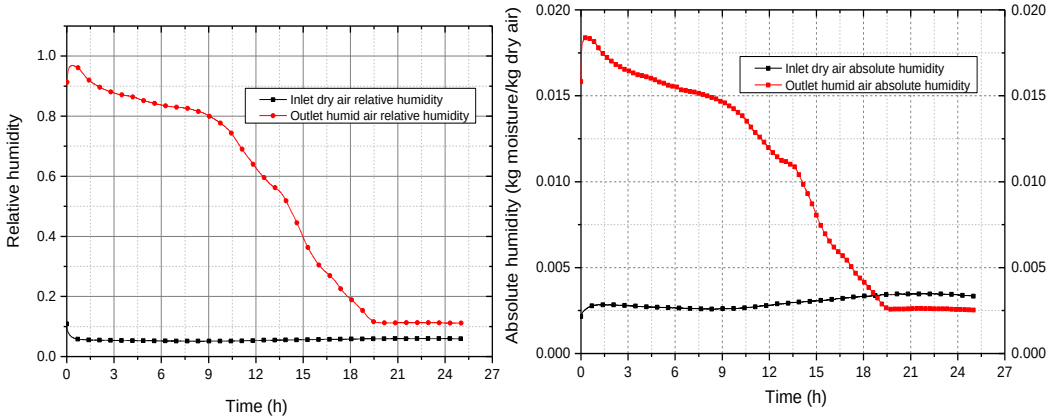

(b)

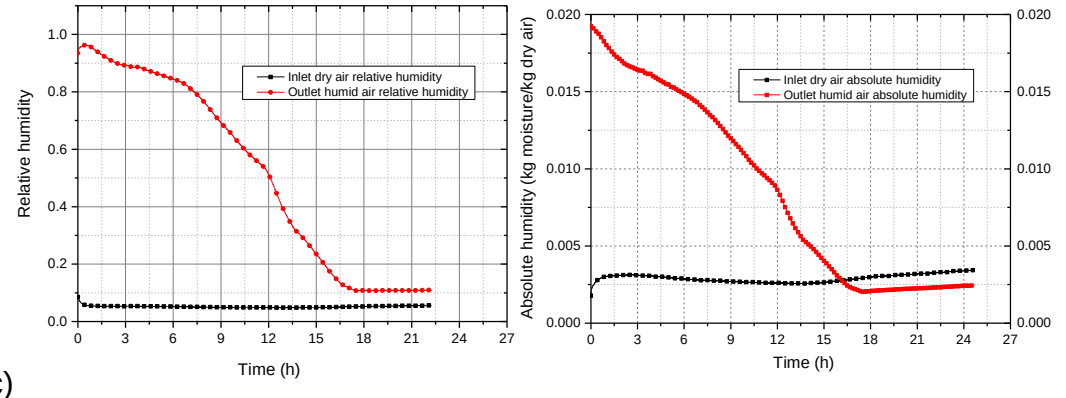

(c)

Figure 9.1 Relative humidity (left) and absolute humidity (right) against time at different flows (a) 8 l/min, (b) 10 l/min, (c) 12 l/min

The higher drying rate results in a faster drying. Within the similar initial solvent content in Figure 9.2, the drying time is 20 h for 8 L/min, 18 h for 10 L/min and 15 h for 12 L/min. The drying rates against solvent content at different flow are plotted in Figure 9.3. The critical moisture content of the wet-cake seems maintain the same regardless of the flow. It might be have a

slightly change due the recrystallization under convective drying. However, the inlet temperature of drying air is between 20-30 °C which has little possibility in changing the particle sizes. That is the reason why the critical solvent content staying the similar value.

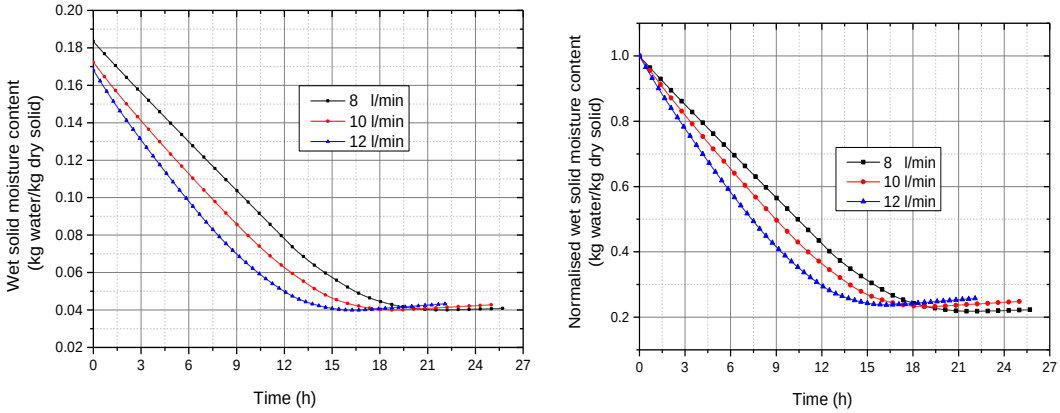

Figure 9.2 Moisture content (left) and normalised moisture content (right) against time at different flow

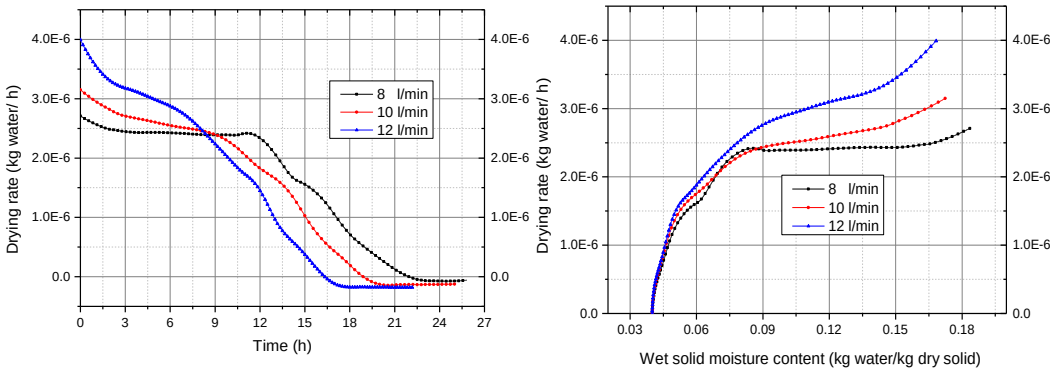

Figure 9.3 Drying rate against time (left) and drying rate against moisture content (right) at different flow

The temperature profile at different flow shows the real temperature distribution along axial direction. From Figure 9.4, it can be seen that cooling effect caused by solvent vaporization initially occurs at the surface of the wet-cake. At the same time, the cake inside temperature also drops down but has a delay along the axial direction. The delay is caused by the dry gas entering from the top of the cake and carrying the moisture vapour away and then exit the cake with saturated humid gas. As the humid gas passing by the middle layer the wet-cake, it can only carry limit amount of moisture until it reaches saturation humidity. According to the previous theory that during through-circulation convective drying, the vaporization occurs layer by layer.

From the temperature profile in Figure 9.4, it can be seen that the moisture vaporization occurs in parallel, but with the limitation of saturation humidity. The temperature of the cake surface often reaches a valley earlier than other axial positions. The value of the valleys should be calculated according to the wet bulb temperature. During this period, because the solid surface is covered by a film of free water, the drying curve start with a higher drying rate. The end of drying process is indicated by the temperature of the bottom of the wet-cake reaches to the inlet gas temperature.

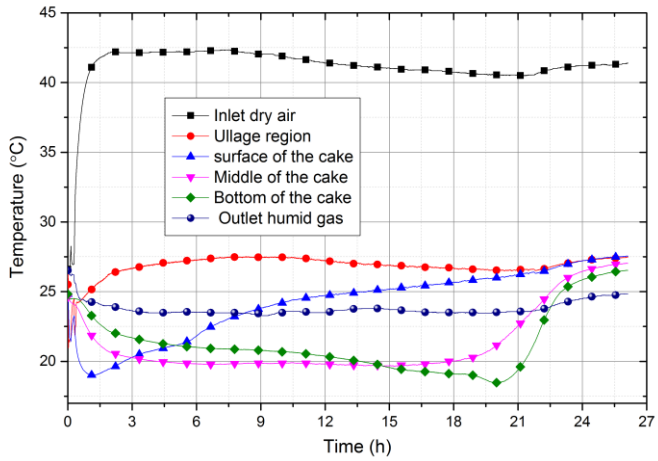

(a)

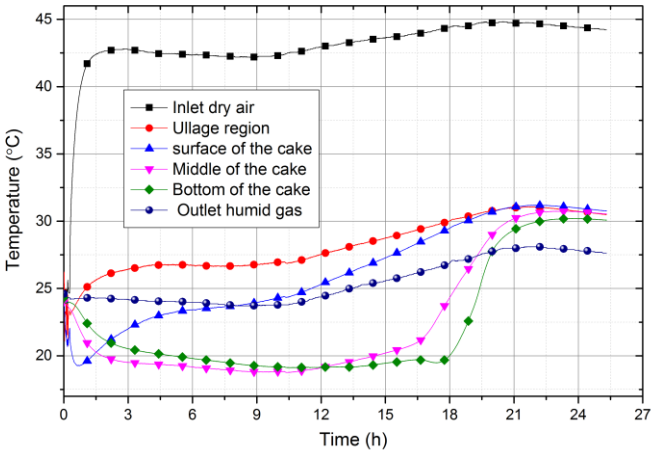

(b)

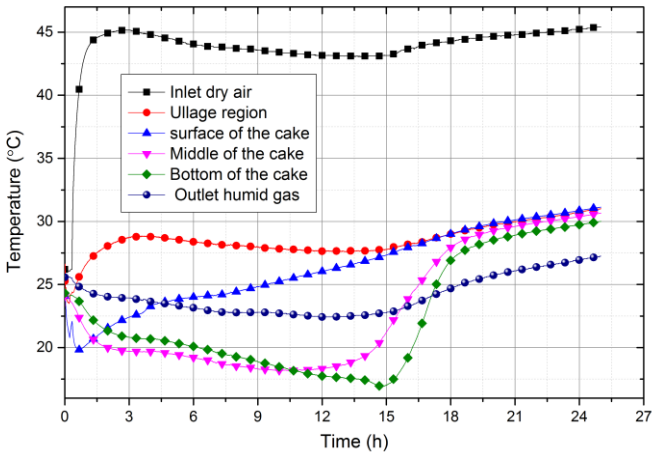

(c)

Figure 9.4 Axial temperature distribution against time at different flows (a) 8 l/min, (b) 10 l/min, (c) 12 l/min

The temperatures of the same location under different flows are presented in Figure 9.5, 9.6 and 9.7. The temperature profile shows that there is a delay for the wet-cake reach the wet bulb temperature. The temperate reaches its valley for higher drying rate 12 L/min earlier than the slower drying rate 8L/min. It can be explained by that the faster drying is resulted from higher gas flow.

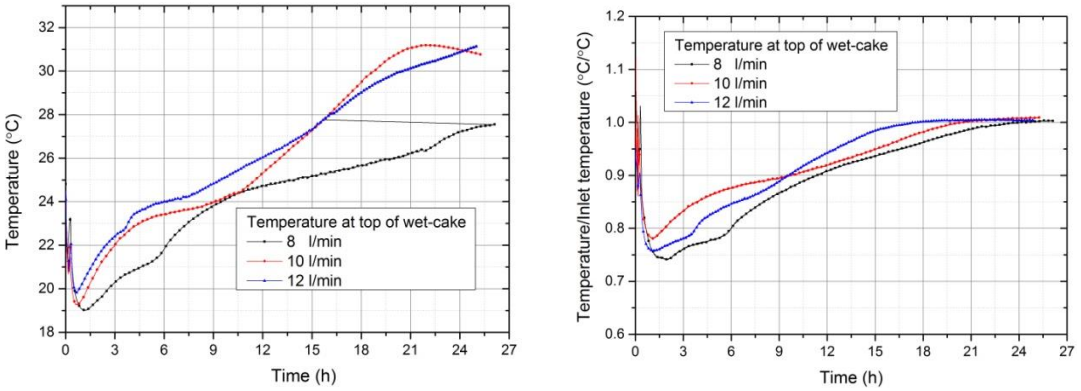

Figure 9.5 Temperature (left) and normalized temperature (right) at the surface of wet-cake at different flow

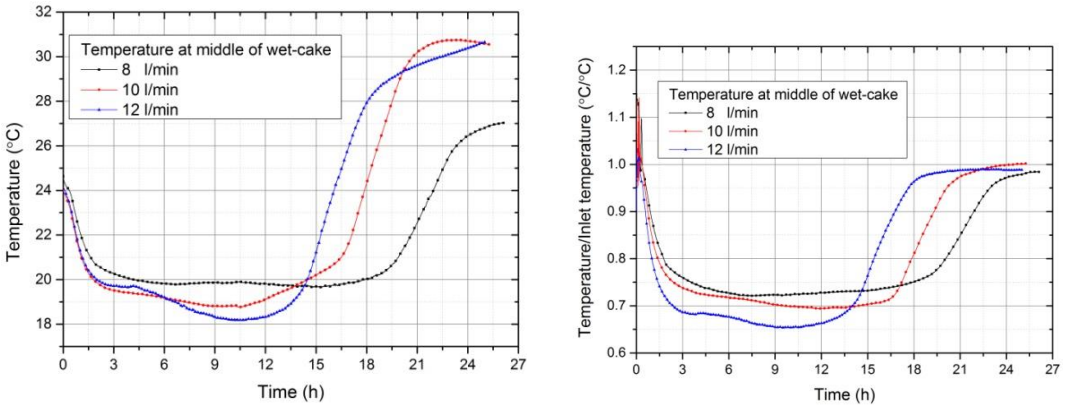

Figure 9.6 Temperature (left) and normalized temperature (right) at the middle of wet-cake at different flow

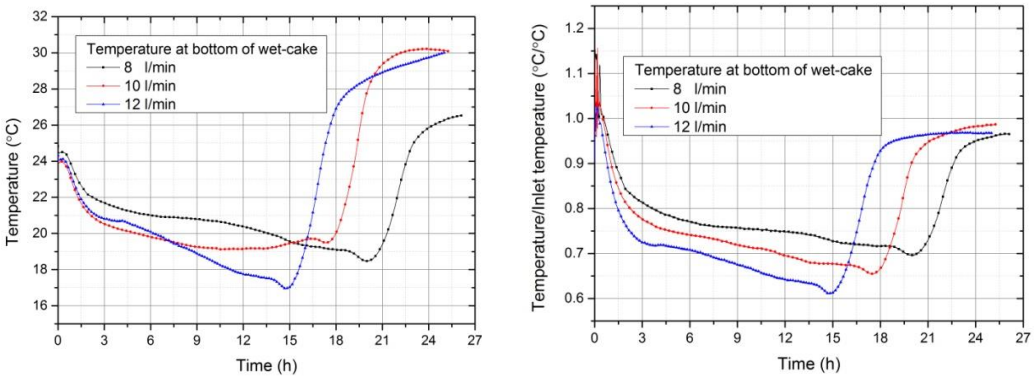

Figure 9.7 Temperature (left) and normalized temperature (right) at the bottom of wet-cake at different flow

9.2.2 Effects of agitation

The effect agitation was investigated by apply different stirring speed to through-circulation convective drying (Figure 9.8). From Figure 9.9, it can be observed that the higher agitation speed results in faster drying rate. But due to the continuous agitation applied, the actual drying rate is not only depending on the extent of agitation, it is also determined by the degree of agglomeration.

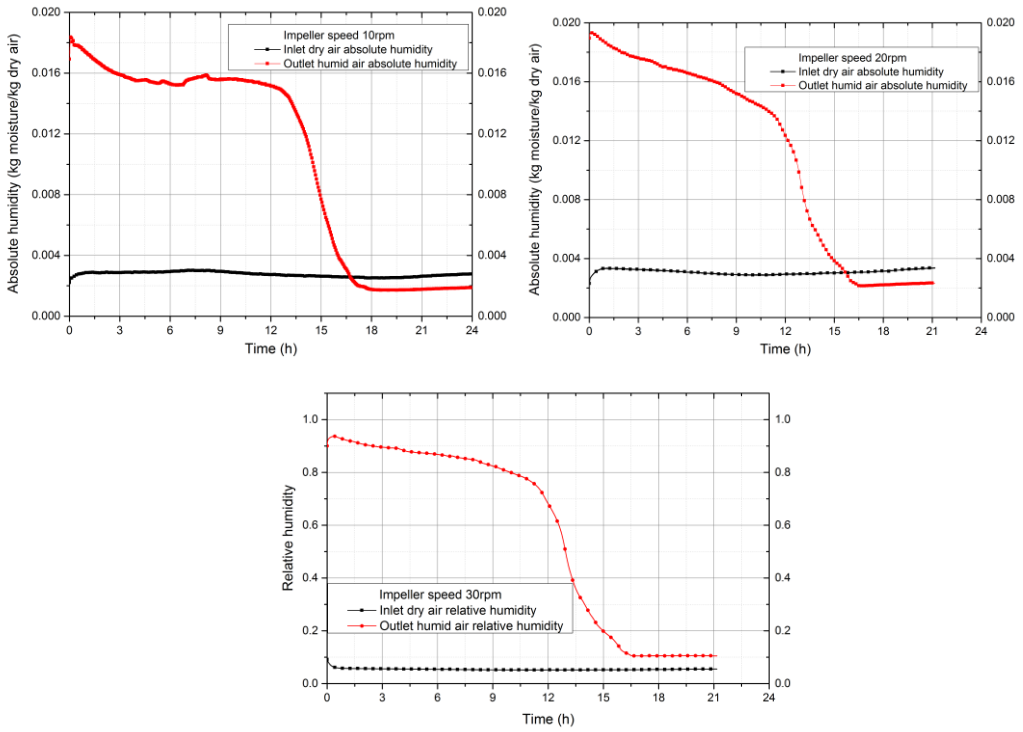

Figure 9.8 The absolute humidity against time with agitation speed at 10rpm, 20rpm and 30rpm

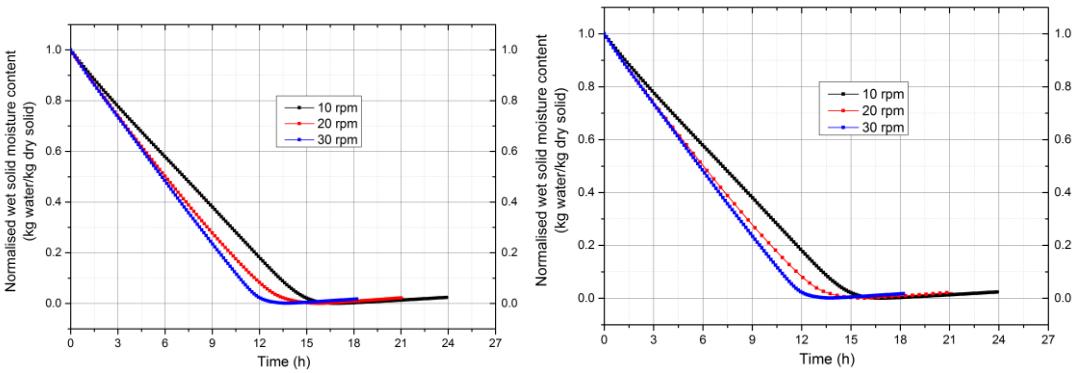

Figure 9.9 The solvent content against time with agitation speed at 10rpm, 20rpm and 30rpm

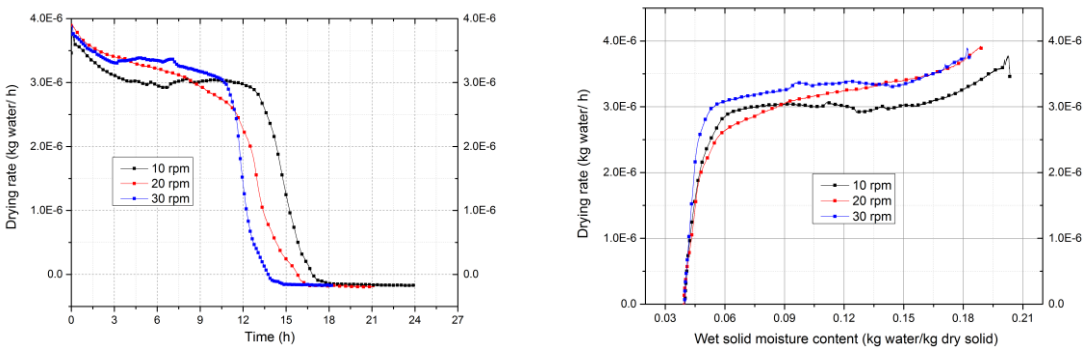

Figure 9.10 The drying rate against the solvent content with agitation speed at 10rpm, 20rpm and 30rpm

The temperature profile for the agitated bed in Figure 9.11 shows that the temperature gap between different layers along the axial direction diminishes as the agitation effects make the cake temperature more homogeneous compared to that of static bed. To determine the best way to agitate, the moisture content flow should be taken into account. The agitation should start at top layer then gradually goes down the bottom the wet-cake. The agitation should start with static bed drying and then when the top layer wet-cake passes the temperature valleys it is the best time to start agitation. Comparing the temperature profile for different agitation speed, it can be seen that for higher agitation speed, the temperature gap is much narrower due to the stronger agitation effects.

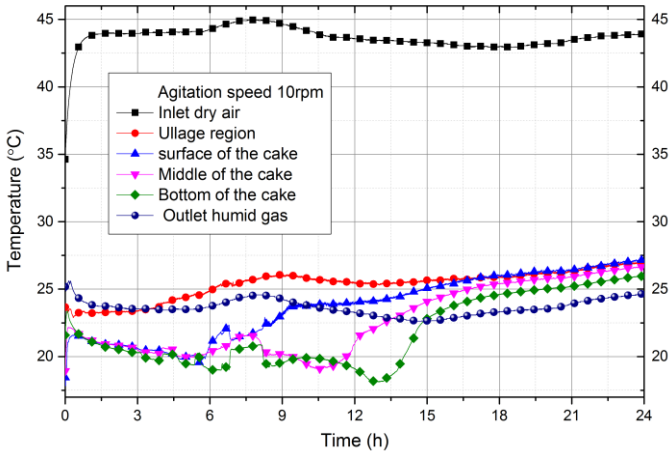

(a)

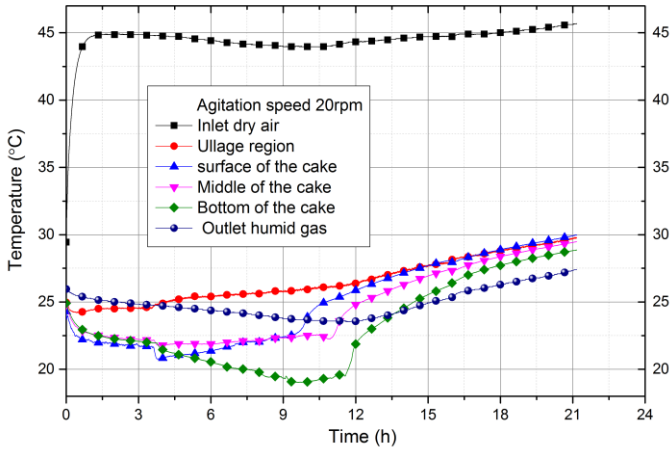

(b)

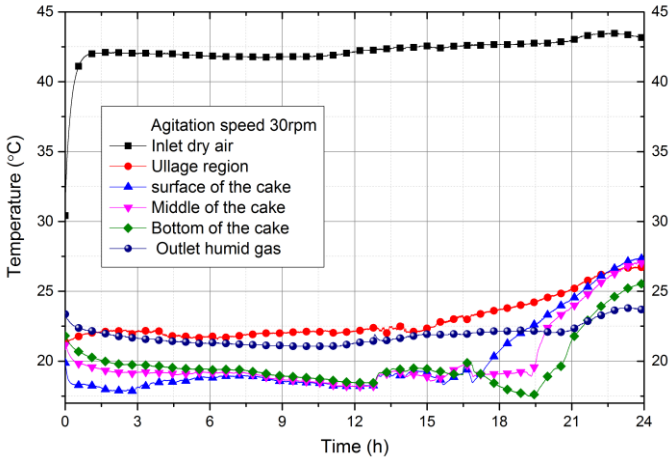

(c)

Figure 9.11 Axial temperature distribution against time at agitation speeds (a) 10rpm, (b) 20rpm, (c) 30rpm

9.2.3 Effects of initial moisture content

The drying behaviours with three initial solvent contents at 13%, 15% and 35% were plotted in Figure 9.12. It can be seen that the drying behaviours with lower solvent content 13% and 15% are much similar to each other while the high initial solvent content 35% shows different drying behaviour.

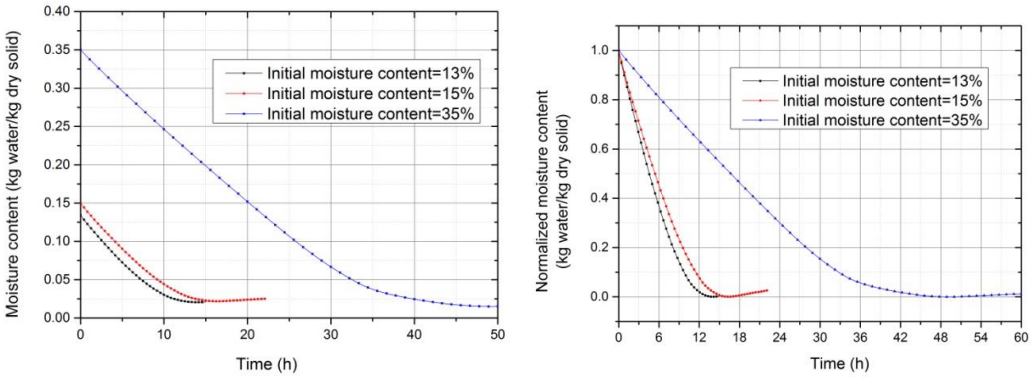

Figure 9.12 Solvent content (left) and normalized solvent content (right) against time with air flow 12 l/min at different initial moisture content

The higher initial solvent content shows that a different transition point indicating that if drying starts from a higher solvent level it may change the crystalline form due to recrystallization during drying process. In Figure 9.13, it can be seen that the upper bound and lower bound of drying rate will not change within the full solvent content range. However, the critical solvent

content was found to change and shift to higher value in that the crystal size increases due to recrystallization process.

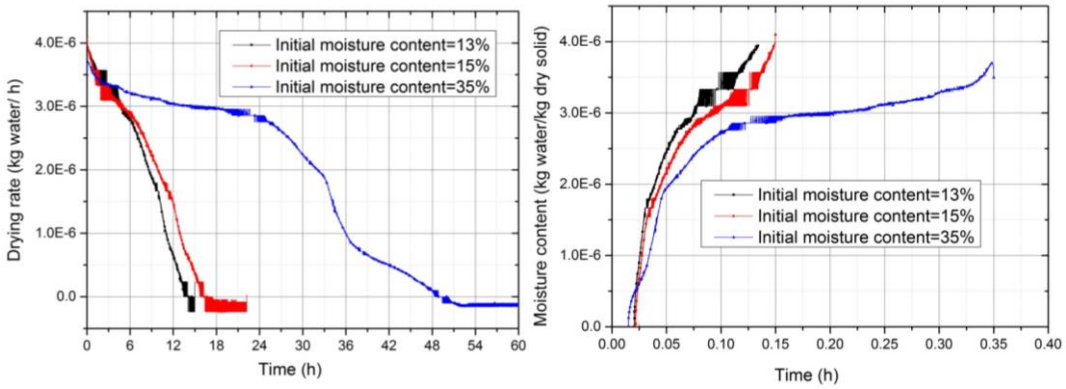

Figure 9.13 Drying rate against time (left), drying rate against moisture content (right) at different initial moisture content

9.3 Simulation results and validation

9.3.1 Estimation of convective heat transfer coefficient

Three different flows pre-set in the operating conditions are 8, 10 and 12 $\mathrm{L\,min^{-1}}$ and then converted to UI as 0.0076, 0.0095, and 0.011 $\mathrm{kgm^{-2}\,s^{-1}}$. The method to calculate the convective heat transfer coefficient from the gas phase to wet solid phase was calculated as follows, here shows one example of the three trials. All the other calculation results were shown in Table 7.1.

Examples of calculation of Reynolds, Prandtl and Nusselt numbers of forced convection of liquid vaporization [19] for mass flow at 0.0076 $\mathrm{kgm^{-2}s^{-1}}$ are shown as follows:

$$\mathrm{Re} = \frac{d_p \dot{G}}{\mu_a} = \frac{4\times10^{-4}\times7.6\times10^{-3}}{1.8\times10^{-5}} = 0.17$$

$$\mathrm{Pr} = \frac{c_{p,a}\mu_a}{\lambda_a} = \frac{1007\times1.8\times10^{-5}}{0.026} = 0.7$$

$$\mathrm{Nu} = 0.0015\,\mathrm{Pr}^{0.33}\,\mathrm{Re}^{0.62} = 0.000445$$

Hence the convective heat transfer coefficient is calculated

$$\alpha_{gs} = \frac{\mathrm{Nu}\,\lambda_a}{d_p} = 0.029 \ \left(\mathrm{Wm^{-2}\ K^{-1}}\right)$$

Table 9.1 Parameters of used in the convective drying experiments for three trials of different gas mass flow at 27 °C

Parameters	**Trial 1**	**Trial 2**	**Trial 3**	**Unit**
Superficial velocity (u_a)	0.0064	0.0080	0.0096	$\mathrm{ms^{-1}}$
Mass velocity of air ($\dot{G}$)	0.0076	0.0095	0.011	$\mathrm{kgm^{-2}s^{-1}}$
Density of air (ρ_a)	1.16	1.16	1.16	$\mathrm{kgm^{-3}}$
Density of dry cake (ρ_{dc})	980	980	980	$\mathrm{kgm^{-3}}$
Surface area* (A_s)	30	30	30	$\mathrm{m^2kg^{-1}}$
Interfacial area per unit volume (A_V)	29400	29400	29400	$\mathrm{m^2m^{-3}}$
Volume distribution based particle size* (d_p)	4.0E-04	4.0E-04	4.0E-04	m
Inlet air temperature (T_1)	27	27	27	°C
Initial solid temperature (T_s)	25	25	25	°C
Wet bulb temperature* (T_W)	19	19	18	°C
Heat of vaporization at T_W (ΔH_W)	2459	2457	2461	$\mathrm{kJkg^{-1}}$
Kinematic viscosity of air (μ_g)	1.8E-05	1.8E-05	1.8E-05	$\mathrm{kgm^{-1}s^{-1}}$

Specific heat of air ($c_{p,g}$)	1007	1007	1007	$\mathrm{Jkg^{-1}\ K^{-1}}$
Thermal conductivity of air (λ_g)	0.026	0.026	0.026	$\mathrm{Wm^{-1}\ K^{-1}}$
Reynolds number (Re)	0.17	0.21	0.25	-
Prandtl number (Pr)	0.707	0.707	0.707	-
Nusselt number (Nu)	0.00045	0.00051	0.00057	-
Initial solvent content (X_o)	0.18348	0.17234	0.16823	-
Critical solvent content (X_C)	0.8	0.8	0.8	-
Equivalent solvent content (X_e)	0.032	0.032	0.032	-
Convective transfer coefficient (α_{gs})	0.029	0.033	0.037	$\mathrm{Wm^{-2}\ K^{-1}}$

* A_s, the interfacial area per unit volume is obtained by average the value of BJH desorption (34.6 $\mathrm{m^2kg^{-1}}$) and adsorption cumulative surface area (26 $\mathrm{m^2kg^{-1}}$) of pores between 1.7 nm and 300 nm diameter.

* d_p, volume distribution based particle size is distribution relevant to the relative proportion of poly modal sample based on their mass or volume.

* T_W, wet bulb temperature is obtained from the thermocouple profile reading from Figure 9.11, according to the temperature profile that the wet bulb temperature is the lowest temperature that can be reached under prevailing conditions by the evaporation of water. An average T_W (18.5) is used for the calculation in section 9.3.2.

9.3.2 Modelling validation

By using the parameters provided in the table above and implement LPM of convective drying to gPROMS software, the predicted drying curves and the experimental results are shown in Figure 9.14. For this model, no parameters needs to be fitted while it can be seen that the predicted drying rate is commonly larger than the actual experimental value. The reason for

may be caused by the following points: first of all, the gap between the wall area and wet-cake can be very important for it is related to the bed thickness as well as the filter cake structure. This may create a short path for the drying air hence facilitate passing through big voids and further reduce the drying efficiency. Meanwhile, the flow direction may change from parallel to turbulent flow. This will further drag the drying rate slowly.

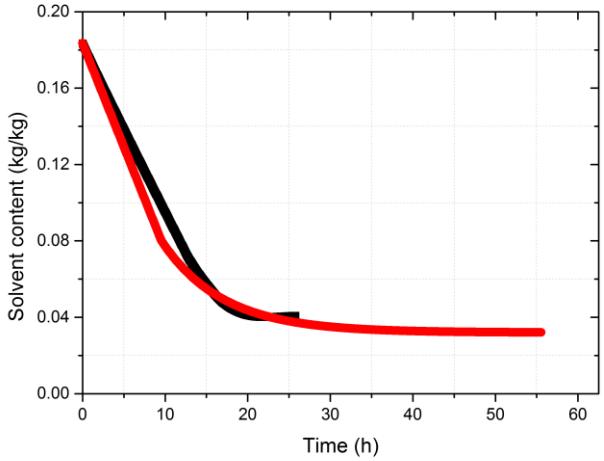

(a)

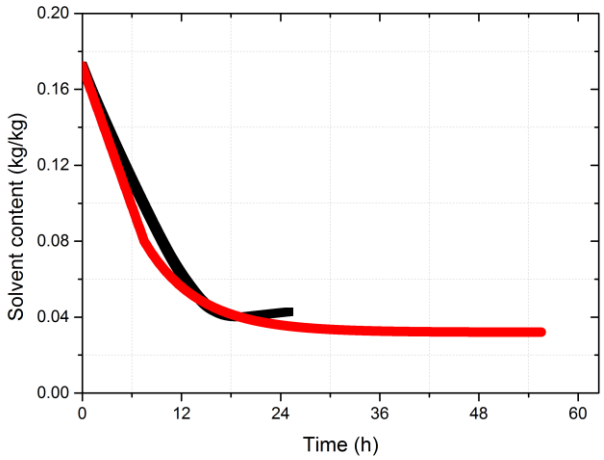

(b)

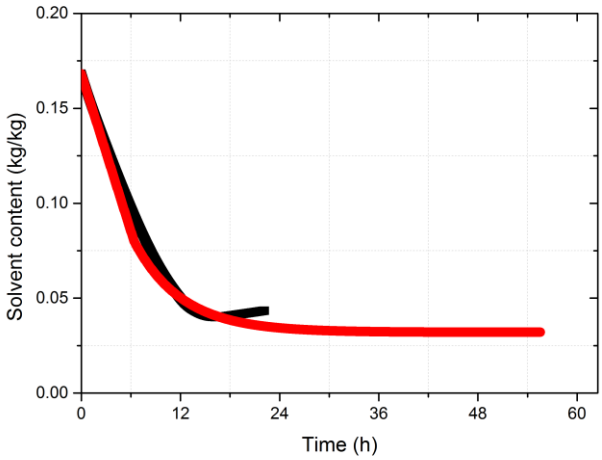

(c)

Figure 9.14 The simulation (——) and experimental result (——) for dry air flow at (a) 8 l/min; (a) 10 l/min and (c) 12 l/min

With regarding the prediction of different initial solvent content , the drying curve were compared between the simulation and experimental results. It can be seen that for it has a good agreement for low initial solvent level of the wet-cake (Figure 9.15 b and c), while when increasing the initial solvent content to 0.35, there is a deviation between the simulation and experimental results in Figure 9.15 a. The reason for that could be possibly caused by the high solvent level at the beginning of the hot air drying resulting in a recrystallization process. Then the heat supplied from dry air is not only used for solvent evaporation but also consumed for recrystallization process. This phenomenon is observed in Figure 9.15 a that the calculated drying rate is faster than the actual drying rate.

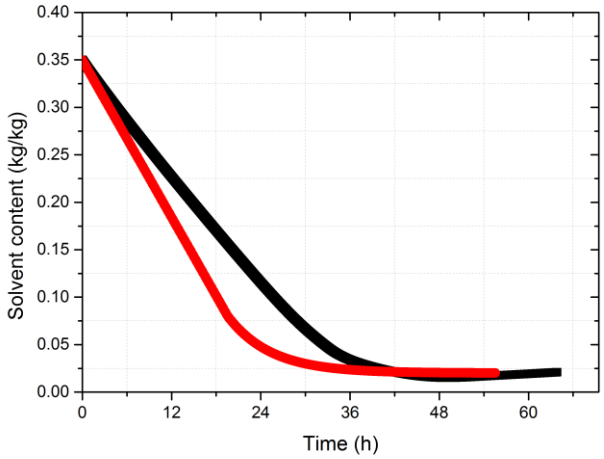

(a)

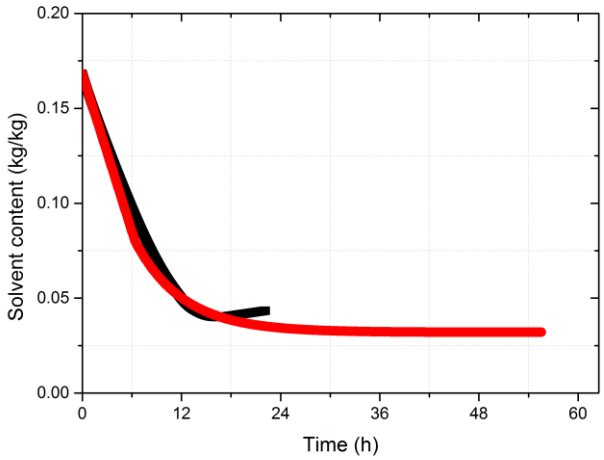

(b)

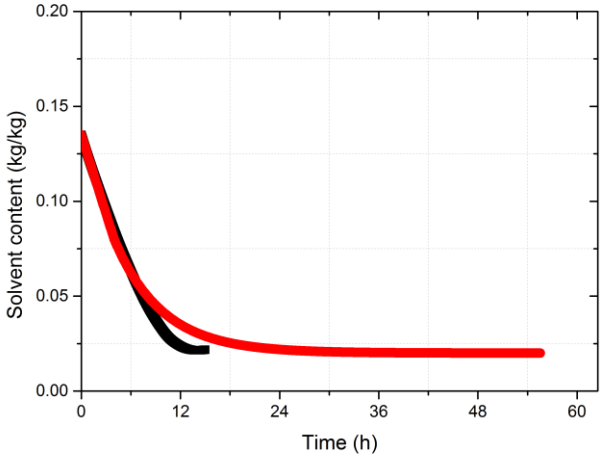

(c)

Figure 9.15 The simulation (——) and experimental result (——) for dry air flow at 12 l/min (a) X_o = 0.35; (a) X_o = 0.16823 and (c) X_o = 0.135

Here shows one example of DPM for convective drying process when flow at 8 l/min. Calculated results are shown in Figure 9.16, 9.17, 9.18 and 9.19. For different phases there is different distribution of the temperature and solvent content. In Figure 9.15, the thermocouple temperatures were compared with the calculated temperature profile along the axial direction of the cake. It is found that the thermocouple temperatures are more similar to the average value of the gas and solid temperature. For the thermocouples placed in the wet-cake, they both contact with the gas phase as well the wet solid phase. Hence, the temperature are more prone to reflect the interfacial temperature between the phases.

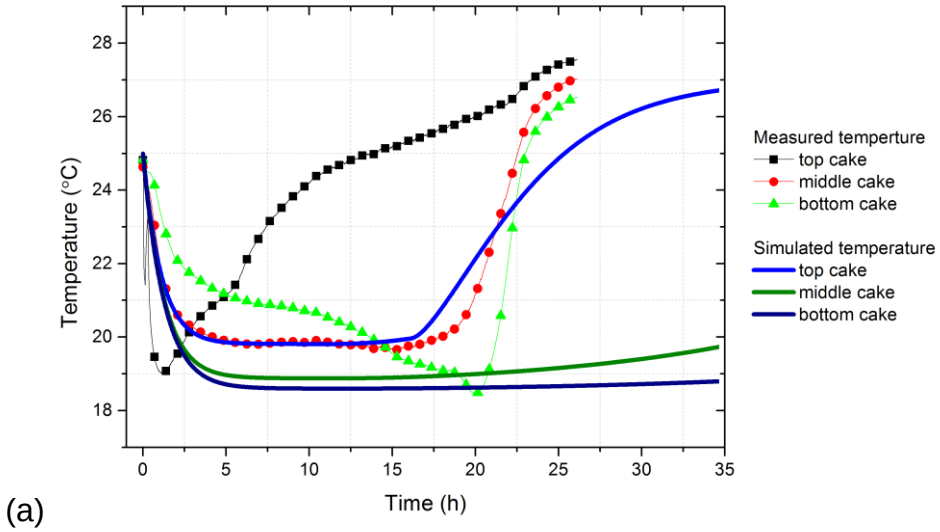

(a)

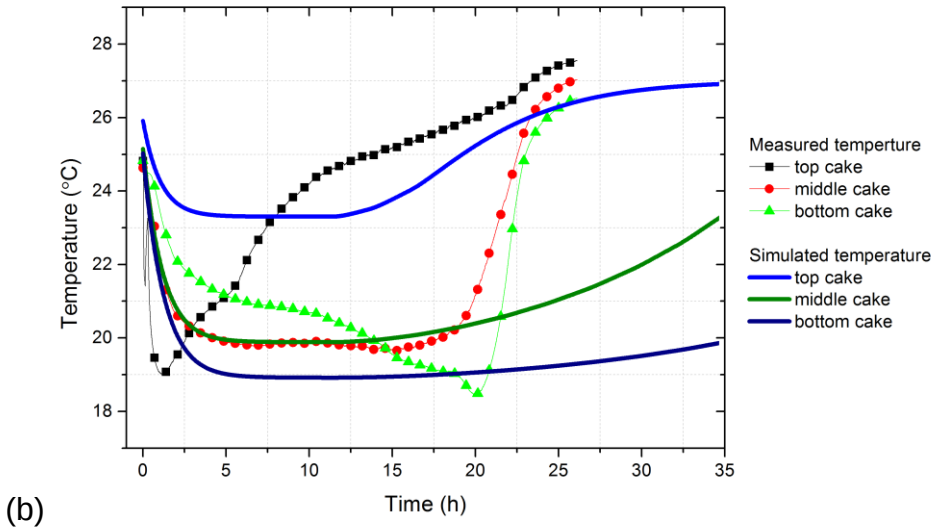

(b)

Figure 9.16 The calculated temperature distribution profile at the axial directions of the wet-cake at 8 l/min (a) comparison the plot of the thermocouple and calculated gas temperatures; (b) comparison the plot of thermocouple and calculated wet solid temperatures

The 3-D plots of solvent content and temperature profile for trial 1 within the bed in Table 9.1 gave an indication of the variables of solvent content and temperature changing with time and location. Give a certain time and location, it can be found the value of solvent content and temperature at that point. Hence, the 3-D plots described not the solvent content but also the temperature profile at different time and locations. It is found that the averaged drying rate is bigger than the local solvent content. As the deeper the wet-cake is, the more difficult to remove the moisture away.

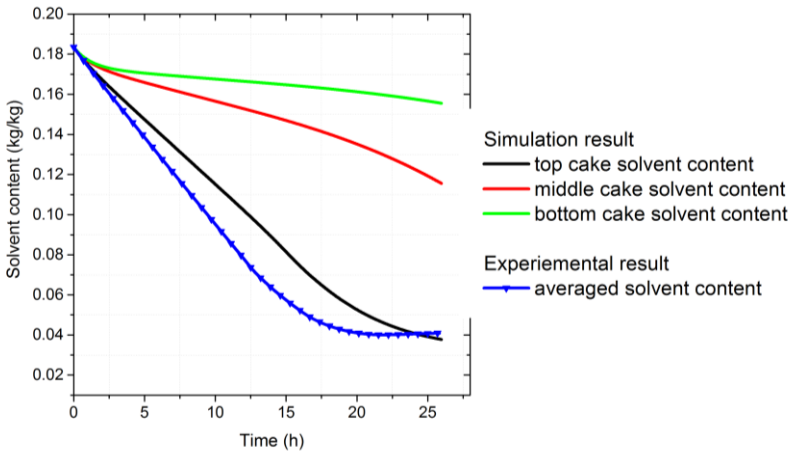

Figure 9.17 The plot of calculated solvent content distribution at top, middle and bottom of the wet-cake compared with averaged experimental solvent content with flow at 8 l/min

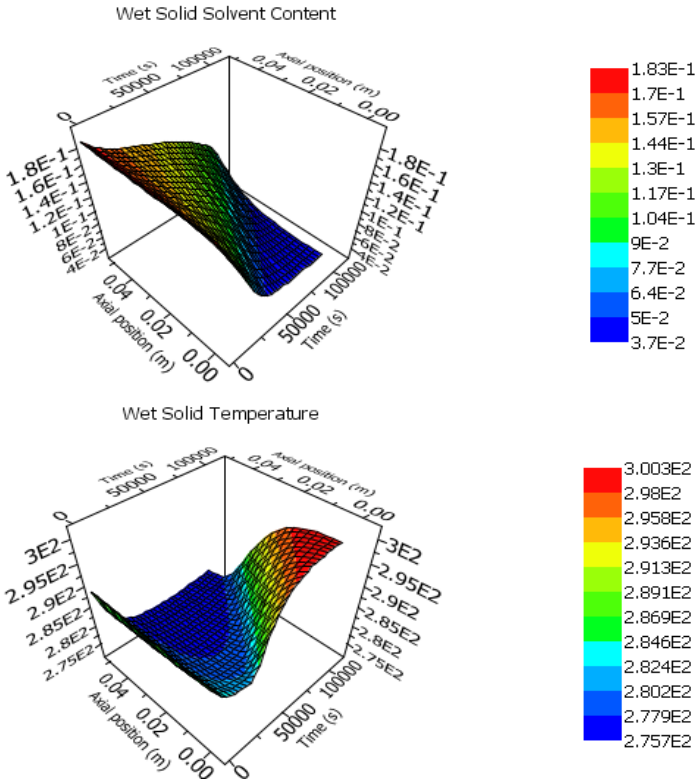

Figure 9.18 The calculated temperature and solvent content distribution for wet solid phase within the wet-cake at 8 l/min

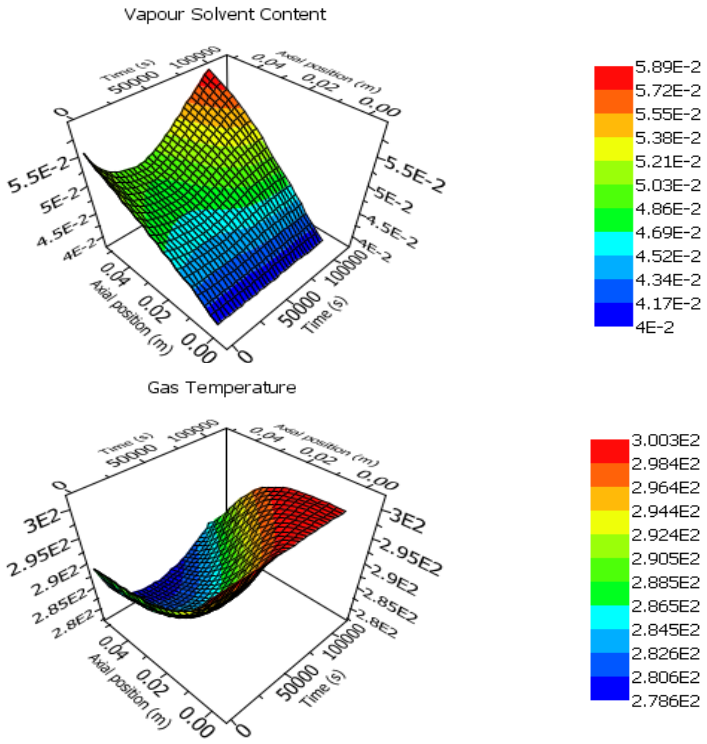

Figure 9.19 The calculated temperature and solvent vapour content distribution for the gas phase within the wet-cake at 8 l/min

9.4 Conclusions

In this chapter, the experimental and modelling work were done for through-circulation convective drying within lab-scale AFD. Influence of process parameters including air flow, agitation speed, initial solvent content on the drying behaviour were investigated. The drying rate was found to be increased with the increase of the air flow, agitation speed.

For the through-circulation drying modelling predictions:

- The calculated drying curves are observed with a faster drying rate compared with the experimental drying process.
- From model simulation process, it can be seen that the critical solvent content for all the convective drying tests are indicating a similar value of 0.8. This phenomenon presents that the critical solvent content are kind of independent with the air flow initial solvent content.
- For different initial solvent content, the drying started from a higher solvent level (0.35) was found a slower drying rate compare to the modelling prediction which may result from recrystallization from a rich solvent slurry at the beginning of drying process.

- The calculated temperature profile of axial direction comparing with the actual temperature at the similar location indicates that the thermocouples inserted into the powder bed are actually the measurement of the gas and wet solid phase temperatures.

The work can be done in future includes the incorporation of the agitation parameters into the current exiting model; the mixed solvents convective drying is also of great interests.

Chapter 10
Conclusions

The chapter provides an overview of the main conclusions drawn from the work presented in this thesis as well as the applicability and development of the techniques to future investigation.

10.1 Introduction

AFDs encompass filtration, washing and drying unit operations into one single piece of equipment. Processing challenges of thermo- and oxygen-sensitive APIs and containment to minimize the potential for worker exposure give rise to the wide use of AFDs in the pharmaceutical industry. Amongst all these unit operations, drying can be the most time-consuming stage. Aggressive drying conditions are often adopted in order to minimize drying cycle time and increase the productivity. However, many APIs are shear sensitive, so agitation in the wet state can lead to agglomeration whilst in the dry state can lead to attrition. Agglomeration is undesired as it causes difficulties in discharging the dry-cake and hence prolongs the cycle time. Attrition can severely affect the downstream operations such as the blending with excipients and the tabletting processes. Both of them can affect the particle size distribution and particle shape which makes a negative impact on the drug product formulation. Hence the best way to dry a wet-cake of an API is to minimise any effects due to improper agitation. A good understanding of the drying behaviour of static and agitated wet-cakes is essential to optimise drying conditions and stirring periods in order to preserve particle integrity without producing lumps or fines. The integrated experimental and modelling study presented in this thesis has aimed to develop a better understanding of the effects of operating parameters on the vacuum contact drying kinetics especially under minimal agitation in a bench-scale AFD.

10.2 Conclusions for this study

The experimental and computational methods are used to study the drying behaviour of a powder bed of the aspirin and organic solvents in a TGA and

AFD. A laboratory-scale AFD was built up and instrumented capturing geometrical and operational features of a pilot-plant scale AFD.

In the TGA experiments using water as a solvent, all drying curves can be observed to have a constant and falling rate period. However, the high ratio of ethanol in the mixed solvents presents the drying curves with no constant-rate period due to higher mass diffusivity of ethanol. Among the different operating conditions examined by TGA, it is found that the drying rate as well as the critical solvent content relies on the vacuum level, temperature, particle size, and solvent volatility. TGA results show that the effect of recrystallization may hinder the drying process especially for solids with a smaller particle size and drying under a high temperature.

In the AFD, among all the drying conditions performed, it is found that an increase in the agitation speed, vacuum level and jacket temperature resulted in a decrease of the drying time. Both the constant- and falling-rate drying stages are observed for a low heating power; while only a falling-rate period is observed for higher heating input due to the capillary flow within the bed is not fast enough to maintain the wetness of the surface of the bed. An increase of the circularity of the aspirin particle with the increase of the agitation speed is observed. A slight increase in the particle mean size is also observed due to the effect of agglomeration. The extensive experimental schemes developed in this research are displayed in Table 10.1. As revealed in the previous work in the literatures presented in section 3.1.4, the categories listed in Table 3.2 is also compared with this research, the result is show in Table 10.1 which demonstrated on a wide range of types of study and drying characterization in this research.

Table 10.1 The drying experimental scheme exerted in this research relative to Table 3.2

Solute/solvent system	**Particle morphology**	**Type of agitation**	**Pressure**	**Cake preparation**	**Temperature (°C)**	**Types of Heating**	**Heating surface**	**Vessel size (volume/ Diameter)**	**Particle characterization**	**Type of study**	**Drying models**
Aspirin/ water/ ethanol	Needle-like	CA /IA	V	Y	50-70	EH	S	169mm	Y	E/ M	LPM DPM

Drying models based on a lumped-parameter approach were developed for a static bed and a more rigorous model incorporating agitation for vacuum contact drying. The modelling approach included both the constant- and falling-rate drying periods. In the former drying period, two heat transfer resistances were considered including the conductive resistance through the vessel wall and the contact resistance between the inner wall and the first layer of particles. For the later period, the model included a vaporization front that moves from the inner wall of the vessel to the centre of the wet bed for both the static and the agitated bed. An additional heat transfer resistance through the layer of dry particles between the wall and the vaporization front was taken into account. In the combined lumped-distributed parameter model for the through-circulation convective drying, a hot gas flows through a packed bed of wet particles in plug flow with temperature and humidity gradient existing along the axial direction but uniformly distributed along the radial direction. Both drying models were developed using the first principles of heat and mass transfer. Comparison between the calculated drying curves and the experimental data obtained from the AFD reveals a good agreement under varied drying conditions. With a less number of model parameter estimation, this makes the models have analytical solution presenting huge expedience to the drying curves prediction. Compared to the previous drying models, the models developed in this research are more liable to implement to industrial pharmaceutical drying applications.

10.3 **Suggestion of future work**

Within the current experimental work, both the contact and convective drying have their own advantages: at a high solvent level, the vacuum contact drying with agitation has a high potential to form agglomerates while drying without agitation needs a longer cycle time. Whilst the alternative convective drying within an AFD indicates a higher drying rate at a high solvent level meanwhile reduce the solvent level to the acceptable low risk agglomeration region. Hence, in order to reduce drying cycle time as well as minimize agglomeration phenomenon, collaboratively executing convective and conduction drying is great prospective in parallel or sequentially within an AFD, via taking advantage of each type of drying in order to improve the productivity and efficiency.

The mechanism of mixed solvents drying remains unclear and still needs to be investigated as the washing solvent and mother liquor may contain more than one solvent within the wet-cake being dried. As the complexity of the mixed solvents drying, for the modelling work, theory of thermal dynamics of each single solvent as well as the solids interactions with the combinative solvents needs to be considered and incorporated into the current model.

Modelling the drying process by introducing interfacial properties: solvent-solid interactions are favoured both in the academia and industry. Modelling prediction of the agglomeration and attrition as a function of agitation speed and regime as well as solid-solvent interactions is still need to be investigated as they are involved in the evolution of PSD and morphology.

List of references

[1] M. Murru, G. Giorgio, S. Montomoli, F. Ricard, F. Stepanek, Model-based scale-up of vacuum contact drying of pharmaceutical compounds, Chemical Engineering Science 66 (2011) 5045-5054.
[2] A. Michaud, R. Peczalski, J. Andrieu, Modeling of vacuum contact drying of crystalline powders packed beds, Chemical Engineering and Processing: Process Intensification 47 (2008) 722-730.
[3] M. Kohout, A.P. Collier, F. Štěpánek, Mathematical modelling of solvent drying from a static particle bed, Chemical Engineering Science 61 (2006) 3674-3685.
[4] M. Kohout, A.P. Collier, F. Štěpánek, Vacuum Contact Drying of Crystals: Multi-scale Modelling and Experiments, in: A. Barbosa-Póvoa, H. Matos (Eds.) Computer Aided Chemical Engineering, Elsevier2004, pp. 1075-1080.
[5] A. Lekhal, K.P. Girard, M.A. Brown, S. Kiang, B.J. Glasser, J.G. Khinast, Impact of agitated drying on crystal morphology: KCl - water system, Powder Technology 132 (2003) 119-130.
[6] A. Lekhal, K.P. Girard, M.A. Brown, S. Kiang, J.G. Khinast, B.J. Glasser, The effect of agitated drying on the morphology of L-threonine (needle-like) crystals, International Journal of Pharmaceutics 270 (2004) 263-277.
[7] W. Pietsch, Agglomeration in industry : occurence and applications, Weinheim: Wiley-VCH2004.
[8] L. Yu, Pharmaceutical Quality by Design: Product and Process Development, Understanding, and Control, Pharm Res 25 (2008) 781-791.
[9] E. Sahni, J. Hallisey, B. Morgan, J. Strong, B. Chaudhuri, Quantifying drying performance of a filter dryer: Experiments and simulations, Advanced Powder Technology (2011).
[10] A.S. Mujumdar, Handbook of industrial drying, Marcel Dekker, Inc, New York and Basel, 1987.
[11] A.S. Foust, Principles of unit operations, 2 ed., John Wiley and Sons (New York)1980.
[12] K. Sattler, H.J. Feindt, Thermal Separation Processes: Principles and Design, Wiley VCH1995.
[13] M.A. Maha, Equilibrium Moisture Sorption Isotherms of Aspirin, Journal of Engineering مجلة الهندسة 19 (2013) 453-463.
[14] A.S. Mujumdar, Handbook of Industrial Drying, Fourth Edition, Taylor & Francis2014.
[15] D. am Ende, M. Birch, S.J. Brenek, M.T. Maloney, Development and Application of Laboratory Tools To Predict Particle Properties upon Scale-Up in Agitated Filter-Dryers, Organic Process Research & Development 17 (2013) 1345-1358.
[16] G.X. Zhou, Z. Ge, J. Dorwart, B. Izzo, J. Kukura, G. Bicker, J. Wyvratt, Determination and differentiation of surface and bound water in drug substances by near infrared spectroscopy, Journal of Pharmaceutical Sciences 92 (2003) 1058-1065.

[17] K.R. Morris, S.L. Nail, G.E. Peck, S.R. Byrn, U.J. Griesser, J.G. Stowell, S.-J. Hwang, K. Park, Advances in pharmaceutical materials and processing, Pharmaceutical Science & Technology Today 1 (1998) 235-245.
[18] D.J. am Ende, M.J. Preigh, K. Hettenbach, P. Ahlijanian, H.W. Ward, On-Line Monitoring of Vacuum Dryers Using Mass Spectrometry, Organic Process Research & Development 4 (2000) 587-593.
[19] R.H. Perry, D.W. Green, Perry's Chemical Engineers' Handbook, 7th ed., McGraw-Hill1997.
[20] J.D. Seader, E.J. Henley, Separation process principles, 2nd ed., Hoboken, N.J. : Wiley.2006.
[21] D.J. am Ende, Chemical Engineering in the Pharmaceutical Industry R&D to Manufacturing, John Wiley & Sons Inc, US, 2010.
[22] Z. Berk, Food Process Engineering and Technology, Academic Press2009.
[23] J.F. Richardson, J.H. Harker, J.R. Backhurst, Coulson and Richardson's Chemical Engineering Volume 2 - Particle Technology and Separation Processes, 5th Edition ed., Elsevier2002.
[24] M. Shi, X. Wang, Investigation on moisture transfer mechanism in porous media during rapid drying process, Drying Technology 22 (2004) 111-122.
[25] L.A. Segura, Modeling at pore-scale isothermal drying of porous materials: liquid and vapor diffusivity, Drying Technology 25 (2007) 1677-1686.
[26] S.E. Papadakis, R.E. Bahu, The Sticky Issues of Drying, Drying Technology 10 (1992) 817-837.
[27] S.M. Iveson, J.D. Litster, K. Hapgood, B.J. Ennis, Nucleation, growth and breakage phenomena in agitated wet granulation processes: a review, Powder Technology 117 (2001) 3-39.
[28] W. Pietsch, Size enlargement by agglomeration, Wiley1991.
[29] H. Rumpf, The strength of granules and agglomerates, in: W.A. Knepper (Ed.) Agglomeration : based on an international symposium held in Philadelphia, New York ; London : Wiley Interscience, Pennsylvania, 1962, pp. 379-418.
[30] T. Schæfer, B. Taagegaard, L.J. Thomsen, H. Gjelstrup Kristensen, Melt pelletization in a high shear mixer. IV. Effects of process variables in a laboratory scale mixer, European Journal of Pharmaceutical Sciences 1 (1993) 125-131.
[31] T. Schæfer, B. Taagegaard, L.J. Thomsen, H. Gjelstrup Kristensen, Melt pelletization in a high shear mixer. V. Effects of apparatus variables, European Journal of Pharmaceutical Sciences 1 (1993) 133-141.
[32] T. Schæfer, Melt pelletization in a high shear mixer. X. Agglomeration of binary mixtures, International Journal of Pharmaceutics 139 (1996) 149-159.
[33] T. Schæfer, Melt pelletization in a high shear mixer VI. Agglomeration of a cohesive powder, International Journal of Pharmaceutics 132 (1996) 221-230.
[34] T. Schæfer, C. Mathiesen, Melt pelletization in a high shear mixer. VII. Effects of product temperature, International Journal of Pharmaceutics 134 (1996) 105-117.

[35] T. Schæfer, C. Mathiesen, Melt pelletization in a high shear mixer. VIII. Effects of binder viscosity, International Journal of Pharmaceutics 139 (1996) 125-138.
[36] T. Lee, H.Y. Lin, H.L. Lee, Engineering Reaction and Crystallization and the Impact on Filtration, Drying, and Dissolution Behaviors: The Study of Acetaminophen (Paracetamol) by In-Process Controls, Organic Process Research & Development 17 (2013) 1168-1178.
[37] T. Schæfer, Growth mechanisms in melt agglomeration in high shear mixers, Powder Technology 117 (2001) 68-82.
[38] A. Michaud, R. Peczalski, J. Andrieu, Optimization of crystalline powders vacuum contact drying with intermittent stirring, Chemical Engineering Research and Design 86 (2008) 606-611.
[39] E.U. Schlünder, Heat transfer to packed and stirred beds from the surface of immersed bodies, Chemical Engineering and Processing 18 (1984) 31-53.
[40] E.U. Schlünder, N. Mollekopf, Vacuum contact drying of free flowing mechanically agitated particulate material, Chemical Engineering and Processing: Process Intensification 18 (1984) 93-111.
[41] A. Dittler, T. Bamberger, D. Gehrmann, S. Ernst-Ulrich, Measurement and simulation of the vacuum contact drying of pastes in a LIST-type kneader drier, Chemical Engineering and Processing: Process Intensification 36 (1997) 301-308.
[42] D. Skansi, S. Tomas, I. Fudic, A. Arapović, The influence of pressure and temperature on the kinetics of vacuum drying of ketoprofen, Drying Technology 15 (1997) 1617-1631.
[43] L. Hoekstra, P. Vonk, L.A. Hulshof, Modeling the Scale-Up of Contact Drying Processes, Organic Process Research & Development 10 (2006) 409-416.
[44] E. Tsotsas, E.U. Schlünder, Contact drying of mechanically agitated particulate material in the presence of inert gas, Chemical Engineering and Processing: Process Intensification 20 (1986) 277-285.
[45] F. Heimann, E.U. Schlünder, Vacuum contact drying of mechanically agitated granular beds wetted with a binary mixture: Vakuum-Kontakttrocknung von mechanisch durchmischten Schütgütern, die mit einem binären Gemisch befeuchtet sind, Chemical Engineering and Processing: Process Intensification 24 (1988) 75-91.
[46] R. Forbert, F. Heimann, Vacuum contact drying of mechanically agitated, coarse, hygroscopic bulk material, Chemical Engineering and Processing: Process Intensification 26 (1989) 225-235.
[47] A. Gevaudan, J. Andrieu, Contact drying modelling of agitated porous alumina beads, Chemical Engineering and Processing: Process Intensification 30 (1991) 31-37.
[48] J.F. Nastaj, Vacuum contact drying of selected biotechnology products, Drying Technology 12 (1994) 1145-1166.
[49] D.I.F. Thumer, Scale-up of contact dryers, Drying Technology 12 (1994) 1367-1385.
[50] S. Laurent, F. Couture, M. Roques, Vacuum drying of a multicomponent pharmaceutical product having different pseudo-polymorphic forms, Chemical Engineering and Processing 38 (1999) 157-165.

[51] R. Dewil, J. Baeyens, E. Neyens, Fenton peroxidation improves the drying performance of waste activated sludge, Journal of Hazardous Materials 117 (2005) 161-170.
[52] M. Kohout, A. Collier, F. Štěpánek, Vacuum Contact Drying Kinetics: An Experimental Parametric Study, Drying Technology 23 (2005) 1825-1839.
[53] M. Kohout, F. Štěpánek, Multi-scale analysis of vacuum contact drying, Drying Technology 25 (2007) 1265-1273.
[54] A. Michaud, R. Peczalski, J. Andrieu, Experimental Study and Modeling of Crystalline Powders Vacuum Contact Drying with Intermittent Stirring, Drying Technology 25 (2007) 1163-1173.
[55] W.-Y. Deng, J.-H. Yan, X.-D. Li, F. Wang, S.-Y. Lu, Y. Chi, K.-F. Cen, Measurement and simulation of the contact drying of sewage sludge in a Nara-type paddle dryer, Chemical Engineering Science 64 (2009) 5117-5124.
[56] J.-H. Yan, W.-Y. Deng, X.-D. Li, F. Wang, Y. Chi, S.-Y. Lu, K.-F. Cen, Experimental and Theoretical Study of Agitated Contact Drying of Sewage Sludge under Partial Vacuum Conditions, Drying Technology 27 (2009) 787-796.
[57] N.K. Nere, K.C. Allen, J.C. Marek, S.V. Bordawekar, Drying process optimization for an API solvate using heat transfer model of an agitated filter dryer, Journal of Pharmaceutical Sciences 101 (2012) 3886-3895.
[58] P. Hamilton, D. Littlejohn, A. Nordon, J. Sefcik, P. Slavin, J. Andrews, P. Dallin, Investigation of factors affecting isolation of needle-shaped particles in a vacuum-agitated filter drier through non-invasive measurements by Raman spectrometry, Chemical Engineering Science 101 (2013) 878-885.
[59] E.K. Sahni, R.H. Bogner, B. Chaudhuri, Systematic investigation of parameters affecting the performance of an agitated filter-dryer, Journal of Pharmaceutical Sciences 102 (2013) 2198-2213.
[60] E.K. Sahni, B. Chaudhuri, Numerical simulations of contact drying in agitated filter-dryer, Chemical Engineering Science 97 (2013) 34-49.
[61] D. am Ende, M. Birch, S.J. Brenek, M.T. Maloney, Development and application of laboratory tools to predict particle properties upon scale-up in agitated filter-dryers, Organic Process Research & Development (2013).
[62] U. Grigull, H. Sandner, Heat conduction, 1984.
[63] J.C.J. H.S. Carslaw, Conduction of heat in solids, 2nd ed. ed., Oxford University Press, Oxford, 1986.
[64] L.M. Jiji, Heat Conduction, 3rd Edition ed., New york, 2009.
[65] E.U. Schlünder, N. Mollekopf, Vacuum contact drying of free flowing mechanically agitated particulate material, Chemical Engineering and Processing: Process Intensification 18 (1983) 93-111.
[66] E.K. Sahni, B. Chaudhuri, Contact drying: A review of experimental and mechanistic modeling approaches, International Journal of Pharmaceutics 434 (2012) 334-348.
[67] D. Marinos-Kouris, Z.B. Maroulis, C.T. Kiranoudis, Computer Simulation of Industrial Dryers, Drying Technology 14 (1996) 971-1010.
[68] K.M. Waananen, J.B. Litchfield, M.R. Okos, CLASSIFICATION OF DRYING MODELS FOR POROUS SOLIDS, Drying Technology 11 (1993) 1-40.

[69] E. Barati, J.A. Esfahani, A new solution approach for simultaneous heat and mass transfer during convective drying of mango, Journal of Food Engineering 102 (2011) 302-309.
[70] N. Boukadida, S.B. Nasrallah, P. Perre, Mechanism of two-dimensional heat and mass transfer during convective drying of porous media under different drying conditions, Drying Technology 18 (2000) 1367-1388.
[71] J.A. Esfahani, H. Majdi, E. Barati, Analytical two-dimensional analysis of the transport phenomena occurring during convective drying: Apple slices, Journal of Food Engineering 123 (2014) 87-93.
[72] M. Ilic, I.W. Turner, Convective drying of a consolidated slab of wet porous material, International Journal of Heat and Mass Transfer 32 (1989) 2351-2362.
[73] B. Zecchi, L. Clavijo, J. Martínez Garreiro, P. Gerla, Modeling and minimizing process time of combined convective and vacuum drying of mushrooms and parsley, Journal of Food Engineering 104 (2011) 49-55.
[74] J.K. Gigler, W.K.P. van Loon, M.M. Vissers, G.P.A. Bot, Forced convective drying of willow chips, Biomass and Bioenergy 19 (2000) 259-270.
[75] A. Mhimid, J.P. Fohr, S. Ben Nasrallah, Heat and Mass Transfer during Drying of Granular Products by Combined Convection and Conduction, Drying Technology 17 (1999) 1043-1063.
[76] A. Mhimid, S. Ben Nasrallah, J.P. Fohr, Heat and mass transfer during drying of granular products — simulation with convective and conductive boundary conditions, International Journal of Heat and Mass Transfer 43 (2000) 2779-2791.
[77] E. Barati, J.A. Esfahani, Mathematical modeling of convective drying: Lumped temperature and spatially distributed moisture in slab, Energy 36 (2011) 2294-2301.
[78] X. Nie, R.W. Besant, R.W. Evitts, Convective heat and mass transfer coefficient measurements and correlations for particle beds using temperature and humidity step changes with air flow through a test bed, Chemical Engineering Science 64 (2009) 3476-3485.
[79] R.G. Taecker, O.A. Hougen, HEAT, MASS TRANSFER OF GAS FILM IN FLOW OF GASES THROUGH COMMERCIAL TOWER PACKINGS, Chemical Engineering Progress 45 (1949) 188-193.
[80] E. Barati, J.A. Esfahani, Mathematical simulation of convective drying: Spatially distributed temperature and moisture in carrot slab, International Journal of Thermal Sciences 56 (2012) 86-94.
[81] E. Barati, J.A. Esfahani, A novel approach to evaluate the temperature during drying of food products with negligible external resistance to mass transfer, Journal of Food Engineering 114 (2013) 39-46.
[82] L. Malafronte, G. Lamberti, A.A. Barba, B. Raaholt, E. Holtz, L. Ahrné, Combined convective and microwave assisted drying: Experiments and modeling, Journal of Food Engineering 112 (2012) 304-312.
[83] P. Sebastian, I.W. Turner, An investigation of the boundary conditions for a vacuum drying problem - introducing the transition layer concept, Drying Technology 12 (1994) 717-760.

[84] A. Geddes, The Filtration and Drying Behaviour of Organic Crystals with Varied Morphologies following their Batch Crystallisation Institute of Particle Science and Engineering, University of Leeds, 2003.
[85] V.V. Komarov, Handbook of dielectric and thermal properties of materials at microwave frequencies, 2012.
[86] R.B. Hammond, K. Pencheva, V. Ramachandran, K.J. Roberts, Application of grid-based molecular methods for modeling solvent-dependent crystal growth morphology: aspirin crystallized from aqueous ethanolic solution, Crystal Growth & Design 7 (2007) 1571-1574.
[87] F.P. Incropera, Fundamentals of heat and mass transfer, 7th ed., John Wiley & Sons2012.
[88] S. Whitaker, Fundamental principles of heat transfer, Elsevier2013.
[89] P.K. Kom, W. Cook, E. Kougoulos, Impact of laboratory vacuum contact drying on material drying Rates and physical properties, Organic Process Research & Development 15 (2011) 360-366.
[90] J.M.R.J.F. Coulson, Coulson & Richardson's chemical engineering. Vol. 1, Butterworth-Heinemann, Oxford, 2003.
[91] E. Tsotsas, M. Kwapinska, G. Saage, Modeling of contact dryers, Drying Technology 25 (2007) 1377-1391.
[92] M. Kohout, A. Collier, F. Štěpánek, Effective thermal conductivity of wet particle assemblies, International Journal of Heat and Mass Transfer 47 (2004) 5565-5574.
[93] W. Ranz, Friction and transfer coefficients for single particles and packed beds, Chemical Engineering Progress 48 (1952) 247-253.
[94] S. Mukayeva, Agitated filter drying of aspirin slurry in mixed solvents, University of Leeds, Leeds, 2014.
[95] D.W.P. Green, Robert H. , Perry's Chemical Engineers' Handbook, 8th Edition ed., McGraw-Hill2008.
[96] J.C.S. Warren L. McCabe, Peter Harriot, Unit operations of chemical engineering, McGraw-Hill, London 2005.
[97] C. Fyhr, I.C. Kemp, COMPARISON OF DIFFERENT DRYING KINETICS MODELS FOR SINGLE PARTICLES, Drying Technology 16 (1998) 1339-1369.
[98] J.W. Mullin, Crystallization, 4th ed., Butterworth-Heinemann2001.
[99] R.C. Progelhof, J.L. Throne, R.R. Ruetsch, Methods for predicting the thermal conductivity of composite systems: A review, Polymer Engineering & Science 16 (1976) 615-625.
[100] N.P. Cheremisinoff, Chapter 6 - Mechanical Separation Equipment, in: N.P. Cheremisinoff (Ed.) Handbook of Chemical Processing Equipment, Butterworth-Heinemann, Woburn, 2000, pp. 334-434.

Bibliography

A.S. Foust, Principles of unit operations, 2 ed., John Wiley and Sons (New York)1980.

A.S. Mujumdar, Handbook of industrial drying, Marcel Dekker, Inc, New York and Basel, 1987.

C.J. Geankoplis, Transport processes and separation process principles, 4th ed.2003.

D.J. am Ende, Chemical Engineering in the Pharmaceutical Industry R&D to Manufacturing, John Wiley & Sons Inc, US, 2010.

D.W.P. Green, Robert H. , Perry's Chemical Engineers' Handbook, 8th Edition ed., McGraw-Hill2008.

F.P. Incropera, Fundamentals of heat and mass transfer, 6th ed., John Wiley & Sons2011.

J.D. Seader, E.J. Henley, Separation process principles, 2nd ed., Hoboken, N.J. : Wiley.2006.

J.F. Richardson, J.H. Harker, J.R. Backhurst, Coulson and Richardson's Chemical Engineering Volume 2 - Particle Technology and Separation Processes, 5th Edition ed., Elsevier2002.

J.M.R.J.F. Coulson, Coulson & Richardson's chemical engineering. Vol. 1, Butterworth-Heinemann, Oxford, 2003.

K. Sattler, H.J. Feindt, Thermal Separation Processes: Principles and Design, Wiley VCH1995.

Z. Berk, Food Process Engineering and Technology, Academic Press2009.

Appendix A
Different complexity of LMPs for static beds

A.1 Constant wall temperature

In the static bed drying model, the solvent vaporises at a much lower temperature due to the very low pressure maintained in the head-space of the vessel shown in Figure 6.1. With the heating jacket supplying heat to the wet-cake, the temperature increases from the room temperature to the boiling point of the solvent and the solvent starts to vaporize. The rate of heat transfer to the wet-cake determines the rate of solvent vaporization. At the beginning, the surface of the cake is completely wet and is covered with a film of solvent. In this period, the solvent is continuously supplied to the surface from the interior of the wet-cake. The constant-rate period will continue as long as enough solvent can be supplied from the interior of the wet-cake by capillary or diffusion to keep the surface of the solid completely wet.

Constant-rate period

The drying model for the constant-rate period is based on the following assumptions:

- The initial heating up period is neglected.
- There are no gradients of temperature and solvent content inside the wet-cake [2].
- Because of a low temperature in the vacuum dryer, radiation heat transfer is neglected.
- The heat supplied from the heating jacket is used for solvent vaporisation.

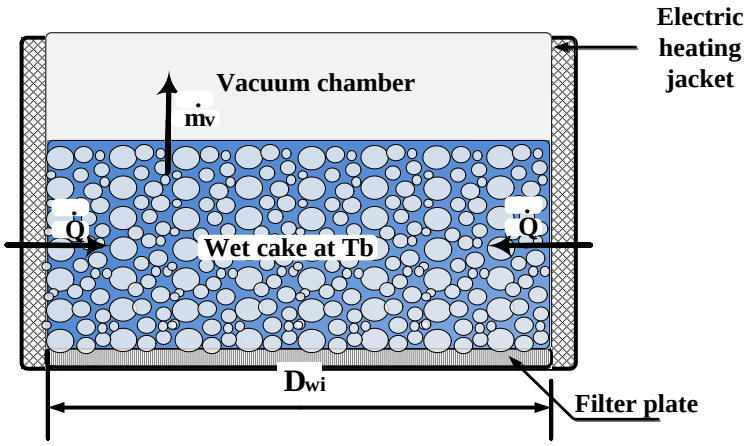

Figure A.1 The schematic of a vacuum contact dryer during the constant-rate period.

The solvent content of the wet solid , X , is solvent content by weight of bone-dry material in the solid which is expressed by solvent solid ratio, m_v/m_{ds} , based on the mass of the dry solid, m_{ds} , and is given by [20]:

$$X = \frac{m_v}{m_{ds}} \qquad \text{A-1}$$

The variation of average solvent content of the wet-cake with time is given by:

$$\frac{\mathrm{d}X}{\mathrm{d}t} = -\frac{\dot{m}_v}{m_{ds}} \qquad \text{A-2}$$

The solvent vaporised at the saturation temperature T_B at the vessel wall under the prevailing pressure. For the vapour phase, the heat flux from heating surface to the solvent vapour is supplied to vaporization heat:

$$\alpha_{ws} A\left(T_{wi} - T_B\right) = \dot{m}_v \Delta H_v \qquad \text{A-3}$$

Falling-rate period

The falling-rate period starts from the point of critical solvent content $\left(X_C\right)$. During this period, no ample solvent can be transferred from inside the wet-cake to the surface to maintain the surface completely wet. The surface between the vessel wall and the wet-cake becomes partly dry and a vaporization front is established which shifts towards inside the cake and the falling-rate period begins (Figure A.2). The solvent on the surface continue to decrease until the surface becomes completely dry which means the first falling-rate period is coming to the end. The plane of vaporisation moves towards the centre of the wet-cake and heat supplied for the vaporisation is

transferred to the wet-zone through the dry solids. The pressure difference between the vessel head and the cake provides the driving force for the mass transfer of the vapour through permeability while the temperature difference facilitates the drying process. The rate of vapour removal dominates the rate of drying in the falling-rate period. A porous solid may contains interconnecting pores and channels of varied pore size. In porous materials, interfacial tension formed by capillary forces between the solvent and the solid provides the driving force to remove the solvent from the wet-zone to the surface. When there is not enough solvent for the solids to maintain a continuous film across the pores to keep the capillary force, the rate of drying decreases suddenly. Then the second falling-rate period starts. If there is still bound solvent inside the individual particles, the solvent may be removed by diffusivity. The rate of diffusion of vapour and contact heat transfer rate controls the drying rate at the second falling-rate period. If there is no bound water inside the particles, no breaking point shows between the first falling-rate and second falling-rate period. In the end of falling-rate period, the solvent content reaches the equilibrium solvent content. The drying model for the falling-rate period is based on the following assumptions:

- Throughout the wet zone the temperature and solvent content are homogeneous.
- The solvent vaporises at the saturation temperate under the prevailing pressure.
- A vaporization front is developed and move from the heating wall to inside the bed.

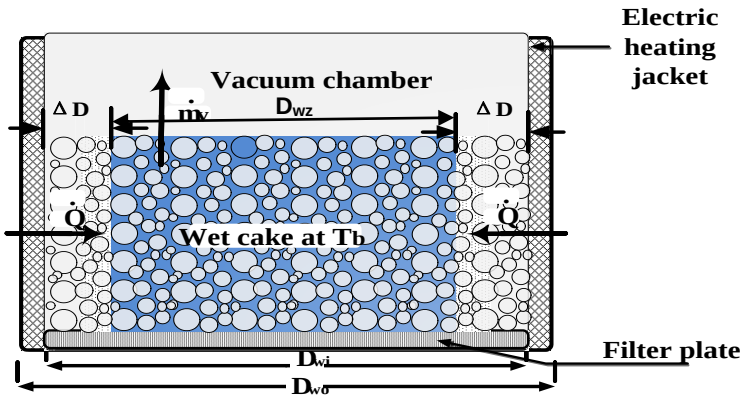

Figure A.2 The schematic of a vacuum contact dryer during the falling-rate period

This equation can be solved directly by integration and this saves the calculation process a lot of time.
The equation changed to format as follows:

$$\frac{dt}{dX} = \frac{m_{ds}\Delta H_v D_{pb}}{(T_{sw}\text{-}T_b)A_{sw}4\lambda_{ds}} \ln X(t) - \frac{m_{ds}\Delta H_v}{(T_{sw}\text{-}T_b)A_{sw}}\left(\frac{1}{\alpha_{ws}} + \frac{D_{pb}\ln X_C}{4\lambda_{ds}}\right)$$
$$\Leftrightarrow \frac{dt}{dX} = A\ln X + B \qquad \text{A-4}$$

Define the constant A as $\frac{m_{ds}\Delta H_v D_{pb}}{(T_{sw}\text{-}T_b)A_{sw}4\lambda_{ds}}$, and the constant B as $-\frac{m_{ds}\Delta H_v}{(T_{sw}\text{-}T_b)A_{sw}}\left(\frac{1}{\alpha_{ws}} + \frac{D_{pb}\ln X_C}{4\lambda_{ds}}\right)$. The drying curve can be obtained by integrating the above equation between the limit of
Time: $t_c \to t$
Solvent content: $X_c \to X(t)$

$$\int_{t_c}^{t} dt = \int_{X_c}^{X} (A\ln X + B)dX = \int_{X_c}^{X} d\left[AX\ln X + (B-A)X\right] \qquad \text{A-5}$$

The time needed to reach certain solvent content X during the falling-rate period is expressed as:

$$t_f = AX\ln X - AX_C\ln X_C + (B-A)(X - X_C) \qquad \text{A-6}$$

The heat transfer across the vessel wall is used for overcoming the heat resistance from the inner wall to the first layer of the particle as well as the resistance from the first layer of the particle to the vaporization front:

$$\dot{Q}_{in} = \frac{1}{1/\alpha_{ws} + 1/\alpha_{ds}} A_{wi}(T_{wi}\text{-}T) \qquad \text{A-7}$$

Furthermore, the heat transfer from inner wall to the first layer of wet-cake is used for solvent vaporisation and heat up the wet-cake:

$$\frac{1}{1/\alpha_{ws} + 1/\alpha_{ds}} A_{wi}(T_{wi}\text{-}T) = \langle mC_p \rangle \frac{dT}{dt} + \dot{m}_v \Delta H_v \qquad \text{A-8}$$

According to Antoine equation, the saturation pressure of vapour $P_{sat} = 10^{\left(A - \frac{B}{C+T}\right)}$ is increased as temperature rises. Hence the solvent vapour drying rate $\dot{m}_v = \frac{K\rho_v}{P_{ul}}(P_{sat} - P_{ul})$ decreases as the actual vapour pressure reducing.

A.2 Varied wall temperature

In the foregoing discussion, it has been shown that the model of constant wall temperature. However, some of agitated vessels are slow to heated up. In this work, the constant heating power was supplied from the electric heating band to the vessel wall, compared to a jacket heating system using circulating fluid, it takes longer time to reach the pre-set value. Hence, the wall temperature was monitored and fitted to a curve. The fitting curve will be then used in a modelling validation rather than a constant temperature value as an input in order to eliminate the influence from the inevitable initial heating up period. First of all, the original wall temperature recorded data was plotted and then find the closest fitting curve to the recorded data. The fitting curve and the original data recorded for the heat wall temperature are plotted in Figure A.3.

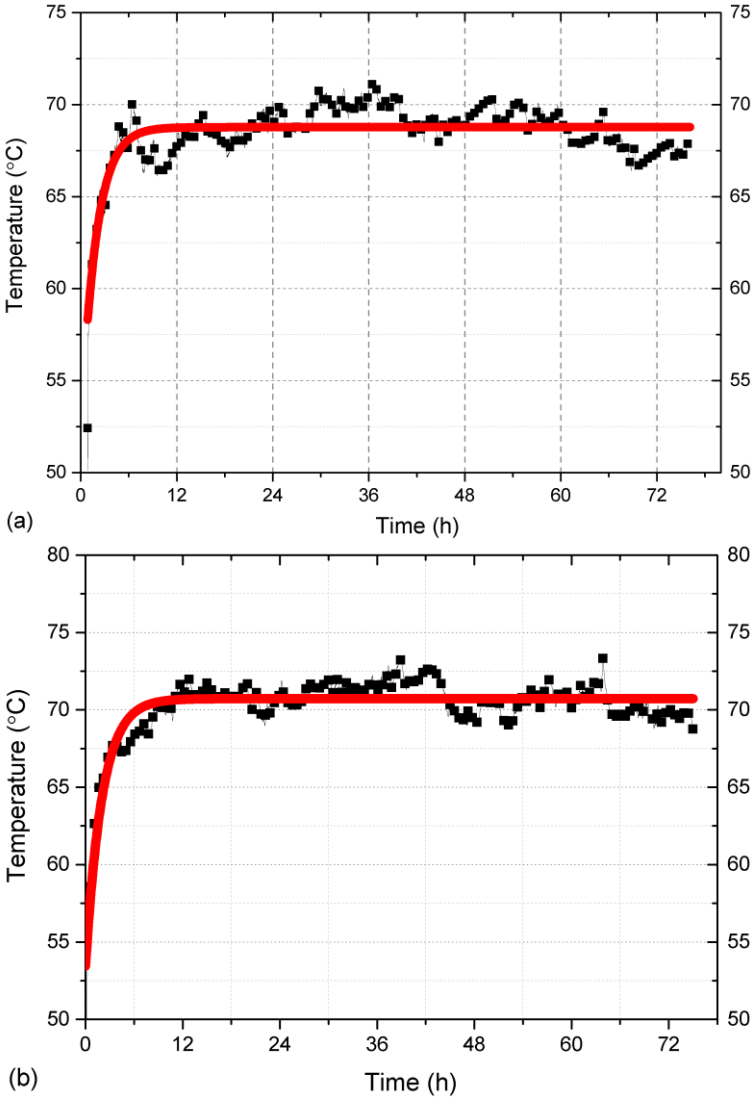

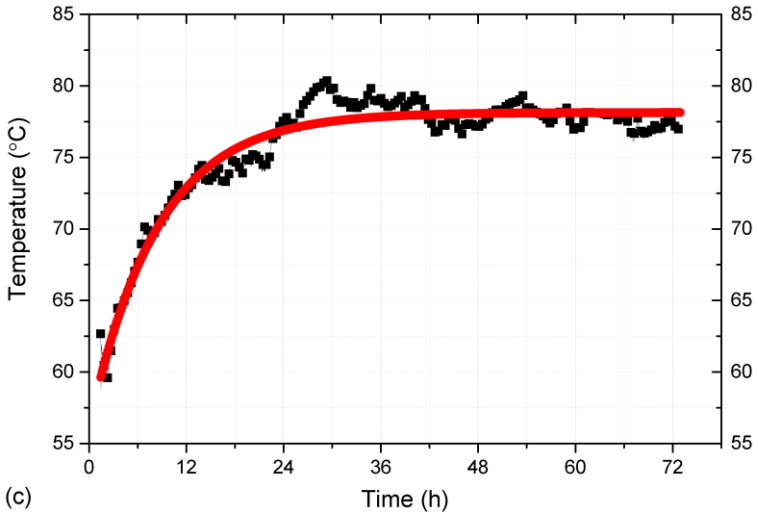

Figure A.3 The fitting curves for heating wall temperature at different electric power: (a) 126 Watts; (b) 144 Watts; (c) 152 Watts

The R-square was calculated for the fitting curve and the fitting equation for temperature against time is shown in table A.1. It can be seen that after fitting the curve of wall temperature is much closer to the actual condition which in turn would improve the degree of accuracy of model prediction meanwhile exclude the influence with the assumption of constant wall temperature from the first model.

Table A.1 The heating wall temperature fitting curve equations as a function of time at three electric heating powers

Electricity power	Equations	R-Square
126 Watts	$T = 68.7 - 16.6 * EXP(-1.48E-4 * t)$	0.79
144 Watts	$T = 70.7 - 17.3 * EXP(-1.36E-4 * t)$	0.83
152 Watts	$T = 78 - 22 * EXP(-3.3E-5 * t)$	0.94

With the heating temperature profile input as variables, it brings the closer connection from the model the actual experiment operating conditions. Use the three equations as the heating wall temperature, a slightly different model will be generated.

A.3 Initial heating up period

For some cases, the heating temperature profile is not easy to obtain. Hence the initial heating up period cannot be ignored here. The solvent starts to vaporise at a much lower temperature and for a special collection of dryers with a long heating up period, it is important to take this part in to account.

The heat supplied from the heating jacket is used for heating up the cake as well as for the vaporisation of the solvent.

At the beginning, the driving force for drying is the temperature difference between the heating jacket (T_{wi}) and the wet-cake (T). The heat supplied from the heating jacket to the wet-cake is used for heating up the cake and solvent vaporization.

$$\alpha_{ws} A(T_{wi}\text{-}T) = \langle mC_p \rangle \frac{dT}{dt} + \dot{m}_v \Delta H_v \qquad \text{A-9}$$

The mean gravimetric heat capacity, $\langle mC_p \rangle$, is calculated from the pure components and the phase mass fractions according to:

$$\langle mC_p \rangle = \frac{m_{ds}}{m_c} C_{p,ds} + \frac{m_v}{m_c} C_{p,l} \qquad \text{A-10}$$

m_{ds}, m_v and m_c are the mass of dry solid, solvent and the cake individually; $C_{p,ds}$ and $C_{p,l}$ is the heat capacity of dry solid and solvent individually. The vaporization was supposed to occur at the heating wall and the drying rate was calculated by solving mass transfer for the vapour phase.

The driving force for mass transfer is the pressure drop between the wet-cake and headspace above the wet-cake. To predict mass transfer rate of the vapour, the theory of gas filtration within a porous media driven by pressure drop is used here. It has been proved that dimensional analysis is most reliable method by yielding an equation for accurate pressure drop prediction [100]. This method is based on dimensional analysis of Darcy's law of flow through porous media and the driving force is created by the pressure drop to the filter porosity. The original Darcy's equation is given by

$$\dot{m}_v = -\frac{\kappa_D A_b \rho_v}{\eta_v} \left(\frac{P - P_{sat}}{Z} \right) \qquad \text{A-11}$$

According to Antoine equation, saturation pressure of solvent vapour, P_{sat} (pa), is expressed as [95]:

$$P_{sat} = 10^{\left(A - \frac{B}{C+T}\right)} \qquad \text{A-12}$$

$$A = 10.196213, \quad B = 1730.63, \quad C = 233.426 \qquad for \quad 0°C < T < 100°C$$

This model containing first-order nonlinear ordinary differential equations is implemented to gPROMS software.

Appendix B
Calculation of TGA drying curves

The original data obtained from TGA was weight loss (mg) vs. time (s) (Figure B.1), the plot was shown as follows:

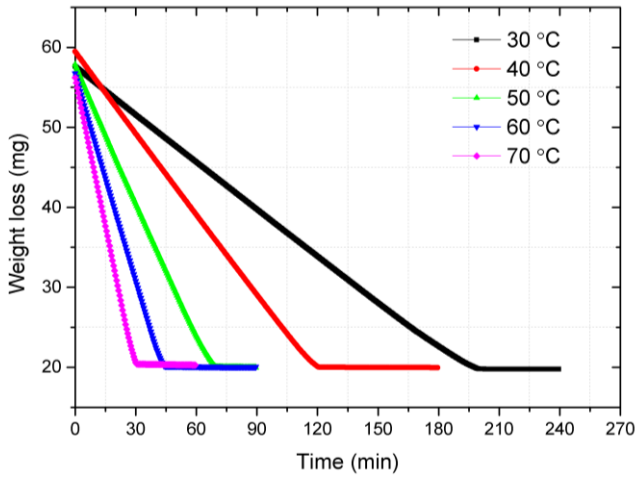

Figure B.1 Weight loss vs. time at different temperatures

By converting the weight loss to the solvent content, the following conversion was used:

$$\text{Solvent content} = \frac{\text{Weight loss} - \text{Weight of dry solid}}{\text{Weight of initial wet cake}}$$

where $\text{Weight of initial wet cake}$ is the weight of wet-cake measured at the beginning of drying process; $\text{Weight of dry solid}$ is the weight of bone-dry materials measured by the end of drying.

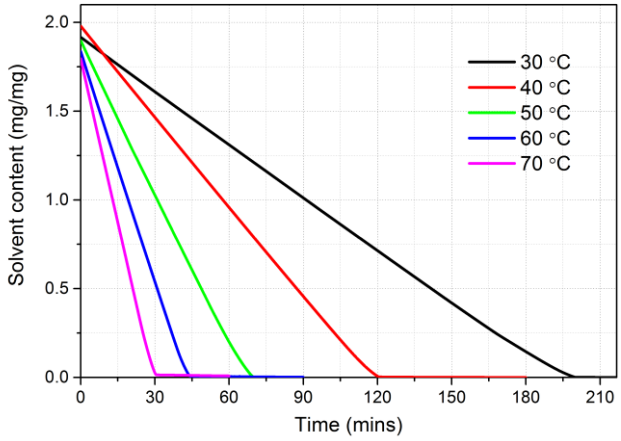

Figure B.2 Solvent content vs. time at different temperatures

By converting the solvent content vs. time in Figure into drying rate curve, the following conversion was used:

$$\text{Drying rate} = -\text{Weight of dry solid}\,\frac{\text{Solvent content (i+1)} - \text{Solvent content (i)}}{\Delta t}$$

Where the solvent content in any time step (i) to the next one (i+1) took time Δt , by differentiating the solvent content vs. time curve, the drying rate vs. solvent content (Figure B.3) could be plotted as follows:

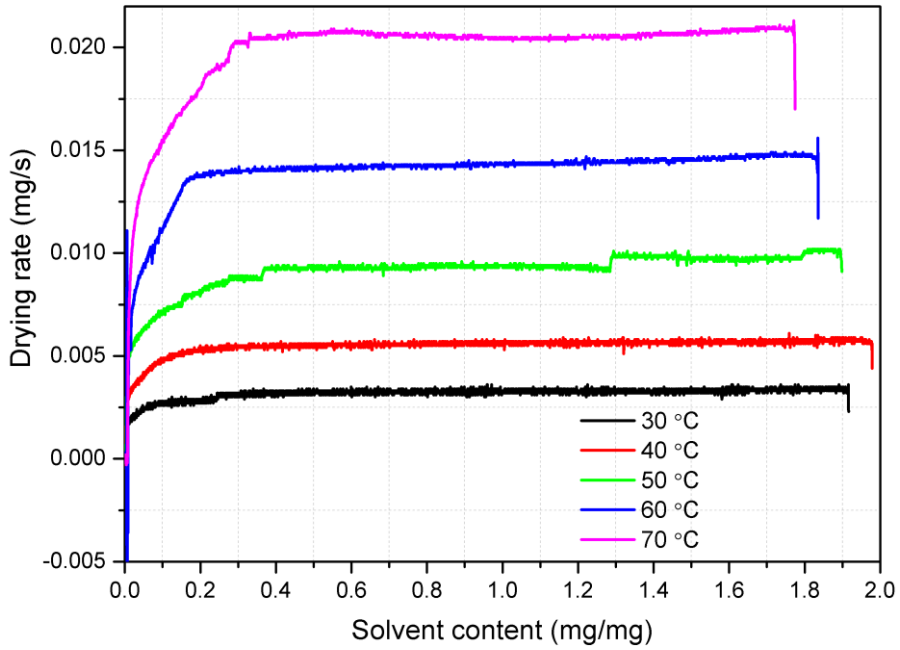

Figure B.3 Drying rate vs. solvent content at different temperatures